"Dynamics and microstructure of entangled supramolecular networks"

Goldansaz, Seyed Hadi

Abstract

Scientists have constantly looked for new routes and methodologies to modify and improve the properties of the synthetic polymers. One of the greatest treatment of all, inspired from the nature, is to incorporate non-covalent transient interactions into polymers. The utilization of hydrogen bonds, coordination chemistry and ion-dipole interactions to obtain so called supramolecular networks has attracted wide spread interest in recent years, since adaptive and functional synthetic polymers with new properties are obtained. The goal of this work is to gain comprehensive understanding over self-organization and molecular dynamics of model entangled supramolecular networks. We investigated the effects of supramolecular assemblies on the relaxation mechanism of entangled associating polymers, from smallest statistical segment to macroscopic flow. In addition, we studied alteration of the self-assembling dynamics of supramolecular moieties in the environment of the polymer melt. The outco...

Document type : *Thèse (Dissertation)*

Université catholique de Louvain

Institut de la Matiére Condensée et des Nanosciences

Bio and Soft Matter Division

Dynamics and Microstructure of Entangled Supramolecular Networks

Seyed Hadi Goldansaz

Dissertation presented in partial fulfilment of the requirements
for the degree of Doctor in Engineering Science
October 2015

Examination Committee:

Chair :	Prof. dr. Jacques Devaux	Université catholique de Louvain
Supervisor:	Prof. dr. Evelyne van Ruymbeke	Université catholique de Louvain
Jury:	Prof. dr. Dimitris Vlassopoulos	Forth Institute of Technology
	Prof. dr. Michael Wübbenhorst	Katholieke Universiteit Leuven
	Prof. dr. Christian Bailly	Université catholique de Louvain
	Prof. dr. Jean-Franois Gohy	Université catholique de Louvain
	Prof. dr. Charles-André Fustin	Université catholique de Louvain

Dedicated to my wife

for her love, passion and kindness.

Preface

Polymers have achieved a privileged position as the class of materials having the highest volume of production, exceeding that of both metals and ceramics. The impressive production and utilization of polymers has been due to advances in three main fields: (i) various synthesis routs which allows the creation of specific and well defined molecular structures, (ii) In-depth knowledge of the relationship between structure and properties and (iii) advances in processing technology and machinery of polymers to develop morphologies which satisfy the desired specifications. In this context, polymers have truly become engineered materials.

To modify and improve the properties of the synthetic polymers, scientists have constantly looked for new routes and methodologies. One of the greatest treatment of all, inspired from the nature, is to incorporate non-covalent transient interaction into polymer. The utilization of hydrogen bonds, coordination chemistry and ion-dipole interactions to obtained so called supramolecular networks has attracted wide spread interest in recent years, since adaptive and functional synthetic polymers with new properties are obtained.

Indeed supramolecular systems based on associating polymers are promising smart materials since they exhibit tunable properties achieved by the incorporation of stimuli responsive supramolecular moieties to polymer backbones. The great advantage of self-assembling supramolecular networks is that their microstructures and dynamics depend on many tunable parameters such as the strength of the transient bonds, temperature, chemistry and architecture of the polymer precursor. As a result of facile tailoring of their dynamics at large, supramolecular networks have been successfully employed in several high-tech applications in which high degree of control over molecular dynamics is required e.g. shock absorbers, polymer electrolytes, self-healing materials, micro switchers and sensors. This research work tries to answer several important questions on the structure-property relationship in model entangled supramolecular networks.

A work such as this one would have been impossible without generous and even

enthusiastic help of family, friends and colleagues. It is a pleasure to express my deep gratitude to Prof. E. van Ruymbke for her supervision, encouragements and kind help throughout these years. I would like to acknowledge my supervising committee members, Professors C. Bailly, J.-F. Gohy and C.-A. Fustin who have great shares in the successes of this work. The benefit of their valuable discussions and suggestions is also greatly acknowledged. I would like to sincerely thank Prof. D. W. Auhl who played an outstanding role in shaping my research capabilities and skills. Several colleagues were most helpful by collaborating in this research project. In this connection, special thanks are due to Professors M. Wbbenhorst, M. E. Ries and B. Goderis, D. Vlassopoulos, O. Hassager and N. J. Alvarez.

It is a great pleasure to acknowledge an outstanding group of friends who participated in this research work, specifically Doctors M. Ahmadi, L. Hawke, A. Shabir and J. Brassine.

Last but not least, I would like to thank my better half, my inspiration, my lovely wife Hoda, who helped me to regain hope after despair, resume life after obstructions, and restart journeys after detours. Without her kindness, I would have never reached the end of this PhD.

Contents

List of Figures

List of Tables

Acronyms

AA	Acrylic Acid Monomer
BA	Butyl Acrylate Monomer
BDS	Broadband Dielectric Spectroscopy
CLF	Contour Length Fluctuations
CPMG	Carr-Purcell-Meiboom-Gill Pulse Sequence
CR	Constraint Release Rouse
CRR	Cooperative Rearranging Region
DMA	Dynamic Mechanical Analysis
DSC	Differential Scanning Calorimetry
EDX	Energy Dispersive X-Ray Spectrometry Analysis
DSIMS	Dynamic Secondary Ion Mass Spectrometry
E_P	Electrode Polarization
FWHM	Full Width at Half Maximum
GPC	Gel Permeation Chromatography
HEA	Hydroxyethy Acrylate
I_P	Interfacial Polarization
LAOS	Large Amplitude Oscillatory Shear
LVE	Linear Viscoelastic
MALDI	Matrix Assisted Laser Desorption/Ionization
MMD	Molar Mass Distribution
M_n	Number average Molar Mass
M_w	Weight Average Molar Mass
MWS	Maxwell-Wagner-Sillars
NLVE	Non-Linear Viscoelastic
NMR	Nuclear Magnetic Resonance
PAA	Poly(Acrylic Acid)
PB	Poly(butadiene)
PEO	Poly(Ethylene Oxide)
PEP	Poly(styrene)
PnBA	Poly(n-Butyl Acrylate)
PS	Poly(styrene)
SAOS	Small Amplitude Oscillatory Shear
SAXS	Small Angle X-Ray Scattering
SEC	Size Exclusion Chromatography
SEP	Poly(syrene-ethylene-butene)
SEPS	Solid Echo Pulse Sequence
SSR	Strong Segregation Region
sSSR	Super Strong Segregation Region
TMA	Time Marching Algorithm
TMS	Trimethylsilyl
tTS	Time Temperature Superposition
UPy	Ureidopyrimidinone
VFT	Vogel-Fulcher-Tammann
WAXS	Wide Angle X-Ray Scattering

Symbols

b_{jk}	Dipole-Dipole Coupling Constant Between Nuclei I and J
b_K	Kuhn Length
$\hat{C}$	Monomer Concentration
C_∞	Number of Backbone Bonds in the Statistical Segment
D_{eff}	Effective Spin-Diffusion Coefficient
e_{jk}	Unit Vector Joining Spins I_j And I_k
F	Force
f	Frequency
$\mathfrak{G}$	Gibbs Free Energy
$G(t)$	Relaxation Modulus
G^*	Complex Modulus
$G^{'}$	Elastic Modulus
$G^{''}$	Viscose Modulus
G_N^0	Plateau Modulus
$\mathfrak{h}$	Plancks Constants
$\hat{H}^{DD}$	Secular Dipole-Dipole Interactions for All Spins
$\hat{H}_{jk}^{DD,full}$	Full Form Of Dipole-Dipole Interactions Between Spins I_j And I_k
$\hat{H}_{jk}^{DD}$	Secular Dipole-Dipole Interactions Between Spins I_j And I_k
$\mathbf{I}$	Spin Angular Moments of Nucleus
k_B	Boltzmann Constant
L	Length
$\mathcal{L}$	Laplace Transformation
$LM(t)$	Recovering Longitudinal Magnetization
$M(t)$	Molar Mass Between the Topological Constraints
M_e	Entanglement Molecular Weight
M_u	Elementary Chain Unit Molecular Weight
M_x	Cross-Linked Strand Molecular Weight
n	Number of Backbone Bonds in the Elementary Chain Unit
N_{CG}	Number of Always- In-Equilibrium Segments
N_{cpx}	Number of Chains Contributing to Each Complex
N_K	Number of Kuhn Segments

P	Polarization
$P(x)$	Probability Distribution of x
$P_{seq}(X)$	Probability of Sequence with X AA Monomers
R	Gas Constant
r	End-To-End Vector
r_{jk}	Distance Between Two Spins
r_{PAA}	PAA Domain Size
S	Number of Orthogonal Directions
$\mathfrak{S}$	Entropy
T	Absolute Temperature
T_1	Spin-Spin Relaxation Time
T_2	Spin-Lattice Relaxation Time
T_2^{PI}	High Temperatures Plateau in Transvers Proton Relaxation
T_2^{RL}	Relaxation Time of Polymer Swollen in Deuterated Solvent
T_{anl}	Annealing Temperature
t_{anl}	Annealing Time
T_g	Glass Transition Temperature
$TM(t)$	Decaying Transverse Magnetization
V	Volume, Unit Volume
X	Mean Displacement of Spin Magnetization
Z	Number of Statistical Segments Between Chemical and Physical Network Junctions
α_d	Dilution Exponent
γ_i	Gyromagnetic Ratio of Nucleus J
δ	Phase Angle, Surface Tension
ε^*	Complex Permittivity
ε_0	Low Frequency Limiting Permittivity
ε_∞	High Frequency Limiting Permittivity
μ^*	Complex Viscosity
Θ_{jk}	Orientation Angle Between Vector Joining Spins I_j And I_k and the Magnetic Field
λ	Wavelength, Inter-Distance Between Collective Assemblies
ξ	Cooperative Rearranging Region Size
ρ	Density
σ	Stress
τ_{cpx}	Association Time
τ_d	Reptation Time
τ_e	Rouse Time of Entangled Strand
τ_R^{Max}	Longest Rouse Time
Φ	Volume Fraction
$\varphi(t)$	Auto Correlation Function of Polarization
$\Phi(t)$	Survival Probability of Chain
ω	Angular Frequency
$\Omega(x)$	Number of Configurations
μ	Dipole Moment
μ_0	Magnetic Constants
2θ	Diffraction Angle

Chapter 1

Introduction, Objectives, Strategy

1.1 Overview

In recent years, stimuli-responsive polymers have gained a large interest, showing dramatic changes in their properties and state under the application of a stimulus that can be easily controlled. Stimulus can be of different nature, such as temperature, pH, shear, irradiation, or magnetic field.[1−10] Possible applications based on this kind of ″smart″ materials are diverse and cover several fields such as food industry, construction, coating and biomedicine.[11,12] Among the stimuli-responsive polymers, supramolecular polymers, which typically consist of chains held together by weak reversible non-covalent interactions, represent a very promising class of systems since these reversible, non-covalent interactions allow the preparation of high molecular weight materials that combine the properties of typical covalent polymers or of a polymeric network with those of low molecular weight molecules.[13−15] Due to their reversible bonds, they can change dramatically their shape or phase under the influence of external parameters and are easy to process, re-use and recycle.[16−18] They also show interesting self-healing properties.[11,19−21]

The properties of such self-assembled polymers depend on several factors such as the functionality of the building blocks,[18,22] the concentration, or the localization, density and the lifetime of associating bonds.[16−18,23−25] Their dynamics can therefore be widely tailored by playing with these parameters. In particular, the nature of the supramolecular interactions will largely influence the properties of the self-assembled structures. While many works have studied the influence of the presence of hydrogen bonds,[18,22,26] supramolecular bonds based on metal-ligand coordination is becoming more exploited today.[1,14,27] Metal-ligand coordination is particularly attractive since the coordinative bond is relatively strong (bond energy ca. $40-120\ kJ/mol$),[27,28] highly directional,[29] and the structure, dynamics, and thermodynamic stability of the complexes can be easily varied by choosing among a broad series of ligands and metal ions comprising nearly half the periodic table.[1,30−35] Such associative bonds

can therefore be of various strengths, from strong bonds that lead virtually to irreversible or static binding of the metal, to weak and labile interactions that allow for reversible and dynamic binding.[36,37] Beside the intrinsic stability of metallo-supramolecular aggregates, external parameters also play an important role in the strength of the binding, such as the nature of the solvent[1] and of the counter-ions.[37] Indeed, the presence of coordinative species can change dramatically their dynamics by altering the dissociation/exchange mechanism between metal complexes.

While the influence of the functionality of the building blocks,[18,22] the solution concentration, or the localization, density and lifetime of the associating bonds[16−18,23−25] on the properties of the transient networks have been largely addressed in literature, only few works have investigated the role played by the own dynamics of the building blocks in the flow properties of such systems. Indeed, most of the supramolecular networks are based on short, non-entangled telechelic building blocks in solution.[13,15,19,22] Several dynamic investigations have been performed in unentagled melt of supramolecular polymers built from oligomers or small molecules. In such systems, viscoelastic properties are almost entirely dominated by the supramolecular bonds.[30,38] Many of such supramolecular polymers have shown a single relaxation time which corresponds to the life time of the supramolecular transient association.[39]
On the other hand, dynamics of supramolecular polymers with entangled polymer precursors have rarely been exploited. A big challenge is to successfully incorporate reversible supramolecular dynamics with disentanglement dynamics of macromolecules, so that the chains relax at the rhythm of association-dissociation of the supramolecular bonds.[40] If relaxation time of the supramolecular bonds is much larger than that of polymer chains, the supramolecular polymer will exhibit properties like a conventional elastomer.[41,42] *Vice versa*, if polymer chains relax much slower than the dissociation of the supramolecular pairs a minor retardation of terminal relaxation is only expected.[43,44] Therefore in order to achieve supramolecular systems in which both entanglement and transient associations contribute to viscoelasticity, the two time scales have to be in the same order of magnitude. In such a case, one should be able to describe their rheological properties by looking at the supramolecular assemblies as if they were entangled covalent networks able to split into several entangled building blocks at the rhythm of the lifetime of the supramolecular bonds, while an unassociated building block is able to move only after the time needed to disentangle from its neighboring chains. This is the main approach of this PhD work, which differs from describing the properties of supramolecular gels made of short building blocks, which are usually investigated based on the rubber elasticity theory.

As a result of hierarchy of different relaxation modes, with different activation energies and time scales, contributing to the relaxation of entangled supramolecular networks, these systems are expected to show pronounced thermo-rheological complexity. Hence state of the art combination of several techniques is required to fully characterize segmental and bulk dynamics of the supramolecular polymers, since time-temperature superposition [tTS] severely fails in these systems. Appropriate combination of different technics, such as

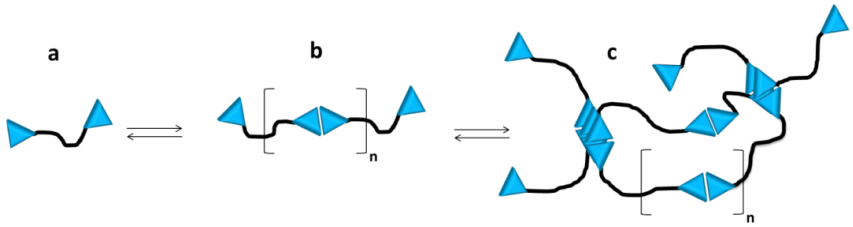

Figure 1.1: Schematic representation of self-assembly in (a) telechelic building block: (b) binary associations lead to chain extension (c) collective and binary associations form supramolecular polymer network.

rheology, broadband dielectric spectroscopy [BDS] and nuclear magnetic resonance [NMR] relaxometry is needed to acquire systematic understanding of dynamics of entangled supramolecular polymers at different time scales. To reach this goal, it is essential to have independent measures of supramolecular dynamics at different time/length scales.[45–54] Dealing with supramolecular associations, one has to consider the stimuli responsive nature of these interactions, meaning that small changes in compositions or conditions can largely change the equilibrium constant between associated and free moieties by several orders of magnitude.[6,27,55,56] For instance, kinetic studies on terpyridine-Fe(II) bis-complexes demonstrated that the equilibrium constant varies up to 5 orders of magnitude by changing polarity of the medium. Also grafting to different organic or oligo(poly)meric groups was shown to largely alter the equilibrium constant.[55] The sensitivity of supramolecular association phenomenon to different chemical or physical stimuli urges the need to investigate their dynamics in the system of interest and at the conditions of implementation, in order to correctly bridge polymer and supramolecular dynamics.

In studying dynamics of supramolecular moieties attached to a polymer backbone, one has to consider different modes of assembly (For a comprehensive review see reference.[57]) In the first level of assembly, complementary moieties associate in often binary (sometimes higher orders) ensembles thanks to directional transient interactions, such as hydrogen bond or metal-ligand coordination. This is the most studied mode of assembly of supramolecular moieties and we refer to it as ″binary″ associations. Depending on the architecture of the supramolecular polymer as well as the chemistry and concentration of the associating motifs, they can spontaneously aggregate into dense rigid domains. The driving forces for ″collective″ association are either reduction of surface tension arising from large amphiphilicity (polarity difference between the polymer backbone and supramolecular moieties[58–60]) or reduction of Gibbs free energy via formation of secondary bonds between supramolecular moieties *e.g.* $\pi - \pi$ interactions between aromatic rings in their architecture.[12,57,61,62] Due to high stability of collective assemblies, the supramolecular systems usually exhibit higher solid-liquid transitions temperature and lower degree of stimuli responsiveness.[63] Figure 1.1 schematically illustrates binary and collective assemblies of moieties in supramolecular polymers.

These two modes of assembly together with other features such as crystallinity lead to complex morphologies in the entangled supramolecular systems. Hence, heterogeneity in molecular dynamics, originated from complex microstructures, is anticipated for these materials. To correctly understand the role of supramolecular interactions on the dynamics of entangled macromolecules is it critical to thoroughly investigate the microstructure of the entangled supramolecular polymers. Morphology studies are critical in drawing the molecular microstructure. In some systems a direct visualization of the morphology is possible for instance by microscopy techniques, whereas in many others, only clues about the possible morphologies can be acquired through indirect technics such as scattering. Therefore a systematic correlation between dynamic and morphological observations is needed to achieve a microstructure picture which appropriately describes the state of assembly and the relaxation mechanism of the polymer segments in the supramolecular network.

1.2 Objectives

The goal of this work is to gain comprehensive understanding over self-organization and molecular dynamics of model entangled supramolecular networks. We would like to understand the effect of supramolecular assemblies on the relaxation mechanism of entangled associating polymers, from the glass transition to the macroscopic flow. In addition, we would like to study alteration of the self-assembling dynamics of supramolecular moieties in the environment of the polymer melt. The outcome will enable us to control mechanical and viscoelastic properties of self-assembling systems by simultaneously taking advantage of both entanglement and transient supramolecular interactions.

Having thermo-rheologically complex systems, we employ several experimental techniques to acquire dynamic information over a wide range of time and length scale. In doing so, it is critical to have deep understanding of the relationship between macroscopic properties and microscopic phenomena which are probed by each experimental technique. Since different techniques probe various aspects of molecular relaxations, we seek for a consistent microstructure which can conclusively explain the various dynamic observations made by different experimental techniques.

In achieving the required comprehensive microstructure, morphology of model supramolecular networks should be investigated. Nevertheless, often sub-micron size of morphological features obtained by collective assembly of supramolecular groups in polymer melt, lack of phase contrast or other experimental limitations do not allow direct visualization of the heterogonous morphology. Hence indirect methods of studying morphology, such as X-ray scattering or calorimetry will be employed.

Having dynamic and morphological observations over wide range of time and length scales and taking into account the chemistry of the supramolecular networks, we would be able to conceive molecular microstructure of the entangled suprameolcular networks, which is in line with all experimental findings. Bridging dynamics and morphology of entangled suprameolcular networks via the microstructure enables us to build thermodynamic-mechanical

models to quantitatively simulate and ultimately predict dynamics of entangled supramolecular systems.

1.3 Strategy

To meet the objectives of the work a careful design of model supramolecular network is required in which hierarchical assembly of supramolecular moieties is understood. In this section we review the strategies in design and characterization of supramolecular networks, and present the model entangled supramolecular networks of this work.

1.3.1 Architecture of Supramolecular Polymers

In literature several strategies have been successfully applied in the rational design of supramolecular polymer networks and gels,[36,37] which can be classified in three distinct categories depending on the architecture of the supramolecular network. The first category involves the combination of supramolecular complexes that can accommodate more than two moieties, each one being connected to the one end of a linear chain. In this way, the complexes act as branching points or as cross-linkers within the polymer network. A typical example of this approach is found in the work of Rowan and coworkers who combined lanthanoid and transition metal ions in conjunction with a ditopic oligomer to produce supramolecular gels that can exhibit thermo-, chemo- and mechano-responses, as well as light-emitting properties,[3,4,64] and to produce thermoresponsive films.[6] The second category involves the combination of functionalized star or branched chains to achieve average functionality > 2 per building block. Unlike the former scenario, here the polymer building blocks give rise to 3D network. A typical example of such system has been reported by van Ruymbeke *et al.* who used multi arm star polymers where each arm was functionalized by a zwitter ionic group, capable of forming binary assembly.[40]

The 3^{rd} strategy is either to graft the supramolecular moieties as short pendant side groups to the chain backbone or to place them along the contour of the chain. Note that very long side groups will lead to systems similar to those described in the 2^{nd} senario. An example of such a network has been reported by Craig and co-workers.[33−35] The coordination motifs were based on poly(4-vinylpyridine) and bifunctional palladium(II) or platinum(II) pincer complexes, which give access to metallo-supramolecular networks that can swell in organic solvents. The dynamic mechanical properties of these materials were tuned by the choice of the metal ion and the structure of the pincer used for coordination. Figure 1.2 schematically represent the 3 strategies to obtain supramolecular networks.

It is imperative to note that networks obtained by the 2^{nd} and the 3^{rd} strategies are identical with regard to molecular dynamics, unless the systems are entangled. In unentangled melts the chains can almost entirely relax by Rouse mechanisms. However, in entangled environments stress relaxation mechanisms of the two type of networks are quite different, since beside Rouse motions other relaxations are required to fully relax the stress. The entangled star

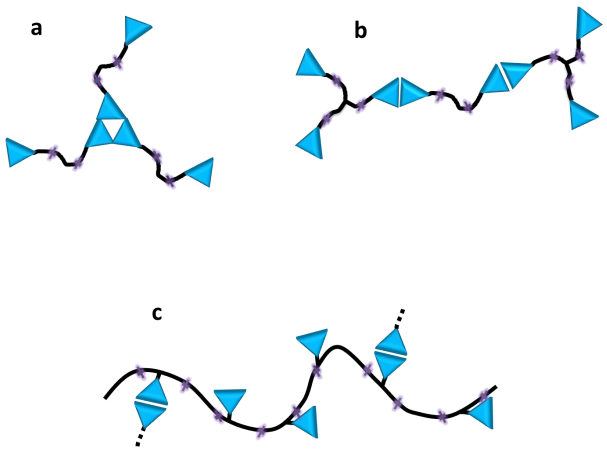

Figure 1.2: Schematic representation of the three distinct strategies to obtain supramolecular networks by hierarchical assembly (a) Employing supramolecular complexes which accommodate more than two moieties (b) using non-linear chains to reach overall functionality above 2 (c) placing the supramolecular moieties along the chain backbone or as short side groups. Crosses represent entanglements. Note that in unentangled systems, with respect to chain dynamics, b and c are indistinguishable.

supramolecules in the 2^{nd} strategy (Figure 1.2.b) can only relax by arm retractions (fluctuations) once the supramolecular motifs at the end of the arms are in unassociated state. On the other hand the entangled backbone relaxation in the last scenario (Figure 1.2.c) is most likely close to the relaxation mechanism of comb polymers or trees with several generations of branches.

The 3^{rd} strategy has a unique advantage compared to the other ones, which is to produce supramolecular networks with tunable segmental Rouse relaxations. Hence all the dynamic features of these networks, from the glass transition to the macroscopic flow are influenced by the presence of supramolecular assemblies. This ultimate adaptiveness increases the complexity of dynamics in these systems.

In this PhD work, examples of all three strategies to obtain supramolecular network are investigated. However with respect to molecular dynamics, networks built from associative polymers with supramolecular groups distributed along the backbone can be considered as the general case for all supramolecular networks. Hence we limit the discussion of this document to the investigation of these systems.

According to the last scenario, two different libraries of entangled supramolecular networks have been designed, in which entanglements and supramolecular dynamics are properly incorporated.

Poly Ether-Metal Salt Systems: Interactions between Poly (ethylene oxide) [PEO] and metallic salts have been intensively investigated due to their important industrial applications as poly electrolytes. The electron-rich ether

oxygen atoms in PEO can form complexes with many alkali, alkaline earth and transition metal ions.[65] These complexes are reversible, hence they exhibit a finite life-time of association. Upon dissociation, a given ion can associate back to the same location or randomly move to adjacent groups along the PEO chain.[39,66] The time scale of this association provides a source of friction for the chain, which hinders its dynamics. The resulting mobility reduction (akin to an increased friction coefficient) of the chain segments is the cause of many anomalous observed phenomena in PEO, such as two distinct glass transition temperatures, retarded terminal relaxation, increased viscosity, formation of a second rubber-like plateau and alteration of the crystallinity of PEO. The life-time of the PEO-metal ion complexes varies by many orders of magnitude, depending on oxidation state, ionic radius and charge of the metal ions as well as cation-anion association and solubility of the metal salt in PEO.[39,66–68]

In this work, PEO-Ni salt interactions are addressed in two different systems. In the first place excess of nickel salt is added to linear entangled telechelic PEO. Thanks to coordination interactions between terpyridine ligands and a fraction of Ni^{2+} ions linear chains can self-assemble into longer linear entities. The remaining ions interact with the PEO backbone and consequently form elastic networks. Hence metal-ligand coordination and PEO-salt complexation are both present in these supramolecular networks.

To better understand the effect of each of these interactions on PEO dynamics, we then study pure PEO-salt systems, where additional information is achieved by systematically varying salt concentration in different linear PEO matrices.

Entangled Linear Monodisperse Hydrogen Bonding Systems: Two series of associative polymers with sticky side groups were synthesized using entangled narrowly dispersed poly(n-butyl acrylate) [PnBA] backbones. PnBA was selected due to its low glass transition temperature [T_g], lack of crystallinity, and easiness of modification.

In the first library, a model well-entangled monodisperse linear PnBA polymer, $M_w = 210\ kg/mol$, $PDI = 1,3$, obtained by anionic polymerization is selectively hydrolyzed to convert a fraction of butyl acrylate side groups [BA] to acrylic acid [AA] side groups, in order to isolate the effect of hydrogen bonding on linear viscoelasticity of entangled polymer melts. The carboxylic acid groups of different chains attract each other by weak hydrogen bonding and form a transient network.[44,11,11]

In the second library of model PnBAs, ureidopyrimidinone [UPy] motifs are grafted to the backbone as pendent side groups. Substitution level is varied from $2-4\%$ of sticker per chain monomers. Here the PnBA backbone is made by atom transfer radical polymerization. The molecular weight and PDI of the backbone PnBA are 140 kg/mol and $1,35$ respectively.

These two libraries enable us to study the effect of supramolecular association strength on the network properties. While AA dimers are relatively weak hydrogen bonding associations, quadrupole hydrogen bonding UPy motifs form much stable complexes with relatively long association time.[38,44,57]

In a similar study Lewis *et. al.* investigated dynamic of supramolecular networks based on unentangled PnBA-AA and PnBA-UPy samples. The molecu-

lar weight of PnBA precursor was only 39 kg/mol and polydispersity was over $2,25$. These unentangled supramolecular networks showed thermo-rheological complexities at low frequencies. Increasing sticker content systematically increased the terminal relaxation time. More over a clear change of slope of $G'(\omega)$ at low frequencies was observed.[44] A discussion on the microstructure of these systems is certainly missing in the work of Lewis *et. al.*

1.3.2 Dynamics Characterization

Various experimental techniques are used to study chain dynamics of polymers, including rheology, dynamic mechanical analysis [DMA], BDS, multinuclear NMR relaxation, quasi-elastic dynamic light scattering, quasi-elastic neutron scattering, transient uorescence depolarization and optical relaxation techniques. Each of these techniques comprises its own, particular molecular probe of the polymer dynamics. Hence molecular theories of relaxation are required to successfully connect the macroscopic observables, *e.g.* dynamic moduli, complex dielectric permittivity, magnetization decay, scattering functions, to the molecular dynamics of the polymer chains. In this part we shortly review basic theoretical correlation between molecular motion and macroscopic properties in the main experimental techniques used in this work to probe polymer chain dynamics *i.e.* rheology, BDS and NMR relaxometry.

Chain Dynamics Probed in the Electric Field: Molecular motions result in dielectric relaxation if molecules possess permanent dipoles. The dielectric properties of a polymer chain depend on the polarization [$\mathbf{P}$] which is the dipole density in a unit volume [V]

$$\mathbf{P} = \frac{1}{V} \sum_{\text{chain}} \sum_{\text{repeating unit}} \boldsymbol{\mu}_i \tag{1.1}$$

where $\boldsymbol{\mu}_i$ is the dipole moment of the repeating unit i. The mean square dipole moment has two separate contributions, self-correlation of the dipole moment of a repeating unit and the cross correlations of dipoles between different repeating units. For long chain macromolecules, the cross correlations of dipoles implies that $\mathbf{P}$ depends on different possibilities for the orientation of a molecular dipole vector with respect to the polymer backbone. Macromolecules with molecular dipoles fixed parallel to the backbone are called Type-A polymers. For the polarization of the whole chain [$\mathbf{P}_A$] one gets

$$\mathbf{P}_A = \mu_p \boldsymbol{r} \tag{1.2}$$

where μ_p is the component of the dipole moment of the repeating unit parallel to the chain contour and $\mathbf{r}$ is the end-to-end vector of the chain. Hence polarization in type-A macromolecules can be attributed to stress relaxation via chain reorientations through $\mathbf{r}$. Although there is no polymer which is exclusively of Type-A there are several examples of macromolecules like poly(cis-1,4-iso-prene) having components of the dipole moment parallel and perpendicular to the chain.

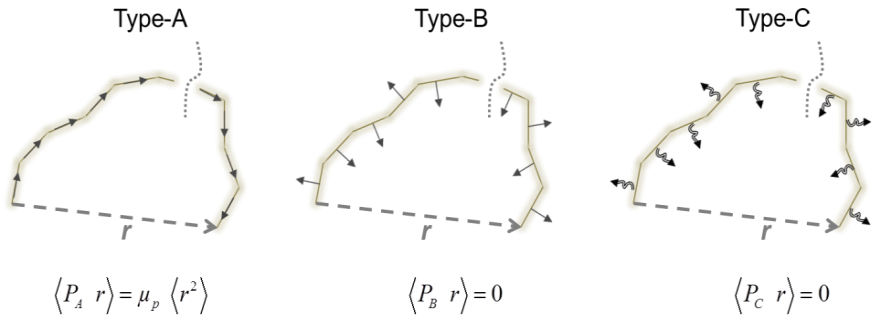

Figure 1.3: Representation of chains with dipoles located parallel or perpendicular to the chain axis or in flexible side groups.

For Type-B polymers the dipole moment is rigidly attached perpendicular to the chain backbone. Therefore no correlation between the polarization and the chain contour exists.

$$\langle \mathbf{P}_B \cdot \mathbf{r} \rangle = 0 \tag{1.3}$$

where $\mathbf{P}_B$ is the polarization of a type-B polymer. Since no long range correlation between dipoles of different repeating units exists in Type-B macromolecules, the fluctuation of the dipole moment are solely due to conformational transitions which are related to segmental mobility. Most macromolecules are of Type-B.

In many cases dipole is located in a more or less flexible side groups. The random fluctuation of dipole orientation do not result is a net polarization along the chain axis, therefore no long range cross correlation between repeating unit exist in this macromolecules. These polymers are known as Type-C. Figure 1.3 summarizes different macromolecules according to the orientation of permanent dipoles with respect to the chain contour.

In the time scale longer than that for the electronic/atomic polarization, the normalized dielectric relaxation function $\phi(t)$ is given by the autocorrelation of microscopic polarization $\mathbf{P}$ as

$$\phi(t) = \frac{\langle \Delta \boldsymbol{P}(0)\ \ \Delta \boldsymbol{P}(t) \rangle}{\langle \Delta \boldsymbol{P}(0)^2 \rangle} \tag{1.4}$$

where $\Delta\mathbf{P} = \mathbf{P} - \langle \mathbf{P} \rangle$ is the fluctuation of polarization $\mathbf{P}$ around its equilibrium value $\langle \mathbf{P} \rangle$. The macroscopic complex dielectric permittivity $\varepsilon^*(\omega)$ can be calculated by Laplace transformation $[\mathcal{L}]$ of $\dot{\phi}(t)$ the first derivative in time :

$$\frac{\varepsilon^*(\omega) - \varepsilon_\infty}{\varepsilon_0 - \varepsilon_\infty} = \mathcal{L}(\dot{\phi}(t)) \tag{1.5}$$

ε_0 and ε_∞ are respectively, limiting permittivity at low and high frequency. By combining Equations (1.1), (1.4) and (1.5), the molecular quantities $\boldsymbol{\mu}_i$ is liked to macroscopic property $\varepsilon^*(\omega)$ through auto correlation function of polarization $\phi(t)$.[71,72]

Chain Dynamics Probed in the Magnetic Field: In the nuclear spin environment, the Hamiltonian of a given nucleus i contains several contributions. The dominant term is the Zeeman interactions with external polarizing filed which describes precession of the nuclei at a Larmor frequency. On the other hand the nuclei experiences magnetic and electric fields originating from the sample itself. Deviations in nuclear Larmor frequency are observed due to local electronic environment imposed by chemical bonds. The Larmor frequency also depends on the presence of other magnetic nuclear spins in close proximities, and the direction of their magnetic moment. A pair of spins can possess direct dipole-dipole interaction or indirect electron mediated ones known as J-coupling. Chemical shifts and dipole-dipole couplings are used in identification of unknown chemical structures. Rotational motion of the molecules also leads to interaction of nuclear spins with the magnetic field. Among different contribution to spin Hamiltonian arising from internal interactions in the sample, J-coupling and spin-rotation interactions are to a good approximation only intramolecular.

In an isotropic liquid, the rotational motion of the molecules average all intramolecular as well as short-range intermolecular spin interactions to their isotropic values, however it does not average out long-range intermolecular interactions. On the contrary, in systems where atomic motion is highly restricted, there is little averaging of internal spin interactions, except by the restricted motions of some molecular groups. Hence both inter- and intermolecular spin interactions survive, and the internal spin Hamiltonian terms depend on the orientation of the sample with respect to the magnetic fields. The full form of the direct dipole-dipole interactions between spin pairs I_j and I_k is represented in the spin Hamiltonian by

$$\hat{H}_{jk}^{DD,full} = b_{jk}(3(\hat{\mathbf{I}}_j.\mathbf{e}_{jk})(\hat{\mathbf{I}}_k.\mathbf{e}_{jk}) - \hat{\mathbf{I}}_j.\hat{\mathbf{I}}_k) \tag{1.6}$$

where $\hat{\mathbf{I}}_j$ and $\hat{\mathbf{I}}_k$ are the spin angular moments of nuclei I_j and I_k and $\mathbf{e}_{jk}$ is the unit vector of the line joining the two nuclei. The magnitude of through space interaction is given by the dipole-dipole coupling constant b_{jk} which has the form of

$$b_{jk} = \frac{\mu_0}{4\pi}\frac{\gamma_j\gamma_k\hbar}{r_{jk}^3} \tag{1.7}$$

γ_j and γ_k are gyromagnetic ratio of the nuclei, μ_0 and $\hbar$ are the magnetic and Plancks constants and r_{jk} is the distance between the two spins. Note that the magnitude of dipole-dipole coupling scales with the inverse of cube of the interdistance between nuclei.

Equation (1.6) shows that unlike Zeeman and chemical shift contributions, dipole-dipole interactions are independent of intensity of the external magnetic field. Hence in a ^{1}H nuclear spin environment dipole-dipole interactions can be investigated without significant interference of other contributions of Hamiltonian by using very small external magnetic field.

$\hat{H}_{jk}^{DD}$ of the same isotropic species (homonuclear case) depends on Θ_{jk} which is the orientation angle between the vector joining spins e_{jk} and the

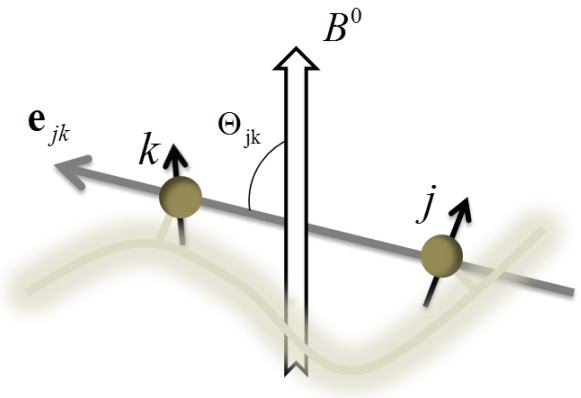

Figure 1.4: The angle Θ_{jk} used in calculation of the dipole-dipole interactions between protons j and k which are attached to the polymer backbone. Solid black arrows represent the spin angular momentum, and the open arrow shows direction of the magnetic field.

direction of the magnetic fields

$$\hat{H}_{jk}^{DD}(\Theta_{jk}) = \frac{b_{jk}}{2}(3\cos^2\Theta_{jk} - 1)(3\hat{I}_{jz}\hat{I}_{kz} - \hat{\mathbf{I}}_j.\hat{\mathbf{I}}_z) \tag{1.8}$$

Figure 1.4 schematically represent Θ_{jk} and e_{jk} for two protons of the polymer backbone.

The dipole-dipole coupling Hamiltonian of the whole sample $\hat{H}^{DD}$ is the summation of interactions over all pairs of nuclei:

$$\hat{H}^{DD} = \sum_{j<k} \hat{H}_{jk}^{DD} \tag{1.9}$$

In isotropic liquids all interactions will be averaged out by translational motion of the molecules hence $\hat{H}_{jk}^{DD} \cong 0$.[73] However entangled polymers the through-space dipole-dipole interactions cannot be ignored. The dephasing of the transverse magnetization in ^{1}H spin environments is due to these residual dipole-dipole interactions that are not averaged by slow molecular motion of polymer chain. For the case of polymers mainly composed of methyl groups, within each proton pair the distance between the two spins is constant at the typical time scale of the NMR experiment and only the angle Θ_{jk} varies with time in a manner determined by the dynamics of the main-chain bonds to which the proton pair is fixed.[74] Using equation (1.8) and (1.9), decay of transverse magnetization can be expressed by reorientation of spins in time as

$$TM(t) = \langle \cos(b_{jk}\int_0^t (3\cos^2\Theta_{jk}(t^{'}) - 1)dt^{'})\rangle \tag{1.10}$$

the bracket represent averaging over all the dynamic configurations of the bond angle Θ_{jk} in the time interval from 0 to t. It is entirely through the term

$TM(t)$ that the NMR relaxometry technique is sensitive to angular anisotropic reorientation, caused by slow relaxation processes, entanglements, crosslinking, or any other process that would lead to a nonzero averaging of the dipole interaction in the time interval t.[74]

For a complex systems such as entangled polymers, the averaging would require sophisticated models considering several assumptions to reach analytical solutions. Cohen-Addad developed a scale-invariant model of the polymer chain by application of the sub-molecule concept, *i.e.* statistical segments.[75] This model was later extended by Brereton for Rouse and entangled dynamics.[74] In entangled polymers, Brereton assumed that the decay of $TM(t)$ is a bi-exponential function arising from fast relaxation of chain ends and slow relaxation of entangled interiors.

In summery, from dipole-dipole interactions between nuclei which determine macroscopic decay of $TM(t)$ in low field NMR, Rouse relaxation time of polymer strands can be extracted with the aid of appropriate models. In addition other information such as degree of cross-linking or entanglement molecular mass can be extracted using several models.[76]

Chain Dynamics Probed in the Stress Field: A polymer molecule can be assumed as a freely jointed chain, in which the orientations of a set of linked rods are uncorrelated. In this approximation the excluded volume has not taken into account, thus the rods can take every angle independent of the neighboring ones. Although non-physical situations can arise from this assumption, it is very helpful in quickly stablishing a link between the macroscopic stress, measured in rheology, and the reorientation of the chains end-to-end vector $\mathbf{r}$. In the free jointed model the step length of the chain corresponds to the shortest independently oriented segment, known as Kuhn length, b_K. This is a material property which depends on the polymer chemistry. Flexible polymers have shorter b_K compared to rigid one. Even in the most flexible polymers b_K is not as small as a monomer length, for instance Kuhn length of PEO is 4-5 backbone bonds. From polymer statistics, for the chain comprises N_K independently oriented segment, the end-to-end displacement is given by

$$\langle r^2 \rangle = N_K b_K^2 \tag{1.11}$$

The probability to have end-to-end vector $\mathbf{r}$, must have a Gaussian form expresses as

$$P(\mathbf{r}) = \Big(\frac{3}{2\pi N_K b_K^2}\Big)^{3/2} \exp\Big(\frac{-3r^2}{2N_K b_K^2}\Big) \tag{1.12}$$

Having $P(\mathbf{r})$ one can estimate the entropy. The number of configurations with fixed end-to-end vector $\mathbf{r}[\Omega(\mathbf{r})]$ is just the corresponding fraction of all configurations $\Omega(\mathbf{r}) = \Omega_{total} P(\mathbf{r})$. The entropy of chain walk with N links and end-to-end distance r is

$$\mathfrak{S}(\mathbf{r}) = k_B \ln \Omega(\mathbf{r}) = Const. - \frac{3k_B r^2}{2N_K b_K^2} \tag{1.13}$$

Since there are no sources of internal energy, there is no enthalpy contribution to the Gibbs free energy of the random walk $\mathfrak{G}(r) = -T\mathfrak{S}(r)$. Therefore

we may derive the entropic force (or 'Brownian tension') $F(r)$ on the chain end-to-end vector as

$$F(\mathbf{r}) = -T\Delta_r \mathfrak{S}(\mathbf{r}) = -\frac{3k_BT}{N_K b_K^2}\mathbf{r} \tag{1.14}$$

Equation (1.14) implies that a single polymer chain simply contract into a state of higher entropy by entropic forces.

By coarse graining we are able to calculate the stress tensor in a dense polymer bulk. To course-grain we need to define a sub-chain having N_{CG} link of b_K length, below which configurations are always in local equilibrium. The choice of always-in-equilibrium segment length determines the level of coarse-graining in different molecular dynamic models. For instance, in Rouse model the shortest statistical segment is considered to be always in equilibrium, whereas in tube models it is the segment between entanglements which is the smallest always-in-equilibrium unit. Knowing the instantaneous configuration of chains at scale above $N_{CG}b_K$, we can average over many subchains (of N_{CG} links) in a local volume large enough to define a macroscopic stress, but small enough to define uniform physical constraints on the polymer chains within it.

Now consider a small cubic volume in a polymer of side length L, which contains $\hat{C}/N_{CG}$ subchains of length N_{CG} , where $\hat{C}$ is the monomer concentration (Figure 1.5). The probability that one subchain of end-to-end vector $\mathbf{r}$ cuts a j-plane (a plane whose normal lies in the jth direction) in the L^3 volume is just r_j/L. r_j is the magnitude of the end-to-end vector $\mathbf{r}$ projection in the j-direction. Using equation (1.14), The ith component of the force transmitted by this chain across the j-plane $[F_{ij}]$ is, $-\frac{3k_BT}{N_{CG}b_K^2}$. So the contribution to the total local stress from this subchain is $-\frac{3k_BT}{N_{CG}b_K^2}\frac{r_ir_j}{L^3}$. The stress arising from all the strands cutting plane-j in the direction i is

$$\sigma_{ij} = \frac{3k_BT\hat{C}}{N_{CG}^2 b_K^2}\langle r_i r_j\rangle \tag{1.15}$$

Since instantaneous configuration of chains at scale above $N_{CG}b_K$ is known, we can define $\mathbf{r}(n,t)$ function that maps the position of the nth always-in-equilibrium segment along the couture length at time t. Then we may replace $\mathbf{r}/N_{CG}$ with $N_{CG}\partial\mathbf{r}/\partial n$. At the end, the stress tensor can be represented as

$$\sigma_{ij} = \frac{3k_BT\hat{C}}{b_K^2}\langle\frac{\partial}{\partial n}r_i\frac{\partial}{\partial n}r_j\rangle \tag{1.16}$$

Equation (1.16) shows that the macroscopic stress measured in defined rheometry fields is related to the averaged second moment tensor of the always-in-equilibrium segments orientation.

1.3.3 Morphology Characterization

Morphology of associative polymers can be largely influenced by the presence of supramolecular groups. For instance, self-assembling supramoleclar moities impact crystallization of polymer backbone in two major ways; firstly, by hinder-

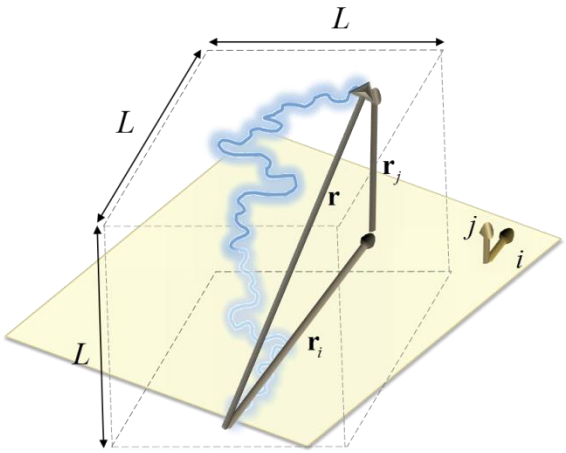

Figure 1.5: Contribution of a single segment to the stress tensor. j is the normal of the plain. r_i and r_j are corresponding projections of the end-to-end vector r of the segment on the j-plain.

ing chain dynamics they slow down the crystallization kinetics. Secondly, they change thermodynamic state of lamella due to their bulkiness and defective nature during the chain folding mechanism.[77] As a result, thinner crystals with lower melting temperature have been reported for telechelic semi-crystalline supramolecular polymers compared to pristine samples.[77]

Additionally, heterogeneous morphologies can be created due to collective assembly of supramolecular moieties for instance through lateral stacking.[57,62] This phenomena will be addressed in details in the next chapter.

The size of the collective assemblies strongly depends on the chemical structure of the supramolecular moieties, surface tension between the polymer backbone and the moieties as well as the architecture of the associating polymer. For example, up to 8 times bigger collective assemblies were observed in telechelic associating polymers compared to side chain-functionalized ones.[78]

In studying morphology of entangled supramolecular polymers, scattering and microscopy techniques can be successfully used. Time and temperature resolved small and wide angle X-ray scattering (SAXS and WAXS, respectively) can be employed to probe short and long range periodicity of structures using electron-density contrast. Wherever possible, transmission and scanning electron microscopy techniques give the advantage to directly monitor the morphological features. In materials loaded with metal salts, energy dispersive X-ray scattering can provide further insight. Thermal analysis can deliver information about temperature dependency of morphology in the systems.

1.4 Structure of This Dissertation

The present work is divided into 8 chapters. Chapter 2 provides a brief introduction to the existing literature on entangled supramolecular polymers. The emphasis is on the works which help clarifying the multi- disciplinary approach of this research and highlight various open questions and concerns in entangled supramolecular polymer melts. Chapters 3,4 and 5 cover the results and discussions of PEO-salt systems, while detailed investigation of the dynamics and microstructure of PnBA based supramolecular networks is presented in Chapters 6 and 7. Main conclusions and comparison of the results in the two systems are addressed in the final chapter.

Chapter 3 addresses the viscoelastic investigations on terpyridine functionalized PEO. The rheology of these samples is extremely sensitive to the salt content. These telechelic supramolecules form weak gels at the excess of Ni salt. The mutual effect of salt interactions with both terpyridine end groups and PEO on rheology is discussed in this chapter.

In Chapter 4, the effect of PEO-metal salt complexation on the dynamics of PEO-nickel chloride systems is investigated by rheology. Annealed PEO-nickel salt systems exhibit network properties above the melting temperature of PEO, characterized by a second elastic plateau, beyond the reptation time of PEO chains. In PEO-$NiCl_2$ networks, it is shown that the linear viscoelastic region is experimentally out of reach meaning that their viscoelastic properties strongly depend on strain and strain rate as well as any deformation history. Despite this limitation, this chapter addresses the fundamental rheology aspects of supramolecular polymer networks. In addition, X-ray scattering is employed to study formation of distinct crystalline structures of PEO-$NiCl_2$ complexes, which are different from those of both neat PEO and nickel salt.

Apart from brittle nature of the PEO-$NiCl_2$ supramolecular networks, PEO crystallinity and thermo-rheological complexity also prevent us from acquiring information about segmental dynamics of PEO chains in the annealed system at low temperature. Therefore in Chapter 5, NMR relaxometry is employed to quantitatively study the relaxation of PEO strands adjacent to and far from PEO-metal complexes. In addition, we calculate the length scale below which the system is heterogeneous due to the PEO-metal interactions. Density, approximate size and vicinity of local homogenous domains are quantified from the transverse NMR relaxation decays. To end with, we present a conclusive microstructure picture for PEO-$NiCl_2$ systems which is consistent with the local and bulk dynamic observations made by NMR transverse relaxometry and rheology, correspondingly, as well as X-ray scattering results.

Chapter 6 focuses on acquiring viscoelastic information on supramolecular networks, in the equilibrium state with the view of studying dynamics of supramolecular assemblies, and their effect on network dynamics. BDS is used to look at the collective assemblies inside the hydrogen bonding networks. Combining BDS and rheology, and taking into account several works on entangled supramolecular networks, a universal microstructure is proposed for the system in which stickers are placed along the chain contour length.

Dynamics and morphology investigations on PnBA-*g*-UPy supramolecular networks are presented in Chapter 7. Large collective assemblies of UPy motifs in the form of crystal domains are found. The effect of UPy crystallization on viscoelastic and thermal properties are addresses. The primary aim of this chapter is to validate the universal microstructure which is proposed in Chapter 6 and provide a basis to build our universal viscoelastic model for entangled supramolecular networks.

In Chapter 8, the universal microstructure and the global viscoelastic behavior of the supramolecular networks is further explained and different systems are compared.

1.5 Summary

Highlights of molecular dynamics in supramolecular polymer networks were presented in section 1.1. The advantages of including transient dynamics of reversible supramolecular groups into disentanglement dynamics of the polymer chains were addressed. Objectives of the work were underlined in section 1.2. Basic strategies in obtaining 3D entangled supramolecular networks were discussed. The model systems used in this work were introduced. The fundamentals of the experimental techniques, and the link between macroscopic observables and microscopic variables in each technique were discussed in section 1.3.

1.6 Bibliography

1 Rossow, T.; Seiffert, S. Supramolecular Polymer Gels with Potential Model-Network Structure. *Polym. Chem.* **2014**, 5 (8), 3018.

2 Rossow, T.; Habicht, A.; Seiffert, S. Relaxation and Dynamics in Transient Polymer Model Networks. *Macromolecules* **2014**, 47 (18), 6473-6482.

3 Beck, J. B.; Rowan, S. J. Multistimuli, Multiresponsive Metallo-Supramolecular Polymers. *J. Am. Chem. Soc.* **2003**, 125 (46), 13922-13923.

4 Rowan, S. J.; Beck, J. B. Metal-Ligand Induced Supramolecular Polymerization: A Route to Responsive Materials. *Faraday Discuss.* **2005**, 128, 43-53.

5 Yerushalmi, R.; Scherz, A.; van der Boom, M. E.; Kraatz, H.-B. Stimuli Responsive Materials: New Avenues toward Smart Organic Devices. *J. Mater. Chem.* **2005**, 15 (42), 44-80.

6 Kumpfer, J. R.; Wie, J. J.; Swanson, J. P.; Beyer, F. L.; Mackay, M. E.; Rowan, S. J. Influence of Metal Ion and Polymer Core on the Melt Rheology of Metallosupramolecular Films. *Macromolecules* **2012**, 45 (1), 473-480.

7 Nath, N.; Chilkoti, A. Creating ″Smart″ Surfaces Using Stimuli Responsive Polymers. *Adv. Mater.* **2002**, 14 (17), 1243-1247.

8 Dhne, L. Multilayer Thin Films. Edited by Gero Decher and Josep B. Schlenoff. Angew. *Chemie Int. Ed.* **2003**, 42 (37), 4426-4428.

9 Stuart, M. A. C.; Huck, W. T. S.; Genzer, J.; Mller, M.; Ober, C.; Stamm, M.; Sukhorukov, G. B.; Szleifer, I.; Tsukruk, V. V; Urban, M.; et al. Emerging Applications of Stimuli-Responsive Polymer Materials. *Nat. Mater.* **2010**, 9 (2), 101-113.

10 Brassinne, J.; Fustin, C.-A.; Gohy, J.-F. Polymer Gels Constructed Through Metal-Ligand Coordination. *J. Inorg. Organomet. Polym. Mater.* **2012**, 23 (1), 24-40.

11 Liu, K.; Kang, Y.; Wang, Z.; Zhang, X. 25th Anniversary Article: Reversible and Adaptive Functional Supramolecular Materials: ″Noncovalent Interaction″ Matters. *Adv. Mater.* **2013**, 25 (39), 5530-5548.

12 Bosman, A. W.; Sijbesma, R. P.; Meijer, E. . Supramolecular Polymers at Work. *Mater. Today* **2004**, 7 (4), 34-39.

13 Nair, K. P.; Breedveld, V.; Weck, M. Multiresponsive Reversible Polymer Networks Based on Hydrogen Bonding and Metal Coordination. *Macromolecules* **2011**, 44 (9), 3346-3357.

14 Seiffert, S.; Sprakel, J. Physical Chemistry of Supramolecular Polymer Networks. *Chem. Soc. Rev.* **2012**, 41 (2), 909-930.

15 Weng, W.; Beck, J. B.; Jamieson, A. M.; Rowan, S. J. Understanding the Mechanism of Gelation and Stimuli-Responsive Nature of a Class of Metallo-Supramolecular Gels. *J. Am. Chem. Soc.* **2006**, 128 (35), 11663-11672.

16 De Greef, T. F. A.; Smulders, M. M. J.; Wolffs, M.; Schenning, A. P. H. J.; Sijbesma, R. P.; Meijer, E. W. Supramolecular Polymerization. *Chem. Rev.* **2009**, 109 (11), 5687-5754.

17 De Greef, T. F. A.; Meijer, E. W. Materials Science: Supramolecular Polymers. *Nature* **2008**, 453 (7192), 171-173.

18 Cordier, P.; Tournilhac, F.; Souli-Ziakovic, C.; Leibler, L. Self-Healing and Thermoreversible Rubber from Supramolecular Assembly. *Nature* **2008**, 451 (7181), 977-980.

19 Montarnal, D.; Tournilhac, F.; Hidalgo, M.; Leibler, L. Epoxy-Based Networks Combining Chemical and Supramolecular Hydrogen-Bonding Crosslinks. *J. Polym. Sci. Part A Polym. Chem.* **2010**, 48 (5), 1133-1141.

20 Leibler, L. Nanostructured Plastics: Joys of Self-Assembling. *Prog. Polym. Sci.* **2005**, 30 (8-9), 898-914.

21 Yuan, J.; Fang, X.; Zhang, L.; Hong, G.; Lin, Y.; Zheng, Q.; Xu, Y.; Ruan, Y.; Weng, W.; Xia, H.; et al. Multi-Responsive Self-Healing Metallo-Supramolecular Gels Based on ″click″ Ligand. *J. Mater. Chem.* **2012**, 22 (23), 11515.

22 Lange, R. F. M.; Van Gurp, M.; Meijer, E. W. Hydrogen-Bonded Supramolecular Polymer Networks. *J. Polym. Sci. Part A Polym. Chem.* **1999**, 37 (19), 3657-3670.

23 Brassinne, J.; Stevens, A. M.; Van Ruymbeke, E.; Gohy, J.-F.; Fustin, C.-A. Hydrogels with Dual Relaxation and Two-Step GelSol Transition from Heterotelechelic Polymers. *Macromolecules* **2013**, 46 (22), 9134-9143.

24 Pensec, S.; Nouvel, N.; Guilleman, A.; Creton, C.; Boue, F.; Bouteiller, L. Self-Assembly in Solution of a Reversible Comb-Shaped Supramolecular Polymer. *Macromolecules* **2010**, 43 (5), 2529-2534.

25 Porte, G.; Ligoure, C.; Appell, J.; Aznar, R. Bridging Interactions due to Telechelic Linkers Balanced by Screened Coulombic Repulsions. *J. Stat. Mech. Theory Exp.* **2006**, 2006 (05), P05005.

26 Feldman, K. E.; Kade, M. J.; Meijer, E. W.; Hawker, C. J.; Kramer, E. J. Model Transient Networks from Strongly Hydrogen-Bonded Polymers. *Macromolecules* **2009**, 42 (22), 9072-9081.

27 Stadler, F. J.; Pyckhout-Hintzen, W.; Schumers, J.-M.; Fustin, C.-A.; Gohy, J.-F.; Bailly, C. Linear Viscoelastic Rheology of Moderately Entangled Telechelic Polybutadiene Temporary Networks. *Macromolecules* **2009**, 42 (16), 6181-6192.

28 Goshe, A. J.; Crowley, J. D.; Bosnich, B. Supramolecular Recognition: Use of Cofacially Disposed Bis-Terpyridyl Square-Planar Complexes in Self-Assembly and Molecular Recognition. *Helv. Chim. Acta* **2001**, 84 (10), 2971-2985.

29 Lawrance, G. A. *Introduction to Coordination Chemistry*; John Wiley & Sons, Ltd: Chichester, UK, 2010.

30 Xu, D.; Craig, S. L. Scaling Laws in Supramolecular Polymer Networks. *Macromolecules* **2011**, 44 (13), 5465-5472.

31 Loveless, D. M.; Jeon, S. L.; Craig, S. L. Rational Control of Viscoelastic Properties in Multicomponent Associative Polymer Networks. *Macromolecules* **2005**, 38 (24), 10171-10177.

32 Serpe, M. J.; Craig, S. L. Physical Organic Chemistry of Supramolecular Polymers. *Langmuir* **2007**, 23 (4), 1626-1634.

33 Yount, W. C.; Loveless, D. M.; Craig, S. L. Strong Means Slow: Dynamic Contributions to the Bulk Mechanical Properties of Supramolecular Networks. Angew. *Chem. Int. Ed. Engl.* **2005**, 44 (18), 2746-2748.

34 Yount, W. C.; Loveless, D. M.; Craig, S. L. Small-Molecule Dynamics and Mechanisms Underlying the Macroscopic Mechanical Properties of Coordinatively Cross-Linked Polymer Networks. *J. Am. Chem. Soc.* **2005**, 127 (41), 14488-14496.

35 Yount, W. C.; Juwarker, H.; Craig, S. L. Orthogonal Control of Dissociation Dynamics Relative to Thermodynamics in a Main-Chain Reversible Polymer. *J. Am. Chem. Soc.* **2003**, 125 (50), 15302-15303.

36 *Self Organized Nanostructures of Amphiphilic Block Copolymers* II; Müller, A. H. E., Borisov, O., Eds.; Advances in Polymer Science; Springer Berlin Heidelberg: 2011; Vol. 242.

37 Schmatloch, S.; Schubert, U. S. Engineering with Metallo-Supramolecular Polymers: Linear Coordination Polymers and Networks. *Macromol. Symp.* **2003**, 199 (1), 483-498.

38 Folmer, B. J. B.; Sijbesma, R. P.; Versteegen, R. M.; Van Der Rijt, J. A. J.; Meijer, E. W. Supramolecular Polymer Materials: Chain Extension of Telechelic Polymers Using a Reactive Hydrogen-Bonding Synthon. *Adv. Mater.* **2000**, 12 (12), 874-878.

39 Chen, Q.; Tudryn, G. J.; Colby, R. H. Ionomer Dynamics and the Sticky Rouse Model. *J. Rheol.* **2013**, 57 (5), 14-41.

40 Van Ruymbeke, E.; Vlassopoulos, D.; Mierzwa, M.; Pakula, T.; Charalabidis, D.; Pitsikalis, M.; Hadjichristidis, N. Rheology and Structure of Entangled Telechelic Linear and Star Polyisoprene Melts. *Macromolecules* **2010**, 43 (9), 4401-4411.

41 Goldansaz, H.; Auhl, D.; Goderis, B.; Voleppe, Q.; Fustin, C.-A.; Gohy, J.-F.; Bailly, C.; van Ruymbeke, E. Transient Metallosupramolecular Networks Built from Entangled Melts of Poly(ethylene Oxide). *Macromolecules* **2015**, 48 (11), 3746-3755.

42 Goldansaz, H.; van Ruymbeke, E.; Gohy, J.-F.; Fustin, C.-A.; Ries, M. E.; Bailly, C. Local Molecular Dynamics and Heterogeneity in PEO-$NiCl_2$ Supramolecular Networks. *Macromolecules* **2015**, 48 (7), 2290-2298.

43 Shabbir, A.; Goldansaz, H.; Hassager, O.; Ruymbeke, E. Van; Alvarez, N. J. The Effect of Hydrogen Bonding on Linear and Nonlinear Rheology of Entangled Polymer Melts; 2015.

44 Lewis, C. L.; Stewart, K.; Anthamatten, M. The Influence of Hydrogen Bonding Side-Groups on Viscoelastic Behavior of Linear and Network Polymers. *Macromolecules* **2014**, 47 (2), 729-740.

45 Hackelbusch, S.; Rossow, T.; van Assenbergh, P.; Seiffert, S. Chain Dynamics in Supramolecular Polymer Networks. *Macromolecules* **2013**, 46 (15), 6273-6286.

46 Choi, U. H.; Ye, Y.; Salas De La Cruz, D.; Liu, W.; Winey, K. I.; Elabd, Y. a.; Runt, J.; Colby, R. H. Dielectric and Viscoelastic Responses of Imidazolium-Based Ionomers with Different Counterions and Side Chain Lengths. *Macromolecules* **2014**, 47 (2), 777-790.

47 Zhang, S.; Painter, P. C.; Runt, J. Coupling of Component Segmental Relaxations in a Polymer Blend Containing Intermolecular Hydrogen Bonds. *Macromolecules* **2002**, 35 (25), 9403-9413.

48 Atorngitjawat, P.; Klein, R. J.; Runt, J. Dynamics of Sulfonated Polystyrene Copolymers Using Broadband Dielectric Spectroscopy. *Macromolecules* **2006**, 39 (5), 1815-1820.

49 Masser, K. a.; Zhao, H.; Painter, P. C.; Runt, J. Local Relaxation Behavior and Dynamic Fragility in Hydrogen Bonded Polymer Blends. *Macromolecules* **2010**, 43 (21), 9004-9013.

50 Müller, M.; Seidel, U.; Stadler, R. Influence of Hydrogen Bonding on the Viscoelastic Properties of Thermoreversible Networks: Analysis of the Local Complex Dynamics. *Polymer*, 1995, 36, 3143-3150.

51 Müller, M.; Stadler, R.; Kremer, F.; Williams, G. On the Motional Coupling between Chain and Junction Dynamics in Thermoreversible Networks. *Macromolecules***1995**, 28, 6942-6949.

52 Müller, M.; Dardin, A.; Seidel, U.; Balsamo, V.; Ivn, B.; Spiess, H. W.; Stadler, R. Junction Dynamics in Telechelic Hydrogen Bonded Polyisobutylene Networks. *Macromolecules* **1996**, 29 (7), 2577-2583.

53 Wübbenhorst, M.; Turnhout, J. Van; Folmer, B. J. B.; Sijbesma, R. P.; Meijer, E. W. Complex Dynamics of Hydrogen Bonded Self-Assembling Polymers. *IEEE Trans. Dielectr. Electr. Insul.* **2001**, 8 (3).

54 Müller, M.; Fischer, E. W.; Kremer, F.; Seidel, U.; Stadler, R. The Molecular Dynamics of Thermoreversible Networks as Studied by Broadband Dielectric Spectroscopy. *Colloid Polym. Sci.* **1995**, 273 (1), 38-46.

55 Henderson, I. *Tuning the Properties of Metal-Ligand Complexes to Modify the Properties of Supramolecular Materials*, University of Massachusetts - Amherst, 2012.

56 Brassinne, J.; Gohy, J. F.; Fustin, C. A. Controlling the Cross-Linking Density of Supramolecular Hydrogels Formed by Heterotelechelic Associating Copolymers. *Macromolecules* **2014**, 47 (13), 4514-4524.

57 Brunsveld, L.; Folmer, B. J.; Meijer, E. W.; Sijbesma, R. P. Supramolecular Polymers. *Chem. Rev.* **2001**, 101 (12), 4071-4098.

58 Semenov, a N. Contribution to the Theory of Microphase Layering in Block-Copolymer Melts. *J. Theor. Exp. Phys.* **1985**, 61 (4), 733-742.

59 Nyrkova, I. A.; Khokhlov, A. R.; Doi, M. Microdomains in Block Copolymers and Multiplets in Ionomers: Parallels in Behavior. *Macromolecules* **1993**, 26 (14), 3601-3610.

60 Semenov, A. N.; Joanny, J.-F.; Khokhlov, A. R. Associating Polymers: Equilibrium and Linear Viscoelasticity. *Macromolecules* **1995**, 28 (4), 1066-1075.

61 Schubert, U. S.; Hofmeier, H.; Newkome, G. R. *Modern Terpyridine Chemistry*; 2006.

62 Burnworth, M.; Tang, L.; Kumpfer, J. R.; Duncan, A. J.; Beyer, F. L.; Fiore, G. L.; Rowan, S. J.; Weder, C. Optically Healable Supramolecular Polymers. *Nature* **2011**, 472 (7343), 334-337.

63 Sivakova, S.; Bohnsack, D. a.; Mackay, M. E.; Suwanmala, P.; Rowan, S. J. Utilization of a Combination of Weak Hydrogen-Bonding Interactions and Phase Segregation to Yield Highly Thermosensitive Supramolecular Polymers. *J. Am. Chem. Soc.***2005**, 127 (51), 18202-18211.

64 Weng, W.; Li, Z.; Jamieson, A. M.; Rowan, S. J. Control of Gel Morphology and Properties of a Class of Metallo-Supramolecular Polymers by Good / Poor Solvent Environments. *Macromolecules* **2009**, 42 (1), 236-246.

65 Armand, M. B.; Bruce, P. G.; Forsyth, M.; Scrosati, B.; Wieczorek, W. Polymer Electrolytes. In *Polymer electrolytes*; 2011.

66 Colby, R.; Zheng, X.; Rafailovich, M.; Sokolov, J.; Peiffer, D.; Schwarz, S.; Strzhemechny, Y.; Nguyen, D. Dynamics of Lightly Sulfonated Polystyrene Ionomers. *Phys. Rev. Lett.* **1998**, 81 (18), 3876-3879.

67 Chen, Q.; Liang, S.; Shiau, H. S.; Colby, R. H. Linear Viscoelastic and Dielectric Properties of Phosphonium Siloxane Ionomers. *ACS Macro Lett.* **2013**, 2 (11), 970-974.

68 Radhakrishnan, S.; Schultz, J. M. Polymer-Induced Crystallization of Inorganic Salts: PEO-$CuCl_2$. *J. Cryst. Growth***1992**, 116 (3-4), 378-386.

69 Lakrout, H.; Creton, C.; Ahn, D.; Shull, K. R. Influence of Molecular Features on the Tackiness of Acrylic Polymer Melts. *Macromolecules* **2001**, 34 (21), 7448-7458.

70 Feng, N.; Dong, J.; Han, G.; Wang, G. Polymer Nanoparticles Based on Pyrene-Functionalized Poly(acrylic Acid) for Controlled Release under Photo and Ph Stimulation. *Macromol. Rapid Commun.* **2014**, 35 (7), 721-726.

71 Kremer, F.; Schönhals, A. *Broadband Dielectric Spectroscopy*; 2003.

72 Watanabe, H.; Matsumiya, Y.; Inoue, T. Rheo-Dielectrics in Oligomeric and Polymeric Fluids: A Review of Recent Findings. *J. Phys. Condens. Matter* **2003**, 15 (11), S909-S921.

73 Levitt, M. H. *Spin Dynamics: Basics of Nuclear Magnetic Resonance*; John Wiley & Sons, 2013.

74 Brereton, M. G. NMR Transverse Relaxation Function Calculated for Constrained Polymer Chains: Application to Entanglements and Networks. *Macromolecules* **1990**, 23, 1119-1131.

75 Cohen-Addad, J. P.; Dupeyre, R. Nuclear Magnetic Resonance Investigations of Properties of the Terminal-Chain Diffusional Spectrum of Molten Poly(dimethylsiloxane). *Macromolecules* **1985**, 18 (6), 1101-1109.

76 Litvinov, V.; Prajna, P. De. *Spectroscopy of Rubber and Rubbery Materials*; 2002.

77 Schmatloch, S.; Berg, A. M. J. Van Den; Alexeev, A. S.; Hofmeier, H.; Schubert, U. S. Soluble High-Molecular-Mass Poly (Ethylene Oxide) S via. **2003**, 9943-9949.

78 Williams, C. E.; Russell, T. P.; Jerome, R.; Horrion, J. Ionic Aggregation in Model Ionomers. *Macromolecules* **1986**, 19 (11), 2877-2884.

Chapter 2

State of the Art

2.1 Introduction

Supramolecular chemistry is the chemistry beyond the covalent bonds, hence it includes every system which take advantage of non-covalent physical or chemical interactions such as dipole-dipole, ion-dipole, hydrogen bond, metal-ligand, $\pi - \pi$ stacking, *etc.* One would agree that in almost every single soft matter system there are significant contributions of non-covalent interactions. Therefore a broad range of soft matters, including macromolecular systems can be categorized as supramolecular ones.

In fact, many deeply investigated polymeric systems, partially owe their properties from the supramolecular interactions. This makes the generalization of the finding extremely difficult if not impossible. In other words, despite the fact that "supramolecular polymer" is a relatively new terminology in soft matter physics, in reviewing the already existing literature, one have to consider a huge body of polymer physics.

Speaking about molecular dynamics and microstructure of supramolecular polymers and networks, which are the main focuses of this work, familiar readers would tend to agree that the environment plays a critical role on the physical, mechanical, thermal, and viscoelastic properties of the supramolecular polymers as well as their corresponding morphology. For instance, by changing the concentration of the AB copolymers in a good solvent of B from dilute solutions to melt, a full spectrum of shape of A block aggregate (*i.e.* sphere, disk, lamellar) is observed. In addition, at different regimes of concentrations various modes of assembly (*i.e.* inter and intra chain, flower-like or bridge) are expected.

As mentioned above, reviewing all these features in various libraries of supramolecular polymers is a tedious work. Hence only to establish a coherent link to the results and discussions of the present dissertation, this chapter builds on knowledge on fundamental aspects of dynamics and morphology of entangled supramolecular polymer networks in the melt state. It is imperative to review the chemical structure and some fundamental physical aspects of the main categories of supramolecular macromolecules. This chapter attempts

to provide a brief overview on the melt dynamics of some important families of the supramolecular associating macromolecules, *i.e* block copolymers, ionomers, metallo-supramolecular and H-bonding associative networks. Note that in view of molecular dynamics, these systems show some fundamental similarities.

In the following sections, before proceeding with studies on molecular dynamics, general considerations on morphology and microstructure of each class of supramolecular network will be addressed. Wherever possible, we will emphasis on the relationship between various microstructures and typical rheological behavior in the systems of interest.

2.2 Block and Random Copolymers with Immiscible Segments

A block copolymer is a chain consists of several types of segments, each one made of different monomers. For a long time, solutions and melts of block copolymers have attracted the attention of polymer specialists, owing to the ability of these systems to transform to a micro layered state. If the segments of types A and B have a positive heat of mixing, then they tend to phase separate and self-assemble into distinct domains. Since the A and B segments are linked into a single chain, self-assembly can only occur on certain scales. Consequently a micro domain structure arises, which gives rise to many valuable properties of the system. The individual domains can have lamellar, cylindrical, or spherical structures. The structures of the two latter types rise whenever the blocks A and B strongly differ in dimensions.[1]

A random copolymer can be treated as a special block copolymer in which A monomers are statistically distributed among the B ones. Randomness implies formation of limited number of segments with several consecutive A monomers. The probability of finding a block of X consecutive A monomers, exponentially decreases with increasing X.[2]

Depending on the architecture of the copolymer, different microphase separated, ordered structures are formed. The equilibrium phases are lamellar, bi-continuous gyroid, hexagonal cylinders, and body centered cubic spheres (see Figure 2.1). Each of these phases has its own characteristic LVE response, schematically represented in Figure 2.2. Independent of the microstructure, nearly every monodisperse block copolymer melts demonstrates three rheological features, which appear to be inherent consequences of the long-range ordering in these systems.

(i) The low-frequency linear viscoelastic response does not exhibit a terminal relaxation time beyond which the material flows like a simple liquid. In other words, slopes of 1 and 2 respectively in $G''(\omega)$ and $G'(\omega)$ are not observed. Long range ordering significantly hinders terminal relaxation time and thus the viscoelasticity persists on time scales that are many orders of magnitude longer than the time required for individual block copolymers to diffuse distances of the order of molecular dimensions.

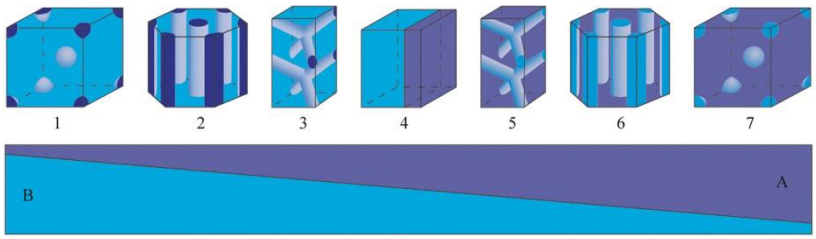

Figure 2.1: Morphologies of AB diblock copolymer structures observed during changes in their composition: (1) and (7) spherical domains; (2) and (6) cylindrical domains; (3) and (5) bi-tetrahedron structure and (4) lamellar structure.

(ii) The rheological properties are extremely sensitive to deformation history. The long-range order is perturbed by strong shear or extensional flows, with direct consequences on viscoelasticity.

(iii) The critical yield strain, below which linear response is observed, becomes smaller at lower frequencies. Often the yield strain limit for LVE regime is considerably less than 1%.[3]

The linear viscoelastic response of the ordered phases of nearly monodisperse block copolymer melts is shown schematically in Figure 2.2. In copolymers with immiscible blocks, it is trivial that the segmental Rouse motion and the packing length of each block are not affected by the presence of the other one as they phase separate into distinct domains. Hence irrespective of the microstructures, all systems, including the disordered ones, have essentially the same response at the highest frequencies shown in Figure 2.2. This includes the entangled rubbery plateau that is a characteristic feature of all polymer melts that have sufficiently long chains for entanglement effects.

The bi-continuous gyroid and spheres phases both have three-dimensional cubic structure, which makes them viscoelastic solids for both diblock and triblock copolymers. The most prominent viscoelastic feature is the formation of a second low frequency plateau. Unlike the first plateau modulus, which is determined by the entanglement density of the continuous matrix, the second plateau modulus is related to the domain spacing d for each of these cubic phases.[4]

$$G^0_{cubic} \cong \frac{40kT}{d^3} \tag{2.1}$$

Based on experimental data a simple scaling law for the hexagonal-packed cylinder phase has been proposed by Ryu *et al.*, who showed that the low frequency complex modulus approximately obeys a power law in frequency.[5]

$$G^*_{hexagonal}(\omega) \sim (i\omega)^{1/3} \tag{2.2}$$

Equation 2.4 indicates that both $G'(\omega)$ and $G''(\omega)$ are proportional to the 1/3 power of frequency. It can be shown that G'' is a factor of 1.7 smaller than G'

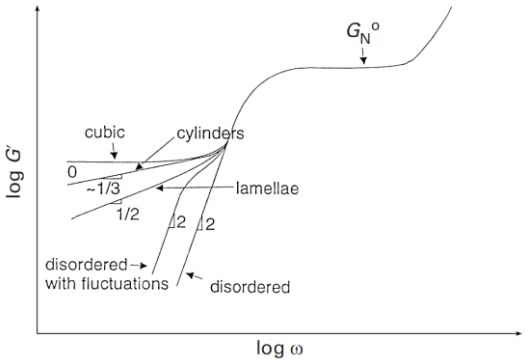

Figure 2.2: Schematic representation of the linear viscoelastic response of diblock copolymers with various equilibrium and non-equilibrium long range ordering structures. Adopted from Kossuth *et al.* J. Rheol. 1999.[4]

in this range of frequency. Contrary to the work of Ryu *et al.*, Rubinstein and Obukhov derived a theory for the hexagonal cylinder phase which predicts that the exponent is 1/4.[6] Note that the ABA triblocks, for which A is the cylinder and B is the matrix, are solids at stress levels below a critical yield stress, when the cylinders are approximately aligned. This result can be understood by considering many trapped chains which simultaneously have A segments in two different cylinders, making a network that can only relax if the A blocks are forced into the B phase. Therefore a behavior similar to that of cubic structures (equation 2.1) is anticipated.

As oppose to hexagonal structures, the lamellar phase of diblock copolymers has been extensively studied in terms of rheology. It is confirmed that the complex modulus shows a power law in low frequencies.[7]

$$G^*_{lamellar}(\omega) \sim (i\omega)^{1/2} \tag{2.3}$$

The experimental observations are well supported by the theories in the lamellar phase.[6]

Self-assembling block copolymers have been used to construct various high tech materials, such as membranes[8] and asymmetric objects,[9] due to ease of modifications of the long range ordering structures. In a very recent study, self-assembly of poly(3-(triethoxysilyl)propyl methacrylate)-block-polystyrene has been used to achieve polymer-grafted nanoobjects of various shape and size. Polymer-grafted nanoobjects are a kind of nanoparticles with persistent geometric shape and densely tethered polymer hairs.[9] These astonishing materials are used in several applications including loading catalysts, drug delivery, medical diagnosing and imaging, and improving performances of polymer materials as nanofillers. The block copolymer was synthesized by RAFT mediated radical polymerization. As mentioned above, the morphology of a block copolymer is controlled by the volume fraction of the two blocks. The volume fraction

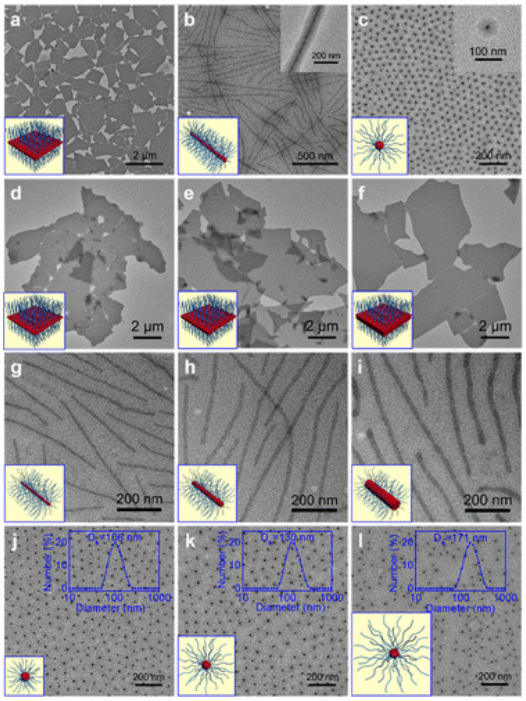

Figure 2.3: TEM images of isolated polymer-grafted nanoobjects with different structures, obtained by self-assembly of a block copolymer. Adopted from Ruan *et al.* ACS Macro Lett. 2015.[9]

of polystyrene (PS) was controlled by introducing PS oligomers to the block copolymer. Since the PS oligomers easily diffused into the PS microdomains of the block copolymers, the total volume fraction of PS component in the blend has increased, and then the morphology of the casting films were changed from the lamellae to the cylinders to the spheres. Finally, ethoxylsilanes contained in other block domain could be cross-linked and the Polymer-grafted nanoobjects with different shapes were obtained by dispersing the bulk samples in solvent. Figure 2.3 shows various nanoobjects which were fabricated by Ruan *et al.*[9]

2.3 Ionomers

Ionomers are usually defined as ion containing polymers with a maximum ionic group content of about 15 *mol*%. To better distinguish ionomers from polyelectrolytes, Eisenberg and Rinaudo described ionomers as polymers in which bulk properties are governed by ionic interactions in discrete regions of the material (ionic aggregates).[10] It is generally accepted that ionomers, owe their peculiar properties to the aggregation of the ions introduced into the organic matrix.

Two distinct types of aggregates, multiplets and clusters, are believed to be formed as a result of ionic associations.

2.3.1 Morphology

Among numerous articles on the microstructure of ionomers, Eisenberg, Hird and Moore model[11] has attracted more attention. Here we summarize this model as some of the its components will be used in this dissertation.

The current model considers a hierarchy of microstructure by considering "multiplets" and "clusters", which are linked to each other by so called "regions of restricted mobility". The formation of multiplets is a crucial element in this model. A multiplet is defined as an aggregate consisting of several ion pairs and containing only ionic material. The formation of multiplets in random ionomers, is determined by both the ionic stickers and the host polymer. Strength of the electrostatic interactions between the ion pairs, which is a direct function of the sizes of the ions and the partial covalent character of the ionic bond, is the most important ionic parameter that affects multiplet formation. A multiplet is formed when the electrostatic interactions between ion pairs overcome the enthropic-elastic forces of the chains to which they are attached. Electrostatic interactions determine the strength of ion pair associations. Hence, at a given charge, small ion pairs interact more strongly than larger ones. Also, higher ion charges increase the affinity to form stronger ion pair associations.

The transient friction of each ion pair in a multiplet effectively anchors the polymer chain at the point to which it is attached. Hence, the polymer chain experiences slower dynamics in the immediate vicinity of a multiplet. Eisenberg *et al.* proposed that around each multiplet there exists a layer in which chain dynamics is much slower than that of bulk. This layer is called region of restricted mobility (see Figure 2.4). The thickness of this layer is believed to be in the range of persistence length of polymer, which is temperature independent.[12] Hence the mobility of rigid polymers such as PS is affected in a greater distance from multiplets compared to flexible macromolecules. Mobility reduction is also controlled by the strength of anchoring ion pair associations. Strong electrostatic interactions lead to rigid multiplets, which restrict the mobility of the chains more than multiplets in which the ions pairs can move relative to one another (*i.e.* small electrostatic forces).

The added value of this model is in description of clusters, which is essential in explaining several observations such as emergence of a second glass transition above the T_g of the polymer, or anomalous plasticization behavior of ionomers. In a random ionomer, the average distance between multiplets decreases, as the ion content is increased. Eventually the regions of restricted mobility surrounding each multiplet start to overlap, while the multiplets themselves remain intact. As this overlap becomes more frequent, relatively large continuous regions of restricted mobility must form (See Figure 2.5). When such a region is large enough to have its own T_g (over 8 nm), it constitutes a cluster and exhibits behavior characteristic of a phase-separated region. In other words, clusters are continuous phases of restricted mobility regions ex-

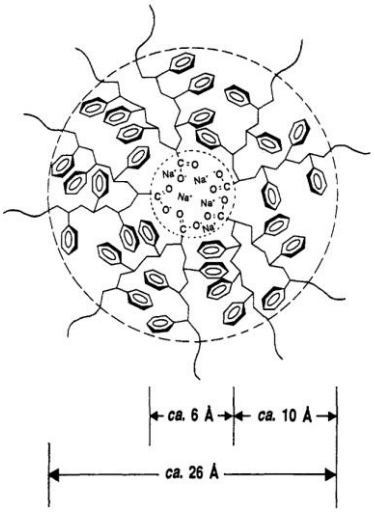

Figure 2.4: Schematic diagram of the region of restricted mobility surrounding a multiplet. Taken from Eisenberg *et al.* Macromolecules 1990.[11]

ceeding the size of cooperative rearranging region. It is important to note that, within the framework of this model, cluster formation gives rise to a new T_g, and not broadening of glass transition temperature. It is important to mention that multiplets effectively act as physical cross-links and thus raise the T_g of the matrix. However, when a sufficient number of multiplets are close enough together to form a continuous region of restricted mobility, the region constitutes a cluster and exhibits its own separate T_g.

2.3.2 Molecular dynamics

Having mentioned the basis of ionomer's microstructure, we now summarize some seminal works on dynamics of entangled ionomers. Familiar readers would agree that ionomers are by far the most studied class of supramolecular networks. Various aspects of their molecular dynamics which were deeply investigated using model ionomers can be generalized to the other classes of supramolecular networks. In the followings we briefly mention some of these highlights.

Influence of Ionic Interaction on Viscoelasticity of Ionomers: Multiplet formation in ionomers restricts the motion of the ionomer chains and thus leads to a delay of stress relaxation in ionomers relative to their neutral polymer counterparts. The terminal response of ionomer chains is governed by the average time for an ion pair to reside in the ionic cluster before its dissociation, referred to as the association life time. The dissociated ion pair can associate back to its original cluster or randomly move to a nearby cluster. The latter process leads to stress relaxation of the portion of chain back-

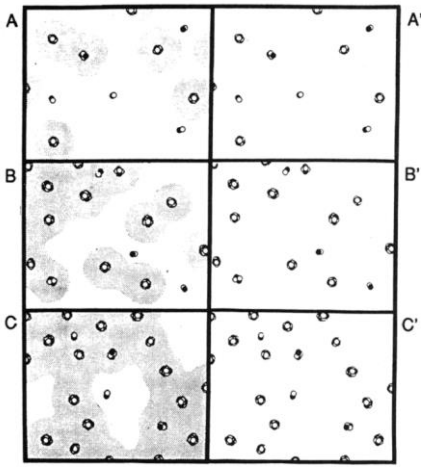

Figure 2.5: Schematic representation of the morphologies of random ionomers at (A) low; (B) intermediate and (C) high ion content. The shaded areas indicate regions of restricted mobility. A', B', and C' are schematic representations of the spatial arrangement of multiplets considering only electron density (seen by X-ray scattering) without regard to chain mobility. Taken from Eisenberg *et al.* Macromolecules 1990.[11]

bones between the ionic associations. Such a dissociation-association process is termed "ion hopping" and the accumulation of these "hops" leads to the terminal relaxation and diffusion of the ionomer chains, making ionomers viscoelastic liquids. Several works have demonstrated the effect of ionic group content and neutralization level on the viscoelastic behavior of ionomers. In a recent work Chen, Tudryn, and Colby showed that LVE of sulfonated PEO and poly(tetramethylene oxide), PTMO, based ionomers can be controlled by the ion content and molecular weight of the associating chains.[13]

Figure 2.6 compares the master curves of storage and loss modulus, $G'(\omega)$ and $G''(\omega)$, for PEO and PTMO based ionomers in refernce[13]. These master curves are reduced at a reference temperature of $Tr = 20\ ^{\circ}C$. Note that, unlike PTMO, the pristine PEO is slightly entangled. For PEO-Na ionomers in Figure 2.6.a, the entire relaxation spectrum is properly captured. This is indeed the great advantage of this work compared to similar literatures. The viscoelastic behavior of PEO-Na ionomers can be divided into three main regions. The glassy plateau in storage modulus at the highest ω followed by a glass transition region, some viscoelastic Rouse-like relaxations, and finally the terminal relaxation of all samples characterized by $G'(\omega) \sim \omega^2$ and $G''(\omega) \sim \omega$ at the lowest ω. Note that both glassy and terminal relaxation times are increasingly delayed with increase of ion content. On the other hand the level of the glassy plateau is not altered by addition of ions.

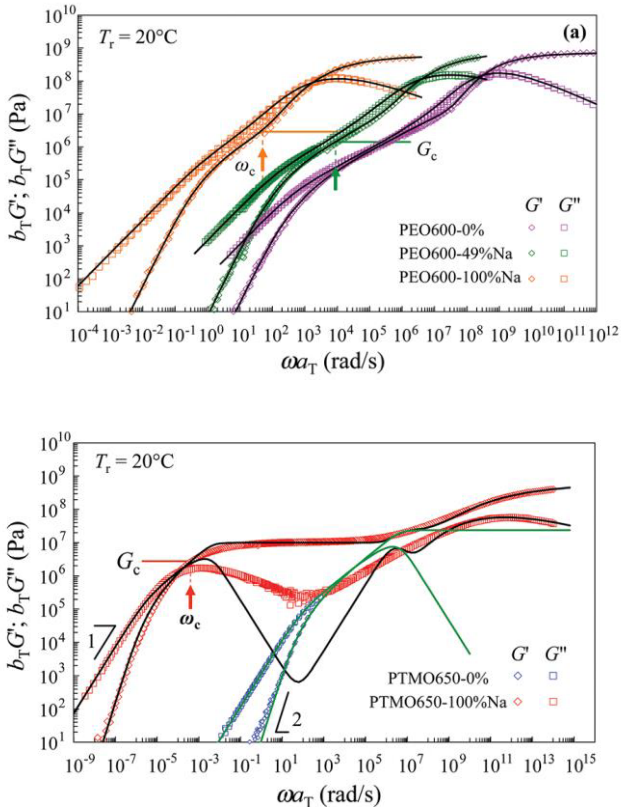

Figure 2.6: Effect of ion content on LVE response of sulfonated (a) PEO (b) PTMO ionomers. Master curves are constructed at reference temperature of 20 $°C$. Adapted from Chen *et al.* J. Rheology 2013.[13]

Some minor changes in the plateau modulus at intermediate frequencies are evident. PTMO-Na ionomers (see Figure 2.6.b) better demonstrate the effect of transient frictions on the plateau modulus of the supramolecular networks. For PTMO 650−0% sample, master curve are limited to $T > 0\ °C$ as crystallization occurs below 0 $°C$. In contrast to the PEO-Na ionomers shown in Figure 2.6.a, the PTMO $650 - 100\%$ Na sample exhibits a plateau covering a wide frequency range of nearly 9 decades, although PTMO $650 - 0\%$ chains are shorter than PEO $400 - 0\%$ ones. Chen *et al.* explained that the energy of an ion pair to move outside the ion cluster is significantly larger in PTMO based ionomers because PTMO has lower dielectric constant and PTMO does not provide the strong specific solvation of Na ions that the PEO provides. Hence the life time of the transient frictions imposed by the ionic associations on the ionomer chains is much larger in PTMO, which results in extremely large terminal relaxation. Although time temperature superposition (tTS) works well in PEO-

Na ionomers, thermo-rheological complexities at intermediate frequencies are observed in PTMO $650 - 100\%$ Na. We address the validity of tTS principle in ionomers in the next part.

Stadler *et al.* investigate the time-dependent linear viscoelastic behavior of alkaline metal- neutralized carboxy-telechelic 1,4-polybutadiene (PB) networks, and compared it with the acid precursor.[14] The terminal relaxation time after neutralization with alkali metal increases by up to 7 decades (see Figure 2.7.a). These authors clearly demonstrated that the level of the plateau modulus in ionomers is higher compared to non-neutralized precursors. Using van Grup-Palmen plot the plateau modulus of polybutadiene acid precursor and its Rb nutralized ionomer were estimated as 1.7 and 2.25 MP, respectively (See Figure 2.7.b). Note large thermo-rheological complexities at intermediate frequencies in the master curve of storage and loss moduli of Rb nutralized PB ionomer, shown in Figure 2.7.a. Unlike PTMO-Na ionomers of Chen *et al.*[13], these telechelic PB chains were moderately entangled.

Astronomic increase of terminal relaxation time almost at every measurable temperature and significant rise of elasticity implies that the zero shear viscosity of ionomers can climb by many orders of magnitude upon addition of minute ion content. The high sensitivity of low frequency viscosity on the nature of ions and counter ions has been addresses by several authors. For instance, 1 $mol\%$ sulfonated PS ionomer neutralized with Na ions has shown apparent viscosity 250000 time greater than that of sulfonated precursor at 220 $^{\circ}C$.[15] As technical difficulties prevented Lundberg and Makowski from determining viscosity in the LVE region, the true value of viscosity is expected to be even higher. To overcome these technical difficulties inherent to rheological experiments, Colby *et al.* measured tracer diffusion coefficients of both well entangled ion-containing PS chains in lightly sulfonated ionomers as a function of ion content, using dynamic secondary ion mass spectrometry (DSIMS).[16] Figure 2.8 shows the measured diffusion coefficients as a function of the number of sulfonated monomers (stickers) per chain, N/Ns. The inset shows DSIMS spectra obtained for the three sulfonated polystyrene ionomer samples allowed to diffuse for 30 min at 160 $^{\circ}C$ into the non-neutralized PS matrix of the closest molecular weight. It is clear that even sulfonating levels as small as 0.85 $mole\%$ ($N/Ns = 8.8$), reduce the diffusion coefficient relative to that of polystyrene by an average factor of 30. The reduction is greater for higher degrees of sulfonation. The error bars shown reflect the 0.5% absolute uncertainty in the degree of sulfonation. Regression suggests that diffusion coefficient scales with sticker content to the power 1.7, $(N/Ns)^{-1.7}$.

The enormous increase of relaxation time and diffusivity in ionomers, and in general supramolecular networks, has raised some serious issues whether the observed microstructure and viscoelastic properties truly reflect thermodynamics equilibrium. In a number of cases, where either the polymer precursors are heavily entangled or the ion content of ionic association is large, it was reported that annealing conditions and thermal history significantly altered the measured properties. There are a number of cases where large differences in duplicate value of properties is observed, which are beyond the measurement errors. The discrepancies are larger when specific thermal histories were

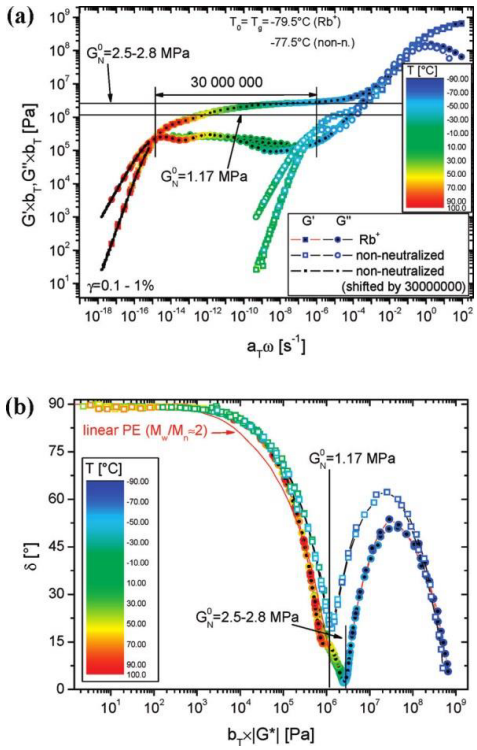

Figure 2.7: Apparent dynamic modulus master curves of the acid precursor and of the rubidium neutralized carboxyl-telechelic 1,4-polybutadiene ionomers at isofriction state ($T_r = T_g$). Black-filled symbols refer to the rubidium neutralized ionomer and the white filled samples refer to the acid precursor, the small black symbols are the data of the acid precursor shifted by a factor of 3×10^7. (a) Storage (G') and loss (G'') moduli (b) Phase angle against complex modulus ($|G^*|$). Taken from Stadler *et al.* Macromolecules 2009.[14]

applied to ionomers. In a classical study, Lundberg and Phillips studied the melt viscoelasticity of sulfonated PS ionomers precipitated from solutions below and above entanglement concentration threshold (c^*). Samples were then freeze-dried and viscosities were measured at 220 $°C$ as a function of time. The samples isolated above c^* showed viscosities similar to that of stock polymer. On the contrary, samples isolated below c^* initially showed one order of magnitude lower viscosities compared to the stock polymer. Time dependent measurements showed that the viscosity level gradually increases towards the stock polymer but even after 45 min it was still only 20% of the reference value. Given that the rate of evolution towards equilibrium decreases as more ionic associations are formed, it can take a considerable time for such samples to reach equilibrium state.

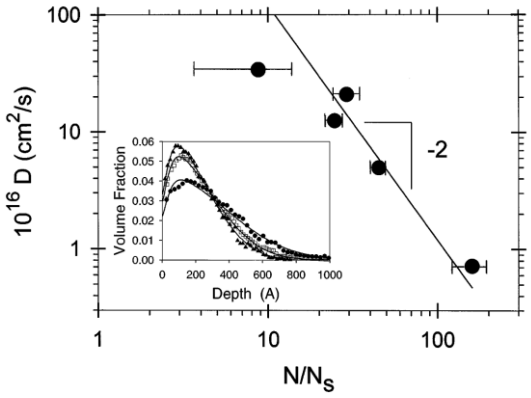

Figure 2.8: Diffusion coefficient in well entangled lightly sulfonated polystyrene at 160 $^{\circ}C$ as a function of the number of stickers per chain, N/Ns. Taken from Colby *et al.* P.R.L. 1998.[16]

Another good example of time-dependent behavior of ionomers is in the work of Litvinov *et al.* who investigated kinetics of physical gelation of unsaturated polyester based ionomers using rheology, solid state NMR relaxometry and X-ray scattering.[17] The system was composed of unsaturated polyester dissolved in 33 $wt\%$ of $\alpha - \omega$ hydroxyl terminated styrene. Unsaturated polyester contained both carboxylic and hydroxyl groups at the chain ends and had a typical number-average molar mass of about 1500 g/mol. The ionomer was thickened with 3 $wt\%$ of MgO. Viscoelastic studies in time showed that the viscosity of the system continuously increase upon addition of Mg ions. The authors tracked the thickening kinetics at 30 $^{\circ}C$ for more than 22 days ($< 1.8 \times 10^6$ s). Figure 2.9 clearly shows that after such a long time no plateau in time was reached, although the rate of evolution has continuously slowed down.[17]

Using dynamics and morphological information captured by NMR, dielectric and X-ray scattering Litvinov *et al.* described the thickening kinetics by defining three time regions. In the first region immediately after adding salt, the carboxylic acid end groups of polyesters react with MgO, which results in the formation of basic and neutral salts. The neutralized Mg-carboxylic complexes eventually form multiplets. Isolated micelles contact each other via the outer parts of their coronas, but bridging chains do not connect them. In the second region electrostatic interactions between multiplets favor their agglomeration, causing phase separated lamella-like crystalline domains to be formed. A continuous network, with bridging chains that interconnect crystalline domains, is formed during this stage. These domains act as multifunctional network junctions. The size of the multiplets could also increase in the second region, since larger multiplets are favorable in telechelics. The increase in the number of network chains and in the fraction of immobilized domains causes a large increase in the viscosity and the storage modulus. At the end of the second step, the major fraction of polyester chains is incorporated in lamella-like domains

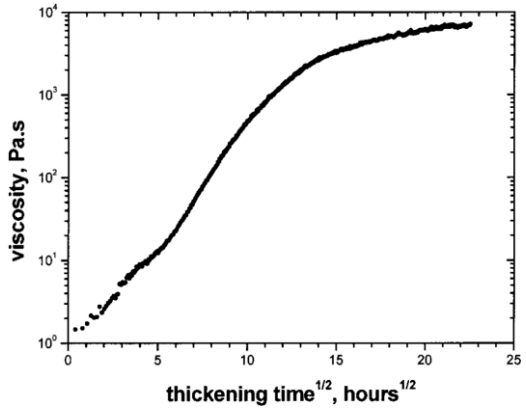

Figure 2.9: Viscosity of telechelic unsaturated Polyester-Mg ionomers as a function of the square root of the thickening time. Thickening was performed at 30 $^{\circ}C$. Taken from Litvinov *et al.* Macromolecules 2001.[17]

and the physical network. This causes the thickening rate to slow down. In the third region the aggregation of multiplets continues, which causes a continuous growth of the immobilized domains at the expense of the mobile network chains. More than half of the polyester chains are built into the immobilized domains two months after the compound was prepared and stored at 30 $^{\circ}C$. This works clearly shows that the slow chain dynamics in ionomers can prevent the systems from reaching its most stable thermodynamic state even after two months.

The desired time to reach equilibrium state can be well beyond the possible experimental time. For instance, in carboxyl-telechelic 1,4-polybutadiene ionomers, Stadler *et al.* reported continuous decrease of terminal crossover frequency, corresponding to the terminal relaxation time. To calculate required equilibration time at room temperature, these authors defined an equivalent equilibration time, *i.e.* the sum of corrected measurement times obtained by dividing the actual time of the experiment by the shift factor corresponding to the experiment temperature. They showed that the equivalent equilibration time for potassium neutralized PB ionomers exceeds 10^8 s.[14]

In summary, transient frictions imposed by ionic associations can significantly change dynamics of polymer chains. The most evident observations are increase of the terminal relaxation time and viscosity, rise of the plateau modulus and in general elasticity and extreme sensitivity to annealing conditions and thermal history. These observations are typically found in other families of supramolecular polymers.

Validity of Time-Temperature Superposition Principle: No single measurement can provide the full viscoelastic spectrum of most ionomers, due to extremely large terminal relaxations and limitations of experimental techniques in frequency and time domains. Inspired by the success of tTS in non-associating

polymers, most authors shift viscoelastic data measured at various temperatures to construct a single (pseudo)master curve, which conceivably represent dynamics of associating polymers over a larger frequency window. As a general rule, for a system to obey tTS all relaxation mechanisms which are active on the experimental time scale must have the same dependence on temperature. Otherwise the system exhibits thermo-rheological complexity. It was mentioned in the previous chapter that dynamics of supramolecular networks are dominated by both disentanglement dynamics of the polymer precursor and sticker dynamics. For tTS to work in such systems these two dynamics have to have very same temperature dependency or If one relaxation totally dominates all others in the experimental time scale. The latter is the case when the activation energies of the two processes are significantly far apart.

Thermo-rheological behavior of supramolecular systems, including ionomers, is quite diverse. In numerous examples tTS was reported to work.[13,18,19] A fraction of literature showed that tTS severely fails to reduce different measurements into a master curve.[20−23] Most surprising, supramolecular interactions were reported to impose thermo-rheological simple behavior in several multiphase or multi components systems, where large thermo-rheological complexities were aniticpated.[24−26]

In a seminal study on validity of tTS in ionomers, Eisenberg and Navratil performed an extensive series of stress relaxation measurements on styrene-sodium-methacrylate copolymers.[22] While ionomers with low ion content ($3.7-mol\%$) were thermo-rheologically simple, using transient measurements covering $4-5$ decades of time, it was shown that break down of tTS becomes noticeable at high ion content ($7.7\ mol\%$). This study reveals that the apparent applicability of tTS in some systems is perhaps due to narrow experimental range.[22]

Beside the ion content, polymer precursor can affect thermo-rheological behavior. Tierney and Register looked at applicability of tTS in a systematic study of well-defined sulfonated polys (tyrene-ethylene-butene) (SEB) ionomers of varying molecular weights and functionalization levels. Figure 2.10 illustrates reduced master curves for different SEB terpolymers and corresponding Na naturalized ionomers. Terpolymers and ionomers are labels as SEBX and NaX-Y, where X refer molecular mass of the terpolymer in kg/mol and Y is the Na $mol\%$ in ionomer. Right panels in Figure 2.10 clearly demonstrate that unfunctionalized terpolymers were all thermo-rheologically simple, although different sets of shift factors were used for each specific molecular mass. On the contrary, ionomers showed strong thermo-rheological complexity at every single molecular mass and ion content (See left panels in Figure 2.10).[20]

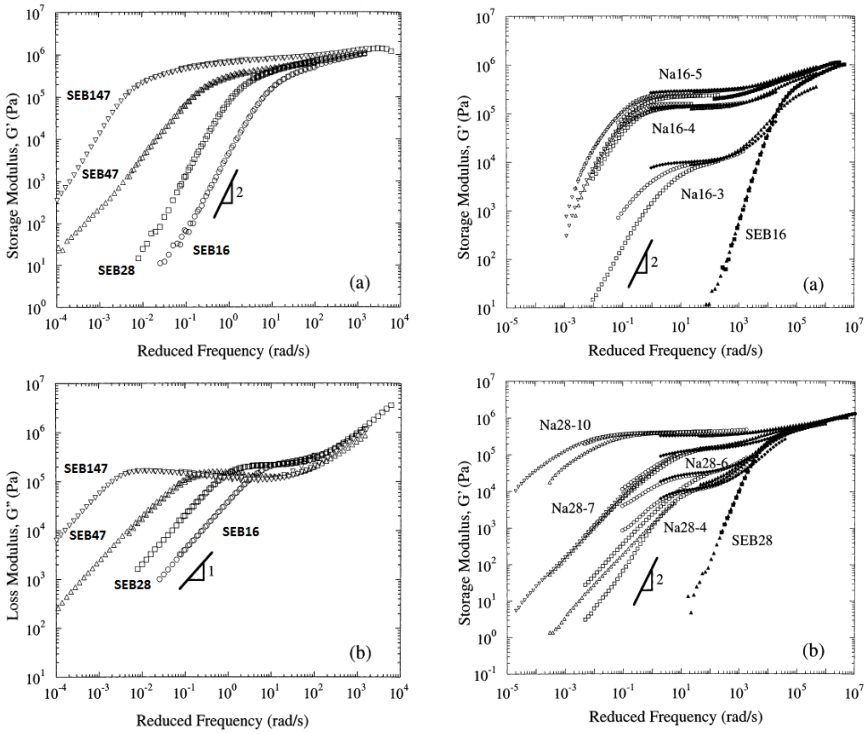

Figure 2.10: (Left Panels) Storage and loss moduli master curves for unneutralized sulfonated styrene-ethylene-butene (SEB) terpolymers at a reference temperature of 30 $^{\circ}C$: (Right panel) Storage modulus (G') pseudo-master curves of Na neutralized ionomers at reference temperature of 120 $^{\circ}C$. Adopted from Tierney and Register Macromolecules 2003.[20]

The breakdown of TTS indicates that multiple relaxation mechanisms are present in this time-temperature window and that these mechanisms do not have the same dependence upon temperature. Moreover, many of the curve segments in Na-SEB ionomers (corresponding to different temperatures) have distinctly different shapes over comparable ranges of reduced frequency, which was attributed to the presence of relaxation mechanism of chains ends (with a different activation energy). On the basis of a well-shaped discussion, Tierney and Register suggested that the failure of tTS observed here is not predominantly due to differences in activation energy between the sticker dynamics and chain terminal relaxation, but rather to the difference between the activation energies for these two processes and that for relaxation of the chains nonionic ends.[20]

From this work one may conclude that heterogeneous microstructure or composition of ionomers can produce heterogeneities in the flow activation energies of different relaxation mechanisms and eventually lead to thermo-

rheological complexity. While this argument is acceptable in many cases, exceptions have also been reported.

Hagen and Wiess assessed tTS of linear viscoelastic behavior of blends of N-methylated nylon-2,6 and $9-12$ $mol\%$ sulfonated PS ionomers.[24] The two components are miscible and exhibit strong intermolecular interactions, as they both contain supramolecular groups. Just like ionic interactions in sulfonated PS, strong hydrogen bonding in polyamides interferes with chain relaxation. Thus both components of the blend are known to exhibit some degree of thermo-rheological complexities. However tTS of the storage and loss shear moduli measured at frequencies of $0.01-500$ rad/s was applicable over the temperature range from 95 to 185 $^{\circ}C$ (See Figure 2.11). The success of tTS in this case is probably due to solvation of the ionic aggregates by complexation of the polyamide with the metal sulfonate groups.

Hagen and Wiess addressed that addition of the polyamide decreases the terminal relaxation time of the ionomer, because interactions of the sulfonate and amide groups also destroy the ionic aggregate microstructure that is responsible for the long relaxation times for the neat ionomer. It is naturally expected that the relaxation times for the polyamide is perturbed by complexation with the ionomer. As a result of strong intermolecular interactions the temperature dependences of the relaxation times for the two species in the blend are probably similar, or identical.[24]

In conclusion, it was shown that the applicability of tTS in various supramolecular systems, specifically ionomers is questionable. Controversial reports of tTS applicability can be found on some ionomers, which might be due to various experiment time/frequency rang or thermal history. To the best of authors knowledge it is yet rather difficult to predict whether an ionomer system would exhibit thermo-rheological complexity, although some crude guide lines do exist.

2.4 Multiple Hydrogen Bonding and Metallo-Supramolecular Polymer Networks

In recent years, highly directional physical interactions have been applied in a fundamentally different way to form supramolecular polymers. In this novel class of materials, functionalization of polymers with active groups that associate via noncovalent interactions results in a strong increase of the virtual molecular weight and in simultaneous changes of mechanical and rheological properties. Among the different non-covalent interactions forming supramolecular bonds, coordination and hydrogen bonding interactions are particularly interesting as they are directional and a wide range of moieties are available. In metallo-supramolecular systems, strength of interactions can be easily fine-tuned by choosing the appropriate metal ion. Furthermore the number of ligands participating in each complex can be changed by the choice of metal cation. For instance, most transition metal ions form bis-complexes with terpyridine derivatives, while lanthanide ions can form tris-complexes.[27] In hydrogen bonding supramolecular networks, the arrangement of donor (D) and

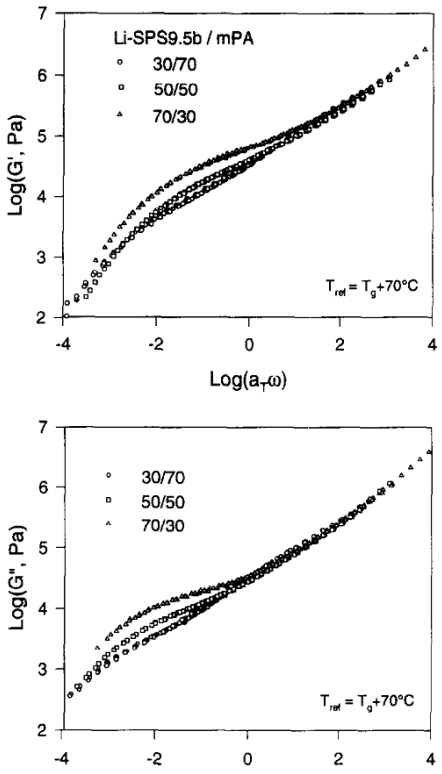

Figure 2.11: Storage and loss moduli , G' and G'', master curves for three compositions of Li sulfonated polystyrene and methylated nylon-2,6 blends. The reference temperature is $T_g + 70\ ^\circ C$.

acceptor (A) bonds determines the strength of association. For instance DDAA arrangement is stronger than DADA array, because of the secondary electrostatic interactions. Due to versatility, tuneability and ease of modification of these two specific interactions a large body of publications exist which addresses mechanical, thermal and viscoelastic properties at incredibly wide range of systems. This section addresses some morphological and dynamic investigations on supramolecular polymer networks obtained by inclusion of multiple hydrogen bonding moieties and coordinating ligands to polymer precursors. Once again we try to emphasis on the properties of entangled systems, whenever possible. However, these associations have been rarely used for the assembly of objects other than small molecules or oligomers.

2.4.1 General Morphological Considerations

Despite inherent differences in composition and structure of various supramolecular networks, several common morphological features are often observed in the majority of these systems. The most common aspect is phase separation, ar-

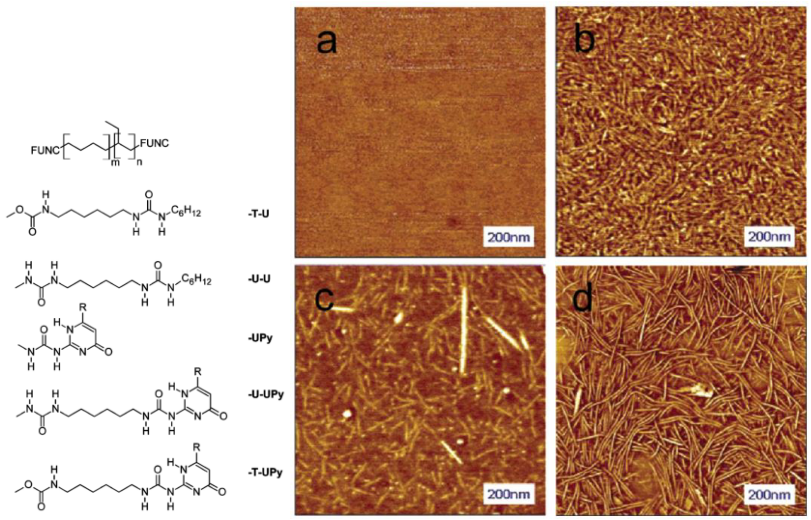

Figure 2.12: (left) Structure of hydrogen bonding telechelics (right) AFM images of thin films of (a) UPy-PEB- UPy, (b) U-U-PEB-U-U, (c) UPy-T-PEB-T-UPy, and (d) UPy-U-PEB-U-UPy. Adpoted from Kautz *et al.* Macromolecules 2006.[28]

rangement or crystalization of the supramolecular motifs into distinct phases, as the core of these motifs generally consists of a planar aromatic groups. The strong $\pi - \pi$ interactions of their cores make these supramolecular motifs prone to aggregate in either polar or apolar solvents, as well as in the melt state. Because of the polarizability and good intermolecular contact of the planar aromatic system, attractive intermolecular stacking interactions occur. In very apolar systems the $\pi - \pi$ stacking may be strengthened significantly by the solvophobic interactions.

Kautz *et al.* studied the effect of directional aggregation of ureidopyrimidinone (UPy) enforced by the lateral interactions of hydrogen bonding motifs and achieved supramolecular thermoplastic elastomers with 1-D aggregation of dimerized end groups. In this study hydroxy-telechelic poly(ethylene- butylene) (PEB, $Mn = 3500\ g/mol$) was functionalized with lateral urea (U) and urethane (T) hydrogen-bonding functionalities (U-U-PEB-U-U and U-T-PEB-T-U), with end-to-end hydrogenbonding functionalities (UPy-PEB-UPy), as well as with both lateral and end-to-end functionalities (UPy-U-PEB-U-UPy and UPy-T-PEB-T-UPy).[28] Molecular structures and corresponding morphologies are shown in Figure 2.12.

Figure 2.12 clearly illustrates that depending on the molecular structure, UPy stacks with various morphologies can form. For instance, strong differences in morphology were observed between films of UPy-PEB-UPy and UPy-U-PEB-U-UPy. In Figure 2.12.a, UPy-PEB-UPy film lacks any distinct features in height or phase mode, while in Figure 2.12.d UPy-U-PEB-U-UPy film features very distinct, micrometer long fibers with estimated widths $< 7\ nm$.

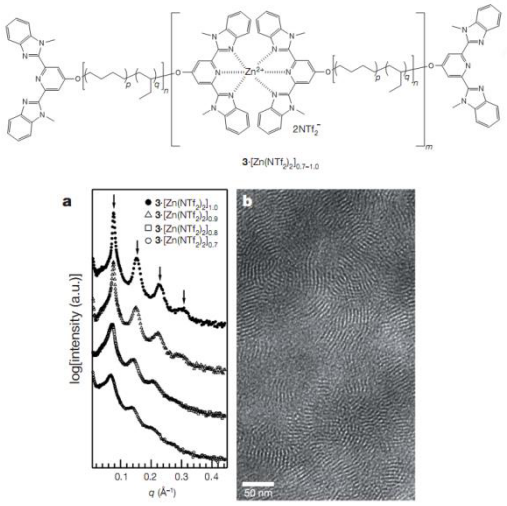

Figure 2.13: (top) Structure of MTPy-PEB-MTPy.Zn supramolecular polymers (bottom-a) SAXS data for metallo-supramolecular polymers at varying metal equivalence. (bottom-b) Representative TEM micrograph showing the lamellar morphology of the networks. Adopted from Burnworth *et al.* Nature 2011.[29]

Note that UPy aggregates in Figure 2.12.d are strictly 1-D and no crossing is observed.

Inspired by this study, Burnworth *et al.* performed an appreciated investigation on morphology of telechelich systems based on poly(ethylene-co-butylene) core terminated with 2,6-bis(19- methylbenzimidazolyl)pyridine, MTPy-PEB-MTPy. The chains were self-assembled using zinc ions.[29] The chemical structure of MTPy-PEB-MTPy.Zn polymers and a representative morphology of the supramolecular networks is shown in Figure 2.13.

SAXS and transmission electron microscopy (TEM) studies of films of MTPy-PEB-MTPy.Zn revealed micro-phase separated lamellar morphologies in which the metal-ligand complexes form a 'hard phase' that physically crosslinks the poly (ethylene-co-butylene) 'soft' domains. The SAXS data show strong Bragg diffraction maxima at integer multiples of the scattering vector, characteristic of well-ordered layered morphologies. The lamellar period was a function of the ion equivalence in this metallo-supramolecular system. Burnworth *et al.* showed that the lamellar spacing is altered by applying light as an external stimulus. TEM images of microstructure revealed a continuous array of $MTPy_2$.Zn complexes filling the entire space (see Figure 2.13).[29]

Such organizations of planar groups dramatically change the mechanical and rheological properties of supramolecular polymer networks. Hence as mentioned in Chapter 1, in studying dynamics of supramolecular systems both binary and collective assemblies of supramolecular groups have to be taken into account.

2.4.2 Entangled Melt Dynamics

Polymer chain dynamics in supramolecular polymer melts is quit complex due to reduction of chain mobility, chain entanglements, phase-segregation of macromolecular parts, and aggregation or crystallization of associating groups (collective assembly). According to Lewis *et al.* most experimental studies of supramolecular polymer melts deviate significantly from the idealized picture of reversibly binding chains. Very few studies have been conducted on model systems that isolate how specific variables influence association/dissociation dynamics of the stickers within polymer melts.[30] The aim of this section is to review some substantial works in which authors have studied both disentanglement dynamics and supramolecular dynamics in entangled associating polymer networks, and correlate the two in regard to the microstructure of the systems.

In a pioneering collection of publications, Stadler *et al.* investigated dynamics of PB modified with 4-phenyl-1,2,4-triazoline-3,5-dione (urazole) groups at 1, 2, 3 and 4 $mol\%$ grafting density. The molecular mass of the PB precursor was 29 kg/mol thus it contained over 18 entanglements.[31–34]

Figure 2.14 shows reduced pseudomater curves of dynamic moduli for PB-urazole at 2, 3 and 4 $mol\%$. It is clear that tTS fails in these supramolecular polymers. The level of thermo-rheological complexity increases with increasing urazole content along the PB chains. Figure 2.14 demonstrates 3 main effects which are usually found in hydrogen bonding and coordination supramolecular networks. i) terminal relaxation is hindered and the cross over is shifted to lower frequencies, ii) there is considerable broadening of relaxation time spectrum and iii) zero shear viscosity is increased dramatically. These observations are in common with basic observations in ionomers, as addressed in Section 5.7.

In the case of the functionalized PB-urazole samples, a small step in the log G' curves occurs within the rubbery plateau region. This relaxation appears in G'' psuedomaster curves as a peak at intermediate frequencies. The relaxation is shown with an arrow in Figure 2.14 and will be referred to as α^*_{DMA}. The maximum failure of tTS is observed around this relaxation, which suggests the presence of an individual relaxation mechanism with different activation energy (see Section 5.7).[31] Stadler *et al.* investigated the origin of this relaxation by combining rheology and BDS, as two independent measures of molecular dynamics in the supramolecular network. As the urazole units are associated with large molecular dipoles, the motion of these groups can be tracked by BDS. Hence this technique offers the opportunity to study not only the dynamics of the polybutadiene segments but also the dynamics of supramolecular associations in the PB-urazole systems. Furthermore, unlike rheology, BDS easily covers 10 decades in frequency at an individual temperature.[33]

Two relaxation processes were observed in the dielectric spectra of unmodified PB ($Mw = 29\ kg/mol$), the α relaxation corresponding to the dynamic glass transition, and the β relaxation attributed to local segmental motions. Figure 2.15 shows that after functionalization of the PB with urazole groups, an additional relaxation occurrs, which is referred to as α^* relaxation. This new α^* relaxation process showed considerably stronger dielectric strength and occurred at frequencies below the α relaxation. Note that the α^* relaxation only appears in the dielectric spectra of functionalized PBs. With increas-

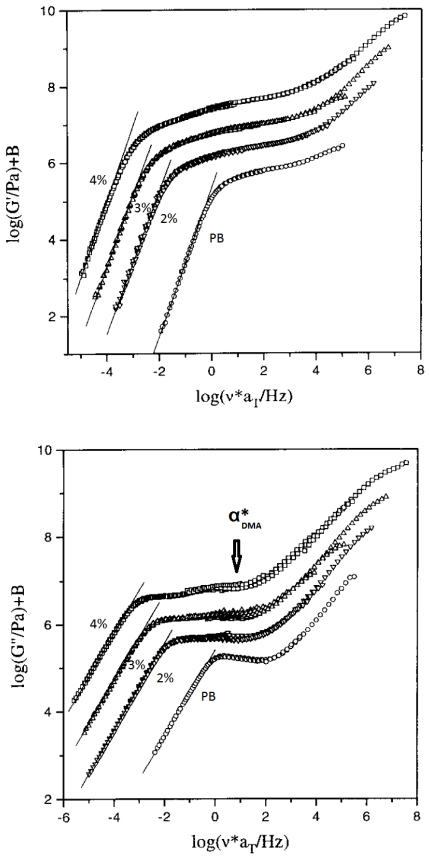

Figure 2.14: (top) Storage and (bottom) loss modulus psuedomaster curves for urazole functionalized polybutadienes at different degrees of substitution ($T_r = -40\ ^\circ C$). The master curves are vertically offset against each other by half a decade for clarity. Adopted from Müller *et al.* Polymer 1995.[31]

ing temperature the product of relaxation strength and temperature of the α^* relaxation decreases which indicates that the relaxation strength of the α^* relaxation is correlated to the number of binary association complexes. Müller *et al.* proved that the α^* relaxation is associated with the binary assemblies of urazole groups, and suggested two different molecular explanations which can account for the α^* relaxation: i) an orientation fluctuation of the binary assembly ii) the dissociation dynamics of the binary assembly. The latter process is a first-order molecular reaction and must follow an Arrhenius law. The fluctuations of associated stickers must be coupled to the motion of adjacent chain segments and thus are expected to show a VFT behavior. The overall relaxation time τ_{asc}, contains both dissociation relaxation and reorientation processes as

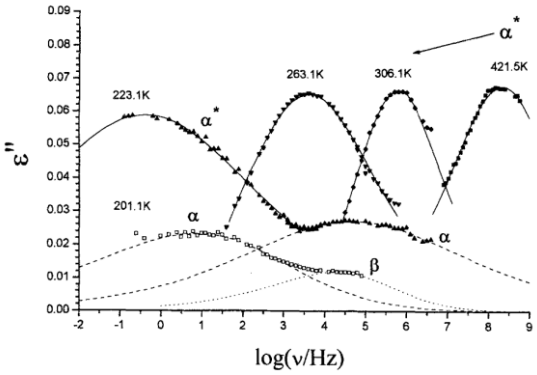

Figure 2.15: Dielectric loss curves for polybutadiene, modified by 4 *mol*% of urazole groups. The lines are fits according to the Havriliak-Negami function. Taken from Müller *et al.* Colloid Polym. Sci. 1995.[33]

$$\frac{1}{\tau_{asc}} = \frac{1}{\tau_{asc}^{Ort}} + \frac{1}{\tau_{asc}^{Ch}} \tag{2.4}$$

where τ_{asc}^{Ort} and τ_{asc}^{Ch}, are respectively characteristic relaxation time of orientation and dissociation of the associated stickers, respectively.

Based on the correlation function approach, a theoretical model was derived for the relaxation behavior of reversible binary assemblies in supramolecular networks.[34] This model had an invaluable share in building some of the discussions in PnBA– r-AA supramolecular systems which will be addressed in Chapter 6. According to Müller *et al.* the complex dielectric function contains two relaxation components, τ_{dsc} describing reorientation relaxation time of uncomplexed stickers and one with the overall relaxation time τ_{asc} of associated stickers.

$$\frac{\varepsilon^* - \varepsilon_\infty}{\varepsilon_s - \varepsilon_\infty} = \frac{N_{dsc}\,\vec{\mu}_{dsc}^{\,2}}{N_{dsc}\,\vec{\mu}_{dsc}^{\,2} + N_{asc}\,\vec{\mu}_{asc}^{\,2}} \frac{1}{1+i\omega\tau_{dsc}} + \frac{N_{asc}\,\vec{\mu}_{asc}^{\,2}}{N_{dsc}\,\vec{\mu}_{dsc}^{\,2} + N_{asc}\,\vec{\mu}_{asc}^{\,2}} \frac{1}{1+i\omega\tau_{asc}} \tag{2.5}$$

Where N and $\vec{\mu}$ refer to the number density and the dipole moment of the associated or dissociated stickers. Note that at equilibrium, number density of each group is fixed and can be determined by the chemical equilibrium constant.

So far only the mean relaxation time of the a^* relaxation was considered. Further important information can be obtained from the relaxation time distribution which determines the peak shape of the dielectric relaxation. Let us first consider the case $\tau_{asc}^{Ch} >> \tau_{asc}^{Ort}$, where the reorientation process dominates the overall relaxation. Reorientations of binary associations couple to the cooperative motion of the polymer matrix. Thus it depends on the relaxation time distribution of chain dynamics. Therefore symmetrically or asymmetrically broadened peaks are obtained. On the other hand, if $\tau_{asc}^{Ch} << \tau_{asc}^{Ort}$,

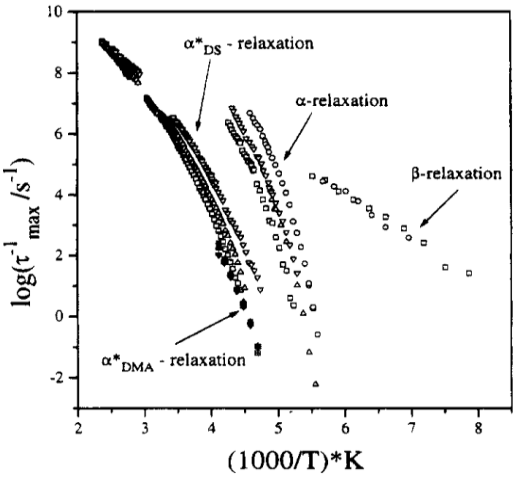

Figure 2.16: Activation plot for dielectric relaxation processes of polybutadienes substituted by different amounts of urazole. BDS data are overlaid with the α^*_{DMA} relaxation times obtained from viscoelastic measurements. In the first place, the quantitative agreement of the α^*_{DMA} and the α^*_{DS} suggests that the two processes have similar origins. Taken from Müller *et al.* Colloid Polym. Sci. 1995.[33]

i.e., if chemical relaxation dominates the overall relaxation, the truly local dissociation leads to a rather narrow relaxation time distribution of the overall relaxation.

For urazole substituted PB networks, Müller *et al.* decoupled both relaxation paths by comparison of the dielectric and dynamic mechanical data (shown in Figure 2.16) and calculated the relaxation time of the reorientation and dissociation of dimeric urazole complexes as a function of temperature. It was shown that at low degrees of urazole substitution (< 2 *mol*%) reorientation occurs much faster than dissociation, whereas at higher degrees, both relaxation times are of the same magnitude.

Sijbesma *et al.* investigated stress relaxation and thermo-mechanical properties of polymeric networks in which part of the cross-links were UPy-based. UPy groups, as non-covalent cross linkers, were introduced in polyester-polyurethane networks. Free-standing films were prepared by dissolving the functionalized triols, cross-linker, and a catalyst in $CHCl_3$, then casting the mixture into a mold, next curing at 50 $^\circ C$ for 3 h followed by an intensive drying at 100 $^\circ C$ at reduced pressure. A scheme of the network structure is shown in Figure 2.17.[35,36]

The glass transition temperatures were reported to increase from 34 to 44 $^\circ C$ when the amount of UPy content in the materials is increased from 0% (fully covalent network) to 40%. Figure 2.18 shows creep and recovery behavior of the partially cross-linked supramolecular networks at $T_g + 16\ ^\circ C$ and $T_g - 14\ ^\circ C$ at constant stress of 0.5 MPa. Above T_g, in the rubbery state, creep behavior

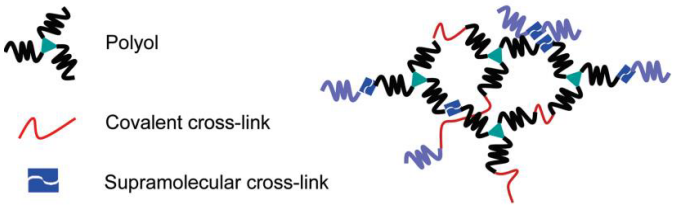

Figure 2.17: Schematic representation of partially cross-linked polyester-polyurethane supramolecular networks. Taken from Dimopoulos *et al.* Macromolecules 2010.[35]

strongly depends on UPy content. At $T_g + 16\ ^\circ C$, equilibrium elongation increases strongly with increasing fraction of UPy cross-links. The rate of creep in UPy containing samples is much slower than in the fully covalently cross-linked material. While the fully crosslinked samples deform instantaneously under constant stress, 40 $mol\%$ UPy network requires ~ 1.2 min to reach 50% of its final strain. Like in the creep part of the experiment, recovery of the UPy containing materials is much slower and is not complete after 20 min.

Also at $T_g - 14\ ^\circ C$, the presence of UPy cross-links results in higher strains, although the differences are much smaller compared to above T_g. Dimopoulos *et al.* successfully demonstrated that the supramolecular dynamics can also affect glassy network dynamics. UPy containing networks elongate to significantly higher strains because at these temperatures the noncovalent UPy cross-links are unable to sustain stress at the time scale of the experiment and the covalent part of the network has a lower cross-link density than in the fully covalent material.[35]

The evolution of the tensile storage moduli with temperature in partially crosslinked supramolecular networks at 10 and 30 $mol\%$ UPy substitution in illustrated in Figure 2.19. The pure covalent network is also shown for comparison. As the materials go from the glassy to the rubbery state, the tensile storage moduli drop by more than 2 orders of magnitude. Fully covalent network (0 $mol\%$ UPy) displays a minimum in the storage modulus, after which it shows the expected slow but constant increase due to entropic elasticity. The transient nature of supramolecular cross-links induces a second, relaxation at higher temperatures. The transition is better resolved at high UPy contents. Once again this second transition will be referred to as α^*_{DMA}. Beyond this second transition, the storage modulus shows again entropic hardening for the low UPy content networks.

Activation plot of the and α^* relaxations, as revealed by mechanical and dielectric measurements, are shown in Figure 2.20. Although the mechanical and dielectric relaxation times are systematically shifted with respect to each other by 2-3 decades, they obey the same temperature dependence according to the VFT formalism. The common temperature dependence for the dielectric and mechanical α-process is generally expected. However the coupling between the α^* and the α dynamics implies that the dynamics of the UPy network are

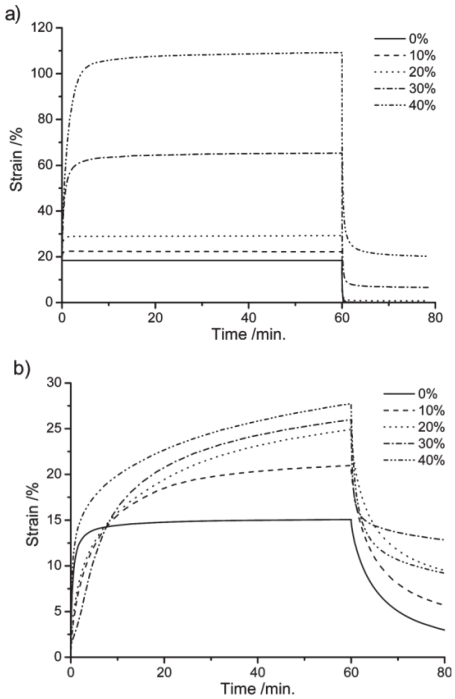

Figure 2.18: Creep measurements in partially UPy cross-linked networks at 0.5 MPa stress at (a) $T_g + 16\ ^\circ C$ and (b) $T_g - 14\ ^\circ C$. Adopted from Dimopoulos *et al.* Macromolecules 2010.[35]

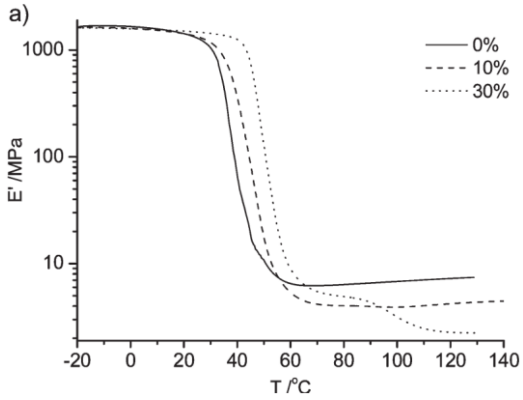

Figure 2.19: Evolution of storage modulous vs temperature in partially UPy cross-linked networks (1 Hz and 3 $^\circ C$/min heating rate). Adopted from Dimopoulos *et al.* Macromolecules 2010.[35]

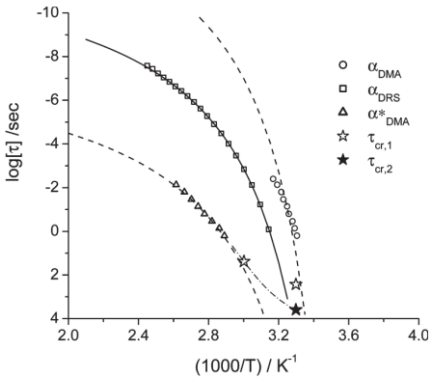

Figure 2.20: Relaxation times of the glass transition (α) and the high temperature relaxation process (α^*) obtained from mechanical and dielectric spectroscopy for 20 $mol\%$ UPy cross-linked network. The stars indicate relaxation times obtained from creep experiments at $T_g - 5\ ^\circ C$ and $T_g + 25\ ^\circ C$.

driven by the segmental mobility.[35] The coupling between sticker dynamics and segmental mobility can explain the dramatic change behavior in transient creep measurements below and above glass transition.

In these two publications, Sijbesma *et al.* successfully tracked supramolecular dynamics within the transient polymer networks and establish a clear link between the two. The extra relaxation α^*, was associated to the dissociation of the UPy groups which follow VFT behavior above glass transition of the network. They also showed that the network dynamics is affected by the hydrogen bonds both below and above its T_g.

In this section we summarized two sets of works on dynamics of entangled supramolecular networks, in which mechanical, thermal and dielectric investigations where coupled to achieve a conclusive understanding on network dynamics. The authors used BDS as an independent measure to look at cooperative dynamics of polymer chain as well as association-dissociation dynamics of the stickers. The works of Stadler *et al.*[31−34] and Sijbesma *et al.*[35,36] well represent the approach of this PhD work, *i.e* to use various techniques in order to maximize understanding of dynamics in entangled supramolecular networks, in which several relaxation mechanisms with different activation energies together with heterogeneous molecular structure and morphologies, limit the applicability of tTS.

2.5 Bibliography

1 Semenov, A N. Contribution to the Theory of Microphase Layering in Block-Copolymer Melts. *J. Theor. Exp. Phys.* **1985**, 61 (4), 733-742.

2 Nyrkova, I. A.; Khokhlov, A. R.; Doi, M. Microdomains in Block Copolymers and Multiplets in Ionomers: Parallels in Behavior. *Macromolecules* **1993**, 26 (14), 3601-3610.

3 Colby, R. H. Block Copolymer Dynamics. *Curr. Opin. Coll. Interface Sci.* **1996**, 1, 454-465.

4 Kossuth, M. B.; Morse, D. C.; Bates, F. S. Viscoelastic Behavior of Cubic Phases in Block Copolymer Melts. *J. Rheol.* **1999**, 43 (1), 167.

5 Ryu, C. Y.; Lee, M. S.; Hajduk, D. A.; Lodge, T. P. Structure and Viscoelasticity of Matched Asymmetric Diblock and Triblock Copolymers in the Cylinder and Sphere Microstructures. *J. Polym. Sci. Part B Polym. Phys.* **1997**, 35 (17), 2811-2823.

6 Rubinstein, M.; Obukhov, S. P. Power-Law-like Stress Relaxation of Block Copolymers: Disentanglement Regimes. *Macromolecules* **1993**, 26 (7), 1740-1750.

7 Rosedale, J. H.; Bates, F. S. Rheology of Ordered and Disordered Symmetric Poly(ethylenepropylene)-Poly(ethylethylene) Diblock Copolymers. *Macromolecules* **1990**, 23 (8), 2329-2338.

8 Mugemana, C.; Gohy, J.-F.; Fustin, C.-A. Functionalized Nanoporous Thin Films from Metallo-Supramolecular Diblock Copolymers. *Langmuir* **2012**, 28 (5), 3018-3023.

9 Ruan, Y.; Gao, L.; Yao, D.; Zhang, K.; Zhang, B.; Chen, Y.; Liu, C. Polymer-Grafted Nanoparticles with Precisely Controlled Structures. *ACS Macro Lett.* **2015**, 4, 1067-1071.

10 Eisenberg, A.; Kim, J.-S. Introduction to Ionomers; Wiley, 1998.

11 Eisenberg, A.; Hird, B.; Moore, R. B. A New Multiplet-Cluster Model for the Morphology of Random Ionomers. *Macromolecules* **1990**, 23 (18), 4098-4107.

12 Wignall, G. D.; Ballard, D. G. H.; Schelten, J. Measurements of Persistence Length and Temperature Dependence of the Radius of Gyration in Bulk Atactic Polystyrene. *Eur. Polym. J.* **1974**, 10 (9), 861-865.

13 Chen, Q.; Tudryn, G. J.; Colby, R. H. Ionomer Dynamics and the Sticky Rouse Model. *J. Rheol.* **2013**, 57 (5), 1441.

14 Stadler, F. J.; Pyckhout-Hintzen, W.; Schumers, J.-M.; Fustin, C.-A.; Gohy, J.-F.; Bailly, C. Linear Viscoelastic Rheology of Moderately Entangled Telechelic Polybutadiene Temporary Networks. *Macromolecules* **2009**, 42 (16), 6181-6192.

15 Lundberg, R.; Makowski, H. A Comparison of Sulfonate and Carboxylate Ionomers. *Ions Polym.* **1980**.

16 Colby, R.; Zheng, X.; Rafailovich, M.; Sokolov, J.; Peiffer, D.; Schwarz, S.; Strzhemechny, Y.; Nguyen, D. Dynamics of Lightly Sulfonated Polystyrene Ionomers. *Phys. Rev. Lett.* **1998**, 81 (18), 3876-3879.

17 Litvinov, V. M.; Braam, a W. M.; van der Ploeg, a F. M. J. Telechelic Ionomers: Molecular Structure and Kinetics of Physical Gelation of Unsaturated Polyester as Studied by Solid State NMR and X-Ray. *Macromolecules* **2001**, 34 (3), 489-502.

18 Chen, Q.; Masser, H.; Shiau, H. S.; Liang, S.; Runt, J.; Painter, P. C.; Colby, R. H. Linear Viscoelasticity and Fourier Transform Infrared Spectroscopy of Polyether-Ester-Sulfonate Copolymer Ionomers. *Macromolecules* **2014**, 47 (11), 3635-3644.

19 Chen, Q.; Liang, S.; Shiau, H. S.; Colby, R. H. Linear Viscoelastic and Dielectric Properties of Phosphonium Siloxane Ionomers. *ACS Macro Lett.* **2013**, 2 (11), 970-974.

20 Tierney, N. K.; Register, R. a. Synthesis and Melt Dynamics of Model Sulfonated Ionomers. *Macromolecules* **2003**, 36 (4), 1170-1177.

21 Eisenberg, A.; Navratil, M. Ion Clustering and Viscoelastic Relaxation in Styrene-Based Ionomers. II. Effect of Ion Concentration. *Macromolecules* **1973**, 6 (4), 604-612.

22 Eisenberg, A.; Navratil, M. Time-Temperature Superposition in Styrene-Based Ionomers. *J. Polym. Sci. Part B Polym. Lett.* **1972**, 10 (7), 537-542.

23 Greener, J.; Gillmor, J. R.; Daly, R. C. Melt Rheology of a Class of Polyester Ionomers. *Macromolecules* **1993**, 26 (24), 6416-6424.

24 Hagen, R.; Weiss, R. A. Assessment of Time-Temperature Superposition of Linear Viscoelastic Behaviour of Strongly Interacting Polymer Blends: N-Methylated Nylon-2,10 and Lightly Sulfonated Polystyrene Ionomers. *Polymer* **1995**, 36 (24), 4657-4664.

25 Masser, K. a.; Zhao, H.; Painter, P. C.; Runt, J. Local Relaxation Behavior and Dynamic Fragility in Hydrogen Bonded Polymer Blends. *Macromolecules* **2010**, 43 (21), 9004-9013.

26 Masser, K. a.; Runt, J. Dynamics of Polymer Blends of a Strongly Interassociating Homopolymer with Poly(vinyl Methyl Ether) and poly(2-Vinylpyridine). *Macromolecules* **2010**, 43 (15), 6414-6421.

27 Kumpfer, J. R.; Wie, J. J.; Swanson, J. P.; Beyer, F. L.; Mackay, M. E.; Rowan, S. J. Influence of Metal Ion and Polymer Core on the Melt Rheology of Metallosupramolecular Films. *Macromolecules*, **2012**, 45 (1), 473-480.

28 Kautz, H.; Van Beek, D. J. M.; Sijbesma, R. P.; Meijer, E. W. Cooperative End-to-End and Lateral Hydrogen-Bonding Motifs in Supramolecular Thermoplastic Elastomers. *Macromolecules* **2006**, 39 (13), 4265-4267.

29 Burnworth, M.; Tang, L.; Kumpfer, J. R.; Duncan, A. J.; Beyer, F. L.; Fiore, G. L.; Rowan, S. J.; Weder, C. Optically Healable Supramolecular Polymers. *Nature* **2011**, 472 (7343), 334-337.

30 Lewis, C. L.; Stewart, K.; Anthamatten, M. The Influence of Hydrogen Bonding Side-Groups on Viscoelastic Behavior of Linear and Network Polymers. *Macromolecules* **2014**, 47 (2), 729-740.

31 Müller, M.; Seidel, U.; Stadler, R. Influence of Hydrogen Bonding on the Viscoelastic Properties of Thermoreversible Networks: Analysis of the Local Complex Dynamics. *Polymer*, **1995**, 36, 3143-3150.

32 Müller, M.; Dardin, A.; Seidel, U.; Balsamo, V.; Iván, B.; Spiess, H. W.; Stadler, R. Junction Dynamics in Telechelic Hydrogen Bonded Polyisobutylene Networks. *Macromolecules* **1996**, 29 (7), 2577-2583.

33 Müller, M.; Fischer, E. W.; Kremer, F.; Seidel, U.; Stadler, R. The Molecular Dynamics of Thermoreversible Networks as Studied by Broadband Dielectric Spectroscopy. *Colloid Polym. Sci.* **1995**, 273 (1), 38-46.

34 Müller, M.; Stadler, R.; Kremer, F.; Williams, G. On the Motional Coupling between Chain and Junction Dynamics in Thermoreversible Networks. *Macromolecules* **1995**, 28, 6942-6949.

35 Dimopoulos, A.; Wietor, J. L.; Wübbenhorst, M.; Napolitano, S.; Van Benthem, R. a T. M.; De With, G.; Sijbesma, R. P. Enhanced Mechanical Relaxation below the Glass Transition Temperature in Partially Supramolecular Networks. *Macromolecules* **2010**, 43 (20), 8664-8669.

36 Wietor, J.-L.; Dimopoulos, A.; Govaert, L. E.; van Benthem, R. a. T. M.; de With, G.; Sijbesma, R. P. Preemptive Healing through Supramolecular Cross-Links. *Macromolecules* **2009**, 42 (17), 6640-6646.

Chapter 3

Melt Rheology of Linear Entangled Metallo-Supramolecular Polymers

Outline

We study in the melt, the linear viscoelastic properties of supramolecular assemblies obtained by adding different amounts of nickel ions into linear entangled PEO building blocks end-functionalized by a terpyridine group. We first show that the elasticity of these supramolecular assemblies is mainly governed by the entanglements dynamics of the building blocks, while the supramolecular interactions delay or suppress their relaxation. By adjusting the amount of metal ions, the relaxation time as well as the level of the low-frequency plateau of these supramolecular assemblies can be controlled. In particular, the addition of metal ions above the 1:2 metal ion/terpyridine stoichiometric ratio allow secondary supramolecular interactions to appear, which are able to link the linear supramolecular assemblies and thus, to lead to the reversible gelation of the system. By comparing the rheological behavior of different linear PEO samples, bearing or not functionalized chain-ends, we show that these extra supramolecular bonds are partially due to the association between the excess of metal ions and the oxygen atoms of the PEO chains. We also investigate the possible role played by the terpyridine groups in the formation of these secondary supramolecular interactions.

3.1 Introduction

In this work, we focus on metallo-supramolecular assemblies based on end-functionalized building blocks. Our main objective is to investigate how the

dynamics of metallo-supramolecular systems can be influenced by the building block architecture. To this end, relatively long building blocks have been selected to ensure that they are entangled with each other, and we focus on their dynamics in the melt state. In particular, we would like to investigate the dynamics of metallo-supramolecular polymeric assemblies made from linear well-defined entangled mono-functional and/or bi-functional building blocks of PEO. These systems have been selected for the simplicity of the building block architecture, which should lead to the creation of linear polymeric assemblies. The rheological behavior of the corresponding supramolecular systems should therefore be interpreted without ambiguity, allowing us to point out any unexpected process.[1] Due to its specific properties, such as its water solubility, biocompatibility, or high crystallinity, the PEO is an interesting polymer for various industrial and biomedical applications.[2,3] By combining these properties with the peculiar dynamics of the reversible bonds, one can therefore expect to further extend its range of possible properties and applications. In order to create supramolecular interactions, the extremities of the PEO building blocks have been functionalized with terpyridine, while nickel ions (Ni^{2+}) have been chosen as metal ions, allowing the creation of terpyridine-nickel bis-complexes, as it has already been demonstrated in literature.[4,5] The terpyridine-nickel bis-complexes are known to be rather stable (with a $log\ \ K_2$ value for the bis-complex of around 11.1 in aqueous solutions).[5,6]

Our first aim is to understand how to control the dynamics of such systems by varying the proportion of metal ions present in the samples, below and above the 1/2 nickel/terpyridine stoichiometric ratio. Since the building blocks are linear and the ligands are localized at their extremities, we expect the creation of linear polymeric assemblies of various lengths, depending on the amount of metal ions added to the system. The addition of metal ions, while keeping their total amount below the 1/2 stoichiometric ratio, should increase the average length of the linear assemblies and thus their corresponding viscosity.[7] On the other hand, the influence of an excess of ions on the dynamics of these systems could lead to a decrease of viscosity, compared to the 1/2 stoichiometric ratio, due to the creation of a larger ratio of mono-complexes.[5] This assumption is tested in Section 3.4.4.

Our second objective is to understand how the viscoelastic response of such systems can be tuned, by playing with the relative proportion of mono- and bi-functional entangled PEO building blocks. By incorporating mono-functional building blocks, we expect to vary the average length of the supramolecular linear assemblies, since they will act as chain stoppers (for the assemblies). It seems therefore important to understand how this ratio will influence the elasticity and flow properties of these supramolecular systems.
In order to analyze the rheological data of the different systems, we use a mesoscopic model based on the tube theory,[8,9] which allows us to determine the molar mass distribution (MMD) of a linear polymer or supramolecular assemblies from its viscoelastic behavior.[10,11]

As detailed in references,[12–14] tube models are usually used to predict the rheology of polymer melts, knowing their composition. However, since we

expect the polymeric assemblies to be linear, it can be used in the inverse way (*i.e.*, from its rheology to its MMD).[15,16]

3.2 Materials: Synthesis and Preparation

The supramolecular systems studied are based on dihydroxy-terminated linear poly(ethylene oxide) and α-methoxy ω-hydroxy- linear poly(ethylene oxide) purchased from Aldrich (see Figure 3.1). The PEOs have a weight averaged molar mass of 11 kg/mol and a dispersity of 1.1.
Both were dried by azeotropic distillation with toluene before use. They were functionalized at the chain-end(s) by a terpyridine ligand following a reported procedure.[17,18]

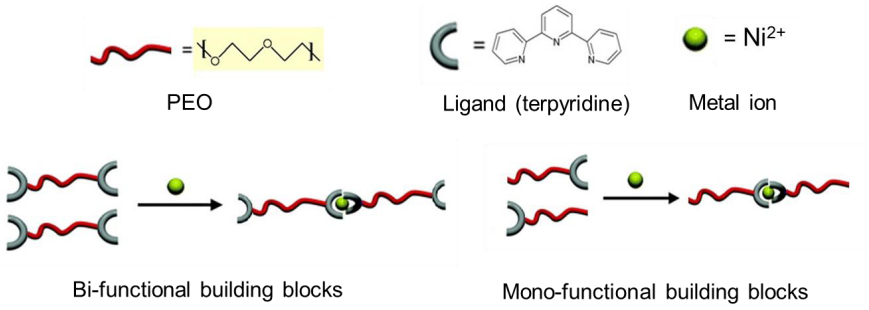

Figure 3.1: Structure of the mono- and bi-functional building blocks used in this study.

Nickel chloride has been added to the samples to promote supramolecular interactions. To this end, functionalized PEO was dissolved in methanol at a concentration of 88 g/L. The desired amount of $NiCl_2$. $6BH_2O$ was dissolved in ethanol, and this solution was added to the PEO solution. The mixture was then stirred for 12 hours at 60 $°C$ under inert atmosphere. Finally, the solvent was removed under reduced pressure, and the obtained solid was further dried at room temperature under vacuum for 15 hours.

Several samples have been prepared and analyzed in this work, containing various amounts of metal ions and based on several ratios between mono- or bi-functional PEO. Their compositions are listed in Table 3.1. It must be noted that, in this chapter the ion concentration in the system is expressed in terms of equivalent with respect to the number of terpyridine end groups. This means, for example, that a supramolecular system with equimolar amounts of bi-functional PEO and ions will contain 0.5 ion equivalents with respect to the terpyridine. Expressed into weight proportions, these amounts are very small (it represents, for example, 0.56 $wt\%$ of Ni^{2+} for Bi_ PEO_ 1eq)

Table 3.1: List of terpyridine functionalized PEO samples

Sample name	Mono-functional PEO/bi-functional PEO $wt\%/wt\%$	Ni^{2+} concentration ion equivalent
PEO_ 11 k	Non functionalized PEO	-
PEO_ 11 k_ Ni^{2+}	Non functionalized	Same proportion as in Bi-PEO_ 1eq
Mono-PEO_ 0.5eq	100/0	0.5
Bi-PEO_ 0.5eq	0/100	0.5
Mono-PEO_ 1eq	100/0	1
Bi-PEO_ 1eq	0/100	1(=0.56 $wt\%$)
(10% Mono-PEO/90% Bi-PEO)_ 1eq	10/90	1
(25% Mono-PEO/75% Bi-PEO)_ 1eq	25/75	1
(10% Mono-PEO/25% Bi-PEO)_ 1eq	75/25	1
Bi-PEO_ 0.25eq	0/100	0.25
Bi-PEO_ 0.75eq	0/100	0.75
Bi-PEO_ 0.85eq	0/100	0.85
Mono-PEO_ 2eq	100/0	2
PEO_ 101 k	Non functionalized	-
PEO_ 231 k	Non functionalized	-
PEO_ 231 k_ Ni^{2+}	Non functionalized	4.5 $wt\%$

In addition to these samples, non-functionalized linear PEO of molecular weight of 101 and 231 kg/mol have been used as reference samples to determine the material parameters used in the tube model (see Section 3.4.2).

Samples were kept in appropriate condition in order to prevent radical oxidative mechanism, which mainly takes place upon UV- irradiation.[3]

3.3 Experimental and Modeling Tools

In order to determine the dynamics and structure of these samples, rheological measurements have been performed in the linear regime (see Section 3.3.1), as well as Small Angle X-ray scattering (see Section 3.3.2). We then use a tube-based model (see Section 3.3.3) to analyze the data and determine the average number of building blocks present in the polymeric assemblies.

3.3.1 Rheology Measurements

Small Amplitude Oscillatory Shear (SAOS) measurements were conducted on a Rheometric Scientific strain controlled rheometer (ARES, TA instrument) equipped with parallel plate fixtures (8 mm − 25 mm diameter). The SAOS tests were performed at a temperature of 70 $°C$. Above the melting temperature (of around 56 $°C$), this temperature was low enough in order to minimize possible degradation of the sample.[3] Dynamic time sweep tests were first performed to ensure the sample equilibrium (see Section 3.4.1). Then, strain sweep experiments were conducted to determine the linear viscoelastic region for the frequency sweeps. For non-functionalized PEO sample, the Time-Temperature Superposition (tTS) principle was applied in order to build a master curve. The stability of the supramolecular samples within the rheometer was checked by looking at the evolution of the viscoelastic response during 30 days. It was found that once equilibrated (after few hours, see Section 3.4.1), the samples did not show further evolution with time.

3.3.2 Small Angle X-ray Scattering (SAXS)

Time- resolved synchrotron SAXS measurements were carried out at the synchrotron beam line 10 of the PETRAIII storage ring at HASYLAB (DESY, Hamburg, Germany). The operating wavelength was 0.154 nm. Data were taken every 8 s with exposure time of 2 s. The scattered intensities are recorded by a 2D detector (Pilatus 300 k) positioned at a distance of $1.03-1.28$ m above the sample. Custom-made polymeric (Kapton, Vespel®) cells, with 0.25 mm thickness, were used to hold the sample. Temperature was controlled using a convection oven, operating with nitrogen. The temperature accuracy is better than ± 0.5 $°C$.

3.3.3 Tube-based model Time Marching Algorithm (TMA)

Stress relaxation function G(t)

In order to relate the molecular weight distribution (MWD) of a sample to its linear viscoelastic properties, we use the time-marching algorithm (TMA) developed in previous works for predicting the LVE of linear, star,[10,19] H, pompom[20] and tree-like[21] polymers. We apply it here to the specific case of linear chains. Starting from the MWD of a linear polymer, this model allows us to determine the corresponding relaxation modulus, $G(t)$ at time t, taking into account both the high frequency - Rouse relaxation of the polymer and the disentanglement relaxation function $G_d(t)$, which includes a classical description of reptation, contour length fluctuations, and constraint release processes:

$$G(t) = G_d(t) + \sum_i \varphi_i \left(\frac{\rho RT}{M_i} \sum_{p=Z_i+1}^{n} \exp\left(\frac{-p^2 t_5}{\tau_R(M_i)}\right) + \frac{1}{4}\frac{\rho RT}{M_i} \sum_{p=1}^{Z_i} \exp\left(\frac{-p^2 t}{\tau_R(M_i)}\right)\right) \tag{3.1}$$

$$G_d(t) = G_N^0 \left(\sum_i \varphi_{linear,i} \int_0^1 p_{rept}(x_{lin}, t)\ p_{fluc}(x_{lin}, t)\ dx_{lin} \right)^{\alpha_d + 1} \tag{3.2}$$

where G_N^0 is the plateau modulus, $\varphi_{linear,i}$ are the weight fractions of the different linear chains, ρ is the polymer density, T is the temperature and $\tau_R(M_i)$ is the Rouse relaxation time of a chain of mass M_i and proportion φ_i. Furthermore $p_{rept}(x,t)$ and $p_{fluc}(x,t)$ are the survival probabilities of the initial tube segments localized at the normalized position x (going from 0 at the chain extremity to 1, at the middle) at time t, for the reptation and contour length fluctuations processes, respectively. The $(\alpha_d + 1)$ exponent takes into account the dynamic tube dilution process, with the dilution exponent α_d being fixed to 1.[22,23] By summing up these survival probabilities along all the chains according to their proportion at time t, the total unrelaxed fraction of the polymer at this specific time is then obtained.

As explained in details in references, [10,20] the survival probabilities $p_{rept}(x,t)$ and $p_{fluc}(x,t)$ can be described by time-decreasing exponential functions, which depend, respectively, on the reptation and fluctuations times of the different molecular segments along the chains. Finally, from the relaxation function $G(t)$, the storage and loss moduli are determined using the Schwarzl functions.[24]

Inverse problem: From LVE to MMD

By adding metal ions to the bi-functional linear building blocks, linear supramolecular chains will be created from the association of several building blocks, which should significantly influence their rheological properties. In order to determine their average number, we use here the TMA model in the inverse direction: starting from the rheological response to determine the corresponding MMD of the supramolecular assemblies.

Since this inverse problem is known to be ill-posed, this approach requires limiting as much as possible the number of unknown parameters to define the MMD of these assemblies. To this end, we start from the assumption that the probability for an end-group to become associated via metal-ligand association does not depend on the length of the chain and can be considered as constant. Since we expect several linear building blocks to associate into a long, linear assembled chain, this assumption allows us describing the statistical MMD of these polymeric assemblies by a Flory distribution[25–27]:

$$n(x) = p_a^{x-1}(1 - p_a) = \frac{N(x)}{N_{tot}} \tag{3.3}$$

where p_a is the probability of a building block to be linked to the growing polymeric assemblies, $N(x)$ and $n(x)$ are the number and the number proportion of chains with a degree of polymerization equal to x, and N_{tot} represents the total number of chains. This last number depends on the initial number of

monomers N_0, being equal to $N_0\ (1-p_a)$. Knowing that x is equal to ratio between $M(x)$, the molar mass of the chain of degree of polymerization x and M_0, the mass of one monomer, the weight fraction of chains of mass M, $w(M)$, is defined as:

$$w(M) = \frac{N(x)M(x)}{N_0 M_0} = \frac{M(x)}{M_0} p_a^{\frac{M(x)}{M_0}-1}(1-p_a)^2 = x p_a^{x-1}(1-p_a)^2 \qquad (3.4)$$

Assuming that the MMD of the linear assemblies are well represented by a Flory distribution, the number of unknown parameters to define their MMD is reduced to only one parameter, the weight average molar mass of the sample, M_w (with $M_n = M_w/2 = M_0/(1-p_a)$). The dispersity of such distributions is, by definition, fixed to 2. The inverse problem can therefore be consistently solved: M_w is determined in order to minimize the relative error, $\varepsilon(M_n)$ between the experimental relaxation moduli ($G^{'}\ exp$ and $G^{''}\ exp$) and the moduli predicted, based on this Mn, ($G^{'}\ _{theo}$ and $G^{''}\ _{theo}$):

$$\varepsilon(M_w) = \frac{1}{2N_\omega}\sum_{i=1}^{N_\omega}\left(\left|\frac{\left(G'_{exp}(\omega_i) - G'_{theo}(\omega_i, M_n)\right)}{G'_{exp}(\omega_i)}\right| + \left|\frac{\left(G''_{exp}(\omega_i) - G''_{theo}(\omega_i, M_n)\right)}{G''_{exp}(\omega_i)}\right|\right), \qquad (3.5)$$

with N_ω, the number of frequencies at which the moduli have been measured. This method is used in Section 3.4.3.

Material parameters:
The material parameters required in our tube-based model are the plateau modulus, the average molar mass between two entanglements and the Rouse time of an entanglement segment. As detailed in Section 3.4.2, these parameters have been fixed by best-fitting procedure, based on the rheological response for non-functionalized PEO chains, and consistently with literature values.[28]

3.4 Results and Discussion

3.4.1 Time Dependent Behavior and Sample Equilibration

As most of the supramolecular polymers, the assemblies studied here evolve in time. These effects need to be taken into account in the measurement protocol. This is illustrated in Figure 3.2, which shows several successive frequency sweep measurements at 70 $°C$, performed just after the loading of the sample in the rheometer. It is observed that the rheological response of this sample becomes stable and reproducible only after several hours of measurement. This time evolution of the viscoelastic properties can be attributed to the reorganization of the system and to the formation of new supramolecular bonds, which takes place as soon as the sample is heated. The natural consequence of these new links is an increase of the zero-shear viscosity of the sample through time. As shown later in Section 3.4.4, this viscosity build-up is reversible, and the supramolecular junctions can be destroyed under large shear rates.

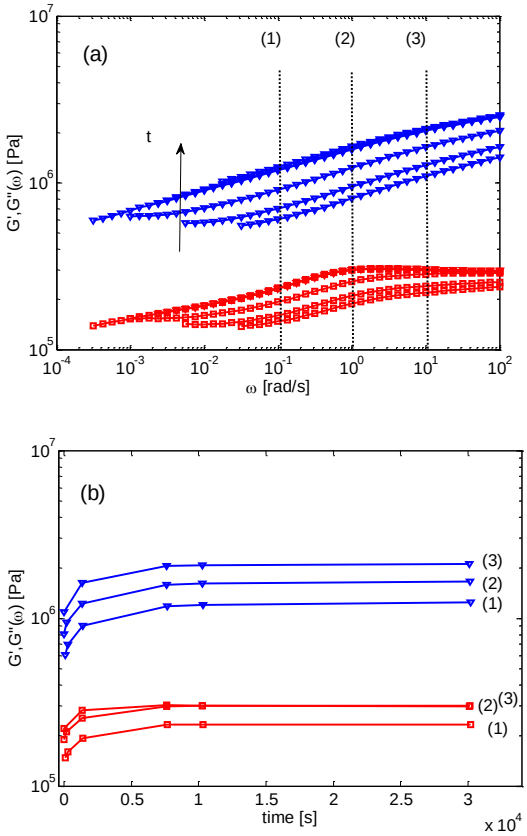

Figure 3.2: (a) Evolution of the storage (blue triangles) and loss (red squares) moduli of sample (10% Mono-PEO/90% Bi-PEO) 1eq, through time, at 70 $^{\circ}C$. (b) Storage and loss moduli versus time, corresponding to a frequency of oscillation of 0.1, 1 and 10 rad/s (related to the dashed lines (1), (2) and (3) in Figure 3.2.a).

Thus, in order to obtain reproducible data, all samples have been first equilibrated during several hours. In order to accelerate the sample equilibration, higher temperature could have been used. However, as it has been described in reference[3], this could also affect the stability of the PEO chains, leading to their partial degradation. We therefore limited the measurement temperature to 70 $^{\circ}C$. Furthermore, in order to check that the samples do keep on evolving after reaching this equilibrium state, one of these samples has been measured for a very long time: after few weeks in the rheometer, no significant further evolution was observed.

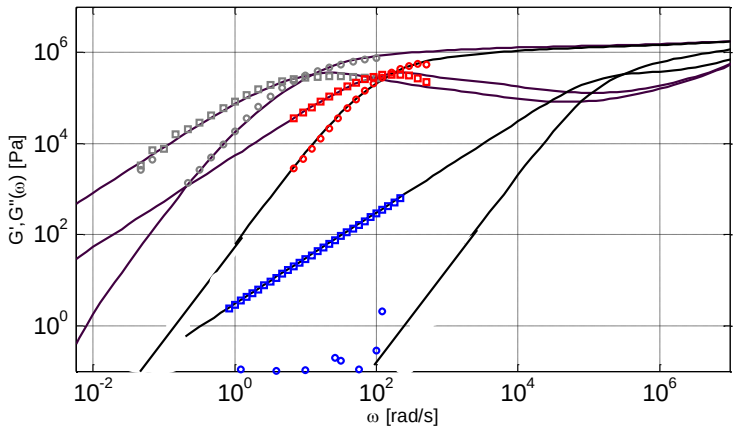

Figure 3.3: Experimental storage (circles) and loss (triangles) moduli of non-functionalized linear PEO samples, of weight averaged molar mass (and dispersity) equal to 11 kg/mol (PDI = 1.14) (blue curves), 101 kg/mol (PDI = 1.06) (red curves) and 231 kg/mol (PDI = 1.2) (grey curves). Continuous curves are predictions from the TMA model.

3.4.2 Rheology of Linear PEO Chains and Tube Model Parameters

In order to translate the viscoelastic response of the metallo-supramolecular polymers into their molecular weight distribution, one needs first to determine the material parameters of the tube model (see Section 3.3.3). To this end, three linear non-functionalized PEO samples have been used as reference samples, having a weight averaged molar mass of 11 kg/mol, 101 kg/mol and 231 kg/mol and respective dispersities of 1.14, 1.06 and 1.2. Their viscoelastic properties are shown in Figure 3.3. Based on these data, and assuming that their MWD are well represented by a log-normal distribution, the plateau modulus, the molar mass between two entanglements and the Rouse time of an entanglement segment have been fixed to 1.45 MPa, 2000 g/mol and 5 10^{-8}s, respectively. As shown in Figure 3.3, the agreement between the experimental data and the storage and loss moduli predicted based on these parameters is indeed very good. Compared to the values proposed in literature[28] the value of the plateau modulus is identical, while the value of the molecular weight of an entanglement segment, M_e, is slightly higher than the one proposed in reference,[28] of 1700 g/mol.

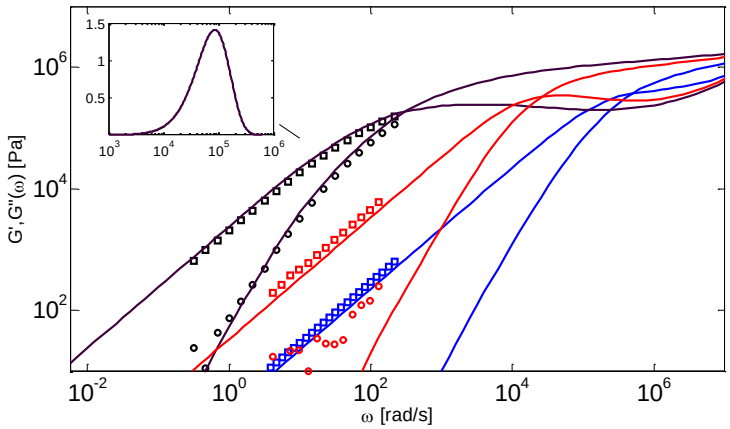

Figure 3.4: Experimental storage (circles) and loss (squares) moduli of the metallo-supramolecular PEO systems obtained by adding nickel ions to bi- (black), mono- (red) or non- (blue) functional PEO building blocks in stoichiometric amount. Continuous curves are predictions from the TMA model, considering a Flory molar mass distribution with $M_w = 86\ kg/mol$ for the bi-functional PEO (see the inset figure), and a log normal distribution with $M_w = 22\ kg/mol$ and PDI= 1.1 for the mono-functional PEO.

3.4.3 Metallo-Supramolecular Chains Based on A Stoichiometric Number of Metal Ions: Influence of the Building Block Functionalization

Rheological Behavior: As already mentioned in the introduction, adding metal ions to the bi-functional linear PEO chains should lead to long linear supramolecular chains containing several of these building blocks. On the other hand, the addition of these metal ions to a sample composed of 100 $wt\%$ of mono-functional PEO should lead to the creation of linear chains with a molar mass equal to twice the molar mass of the building blocks. This picture is validated in Figure 3.4, which presents the viscoelastic data of these samples, as well as the data corresponding to the non-functionalized PEO building blocks: the influence and efficiency of the metal-ligand interactions is clearly demonstrated by a large viscosity increase. In particular, the linear rheology of the assemblies based on the bi-functional PEO building blocks shows a much longer terminal relaxation time than the samples based on the mono-functional or the non-functionalized PEO building blocks, which corresponds to the larger average molar mass of the supramolecular assemblies. The assemblies based on the mono-functional building blocks also show a relaxation time longer than the relaxation of the pure PEO chains.

In order to quantify the degree of association of the bi-functional building blocks, the inverse model presented in Section 3.3.3 is used. To do so, the material parameters determined in the case of non-functionalized linear PEO (see

Section 3.4.2) are considered, and the MWD of the supramolecular assembly of bi-functional building blocks is assumed to be correctly described by a Flory distribution (see Equation 3.4). The only unknown parameter, M_w, is then fixed by best-fitting procedure, in order to minimize the relative error between predicted and experimental viscoelastic data (see Equation (3.5)). Its value is found to be equal to 86 kg/mol, which correspond to an number average molar mass, M_n, equal to 43 kg/mol. As shown in Figure 3.4, the shape of the predicted storage and loss moduli is in good agreement with the experimental data, which allows us to conclude that a Flory distribution, with a fixed dispersity of 2, is indeed suitable to describe the molar mass distribution of this sample. On the other hand, the sample based on mono-functional building blocks can be reasonably well approximated by considering that the supramolecular assemblies are all built from the combination of two building blocks.

From the comparison between experimental and predicted viscoelastic data, we observe that at the timescale and temperature of the measurement, the metal-ligand associations seem to behave like permanent bonds, and the supramolecular assemblies relax similarly to covalent linear chains with same Flory distribution, *i.e.* mainly by reptation process. It is easier for the whole assemblies to diffuse in the melt in order to relax their stress, than for the supramolecular bonds to break. This result can be understood, based on the results found in previous publications, where it was shown that the lifetime of such bis-complexes is around $10^{5.8}$ s.[6,29] Thus, in this case, the relaxation times of the supramolecular assemblies depends on their molar mass distribution, and cannot be represented by a single Maxwell element, as usually observed for supramolecular gels in which the relaxation is fully governed by the dynamics of the supramolecular bonds.[1,30]

Melt Morphology: Assembly of planar structures is a well-known root to achieve 3D networks of supramolecular polymers. Planar aromatics such as pyridine derivatives with simultaneous possibility of pi-pi stacking and metal-ligand association can build up highly ordered columnar or discoid structures, as reported by several authors.[75] The crystalline ordering tendency, rigidity and hydrophobicity of these planar structures can lead to phase separation into fibrillar or rod like assemblies, evidenced by X-ray scattering and transmission electron microscopy.[31−33]

Lateral assembly of chain ends in the telechelic supramolecular systems converts a linear chain extended system to a branched self-assembled one in which chains are interconnected as in networks. The alteration of degree and mode of assembly hence largely affects dynamics of the supramolecur polymer both in the melt and solid state. Plannar aggregation of end groups were reported to increase the melt elasticity, and the tensile modulus, while decreasing the stress relaxation rate and the strain at break.[32,34]

In view of molecular dynamics, the growth of plannar aggregation of chain ends changes the relaxation mode and hierarchy of the system, by retarding or preventing chain reptation and activating late fluctuation mechanism controlled by the life time of reversible supramolecular interactions. Thus it further adds to the complexity of the melt dynamic of supramolecular polymers.

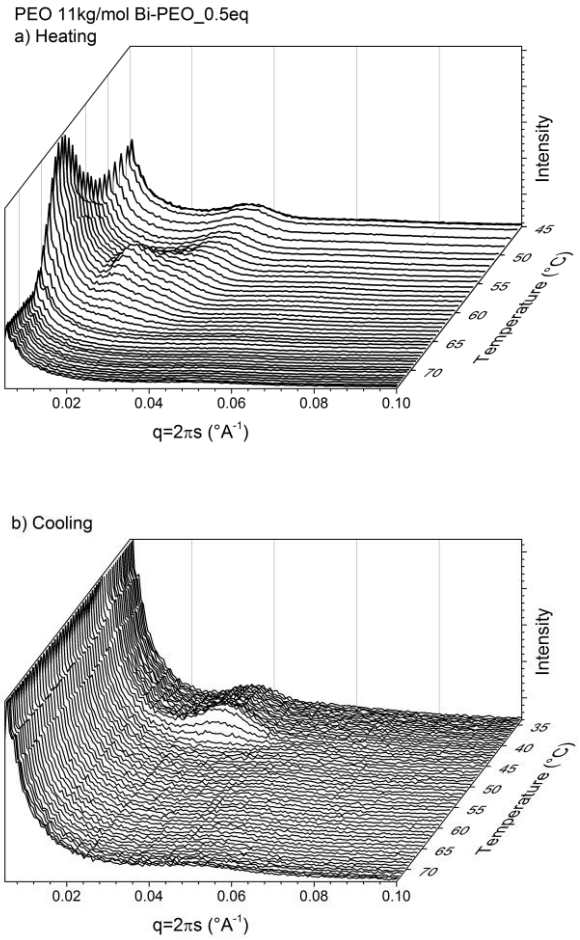

Figure 3.5: Temperature resolved SAXS spectra of sample Bi-PEO_ 0.5 eq upon (a) heating and (b) cooling. Above melting temperature no long range ordering was observed in the q space spanning from $0.005 - 0.14\ ^{\circ}A^{-1}$.

Since pi-pi stacking of terpyridine derivatives, *e.g.* 2,6-bis(1'-methyl-benzimidazolyl)pyridine and 2,2:6,2-terpyridine has been reported by several authors, here we investigated the microstructure of terpyridine groups in PEO melt, to demonstrate that the assembly of $Bi-PEO\_0.5\ eq$ sample, discussed in Section 3.4.3, is solely due to complexation of chelating terpyridine ligands with metal ions, which results in linearly structured supramolecular polymers.
To confirm that the complexation of terpyridine only results in linearly structured supramolecular polymers in the melt state, the configuration of terpyridine groups in the PEO melt for sample Bi-PEO_ 0.5 eq has been investigated

by SAXS. Figure 3.5 shows the evolution of the scattering data of the sample upon cooling and heating

It can be observed in Figure 3.5.a that upon heating, SAXS data shows four different thermal regions. First, below the onset of melting ($T < 52\ ^{\circ}C$), almost constant long range ordering and scattering intensity are observed, which address constant lamellar thickness and crystalline content. Then, in the second temperature region, which is between the onset of melting and the melting peak ($52\ ^{\circ}C < T < 59\ ^{\circ}C$), we observe an increase in lamellar thickness and overall crystallinity. We shall note that similar lamellar thickness evolution was reported by Cheng *et. al.*, and was attributed to the transformation of non-integral folding to integral folding chain crystals.[35,36] Then, in region 3 ($59\ ^{\circ}C < T < 65\ ^{\circ}C$), Bragg maxima disappear without much change in lamellar thickness. Finally region 4 corresponds to temperature above the melting temperature, in which viscoelastic measurements are performed. Clearly, in this region, the data does not show any Bragg diffraction maximum and thus, does not reveal any long range ordering neither in heating nor in cooling. Note that the reciprocal space in Figure **??** covers $0.005 - 0.14\ ^{\circ}A - 1$ which corresponds to long range ordering between $125 - 4.5\ nm$ in the real space. The end-to-end distance and contour length of PEO 11 kg/mol chains is well within this range. Therefore it can be concluded that in the Bi-PEO_ 0.5 eq sample, there is no lateral structure due to pi-pi stacking of terpyridine groups in the melt state. It is indeed due to the relatively large size of PEO precursors, which dilute the terpyridine groups.

3.4.4 Influence of the ion Content on Bi-Functional PEO Building Blocks

By adding a lower amount of metal ions to the bi-functional PEO building blocks, compared to the 1:2 metal/terpyridine stoichiometric ratio, the probability to create metal-ligand bis-complexes able to bridge two functionalized building blocks is reduced. As a consequence, it is expected that the supramolecular assemblies of such samples are of smaller length, compared to sample Bi_ PEO_ 0.5eq. This is tested in Figure 3.6, which presents the rheological response of sample Bi-PEO_ 0.25 eq (see Table 3.1). This sample, which only contains 0.25 equivalent of ions, relaxes much faster than the reference sample Bi-PEO_ 0.5eq, which contains 0.5 equivalent of ions, while it relaxes much slower than the pure sample. Thus, this result confirms the ability to create shorter supramolecular assemblies by varying the metal ions content. Using our TMA model in the inverse direction (see Section 3.3.3), the weight-averaged molar mass of this sample is estimated to be equal to 25 kg/mol, *i.e.* slightly more than twice the molar mass of the building blocks. In the case of these bi-functional building blocks, it is thus possible to vary the average molar mass of the assemblies, (and consequently their viscosity,) from $M_w = 11\ kg/mol$ (in the case of the pure sample) to $M_w = 86\ kg/mol$ (in the case of the stoichiometric metal/terpyridines ratio).

On the other hand, adding a larger amount of metal ions to the bi-functional PEO building blocks, compared to the 1:2 metal/terpyridine stoichiometric ra-

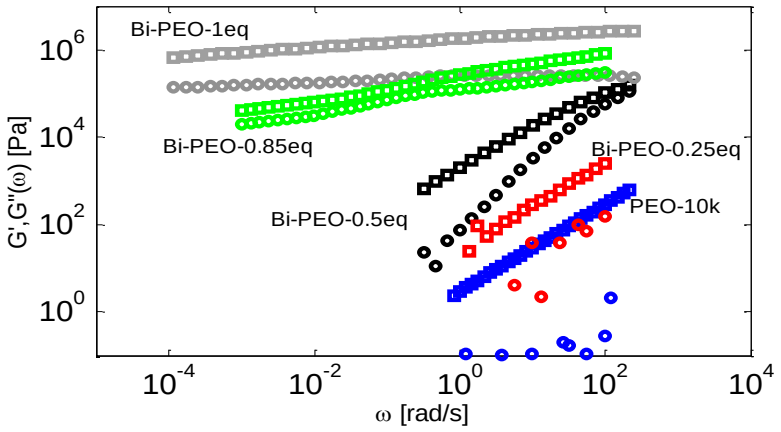

Figure 3.6: Storage and loss moduli of the metallo-supramolecular systems obtained by adding different equivalents of nickel ions to the bi-functional PEO building blocks. The amount of metal ions is either smaller than the stoichiometric amount of 0.5 eq. (as with 0.25 and 0 eq of ions), either larger (as with 0.85 or 1 eq. of ions).

tio, leads to more surprising results, as illustrated in Figure 3.6 for samples containing 0.85 or 1 equivalent of ions: the supramolecular systems are not able to flow anymore, showing a gel-like behavior. This behavior differs from the results shown in previous solution studies for other metallo-supramolecular systems, which have shown that a too large amount of metal ions, *i.e.* exceeding the stoichiometric ratio, usually leads to a large reduction of viscosity[5,37] due to the creation of terpyridine-metal ion mono-complexes and thus to a reduction of the average length of the polymeric assemblies. In particular, it was shown that the complexation behavior in solution of terpyridine bi-functionalized PEO with several metal-ions such as Co^{2+}, Cd^{2+} or Cu^{2+}, leads to a viscosity decrease when adding excess of metal-ions. It must be noted however that by adding an excess of Ni^{2+} salt to the PEO solution, only a small viscosity decrease was observed, contrary to the effect observed with the other metal ions. Based on this result, the authors concluded that with Ni^{2+} ions, the formation of bis-complexes is preferred compared to the creation of mono-complexes in agreement with the respective stability constants,[6] which seems to be also the case here. However, while this fact could explain why long linear assemblies do not decompose into shorter assemblies, it does not suffice to explain the network formation that we observe here in the melt for entangled PEO systems.

The observed viscoelastic response cannot be only attributed to the creation of complexes involving the terpyridine groups and the metal ions since the building blocks are linear and the nickel ions allow the association of only two terpyridine ligands. In order to obtain such viscoelastic behavior with terminal

relaxation time larger than 10^4 s, the linear assemblies should have, at least, a molar mass of 1.5×10^7 g/mol, which is not realistic.

Based on Figure 3.6, one can therefore conclude that there is a second type of interaction that takes place, which allows the chains to associate in order to create a network, and that these interactions occur only if there is an excess of metal ions (compared to the stoichiometric amount) which are not trapped into terpyridine-metal complexes.

It is important to note that the network properties obtained by adding an excess of metal ions are reversible. This is illustrated in Figure 3.7 for sample Bi-PEO-0.75 eq: a supramolecular network is created through time (see Figure 3.7.a), which can be destroyed under large shear deformation (see Figure 3.7.b). The state of the network after destruction (see the red triangles of Figure 3.7.a) corresponds to the moduli which have been reached at the largest amplitude of deformation, $\gamma_{max} = 200\%$. Then, starting from this new state, the system will again evolve through time in order to recover its equilibrium state.

Furthermore, one can observe on Figure 3.6 that the level of the elastic plateau of the sample containing 1 equivalent of nickel ions is nearly constant, and the value of the observed plateau is close to 1.45 MPa, *i.e.* close to the value of the plateau modulus of the covalent PEO systems (see Section 3.4.2). This suggests that adding a low amount of metal ions (of around 1 $wt\%$) is enough to freeze the motion of nearly 100 $wt\%$ of the PEO chains.

From these results, we conclude that this gel-like behavior is due to extra junctions, able to connect together the linear polymeric assemblies made of linear building blocks. Based on literature, we point out three different mechanisms which could lead to the observed gel-like behavior:

The first one is the fact that part of the metal ions in excess can be trapped by the PEO chains themselves, which are able to create coordination complexes with a wide variety of metal cations owing to their simple, regular chemical structure, to the presence of donating oxygen atom in each segment and to their high flexibility.[3] Thus, in this case, while weaker than the terpyridine, the oxygen atoms are also expected to play the role of ligands, able to trap the extra cations and create loops of same size as the ion diameter.[38,39] Such a process is, for example, exploited in electrolyte applications. In the case of the systems described here, this mechanism can indeed consistently explain the observed viscoelastic behavior if we assume that the metal ions can be surrounded by the oxygen atoms from at least two different chains. In this way, as proposed in the cartoon of Figure 3.8.a, associations between the PEO chains are created, leading to the formation of a supramolecular network. The extra nickel ions play thus the role of bridges between different PEO chains, which leads to an important increase of the sample viscosity. This idea is further tested in Section 3.4.5 by adding metal ions in a pure PEO chain.

As already mentioned, in the experimental conditions considered here, the lifetimes of the metal ion-terpyridine bonds between the PEO chains are long enough to be considered as stable during the measurement. Similarly, based on this picture, the lifetime of these secondary interactions between the PEO chains and the metal ions should be long enough to prevent the relaxation of the sample during the measurement.

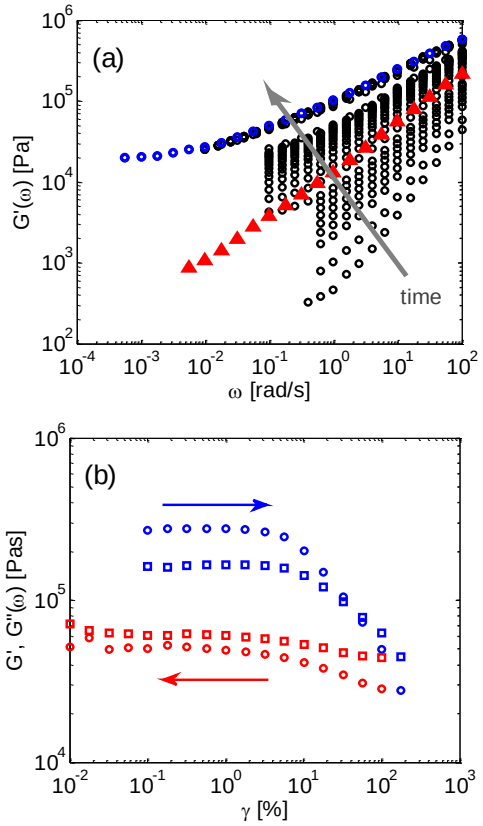

Figure 3.7: (a) Evolution through time of the storage modulus of the metallo-supramolecular systems obtained by adding 0.75 eq. of nickel ions to the bi-functional PEO building blocks (black ○), toward its equilibrium state (blue ○). The data represented by the triangle symbols have been measured right after the strain sweep measurements (see Figure b), and show the partial breaking of the supramolecular network. (b): Storage (○) and loss (□) moduli of the same sample, measured as a function of the amplitude of deformation, at a freq. of 10 rad/s. First from low to high, then from high to low amplitude of deformation.

A second process which can lead to a transient network formation of these linear building blocks is the possible clustering of the supramolecular linking motifs. Indeed, several works in literature mention that clustering and stacking of the reversible junctions in supramolecular polymer networks have been observed, leading to a high elastic energy storage, higher than the value expected by the supramolecular junctions only.[1,40] In particular, in referenc[1], which investigated the network properties of unentangled, end-functionalized star-like building blocks in solution, mechanical reinforcement of the gels was attributed to the strong electrostatic interaction between the metal-ligand complexes. Another example is shown in references[41,42] for metallo-supramolecular

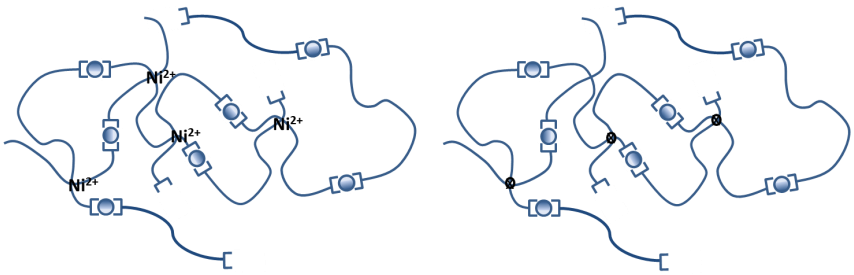

Figure 3.8: Cartoon showing the possible interactions between the chains observed with bi-functional PEO building blocks, in presence of nickel ions in a proportion larger than the stoichiometric ratio. The metal ions are represented either by the symbol • or by the symbol Ni^{2+}, while the terpyridines are represented by the symbol [. (a) Coordination complexes are created between the PEO chains and the nickel ions. (b) The extra uncoordinated Ni^{2+} ions react locally to generate covalent branc hing chains.

polystyrene-[Ru^{2+}]-poly(ethylene oxide) diblock copolymers. The charged complexes and the counter-ions associate into aggregates and therefore, create 'association points' between several terpyridines, acting as branching points.

Since this association mechanism was not observed with sample Bi-PEO_0.5 eq (see Section 3.4.3), neither in the rheological behavior nor in the SAXS data, clustering of the metal-ligand complexes should necessary involve the contribution of the metal ions in excess.

The third process which could explain the creation of the observed transient network is the creation of few covalent bonds between PEO chains, due to the extra uncoordinated $NiCl_2$ salts in the material, which can react locally and which can be consumed to generate chemical, *i.e.* covalent, branching or cross-linking. The fact that metal salts can act as cross-linking agents upon heating has already been reported in literature, for example with PVC.[43] In such as case, only few cross-linking molecules are enough to build a transient network, combining covalent cross-linking points and supramolecular metal-ligand interactions. Furthermore, as illustrated in Figure 3.8.b, the network is still breakable, through its reversible metal-ligand bonds.

In order to determine which of these possible mechanisms is at the origin of the gel-like behavior observed with bi-functional PEO building blocks, we investigate in the next Section the viscoelastic properties of samples composed of mono- or non-functionalized building blocks in presence of nickel ions.

3.4.5 Influence of the Ions Content on Mono-Functional PEO and Non-Functionalized Building Blocks

As shown in Figure 3.9, adding nickel ions in excess (compared to the stoichiometric value) to mono-functional building blocks also leads to the apparition of a clear low-frequency plateau observed in the storage modulus of these sam-

ples. As mentioned in Section 3.4.4, this second plateau cannot be only due to the presence of metal ion-terpyridine associations since there is only one associative extremity per chain and it has been shown that the assemblies made of two building blocks behave like liquid-like samples (see Figure 3.4). Furthermore, this plateau cannot be explained by the possible clustering effect of the supramolecular linking motifs: this process would lead to the creation of star-like PEO structures containing several arms of molar mass of around 11 kg/mol and, as shown in Figure 3.9. Such star-like architectures are relaxing too fast to lead to this very long low-frequency plateau. Also, if we consider that the second low-frequency plateau is due to the presence of large assemblies obtained via cross-linking reactions, this implies that, in order to reach terminal relaxation times larger than 1000 s, these assemblies, which are a small proportion, contain a large number of branching points in order to ensure the presence of very deep, slow relaxing, molecular segments, *i.e.* of generations corresponding to a very large seniority value.[44] This inhomogeneous repartition of the branched monomers cannot be consistently explained based on a statistical rule of branching.

Therefore, based on these first results, the hypothesis of secondary interactions between the oxygen atoms and the extra metal ions (see Section 3.4.4) seems the most appropriate to explain the presence of a second plateau in the elastic modulus of mono-functional building blocks. However, it does not mean that this process alone is sufficient to justify the viscoelastic properties of sample Bi-PEO_1 eq since there is an important difference between these systems. On Figure 3.9, one can observed that the level of the low frequency plateau of sample Mono-PEO-1eq is much lower, by nearly three orders of magnitude, than the value of the plateau modulus of the sample composed of bi-functional building blocks, which is comparable to the one of the PEO samples, equal to 1.45 MPa (see Section 3.4.2). By adding a larger amount of extra Ni^{2+}, as in system Mono-PEO_2 eq, the value of this second plateau slightly increases but still stays clearly below the plateau observed with bi-functional building blocks (which contains the same $wt\%$ if ions). Assuming that the plateau level scales with the square of the unrelaxed polymer fraction (see Eq. (3.2)), one can estimate that the proportion of mono-functional building blocks which participates to the supramolecular network is around 3 $wt\%$ with 1 equivalent of ions, and 12 $wt\%$ with 2 equivalents of metal ions, to be compared to the almost 100 $wt\%$ of trapped building blocks for sample Bi-PEO-1eq.

In order to validate the proposition of secondary interactions between nickel ions and the oxygens of the PEO chains, which appear in systems containing an excess of Ni^{2+} ions, we then study the linear viscoelastic properties of pristine PEO chains, *i.e.* without terpyridine chain-ends, in which a small amount of ions is added. As shown in Figure 3.10, which compares the linear viscoelastic properties of the bi-, mono- or non-functionalized linear building blocks in the presence of an equal amount of nickel ions (corresponding to 1eq. for the bi-functional building block), one can observe a clear second plateau in the storage modulus for the non-functionalized PEO chains. The presence of this plateau, which is reversible, and thus cannot be due to covalent cross-linking,[88] supports again the idea of supramolecular metal-ligand interactions between the metal

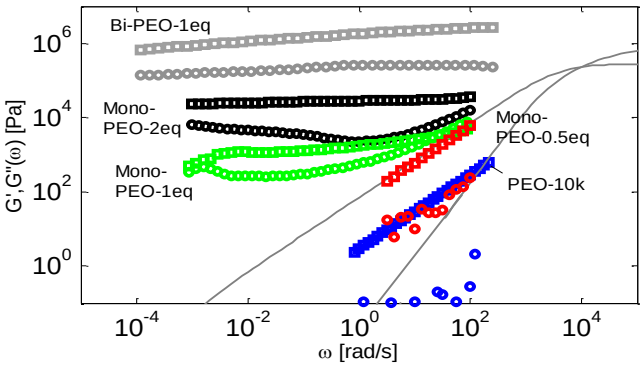

Figure 3.9: Storage and loss moduli of the metallo-supramolecular systems obtained by adding different equivalents of nickel ions to the mono-functional PEO building blocks. For comparison, the rheological data of sample Bi-PEO-1eq are also shown. The continuous curve (-) corresponds to the predicted moduli for star-like PEO chains with arms of 11 kg/mol.

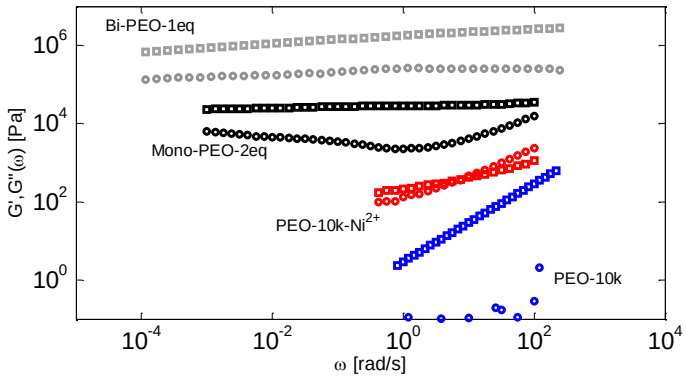

Figure 3.10: Storage and loss moduli of the metallo-supramolecular systems obtained by adding 1 equivalent of nickel ions to the mono-functional, bi-functional or non-functionalized PEO building blocks.

ions and the oxygen atoms of the PEO building blocks,[44,81,82] leading to the creation of PEO loops around the ions and with at least two different polymer chains surrounding a metal ion.

We also observe that, despite the larger proportion of free ions in the non-functionalized PEO sample, the level of its second plateau is even weaker than in the case of mono-functional building blocks. This difference in the plateau level could be attributed to the fact that, for a fixed proportion of 'branching agents', the polymer fraction which is immobilized between two of these branching points, depend on the length of the chains since the short chains

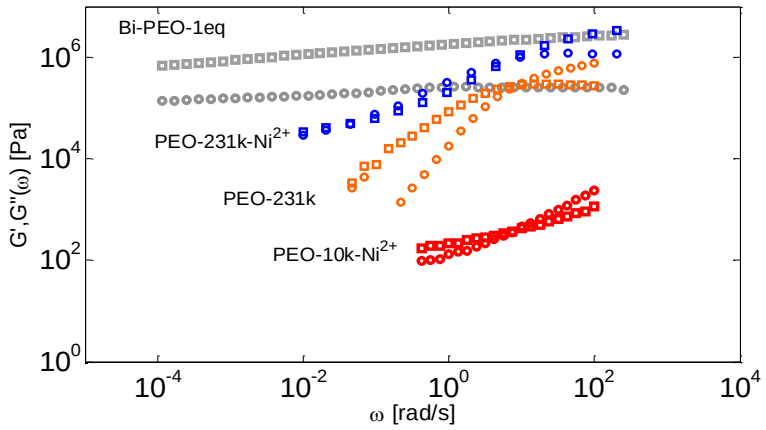

Figure 3.11: Storage and loss moduli of the metallo-supramolecular systems obtained by adding 1 equivalent of nickel ions to the blends of mono-functional, bi-functional or non-functional PEO building blocks.

contain a larger proportion of free dangling ends. Indeed, here, the linear assemblies of sample Bi-PEO-1 eq obtained by metal-terpyridine associations are much longer than the linear assemblies of sample Mono-PEO-2 eq, which are twice longer than the non-functionalized PEO chains. In order to determine if this difference in length is sufficient to explain the different plateau levels and thus, in order to determine if oxygen-metal interactions could explain the network-like response of sample Bi-PEO_ 1 eq, we investigate the viscoelastic properties of a very long non-functionalized PEO sample, PEO-231k-Ni^{2+}, in which a large proportion of Ni^{2+} ions has been added. With a molar mass of 231 kg/mol, the chains are longer than the supramolecular assemblies made of bi-functional building blocks in sample Bi-PEO_ 1 eq. We therefore expect that, if oxygen-metal interaction is the only mechanism needed to obtain the full immobilization of the assemblies made of bi-functional building blocks, sample PEO-231k-Ni^{2+} should also show a gel-like behavior. Results are shown in Figure 3.11. It is clear that again, part of the sample is trapped into a reversible network. However, similarly to the shorter non-functionalized sample and to the assemblies made of mono-functional building blocks, a large part of the polymer is still able to flow. This result suggests that the important length of the PEO assemblies based on bi-functional building blocks combined with metal ions in excess is not enough to explain the full immobilization of sample Bi-PEO-1 eq. Obviously, the terpyridine groups play a role in the network formation of this last sample.

Thus, from Figures 3.9-3.12, we conclude that 1) In the presence of metal ions in excess, oxygen-metal interactions between these ions and PEO chains take place and lead to the immobilization of a fraction of the polymer melt. However, it does not allow the freezing of the motions of the whole sample, 2) Nearly 100 $wt\%$ of the assemblies made of bi-functional building blocks par-

ticipate to the network, which cannot be only attributed to their long length compared to the assemblies made from the mono-functional building blocks, 3) Since cross-linking reactions are not observed with the PEO 231 kg/mol in which Ni^{2+} ions are added, one cannot explain the origin of the network formation by possible chemical cross-linking enhanced by the presence of uncomplexed ions.

The only remaining process is a possible clustering of the terpyridine groups favored by the metal ions in excess. In the specific case of bi-functional building blocks, this could indeed lead to a freezing of the motion of the building blocks, which are fully trapped between terpyridine groups, while this process should not significantly affect the dynamics of the mono- and non-functionalized building blocks, which always keep a chain extremity which is free to move and relax.

3.4.6 Controlling Rheology by Mixing Mono- and Bi- Functional Building Blocks

As it has been observed in Section 3.4.3, the functionalized building blocks mixed with a stoichiometric amount of nickel ions are flowing, and their storage and loss moduli show a terminal regime. Their corresponding terminal relaxation time directly depends on the length of the supramolecular assemblies, which can vary from a weight averaged molar mass of 11 kg/mol for a single PEO chain to 86 kg/mol for the supramolecular chains based on the bi-functional building block (with 0.5 eq of metal ion). By blending bi- and mono-functional building blocks, one should be able to gradually vary this average length between these two extremes. On the other hand, it has been observed in the previous Sections that functionalized building blocks mixed with a larger amount of nickel ions do not flow anymore, mainly due to secondary interactions between the oxygen atoms of the PEO chains and the nickel ions. We have also observed that, for a given amount of metal ions, the level of the storage modulus plateau strongly varies with the functionality of the building blocks (see Section 3.4.5). Mixing bi- and mono- functional building blocks (while keeping the same equivalent amount of metal ions) should therefore allow us to control the level of this plateau. This is tested in Figure 3.12, which presents the viscoelastic data of mixtures of bi- and mono-functional linear building blocks in different proportions. It is found that while for the blends containing less than 25 $wt\%$ of mono-functional building blocks, the viscoelastic behavior is similar to the sample containing 100 $wt\%$ of bi-functional building blocks, larger proportions of the mono-functional PEO block strongly influence this plateau level.

As mentioned in Section 3.4.5, the level of this low frequency plateau depends on the fraction of the samples which still contributes to the total stress once the dangling ends of the supramolecular assemblies as well as the unassociated chains have relaxed. It therefore corresponds to the chain fraction which is participating to the supramolecular network and cannot relax within the experimental frequency window. From the results shown in Figure 3.12, one can see that by adding mono-functional building block, the supramolecular network

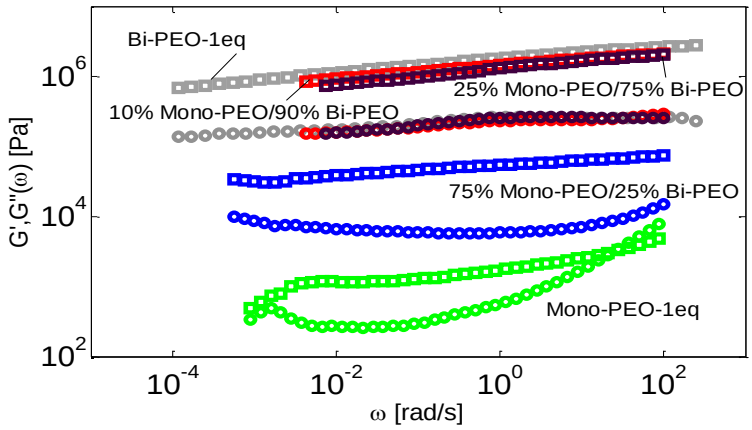

Figure 3.12: Storage and loss moduli of the metallo-supramolecular systems obtained by adding 1 equivalent of nickel ions to the blends of mono-functional and bi-functional PEO building blocks.

becomes softer. This can be first explained by the fact that, in average, the supramolecular assemblies obtained by using mono-functional building block have a lower molar mass than the one created from the association of 100 $wt\%$ of bi-functional building block. As a consequence, the proportion of dangling ends, which are able to relax at very high frequencies, increases. Furthermore, as described in Section 3.4.4, in presence of extra metal ions (compared to their stoichiometric ratio), clusters between the metal-ligand complexes act as extra branching points.

From these results, we conclude that the level of the low frequency plateau can be controlled by varying the association degree of these assemblies via the relative proportion of bi- and mono-functional building blocks.

3.5 Conclusion

We have studied the linear viscoelastic properties of supramolecular assemblies obtained by adding different amount of nickel ions into linear entangled PEO building blocks which have been end-functionalized by terpyridine groups. We have shown that by adjusting the amount of metal ions and the proportion of mono- versus bi-functional building blocks, one could control the relaxation time as well as the level of the low-frequency plateau of these supramolecular assemblies. In particular, we have shown that linear supramolecular assemblies of different length can be obtained, depending on the amount of nickel ions added to the system. For polymeric assemblies containing several building blocks, we could correctly describe their viscoelastic behavior based on the assumption that their molar mass distribution is well described by a Flory distribution. Also, in the melt state, for the systems containing a proportion of metal ions smaller or equal to the stoichiometric ratio, SAXS data revealed

no aggregation of the terpyridine groups. Then, it was shown that by adding metal ions in an amount larger than the stoichiometric amount (but still in very low weight proportion representing a maximum of 0.56 $wt\%$ of the sample), secondary interactions are taking place, which lead to the creation of a reversible polymeric network. Also observed in the viscoelastic properties of supramolecular assemblies made of mono- and non-functionalized PEO building blocks containing an excess of metal ions, we attributed these reversible interactions to metal-oxygen interactions between these extra metal ions and the PEO chains themselves, as it has been already reported in literature and often used in electrolyte applications. It seems here that an ion can interact with several chains at the same time and thus, could play the role of bridge between these different chains towards the creation of a network. However, while this extra association leads to the partial gelation of the system, it stays relatively weak and does not allow explaining the nearly full gelation of the assemblies made of bi-functional PEO building blocks.

By confronting the viscoelastic properties of a long, non-functionalized PEO polymer to the behavior of the assemblies created from bi-functional building blocks, both systems containing an excess of free nickel ions, we concluded that another association process is taking place in the sample containing bi-functional building blocks, in which both the metal-terpyridine complexes and the free metal ions play an active role. This could be due to possible clustering of the supramolecular motifs, as it has been observed in references [1,41,42].

This work gives us a solid starting point to explore more complex architectures of building blocks, based on both supramolecular and covalent cross-linking points. In the next chapters, we investigate the immobilization effect of nickel ions on pure PEO chains, in relation with the architecture of the chains.

3.6 Bibliography

1 Rossow, T.; Seiffert, S. Supramolecular Polymer Gels with Potential Model-Network Structure. *Polym. Chem.* **2014**, 5 (8), 3018.

2 Kaczmarek, H.; Kamiska, a; Kowalonek, J.; Szalla, a. Changes of Poly (Ethylene Oxide) Photostability by Doping with Nickel (II) Chloride. *J. Photochem. Photobid.* **1999**, 128, 121-127.

3 Kaczmarek, H.; Sionkowska, A.; Kamiska, A.; Kowalonek, J.; witek, M.; Szalla, A. The Influence of Transition Metal Salts on Photo-Oxidative Degradation of Poly(ethylene Oxide). *Polym. Degrad. Stab.* **2001**, 73 (3), 437-441.

4 Stadler, F. J.; Pyckhout-Hintzen, W.; Schumers, J.-M.; Fustin, C.-A.; Gohy, J.-F.; Bailly, C. Linear Viscoelastic Rheology of Moderately Entangled Telechelic Polybutadiene Temporary Networks. *Macromolecules* **2009**, 42 (16), 6181-6192.

5 Schmatloch, S.; Schubert, U. S. Engineering with Metallo-Supramolecular Polymers: Linear Coordination Polymers and Networks. *Macromol. Symp.* **2003**, 199 (1), 483-498.

6 Holyer, R. H.; Hubbard, C. D.; Kettle, S. F. A.; Wilkins, R. G. The Kinetics of Replacement Reactions of Complexes of the Transition Metals with 2,2,2"-Terpyridine. *Inorg. Chem.* **1966**, 5 (4), 622-625.

7 Montarnal, D.; Cordier, P.; Souli-Ziakovic, C.; Tournilhac, F.; Leibler, L. Synthesis of Self-Healing Supramolecular Rubbers from Fatty Acid Derivatives, Diethylene Triamine, and Urea. *J. Polym. Sci. Part A Polym. Chem.* **2008**, 46 (24), 7925-7936.

8 Doi, M.; Edwards, S. F. *The Theory of Polymer Dynamics*; 1988.

9 Van Ruymbeke, E.; Liu, C.; Bailly, C. Quantitative Tube Model Predictions For The Linear Viscoelasticity of Linear Polymers. *Rheology* **2007**, 53-134.

10 Van Ruymbeke, E.; Keunings, R.; Bailly, C. Prediction of Linear Viscoelastic Properties for Polydisperse Mixtures of Entangled Star and Linear Polymers: Modified Tube-Based Model and Comparison with Experimental Results. *J. Nonnewton. Fluid Mech.* **2005**, 128 (1), 7-22.

11 Van Ruymbeke, E.; Vlassopoulos, D.; Mierzwa, M.; Pakula, T.; Charalabidis, D.; Pitsikalis, M.; Hadjichristidis, N. Rheology and Structure of Entangled Telechelic Linear and Star Polyisoprene Melts. *Macromolecules* **2010**, 43 (9), 4401-4411.

12 Dealy, J. M.; Larson, R. G. Structure and Rheology of Molten Polymers: *From Structure to Flow Behavior and Back Again*; Hanser Publishers, **2006**.

13 McLeish, T. C. B. Tube Theory of Entangled Polymer Dynamics. *Adv. Phys.* **2002**, 51 (6), 1379-1527.

14 Watanabe, H. Viscoelasticity and Dynamics of Entangled Polymers. *Prog. Polym. Sci.* **1999**, 24 (9), 1253-1403.

15 Van Ruymbeke, E.; Keunings, R.; Bailly, C. Determination of the Molecular Weight Distribution of Entangled Linear Polymers from Linear Viscoelasticity Data. *J. Nonnewton. Fluid Mech.* **2002**, 105 (2-3), 153-175.

16 Carrot, C. From Dynamic Moduli to Molecular Weight Distribution: A Study of Various Polydisperse Linear Polymers. *J. Rheol.* **1997**, 41 (5), 1203.

17 Piogé, S.; Fustin, C.-A.; Gohy, J.-F. Temperature-Responsive Aqueous Micelles From Terpyridine End-Capped Poly(N-Isopropylacrylamide)-Block-Polystyrene Diblock Copolymers. *Macromol. Rapid Commun.* **2011**, 1-6.

18 Lohmeijer, B. G. G.; Schubert, U. S. Supramolecular Engineering with Macromolecules: An Alternative Concept for Block Copolymers. *Angew. Chem. Int. Ed. Engl.* **2002**, 41 (20), 3825-3829.

19 Hofmeier, H.; Hoogenboom, R.; Wouters, M. E. L.; Schubert, U. S. High Molecular Weight Supramolecular Polymers Containing Both Terpyridine Metal Complexes and Ureidopyrimidinone Quadruple Hydrogen-Bonding Units in the Main Chain. *J. Am. Chem. Soc.* **2005**, 127 (9), 2913-2921.

20 Van Ruymbeke, E.; Coppola, S.; Balacca, L.; Righi, S.; Vlassopoulos, D. Decoding the Viscoelastic Response of Polydisperse Star/linear Polymer Blends. *J. Rheol.* **2010**, 54 (3), 507.

21 Van Ruymbeke, E.; Masubuchi, Y.; Watanabe, H. Effective Value of the Dynamic Dilution Exponent in Bidisperse Linear Polymers: From 1 to 4/3. *Macromolecules* **2012**, 45 (4), 2085-2098.

22 Van Ruymbeke, E.; Shchetnikava, V.; Matsumiya, Y.; Watanabe, H. Dynamic Dilution Effect in Binary Blends of Linear Polymers with Well-Separated Molecular Weights. *Macromolecules* **2014**, 47 (21), 7653-7665.

23 Van Ruymbeke, E.; Bailly, C.; Keunings, R.; Vlassopoulos, D. A General Methodology to Predict the Linear Rheology of Branched Polymers. *Macromolecules* **2006**, 39 (18), 6248-6259.

24 Ahmadi, M.; Bailly, C.; Keunings, R.; Nekoomanesh, M.; Arabi, H.; van Ruymbeke, E. Time Marching Algorithm for Predicting the Linear Rheology of Monodisperse Comb Polymer Melts. *Macromolecules* **2011**, 44 (3), 647-659.

25 Flory, J. Molecular Size Distribution. *Engineering* **1940**, 1569 (9).

26 Fradet, A.; Tessier, M. Average Degrees of Polymerization and Molar Masses of Branched and Hyperbranched Condensation Polymers: Recursive Probability Approach. *Macromolecules* **2006**, 39 (18), 6238-6247.

27 Durand, D.; Bruneau, C.-M. Graph Theory and Molecular Distribution. 2. Copolycondensation of A-Group Polyfunctional Monomers with B-Group Polyfunctional Monomers. *Macromolecules* **1979**, 12 (6), 1216-1222.

28 Fetters, L. J.; Lohse, D. J.; Richter, D.; Witten, T. A.; Zirkel, A. Connection between Polymer Molecular Weight, Density, Chain Dimensions, and Melt Viscoelastic Properties. *Macromolecules* **1994**, 27 (17), 4639-4647.

29 Hogg, R.; Wilkins, R. G. 57. Exchange Studies of Certain Chelate Compounds of the Transitional Metals. Part VIII. 2,2?,2?-Terpyridine Complexes. *J. Chem. Soc.* **1962**, 341.

30 Cates, M. E. Reptation of Living Polymers: Dynamics of Entangled Polymers in the Presence of Reversible Chain-Scission Reactions. *Macromolecules* **1987**, 20 (9), 2289-2296.

31 Fox, J. D.; Rowan, S. J. Supramolecular Polymerizations and Main-Chain Supramolecular Polymers. *Macromolecules* **2009**, 42 (18), 6823-6835.

32 Kautz, H.; Van Beek, D. J. M.; Sijbesma, R. P.; Meijer, E. W. Cooperative End-to-End and Lateral Hydrogen-Bonding Motifs in Supramolecular Thermoplastic Elastomers. *Macromolecules* **2006**, 39 (13), 4265-4267.

33 Brunsveld, L.; Folmer, B. J.; Meijer, E. W.; Sijbesma, R. P. Supramolecular Polymers. *Chem. Rev.* **2001**, 101 (12), 4071-4098.

34 Burnworth, M.; Tang, L.; Kumpfer, J. R.; Duncan, A. J.; Beyer, F. L.; Fiore, G. L.; Rowan, S. J.; Weder, C. Optically Healable Supramolecular Polymers. *Nature* **2011**, 472 (7343), 334-337.

35 Cheng, S. Z. D.; Zhang, A.; Barley, J. S.; Chen, J.; Habenschuss, A.; Zschack, P. R. Isothermal Thickening and Thinning Processes in Low-Molecular-Weight Poly(ethylene Oxide) Fractions. 1. From Nonintegral-Folding to Integral-Folding Chain Crystal Transitions. *Macromolecules* **1991**, 24 (13), 3937-3944.

36 Lee, S.; Chen, E.; Zhang, A.; Yoon, Y.; Moon, B. S.; Lee, S.; Harris, F. W.; Cheng, S. Z. D.; Meerwall, E. D. Von; Hsiao, B. S.; et al. Isothermal Thickening and Thinning Processes in Low Molecular Weight Poly (Ethylene Oxide) Fractions Crystallized from the Melt . 5 . Effect of Chain Defects. *Macromolecules* **1996**, 9297 (96), 8816-8823.

37 Schmatloch, Van Den S.; Berg, A. M. J.; Alexeev, A. S.; Hofmeier, H.; Schubert, U. S. Soluble High-Molecular-Mass Poly (Ethylene Oxide) *Macromolecules* . **2003**, 9943-9949.

38 Costa, L.; Luda, M. P.; Cameron, G. G.; Qureshi, M. Y. Thermal and Thermo-Oxidative Degradation of Poly(tetrahydrofuran) and Its Complexes with LiBr and LiI. *Polym. Degrad. Stab.* **2000**, 67 (3), 527-533.

39 Bruce, P. G. Ion-Polyether Coordination Complexes: Crystalline Ionic Conductors for Clean Energy Storage. *Dalton Trans.* **2006**, No. 11, 1365-1369.

40 Herbst, F.; Schröter, K.; Gunkel, I.; Gröger, S.; Thurn-Albrecht, T.; Balbach, J.; Binder, W. H. Aggregation and Chain Dynamics in Supramolecular Polymers by Dynamic Rheology: Cluster Formation and Self-Aggregation. *Macromolecules* **2010**, 43 (23), 10006-10016.

41 Al-Hussein, M.; Lohmeijer, B. G. G.; Schubert, U. S.; de Jeu, W. H. Melt Morphology of Polystyrene-Poly(ethylene Oxide) Metallo-Supramolecular Diblock Copolymer. *Macromolecules* **2003**, 36 (25), 9281-9284.

42 Al-Hussein, M.; de Jeu, W. H.; Vranichar, L.; Pispas, S.; Hadjichristidis, N.; Itoh, T.; Watanabe, J. Bulk and Thin Film Ordering in Side-Chain Liquid-Crystalline/Amorphous Diblock Copolymers: The Role of Chain Length. *Macromolecules* **2004**, 37 (17), 6401-6407.

43 Pike, R. D.; Starnes, W. H.; Jeng, J. P.; Bryant, W. S.; Kourtesis, P.; Adams, C. W.; Bunge, S. D.; Kang, Y. M.; Kim, A. S.; Kim, J. H.;

et al. Low-Valent Metals as Reductive Cross-Linking Agents: A New Strategy for Smoke Suppression of Poly (Vinyl Chloride). **1997**, 9297 (Vi), 6957-6965.

44 Blackwell, R. J.; Harlen, O. G.; McLeish, T. C. B. Theoretical Linear and Nonlinear Rheology of Symmetric Treelike Polymer Melts. *Macromolecules* **2001**, 34 (8), 2579-2596.

Chapter 4

Transient Metallo-Supramolecular Networks Built from Entangled Melts of Poly(ethylene oxide)

Outline

The effect of PEO-metal salt complexation on the dynamics and microstructure of PEO-nickel chloride [$NiCl_2$] systems is investigated by rheology and X-ray scattering. Annealed PEO-nickel salt systems exhibit network properties above the melting temperature of PEO, characterized by a second elastic plateau, beyond the reptation time of PEO chains. The level of the second plateau strongly depends on the annealing conditions and the ion content. In PEO-$NiCl_2$ networks, the linear viscoelastic region is experimentally out of reach meaning that their viscoelastic properties strongly depend on strain and strain rate as well as any deformation history. The network can be broken down by large amplitude shear and reversibly reformed under quiescent conditions.
X-ray scattering reveals formation of distinct crystalline structures of PEO-$NiCl_2$ complexes, which are different from those of both neat PEO and nickel salt. The combined rheology and X-ray scattering results indicate that the network results from a small fraction of trapped PEO chains, which are bridging the crystalline domains of PEO-$NiCl_2$ complexes.

4.1 Introduction

Polyether-ion complexation is one of the most promising fields of supramolecular chemistry since it allows obtaining a variety of electric, magnetic and

optical properties. Polyether-ion complexes were reported in many different systems combining open shell metal ions with various polymer ligands, in which ether bonds are interacting with metal ions and form macrocyclic coordination complexes.[1−7] Among all possible polymer ligands, PEO produces by far the most studied complexes with metal ions. A rich library of acyclic "crown-ether-like" structures has been reported for such PEO-metal salts complexes. The structure of the complex primarily depends on the size and charge of both anions and cations, as well as the ratio between ether oxygens and cations.[5,7] The formation of the complex can lead to significant conformational changes of the PEO chains as the number of ether oxygens involved in the complex can vary from 1 to 7 per cation.[2,5,7−11] For instance, in PEO_3:$LiAsF_6$, two PEO chains adopt counter rotating 3D helical structures to provide 6 ether oxygens to each Li^+, [9] while in PEO_8:$NaBPh_4$ a single chain wraps around a cation to provide seven interacting oxygen sites.[10] In addition to 3D nonrandom coil conformations, the unit cell structure of the PEO-ion complexation can force the chains to adopt a 2D conformation, with large entropic penalties, such as the stretched zigzag or square wave planar structures observed in PEO_1:$NaCF_3SO_3$ and PEO_2:$ZnCl_2$, respectively.[7,11]

Transient dynamics of PEO-metal salt complexation is another distinct feature of these coordinating compounds. PEO-ion complexation is a reversible supramolecular interaction, thus characterized by a certain lifetime. In other words, the coordination of ether oxygens in PEO to the metal cation has a particular dissociation-association time scale, controlled by the thermodynamic state of the system.[2,12] Once a complex dissociates, the ether bonds associate again to the original cation or to an adjacent one after a certain time scale. This continuous exchange of ether oxygens and cations leads to what is usually referred to as "ion hopping". Some generally observed dynamic behavior in PEO-ion systems such as retardation of full relaxation of the chains, alteration of viscoelastic properties and increase in conductivity originate from this ion hopping process.[13−18] For instance, it was found that the apparent glass transition temperature and viscosity are increasing with increasing metal ion to ether bond ratio according to Vogel-Tamman-Fulcher formalism.[19,20] The terminal relaxation time of the glassy plateau can also increase with the ion content, as it has been observed for example in unentangled PEO$-Li^+$ and PEO$-Na^+$.[14,16] Furthermore, the conductivity in these systems was shown to be a direct function of the glass transition of the polymer, which determines the segmental mobility at the application temperature, as well as mobility and density of conducting cations.[14] It is understood that the ion hopping process can alter the molecular motion of the chains by acting as temporary topological constraints.[21−23]

Despite numerous investigations on PEO with alkali and alkaline-earth metal salts, the complexation of PEO with transition metal ions is rarely studied. Recently, the extensive use of functionalized PEO as building block to achieve self-assembled metallo-supramolecular architectures via metal-ligand association [24−26] strongly reinforced the need to understand the possible coordination of transition metal ions with the oxygen atoms of PEO chains, which could appear in addition to the expected metal-ligand interactions. In these

systems, PEO has been used as linker between supramolecular metal-ligand complexes *e.g.* (pyridine based) ligands and divalent transition metal ions. In recent years, several works elucidated that the interaction of transition metal ions with the PEO linker significantly alter the properties of these metallo-supramolecular polymers, most importantly the degree of association of the building blocks. For instance, in the metallo-supramolecular networks created from pyridine based ligands and zinc chloride, Kumpfer *et al.*[27] reported that the viscoelastic properties of the polar poly(alkyl oxides) are different from those of apolar polyolefin backbones. They then suggested that the observed difference is potentially due to the coordination of the metal ions with ether bonds along the chains. It has to be mentioned that noticeable viscosity increase, due to PEO-ion complexation, is often seen in PEO melts but not in PEO solutions. For instance, Schmatloch *et al.*[28] investigated the viscosity of terpyridine functionalized as well as pure PEO solutions with acetate salts of nickel, cobalt, copper and cadmium, above stoichiometric salt concentrations, and reported no alteration of viscosity due to complexation between PEO and the metal salts.

Contrary to solutions, in supramolecular PEO melts containing metal salts, we previously reported that adding an excess of transition metal-ions compared to the stoichiometric ratio, affects the degree of assembly and leads to an increase of the viscosity of the system by orders of magnitude.[29,30] We demonstrated that this phenomenon is, at least partially, due to weak complexation between metal ions and ether bonds in PEO. In these previous studies, we observed that the chemistry of the metal salt plays an important role on the viscoelastic properties of the network. For instance, while elastic PEO networks are formed in presence of $NiCl_2$ and $FeCl_2$, the viscoelasticity of the PEO melt is not modified by $ZnCl_2$,[31] despite the fact that strong PEO-ion complexation is reported for all these metal salts.[2,5]

In this work we aim at studying in more details the coordination interaction between non-functionalized linear PEO chains and nickel salts and its influence on the dynamics of these systems, which is an essential step towards the understanding and control of metallo-supramolecular systems based on functionalized PEO building blocks. In particular, we would like to focus on PEO$-Ni_2^+$ complexes since among all transition metals, they have shown the strongest impact on the dynamics of PEO melts.[31] Our objective is to study the melt rheology of PEO systems containing small amount of metal salts, in order to understand the influence of the latter on the bulk viscoelasticity as well as the microstructure of the PEO systems.

4.2 Materials and Methods

Hexahydrate chloride and perchlorate as well as anhydrous iodide salts of nickel were purchased from Sigma-Aldrich. α - ω-hydroxy and mono-methyl terminated linear PEO of different molar masses with narrow distributions (<1.2) were purchased from Sigma-Aldrich and Polymer Source.

PEO-metal salt systems were prepared by solution mixing. PEO was first dried at 37 $^\circ C$ in vacuum for at least 2 days. Nickel salts and dried PEO were

dissolved in methanol separately and then were incorporated in the desired amount. The solutions of PEO and nickel salt were then stirred for at least 1 hour at room temperature and dried by rotavapor. To ensure removal of all solvent and moisture residues, the obtained powder was placed in vacuum at 42 $°C$ for up to 3 days.

To quantify the ion content we define the ion equivalence as the moles of salt per moles of PEO chains. In order to identify samples, we use PEO Xk Y eq Z formalism, in which X, Y and Z are number-averaged molar mass of PEO in kg/mol, equivalent number and name of salt, respectively. The systems investigated in this work are listed in Table 4.1.

Viscoelastic properties were investigated by small amplitude oscillatory shear (SAOS) rheology using Kinexus (Malvern Instruments) and MCR 301 (Anton Paar) rheometers. A 8, 15 or 20 mm diameter parallel plate geometry was used depending on the viscosity level of the system at the measurement temperature. Different geometries were used to ensure accounting for the tool compliance.

Table 4.1: Overview of the PEO metal salt systems used in this work

PEO molar mass(M_w) kg/mol	Metal salt	Nickel equivalence mol/mol chains	Nickel content $Weight\%$	Nickel content mol/mol $monomer$	Sample code
11	-	-	-	-	PEO 11k
28	-	-	-	-	PEO 28k
231	-	-	-	-	PEO 231k
11	Nickel chloride	0.5	0.25	1/520	PEO 11k 0.5 eq $NiCl_2$
11	Nickel chloride	1	0.5	1/260	PEO 11k 1 eq $NiCl_2$
11	Nickel chloride	2	1.0	1/130	PEO 11k 2 eq $NiCl_2$
11	Nickel chloride	4	2.0	1/65	PEO 11k 4 eq $NiCl_2$
11	Nickel perchlorate	2	1.0	1/130	PEO 11k 2 eq $Ni(ClO_4)_2$
11	Nickel iodide	2	1.0	1/130	PEO 11k 2 eq NiI_2
28	Nickel chloride	2	0.44	1/1300	PEO 28k 2 eq $NiCl_2$
231	Nickel chloride	4	0.1	1/1312	PEO 231k 4 eq $NiCl_2$
231	Nickel chloride	15	0.37	1/350	PEO 231k 15 eq $NiCl_2$
231	Nickel chloride	200	4.5	1/26	PEO 231k 200 eq $NiCl_2$

Evolution of viscoelastic properties of the samples with time was monitored by consecutive frequency sweep measurements. SAOS measurements were performed in shear controlled mode with low angular deformation (0.5%-0.01% strain) in order to minimize possible destructive effects of shear on network formation. Transient creep and recovery experiments were used to capture long time viscoelastic behavior and to extend oscillatory data. The time do-

main data were then converted to frequency domain, by the method of Evans *et al.*[32]

Energy dispersive X-ray spectrometry analysis (EDX) were performed using a JEOL FEG SEM 7600F scanning electron microscope equipped with an EDX system (Jeol JSM2300 with a resolution $< 129 \ eV$) operating at 15 keV with a working distance of 8 mm. The acquisition time for the chemical spectra lasted 300 s with a probe current of 1 nA. The resolution of the EDX is about 0.5 μ_m.[33] Specimens for EDX were mounted on stubs and analyzed without metallization. Small (SAXS) and wide angle (WAXS) X-ray scattering measurements using a 12 keV energy X-ray beam were performed at DUBBLE, the Dutch-Flemish CRG beam line (BM26B) at the European Synchrotron Radiation Facility (ESRF) in Grenoble, France. The SAXS patterns were collected on a two-dimensional Pilatus 1M detector placed at 450 cm from the sample after an evacuated tube. The WAXS signals were captured on a Pilatus $300K-W$ detector at 30 cm from the sample. The angular calibration was performed using silver behenate and high density polyethylene (HDPE) standards for respectively SAXS and WAXS. A Linkam HFS 191 Heating/Freezing stage (Surrey, United Kingdom) was used for temperature control. The transmitted beam intensity was measured by a photo diode placed downstream from the sample at the SAXS beam stop. The scattered intensities were corrected for the scattering of the empty setup, taking differences in transmission and direct beam intensity into account. The 2D SAXS and WAXD data were azimuthally averaged using the program ConeX.[34] The scattering intensity is expressed as a function of the scattering vector modulus, q, and scattering angle, $^\circ 2\theta$, for SAXS and WAXS respectively. Scattering angles are shown at 8 keV (Cu K^α).

Matrix assisted laser desorption/ionization (MALDI) mass spectra were recorded on a Waters QToF Premier mass spectrometer using a nitrogen laser, operating at 337 nm with a maximum output of 500 Jm^{-2} delivered to the sample in 4 ns pulses at 20 Hz repeating rate. Time-of-flight mass analyses were performed in the reflectron mode at a resolution of about 10,000. The matrix used for sample preparation was *trans*-2-[3-(4-tertbutylphenyl)-2-methylprop-2-enylidene]-malononitrile (DCTB) that was initially dissolved in chloroform at a concentration of 40 mg/mL. This solution (1 μL) was further deposited on a stainless steel target and air-dried. Polymer samples were dissolved in THF to obtain 1 mg/mL solutions, 20 μL of sodium iodide 2 mg/mL (1:1; water:acetonitrile) were added to this solution. 1 μL aliquots of those polymer solutions were casted onto the target area previously covered with the matrix crystals, and air-dried. For the acquisition of the single-stage MS spectra, the quadrupole (rf-only mode) was set to pass all the ions of the distribution, and they were transmitted into the pusher region of the time-of-flight analyzer where they were mass analyzed with 1 s integration time. Data were collected in continuum mode until acceptable averaged data were obtained.

Gel permeation chromatography (GPC) was carried out on a system composed of two PSS Gram columns, with 100 Å and 1000 Å mesh size, connected to a Waters 410 differential refractometer, all working isothermally at 37 $^\circ C$.

DMF with 5 mM NH_4PF_6 was used as the carrier solvent with volume rate 0.5 mL/min. Calibration was performed using PEO standards.

4.3 Results and Discussion

4.3.1 Viscoelastic Properties of PEO$-Ni^{2+}$ Melt

As we first observed in our previous work,[29] adding a small amount of nickel salt in pure linear PEO leads to the creation of a second, low frequency plateau in the storage modulus curve, which has been attributed to the fact that a fraction of the PEO chains is partially trapped into a reversible network, originating from the weak interactions between the metal ions and the PEO chains. In order to observe such an effect in the viscoelastic response, these weak reversible interactions should involve at least two different chains, interacting with the metal ion. Within this picture, ions can therefore be seen as cross-linking points for the PEO chains, with the main feature that these cross-linking points are reversible. Here, we would like to further investigate the influence of these supramolecular interactions as well as their dependence on parameters such as the molar mass of the PEO chains, the ions content, the amplitude of deformation, the temperature or the time.

Time and Temperature Effect

Reversible polymeric networks are known to show thixotropic properties.[35,36] Indeed, just after loading the sample into the rheometer, a fraction of the reversible bonds is destroyed and needs time to build the network again. Therefore, in order to determine the best protocol and ensure reproducibility of the data, the evolution through time of the viscoelastic properties of sample PEO $11k$ 2 eq $NiCl_2$ was first studied, by consecutive frequency sweeps above the melting temperature of PEO. Main results are shown in Figure 4.1. First, at 70 $°C$, we observe that both the storage and loss moduli of the sample increase with time. At this temperature, one can observe that the rate of increase of elasticity starts to slow down after 2 h. However, upon increasing temperature to 90 $°C$, large evolution through time is again observed and the low frequency second plateau becomes much more pronounced, as the elasticity of the gel formed at 90 $°C$ is one order of magnitude higher than the elasticity of the gel annealed at 70 $°C$. One can also observe that the gel properties are maintained upon cooling the sample back to 70 $°C$. This result could suggest that the system is at least partially kinetically trapped, on the way towards full thermodynamic equilibrium due to the competition between thermodynamics of PEO-ion complexation and hindered mobility of the PEO chains involved in these complexes, which prevents the supramolecular systems to reach their most stable equilibrium state.[28]

The insert in Figure 4.1 shows that the PEO-nickel salt melt gradually evolves from a viscous fluid, in which $d\log G^{'}/d\log\omega = 2$ and $d\log G^{''}/d\log\omega = 1$ to a critical gel, where dynamic moduli are parallel ($G^{'} \propto G^{''} \propto \omega^{\alpha}$) and then to an elastic network, characterized by a low rubbery plateau (See Figure 4.2 for more information). Compared to the plateau modulus of PEO chains in the melt state, the level of this second plateau remains quite low.

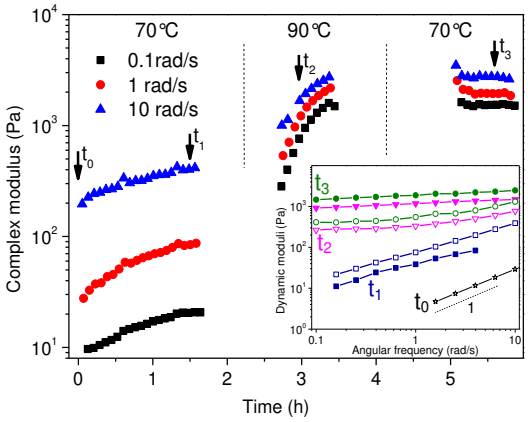

Figure 4.1: Evolution of complex modulus of PEO $11k$ 2 eq $NiCl_2$ during annealing at 70 and 90 $^{\circ}C$, captured by consecutive frequency sweeps. Insert shows the storage and loss moduli (closed and open symbols, respectively) at 4 snapshots indicated by the arrows in the main figure. Upon annealing, PEO 11k 2 eq $NiCl_2$ melt evolves from a viscous liquid (t_0) to a critical gel (t_1) and then to an elastic network (t_2 and t_3).

Figure 4.1 shows that the final viscoelastic properties of the PEO$-Ni^{2+}$ melt strongly depend on the annealing temperature (T_{anl}) as well as the residence time (t_{anl}). Hence T_{anl} is mentioned for each set of data presented below. It has to be mentioned that viscoelastic properties of the samples were continuously measured until the changes of dynamic moduli were insignificant for > 2 h.

Influence of the PEO Molar Mass on the Reversible Network

Since the proportion of metal ions in the samples analyzed here is very low (see table 4.1), the origin of the second plateau observed in the storage modulus cannot be attributed to the unique presence of these metal ions as colloidal particles or fillers, but it is rather due to their capability of acting as reversible cross-linking points for the PEO chains. The likelihood that chains are being bridged by complexes, and hence participate to the transient network, increases with increasing chain length. [30] Therefore we expect that the level of the second plateau increases with the molar mass of the PEO chains. This is tested in Figure 4.2, which presents the relaxation moduli of the PEO chains of molar mass of 11, 28 and 231 kg/mol, with or without adding a small amount of salt. However, the results are non-trivial. Considering PEO 11 and 28 kg/mol, both with 2 equivalents of nickel salt per polymer chain, we see a significant increase of the level of the second plateau when increasing the molar mass of the chains. However, comparing PEO $28k$ 2 eq $NiCl_2$ with PEO $231k$ 15 eq $NiCl_2$, in which there are similar weight fractions of salt, we see that the lower molar mass PEO system shows a second plateau more than one decade higher, compared to the long PEO system. As discussed later, this discrepancy may arise from the high magnitude of non-linearity in the viscoelastic measurement (See Figures 4.5 and 4.6 and the corresponding discussions).

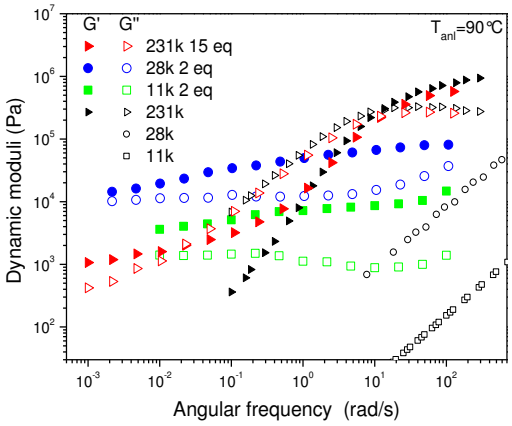

Figure 4.2: Dynamic storage and loss moduli against frequency of annealed PEO 11, 28 and 231 kg/mol samples, without and with $NiCl_2$ salt. The shear strain is fixed to 0.1% strain in all measurements.

Despite the complexity observed in Figure 4.2, the data confirm that the chains lose their capability to relax through reptation mechanisms, as they are partially trapped between complexes. Also, one can observe that at high frequencies, the plateau modulus of these samples is not affected by the small amount of salt which has been added, meaning that at high frequencies, entanglements continue to govern the elasticity of these samples.

Influence of the Proportion of Metal Ions Added to the System

As shown in Figure 4.3.a, if a larger amount of salt is added to PEO $11k$, the importance of the second plateau modulus increases, from liquid-like behavior (*i.e.* no second plateau is observed) to weak network behavior, characterized by a second plateau with a value of around 10^4 Pa for the sample containing 4 equivalents (2 $wt\%$) of metal ions. It must be noted that in this case, the first plateau of the storage modulus (*i.e.* the plateau modulus) cannot be seen experimentally since the relaxation of the free chains takes place at very short times which are outside the experimental frequency window.

In order to acquire information about the plateau modulus and the reptation time of PEO chains in presence of PEO$-Ni^{2+}$ complexes, longer PEO chains have been tested. The effect of adding $NiCl_2$ in sample PEO $231k$ is shown in Figure 4.3.b. Since the chains are much longer compared to PEO $11k$, the $G^{'}-G^{''}$ cross-over point as well as a part of the plateau modulus can now be observed. Again, the importance of the supramolecular network increases with the salt concentration. In particular, at low salt concentrations, the density of complexes seems too low to compete with the density of entanglements: as already mentioned, the plateau modulus as well as the cross-over between $G^{'}$ and $G^{''}$ remain unchanged. This suggests that the dynamics of the chains at the length scale of an entanglement segment is not affected by the presence of the metal ions, and that the only effect of the latter is to prevent the terminal relaxation of a fraction of the chains. On the other hand, at high concentration

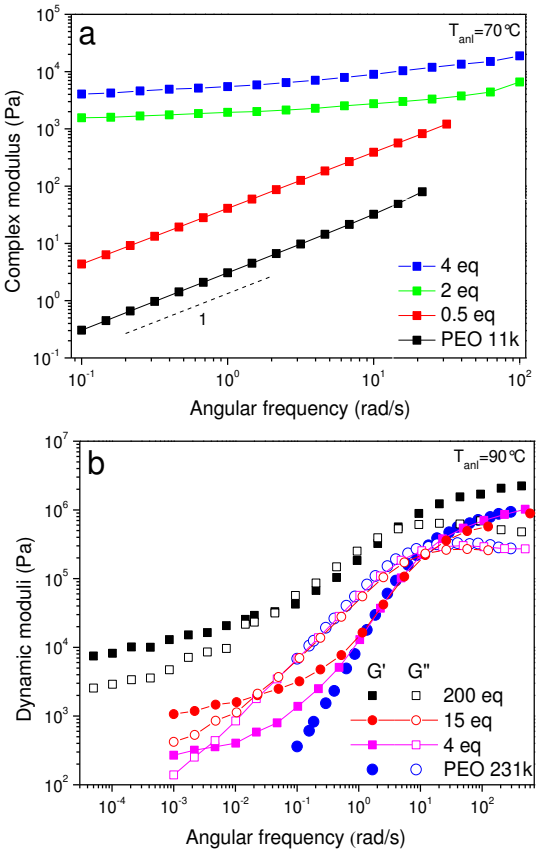

Figure 4.3: Effect of $NiCl_2$ salt content on viscoelastic properties of (a) PEO $11k$ annealed at 70 $^{\circ}C$ (b) PEO $231k$ annealed at 90 $^{\circ}C$. The shear strain is fixed to 0.1% strain in all measurements The PEO$-NiCl_2$ complexion leads to a second plateau, the level of which increases with the proportion of $NiCl_2$.

(as for sample PEO $231k$ 200 eq $NiCl_2$), the plateau modulus and its following cross-over clearly depart from their original values for PEO. In such a case, the number of elastically active strands increases, being influenced by both entanglements and reversible PEO-ion complexes. Furthermore, in Figure 4.3.b, it can be seen that the metal ions act as physical cross-linkers during a long time. Creep and recovery data reveal that the second plateau continues down to frequency 10^{-5} rad/s and the system is still unable to relax.

Evolution of the complex modulus with the proportion of metal ions, is presented in Figure 4.4 for specific frequencies. It can be seen that the second plateau shows exponential dependency on the salt content. In other words, below a critical concentration, which is the minimum concentration needed to suppress the terminal relaxation of the sample (within the experimental fre-

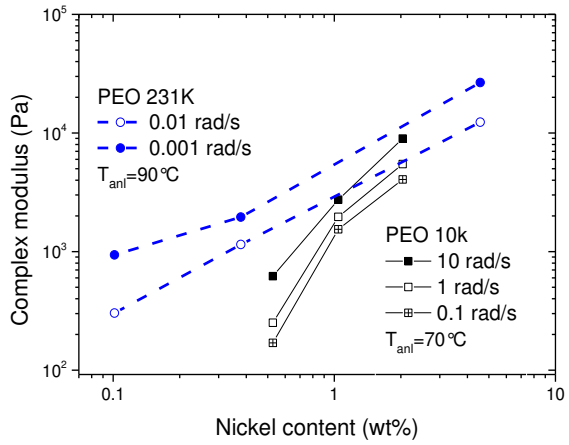

Figure 4.4: The second plateau level against nickel content in PEO $NiCl_2$ exhibits exponential dependence. The shear strain is fixed to 0.1% strain in all measurements.

quency window), the second plateau level strongly increases with small changes in salt content. By contrast, at high concentrations the second plateau almost saturates and becomes independent of salt content.

Assuming that the plateau modulus of pure PEO chains is around 1.45 MPa, as proposed in ref. 29 one can estimate that the level at which the second plateau seems to saturate corresponds to a fraction of roughly 12 $wt\%$ (*i.e.* $\sqrt{G_N^0/10^4}$) of chains trapped into the transient network. This proportion is relatively small compared to the whole polymer.

By adding a large amount of salt, one could have expected a stronger supramolecular gel, in which the relaxation of the whole sample is frozen, but this is not observed. In particular, when 200 eq of $NiCl_2$ are added into the polymer (for PEO 231k 200 eq $NiCl_2$), the level of the second plateau is again around 10^4 Pa, similarly to the value observed with sample PEO 11k. Furthermore, if we focus on sample PEO 231k 200 eq $NiCl_2$, results seem contradictory: on one hand, many complexes are formed, which are able to influence the level of the (first) plateau modulus, but on the other hand, only around 10 $wt\%$ of the chains are not able to relax, being trapped for very long times by these complexes. This result suggests that a large fraction of the complexes is easily destroyed, and that the network partially breaks at short times. In order to better understand the origin of this mechanism, the role played by the amplitude of deformation on the strength of the supramolecular network is investigated in the next point.

Influence of Deformation Amplitude on the Lifetime of the Complexes
In order to determine the influence of the amplitude of deformation on the stability of the complexes created between the metal ions and the oxygen atoms of the PEO chains, amplitude strain sweep data are presented in Figure 4.5

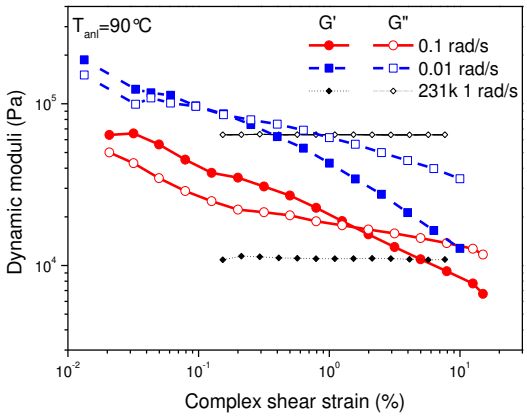

Figure 4.5: Dynamic moduli against shear strain of annealed PEO 231k 200 eq $NiCl_2$ at 0.1 (red) and 0.01 rad/s (blue) and PEO 231k at 1 rad/s (black). For PEO 231k 200 eq $NiCl_2$, the linear viscoelastic region (LVE) is out of reach.

for sample PEO 231k 200 eq $NiCl_2$. Results are surprising: contrary to pure PEO chains, which show a linear response well above 10% of deformation, when adding metal ions, we observe that even at very low deformation amplitudes, the linear regime is out of reach. It seems that any small deformation is sufficient to partially destroy the supramolecular network. Hence, it can be concluded that the PEO-metal ion networks are weak and easy to break.

Due to the inaccessibility of the linear regime, despite the very low level of deformation applied to the sample, the magnitude of shear strain strongly influences the storage and loss moduli in the frequency window where the viscoelastic response is dominated by the transient weak complexation. This is illustrated in Figure 4.6.a: the second, low frequency plateau, which is a measure of the polymer fraction trapped into the supramolecular network at a time equal to the inverse of the frequency, significantly increases when the amplitude of deformation is decreased, and *vice versa*. Thus, the level of the second plateau strongly depends on the amplitude of deformation, more than on the molar mass of the PEO chains (See Figure 4.1 and the corresponding discussion).

Figure 4.6.b shows dynamic moduli of PEO 231k 200 eq $NiCl_2$ at 0.1% shear strain, before and after the amplitude strain sweep measurement presented in Figure 4.5. When performing the amplitude strain sweep up to 10% (See Figure 4.5), a large part of the reversible network breaks down and needs some time to reestablish. It can be seen that after large amplitude shear, a higher fraction of PEO chains is able to flow and no clear plateau is observed at low frequencies. The viscoelastic behavior is entirely reversible, *i.e.* with time, the network reforms and the second plateau is reached again.

Brittle Behavior of the Supramolecular Network

As discussed earlier, the onset of non-linear viscoelasticity is governed by the

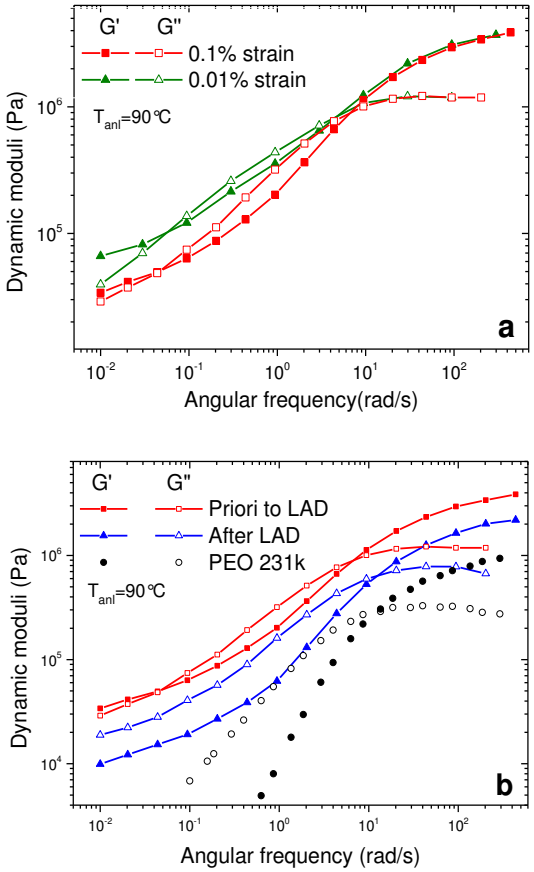

Figure 4.6: Destructive effect of deformation on viscoelastic properties of PEO 231k 200 eq $NiCl_2$ network annealed at 90 $°C$: (a) impact of deformation amplitude in oscillatory shear field on the second plateau, (b) dynamic moduli in oscillatory shear field with 0.1% strain, before and after a large amplitude deformation (LAD).

supramolecular interactions between the metal ions and PEO, which easily break under oscillatory shear. On the other hand the reversible nature of the ion-dipole interactions between PEO and Ni^{2+} ions pushes the network to reform. This autonomous mechanism of network breakage and reformation under shear can be observed by looking at the evolution of the complex modulus with time. This is illustrated in Figure 4.7 for sample PEO $11k$ 2 eq $NiCl_2$: under oscillatory shear at 0.5% amplitude, no stable viscoelastic response is obtained; *i.e.* the network is continuously broken and reformed. This shows the extremely brittle behavior of such supramolecular network. Once the shear amplitude is reduced to 0.05%, the PEO $11k$ 2 eq $NiCl_2$ network can reach one order of magnitude higher elasticity.

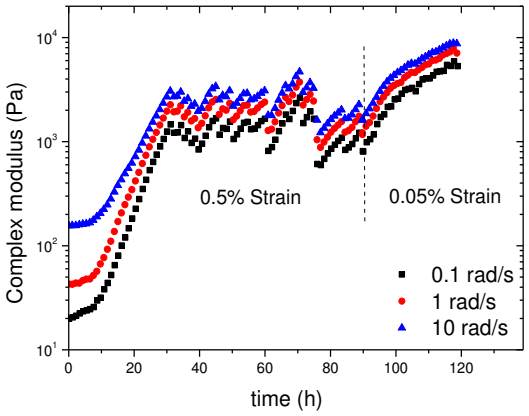

Figure 4.7: Evolution of complex modulus of PEO $11k$ 2 eq $NiCl_2$ with time, at 90 $^{\circ}C$. Flow instabilities occur due to continuous network formation and shear disruption.

This unusual behavior gives high damping capability to PEO-$NiCl_2$ supramolecular networks and makes them novel candidates to be used as shear responsive materials like dampers and shock absorbers at medium temperatures.

Effect of the Counter Ion on the Reversible Network

In order to investigate the effect of counter ion on the rheology of PEO-Ni^{2+} melt, chloride, perchlorate and iodide salts of nickel were incorporated to PEO $11k$ at identical concentrations of 2 ions equivalents. To avoid possible degradation of perchlorate, all three systems were annealed at 70 $^{\circ}C$, in which perchlorate is reported to be stable. Figure 4.8 illustrates the effect of the three counter ions on the viscoelastic behavior of PEO-Ni^{2+} salt systems. PEO-nickel chloride system has the highest elasticity and shows a complex viscoelastic behavior with a second plateau and a transition region in the frequency range of observation, while perchlorate and iodide systems are characterized by a viscous behavior, *i.e.* $\log G^* / \log \omega = 1$. NiI_2, unlike the other two salts, shows no effect on the viscoelastic properties of PEO, even when changing temperature.

In general, success of network formation via PEO-ion complexation depends on the number of chains contributing in each complex (N_{cpx}) and its association time (τ_{cpx}) as well as long range arrangements of the complexes in the PEO melt, *i.e.* crystallization. PEO-ion complexation only leads to network formation if either $N_{cpx} > 1$ or complexes arrange into stable crystalline domains in the PEO melt (see section 4.3.2). It is worth noting that N_{cpx} is a structural parameter of the complex, which depends on the size and charge of both metallic ion and counter ion, and ratio of salt to PEO monomers.[5] The stability of possible crystal domains depends on their melting temperature, which is proportional to the crystal size. For instance, in PEO-$ZnCl_2$ system, in which each cation only binds to two adjacent ether oxygens of a single chain ($N_{cpx} = 1$) and form crystal structures with low melting temperature,[7] no viscoelastic impact on PEO melt was observed.[31]

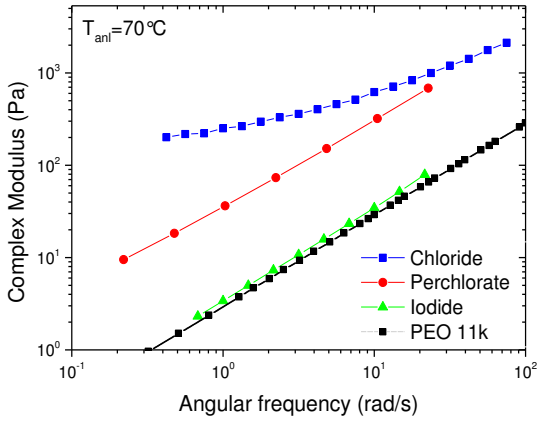

Figure 4.8: Effect of chloride, perchlorate and iodide counter ions on elasticity of PEO-nickel salt system. All samples were annealed at 70 $^{\circ}C$ and contained 2 eq of nickel salts. Contrary to chloride and perchlorate nickel salt, nickel iodide shows no sign of affecting PEO dynamics.

The association time τ_{cpx} is reported to have Vogel-Fulcher-Tammann (VFT) temperature dependency, and can be varied by orders of magnitude via external stimuli.[15] The impact of transient friction of the complex on the chain dynamics depends on the ratio between reptation time of the chain (τ_r) and τ_{cpx}. If $\tau_{cpx} > \tau_r$, reptation mechanism is suppressed in the chains attached to the complex. The relaxation scenario for these chains consists of fluctuations of dangling ends and constraint release Rouse process for strands between complexes. These physically cross-linked strands can also relax by fluctuation at the rhythm of dissociation of the complex. However when $\tau_{cpx} < \tau_r$ chains will be able to reptate once the complex is dissociated, like a branched polymer chain.

To the best of our knowledge among the transition metal salts, only the structures of PEO_4:$ZnCl_2$ and PEO_4:$HgCl_2$ are understood to this date.[7,8] Since the structures of PEO-Nickel complexes are unknown, and taking into account different parameters affecting melt rheology, interpretation of Figure 4.8 is uncertain. In the section 4.3.2, we prove that network formation in PEO-$NiCl_2$ originates from the stable crystalline structure of PEO-ion complexes.

4.3.2 Morphology of PEO-Ni^{2+} Melt

In the previous section, rheology was used to investigate the influence of the PEO-nickel salt complexation on the mechanical properties of PEO melts, and we observed that the elasticity level significantly depends on the annealing temperature (T_{anl}) and on the residence time (t_{anl}). In this section, we discuss the evolution of morphology upon network formation in PEO-$NiCl_2$ melts. Our goal is to acquire structural information about the PEO-$NiCl_2$ complexes, as

well as to understand correlation between the dynamics and microstructure of the network.

The distribution of nickel salt inside PEO matrix was first mapped by EDX, which reveals the dominant effect of annealing at high temperature on the morphology of PEO-$NiCl_2$. Figure 4.9.a shows that fresh PEO $11k$ 2 eq $NiCl_2$ powders, which were prepared by drying solutions of PEO and nickel salt under vacuum, contain large aggregates of metal salts. The size of nickel aggregates exceeds 25 μm in some case, but once the sample is annealed at $90°C$, a homogenous distribution of the salt in the PEO is observed with no residual aggregate (Fig 4.9.b). It is worth noting that the EDX map exaggerates the salt content due to high energy beam charging effects on the polymer matrix and the large number of scans.

Figure 4.10.a shows the diffraction pattern of PEO $231k$ 200 eq $NiCl_2$ at 90 $°C$, before and after annealing at 90 $°C$, in comparison to the diffraction pattern of the pure PEO sample. At 90 $°C$, the pure PEO sample shows an amorphous halo as it is well above its melting point. On the contrary, the WAXS pattern of the annealed PEO 231k 200 eq $NiCl_2$ (which shows highly retarded dynamics with a clear second plateau modulus; see Figure 4.3.b.) shows a number of sharp reflections on top of the PEO amorphous halo. The diffraction angles do not correspond to the crystal structures of PEO or $NiCl_2$, suggesting the formation of a unique crystalline phase of the metallic salt patterned by PEO structure in the melt state. The presence of these peaks suggests that the PEO-nickel complexation acts as driving force for crystallization of the inorganic phase and PEO. The peak center and width of WAXS patterns were used to estimate minimum crystallite sizes using Scherrer model:

$$L = \frac{0.94\lambda}{FWHM(2\theta)\cos(\theta)} \tag{4.1}$$

where $\lambda, 2\theta$ and FWHM(2θ) are the wavelength, the diffraction angle, and the full width at half maximum of the diffraction angle. Table 4.2 summarizes the peak center and full width at half maximum (FWHM), relative intensities and estimated sizes for the diffraction patterns of PEO $231k$ 200 eq $NiCl_2$ and pure PEO $231k$ at different temperatures. Analyzing the width of the diffraction peak of annealed PEO $231k$ 200eq $NiCl_2$ at 19.6 $°2\theta$ with the Scherrer equation yields crystal sizes of 276 and 229 Å at 90 and 25 $°C$ respectively.

Figure 4.10.b shows that the distinct peaks observed in the PEO-$NiCl_2$ melt, can also be unambiguously identified in the diffraction pattern of annealed PEO $231k$ 200 eq $NiCl_2$ measured at room temperature, proving the existence of these specific crystal domains even in the semi crystalline PEO. However, intensities of these peaks are smaller and their width is slightly larger compared to that of the melt (See table 4.2 for more information), presumably due to a destructive effect of the PEO crystallization, similar to the effect of shear presented in section 4.3.1.

Contrary to the annealed PEO $231k$ 200 eq $NiCl_2$, the diffraction pattern of the fresh sample, *i.e.* before its annealing at $90°C$, presents a large number of small peaks besides a single strong reflection at about $14°2\theta$. These peaks are also different from pure PEO or $NiCl_2$, suggesting that another crystalline

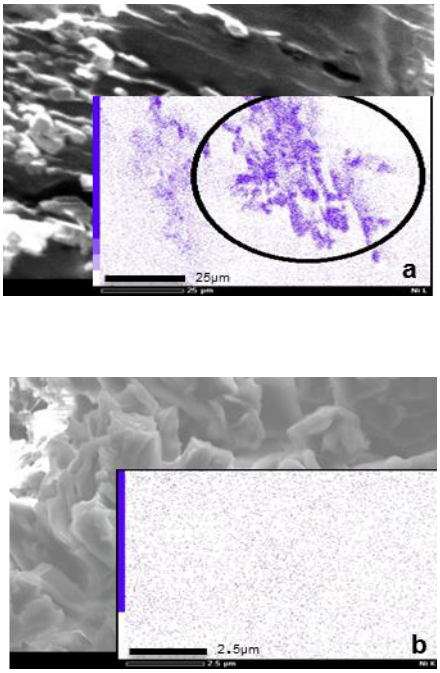

Figure 4.9: SEM and EDX picture of the microstructure of PEO $11k$ 2 eq $NiCl_2$ (a) before and (b) after annealing at 90 $°C$. Unlike the initial state which contains big aggregates of $NiCl_2$, salt is homogenously dispersed in the annealed sample.

form of PEO in conjunction with the metal salt exists, which transforms with time into the structure that produces the strong reflections in the annealed system (See Figure 4.10.a).

Figure 4.11 presents the SAXS patterns of fresh and annealed PEO $231k$ 200 eq $NiCl_2$ at 90 $°C$. We can see that a shoulder is observed in the non-annealed sample, which does not appear in the annealed one. This shoulder, occurring at q-values smaller than 0.1 Å suggests the presence of structural features larger than 6 nm. This length scale may represent a substructure of the actual larger nickel rich morphologies seen by EDX (See Figure 4.9.a). The slope of -4 in the double logarithmic plot of Figure 4.11 for the annealed sample points at the presence of large structures with sharp interfaces and no substructure at the observed SAXS length scale, typical of crystals.

Based on the morphology results, we can conclude that well-defined peaks in the diffraction pattern of the equilibrated PEO metal salt system are due to crystal domains formation induced by PEO-ion complexation. This is in line with the results of Radhakrishnana *et al.*[37,38] who studied complexation of PEO with $CuCl_2$ using WAXS and optical microscopy and reported the formation of crystal domains of inorganic phase assisted by PEO structure

Table 4.2: Analysis of X-ray diffraction data for PEO 231k 200 eq $NiCl_2$ annealed at 90 $^\circ C$, and its PEO precursor

Sample	Peak Center	FWHM	Relative intensity	Crystallite size
	($^\circ 2\theta$)	($^\circ 2\theta$)	(%)	(nm)
PEO 231k	14.8	0.12	2.4	68.1
WAXS at 25 $^\circ C$	15.2	0.19	2.0	45.1
	18.7	0.23	48.1	36.6
	21.6	0.39	21.1	21.7
	22.6	0.67	100.0	12.6
	25.3	0.39	8.8	22.0
	26.0	0.38	9.0	22.5
	26.9	0.29	1.4	29.3
PEO 231k 200 *eq* $NiCl_2$	14.7	0.17	1.4	49.5
	15.1	0.17	1.3	50.1
Annealed at 90 $^\circ C$	15.9	0.35	10.4	23.7
	16.4	0.22	5.5	37.8
WAXS data at 25 $^\circ C$	18.1	0.32	6.2	26.4
	18.7	0.23	35.5	35.8
	19.6	0.37	3.8	22.9
	22.5	0.68	100.0	12.4
	25.3	0.32	7.9	26.6
	26.0	0.29	6.4	29.8
	26.9	0.23	1.6	37.6
	29.7	0.59	6.7	14.5
	31.7	0.41	3.3	20.9
PEO 231k 200 eq $NiCl_2$	15.9	0.25	100.0	34.0
	16.3	0.21	92.6	40.1
Annealed at 90$^\circ C$	19.6	0.31	85.1	27.6
	29.7	0.46	52.8	18.7
WAXS data at 70 and 90 $^\circ C$	31.8	0.56	54.8	15.4

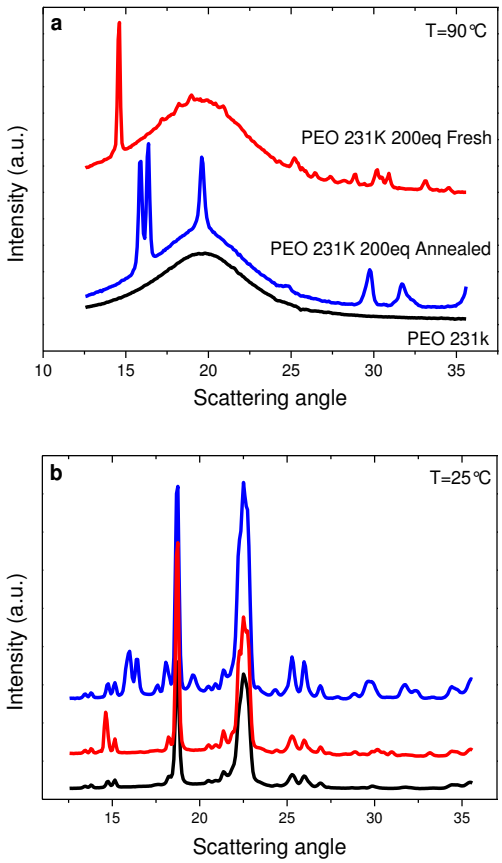

Figure 4.10: Wide angle diffraction pattern of PEO 231k 200 eq $NiCl_2$ before (red) and after annealing (blue) compared to pure PEO 231k (black) at (a) 90 $^{\circ}C$ and (b) 25 $^{\circ}C$.

in the melt. However, they observed nucleation of these emerging patterns only for salt to monomer concentrations higher than 1/8 and at temperatures superior than 100 $^{\circ}C$ while, here, we could observe stable patterns at much lower salt concentrations such as 1/26, using the annealing treatment described in section 4.3.1.

It is also interesting to note that at very low concentrations (such as the 1 : 130 salt/ monomer concentration in sample PEO 11k 2 eq $NiCl_2$, only the amorphous halo of PEO is observed at temperatures higher than its melting point, even though rheology data show enhanced viscoelasticity and the creation of an extended second plateau due to complexation (See Figures 4.2 and 4.3). We believe that this discrepancy is a result of different sensitivity level of each technique.

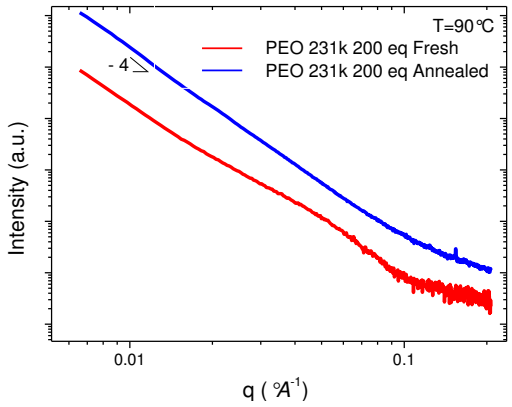

Figure 4.11: Small angle X-ray scattering pattern of PEO $231k$ 200 eq $NiCl_2$ at 90 $^{\circ}C$.

4.3.3 Thermal Stability of the PEO-Ni^{2+} System

Evolution of the dynamics and microstructure of PEO-metal salts above melting temperature of PEO has been continuously investigated for up to 10 days, as it is presented in section 4.3.1. Hence it is critical to ensure that the structure of linear PEO chains is stable enough in these critical conditions and do not experience large scale degradation or crosslinking. Specifically, taking into account thermal-oxidation and photo-degradation of PEO and its coordination complexes with transition metal ions, particularly $NiCl_2$, which have been reported by various authors, [40–47] it is necessary to outline possible structural changes in PEO. Degradation of PEO is characterized by change in molar mass distribution, reduction of melting temperature and heat of fusion, as well as presence of new absorption bands in the FTIR spectrum of PEO. For instance, Scheirs *et al.*[44] studied solid state thermal oxidation of PEO upon aging at 60 $^{\circ}C$ and observed constant decrease in viscosity of the materials over the course of 23 days. They also reported significant morphological changes upon degradation. In another work, Kaczmarek *et al.*[43] investigated photo-degradation of PEO as a function of UV exposure time at ambient temperature. They observed that the presence of $NiCl_2$ can accelerate the photo degradation rate by an order of magnitude. Nonetheless the observed phenomenon was independent of the nickel salt concentration.

Degradation of PEO both by oxygen and by UV exposures is believed to be due to random weak link scission reaction of carbon-oxygen bonds. This has been studied by Afifi-Effat and Hay,[46] who reported that PEO treatment in ethanol for a few minutes stabilizes the polymer which is precipitated from solution. They assigned the origin of degradation of PEO to the decomposition of a limited number of peroxide groups along the chain, formed upon storage in the presence of oxygen. They proposed that ethanol interferes with the chain scission mechanism by converting peroxide to hemi-acetal structures, which are

thermally stable up to 170 $°C$. Han *et al.*[45,48] showed that addition of different anti-oxidants can also suppress thermo-oxidation of PEO melts in air at 80 $°C$.

In addition to thermo-oxidation decomposition, PEO cross-links at high temperature through free radical recombination.[49,50] Taoda *et al.*[49] reported that upon several heating and cooling cycles between $35-150$ $°C$, molar mass distribution of PEO broadened in both sides. They observed that the fraction of high molar mass species formed via crosslinking was much smaller than the low molar mass one, produced by chain scission.[49] The crosslinking reaction is mediated by transition metal salts, which can act as Lewis acids and stimulate reductive coupling.[51]

As a first treatment to enhance PEO stability, polymer and salt solutions were prepared in methanol, as described in Section 4.2. Methanol was carefully selected to prevent PEO degradation as, similarly to ethanol, it reacts with the peroxides which are formed by oxidation of ether bonds upon storage. In addition to the methanol treatment, the PEO samples were extensively dried and kept away from moisture. Our study shows remarkable thermal degradation of PEO when it is annealed in non-dried environment, *e.g.* in an air oven. MALDI-TOF mass spectrometry revealed that both PEO and of PEO $11k$ 2 eq $NiCl_2$, annealed at 90 $°C$ for 72 h in the air oven with ambient moisture, fully degrade into PEO oligomers with molar mass ranging between $500-1200$ g/mol (See Figure 4.12.c). Upon degradation, these PEO samples turn from solid powders into waxy liquids at room temperature, with no melting and crystallization peaks. Hence it is critical to avoid moisture throughout the experiment. This is achieved by annealing the samples in a vacuum oven as well as using extensively dried compressed air to control temperature in the rheometer.

Thermal stability of the nickel salt containing PEO systems was investigated using MALDI-TOF and SEC. While MALDI-TOF has the best precision in low molar mass region (< 5 kg/mol), SEC is powerful in determining distribution of high molar mass fractions. Therefore by combining these two techniques, full spectrum of molar mass distribution can be obtained. The main results are shown in Figure 4.12. First, the molar mass distributions of the PEO $11k$ pure sample and of PEO $11k$ 2 eq $NiCl_2$ sample, which was annealed in the rheometer for 5 days at 90 $°C$, are compared. One can observe that the main distribution around the molar mass of 11000 g/mol remains almost unchanged, though, some indications of minor degradation are observed, which beside thermal-oxidation can occur due to fragmentation during the desorption/ionization process. SEC reveals the presence of a small fraction of higher molar mass PEO chains (See Figure 4.12.d), which cannot be seen in the MALDI-TOF spectrum since it is outside the detectable experimental range. Figure 4.12.f shows that molar mass distribution of PEO $231k$ 200 eq $NiCl_2$ broadens on both sides after 5 days of continuous measurement at 90 $°C$ in the rheometer.

Data in Figure 4.12 confirm that in the experimental conditions of this work, the main molar mass distribution in nickel containing PEO systems is sustained. However a minor fraction of high molar mass chains is observed, which is consistent with the observations in references 49 and 50. Despite

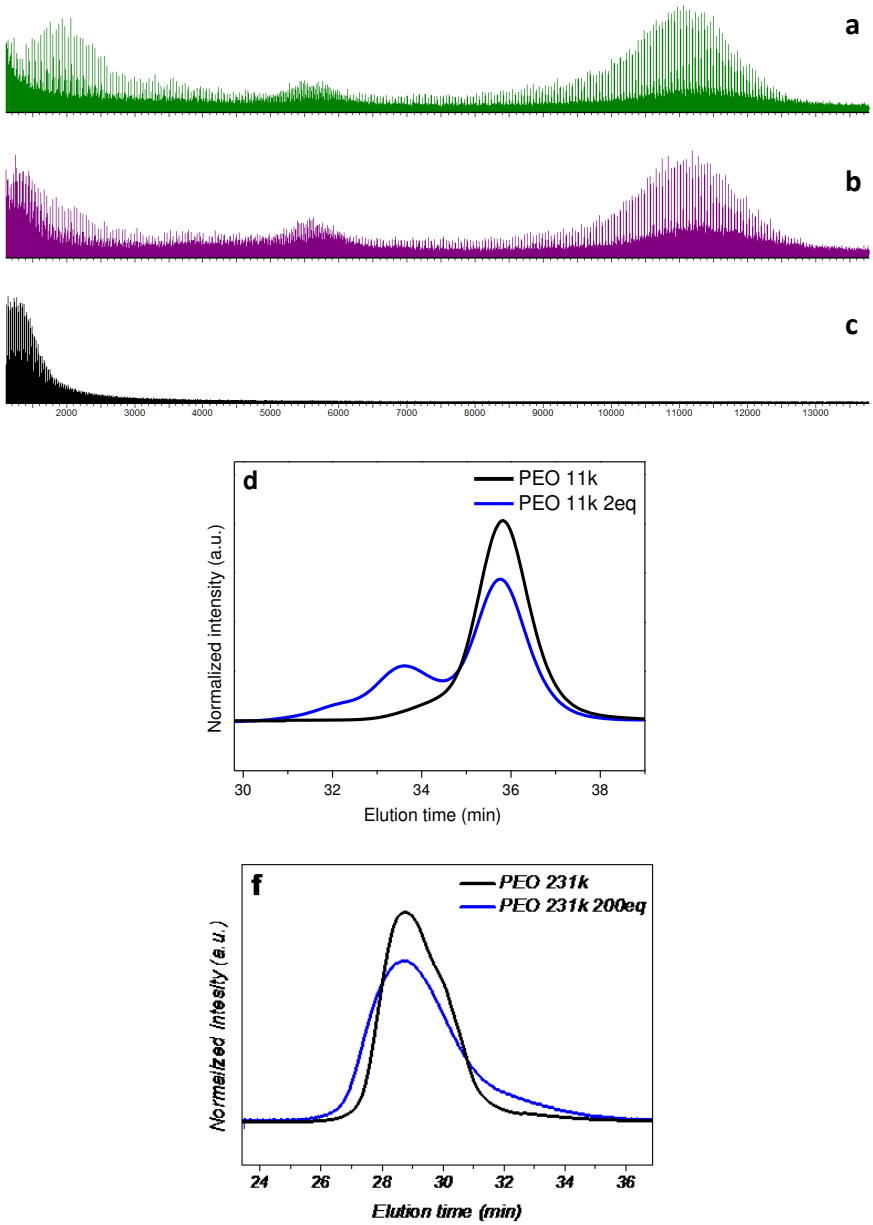

Figure 4.12: MALDI-TOF spectra of (a) pristine PEO 11k and PEO 11k 2 eq $NiCl_2$ annealed at 90 $^{\circ}C$ for (b) 5 days in rheometer and (c) 3 days in a non-dry environment. SEC traces of (d) PEO 11k 2 eq $NiCl_2$ and (f) PEO 231k 200 eq $NiCl_2$, both annealed for 5 days at 90 $^{\circ}C$ in the rheometer.

these structural modifications with time, the PEO-Ni^{2+} systems are stable enough for the analysis proposed in this work. It is worth noting that formation

of a fraction of high molecular weight PEO chains, as shown in Figure 4.12, cannot be attributed to the network formation observed in PEO-$NiCl_2$ systems. Indeed, the covalent networks formed by cross-links are permanent, while the PEO-$NiCl_2$ network is highly reversible, and can be broken by shear and reform in time. Also the relaxation of longer molecules, observed by SEC, is still too fast to lead to a second plateau. Therefore, it can be concluded that the viscoelastic impact of structural changes observed in MALDI-TOF and SEC is negligible, with respect to the dominant effect of PEO-ion complexation.

4.4 Conclusion

PEO nickel salt systems exhibit network formation above the melting temperature of PEO, characterized by a second elastic plateau, beyond the reptation time of PEO chains. The network requires time and high temperature to establish. The level of the second plateau depends on the ion content, molar mass of the PEO chain, temperature and the annealing time. Upon gel formation in PEO-$NiCl_2$ the linear viscoelastic region observed in the strain sweep measurements is reduced and eventually a brittle network is formed. The elasticity of this network strongly depends on any deformation history.
The network formation is attributed to the formation of crystalline structures of PEO-$NiCl_2$ complexes, observed by *X*-ray diffraction spectroscopy. The crystalline domains are surrounded by a matrix of PEO chains. If some chain fractions are trapped between two crystalline domains, they act as bridging chains, leading to the formation of a network. Consequently, a second plateau is observed in the storage modulus.

4.5 Bibliography

1 Marzantowicz, M.; Dygas, J. R.; Krok, F.; Tomaszewska, A.; Czyk, Z. F.; Zygado-Monikowska, E.; Lapienis, G. Star-branched poly(ethylene oxide) $LiN(CF_3SO_2)_2$: A promising polymer electrolyte. *J. Power Sources* **2009**, 194, 51-57.

2 Armand, M. B.; Bruce, P. G.; Forsyth, M.; Scrosati, B.; Wieczorek, W. Polymer electrolytes. In *Energy Materials*; Bruce, D. W., OHare, D., Walton, R. I., Eds.; John Wiley & Sons, Ltd: New York, 2011.

3 Ren, C.; Tian, W.; Szleifer, I.; Ma, Y. Specific salt effects on poly(ethylene oxide) electrolyte solutions. *Macromolecules* **2011**, 44, 1719-1727.

4 Stephan, A. M.; Kumar, T. P.; Kulandainathan, M. A.; Lakshmi, N. A. Chitin-incorporated poly(ethylene oxide)-based nanocomposite electrolytes for Lithium batteries. *J. Phys. Chem. B* **2009**, 113, 1963-1971.

5 Bruce, P. G. Ion-polyether coordination complexes: crystalline ionic conductors for clean energy storage. *Dalton Trans.* **2006**, 1365-1369.

6 Niklasson, G. A. Proton diffusion in polyethylene oxide: Relevance to electrochromic device design. *Sol. Energy Mater. Sol. Cells* **2008**, 92, 1293-1297.

7 Staunton, E.; Christie, A. M.; Martin-Litas, I.; Andreev, Y. G.; Slawin, A. M. Z.; Bruce, P. G. Structure of the poly(ethylene oxide)zinc chloride complexes. *Angew. Chem.* **2004**, 116, 2155-2157.

8 Iwamoto, R.; Saito, Y.; Ishihara, H.; Tadokoro, H. Structure of poly(ethylene oxide) complexes. II. Poly(ethylene oxide)mercuric chloride complex. *J. Polym. Sci., Part A-2: Polym. Phys.* **1968**, 6, 1509-1525.

9 MacGlashan, G. S.; Andreev, Y. G.; Bruce, P. G. Structure of the polymer electrolyte poly(ethylene oxide)$_6$:$LiAsF_6$. *Nature* **1999**, 398, 792-794.

10 Staunton, E.; Christie, A. M.; Andreev, Y. G.; Slawin, A. M.; Bruce, P. G. The structure of poly(ethylene oxide)$_8$:$NaBPh_4$ from a single crystal oligomer and polycrystalline polymer. *Chem. Commun.* **2004**, 2, 148-149.

11 Andreev, Y. G.; MacGlashan, G. S.; Bruce, P. G. Ab initio solution of a complex crystal structure from powder-diffraction data using simulated-annealing method and a high degree of molecular flexibility. *Phys. Rev. B* **1997**, 55, 12011.

12 Thomas, K.; Koster, J.; van Wullen, L. Cationanion coordination, ion mobility and the effect of Al_2O_3 addition in PEO based polymer electrolytes. *Solid State Ionics* **2010**, 181, 489-495.

13 Niedzwiedz, K.; Wischnewski, A.; Pyckhout-Hintzen, W.; Allgaier, J.; Richter, D.; Faraone, A. Chain dynamics and Viscoelastic properties of poly(ethylene oxide). *Macromolecules* **2008**, 41, 4866-4872.

14 Tudryn, G. J.; OReilly, M. V.; Dou, S.; King, D. R.; Winey, K. I.; Runt, J.; Colby, R. H. Molecular mobility and cation conduction in polyether-estersulfonate copolymer ionomers. *Macromolecules* **2012**, 45, 3962-3973.

15 Chen, Q.; Liang, S.; Shiau, H.; Colby, R. H. Linear viscoelastic and dielectric properties of phosphonium siloxane ionomers. *ACS Macro Lett.* **2013**, 2, 970-974.

16 Chen, Q.; Masser, H.; Shiau, H. S.; Liang, S.; Runt, J.; Painter, P. C.; Colby, R. H. Linear viscoelasticity and Fourier transform infrared spectroscopy of polyetherestersulfonate copolymer ionomers. *Macromolecules* **2014**, 47 (11), 3635-3644.

17 Yanga, X. Q.; Leea, H. S.; Hansona, L.; McBreena, J.; Okamoto, Y. Development of a new plasticizer for poly(ethylene oxide)-based polymer electrolyte and the investigation of their ion-pair dissociation effect. *J. Power Sources* **1995**, 54, 198-204.

18 Matsumiya, Y.; Balsara, N. P.; Kerr, J. B.; Inoue, T.; Watanabe, H. In situ dielectric characterization of poly(ethylene oxide) melts containing lithium perchlorate under steady shear flow. *Macromolecules* **2004**, 37, 544-553.

19 Ries, M. E.; Brereton, M. G.; Cruickshank, J. M.; Klein, P. G.; Ward, I. M. NMR study of poly(ethy1ene oxide) complexes with $LiCF_3SO_3$. *Macromolecules* **1995**, 28, 3282-3289.

20 Ries, M. E.; Klein, P. G.; Brereton, M. G.; Ward, I. M. Proton NMR study of Rouse dynamics and ideal glass transition temperature of poly(ethylene oxide) $LiCF_3SO_3$ complexes. *Macromolecules* **1998**, 31, 4950-4956.

21 Chen, Q.; Tudryn, G. J.; Colby, R. H. Ionomer dynamics and the sticky Rouse model. *J. Rheol.* **2013**, 57 (5), 1441-1462.

22 Weiss, R. A.; Yu, W. C. Viscoelastic behavior of very lightly sulfonated polystyrene ionomers. *Macromolecules* **2007**, 40, 3640-3643.

23 Colby, R. H.; Zheng, X.; Rafailovich, M. H.; Sokolov, J.; Peiffer, D. G.; Schwarz, S. A.; Strzhemechny, Y.; Nguyen, D. Dynamics of lightly sulfonated polystyrene ionomers. *Phys. Rev. Lett.* **1998**, 81, 3876-3879.

24 Fustin, C.-A.; Guillet, P.; Misner, M. J.; Russell, T. P.; Schubert, U. S.; Gohy, J.-F. Self-assembly of metallo-supramolecular block copolymers in thin films. *J. Polym. Sci., Part A: Polym. Chem.* **2008**, 46, 4719-4724.

25 Brassinne, J.; Stevens, A. M.; Van Ruymbeke, E.; Gohy, J.-F.; Fustin, C.-A. Hydrogels with dual relaxation and two-step gelsol transition from heterotelechelic polymers. *Macromolecules* **2013**, 46(22), 9134-9143.

26 Weng, W.; Li, Z.; Jamieson, A. M.; Rowan, S. J. Control of gel morphology and properties of a class of metallo-supramolecular polymers by good/poor solvent environments. *Macromolecules* **2009**, 42, 236-246.

27 Kumpfer, J. R.; Wie, J. J.; Swanson, J. P.; Beyer, F. L.; Mackay, M. E.; Rowan, S. J. Influence of metal ion and polymer core on the melt rheology of metallosupramolecular films. *Macromolecules* **2012**, 45 (1), 473-480.

28 Schmatloch, S.; van den Berg, A. M. J.; Alexeev, A. S.; Hofmeier, H.; Schubert, U. S. Soluble high-molecular-mass poly(ethylene oxide)s via self-organization. *Macromolecules* **2003**, 36, 9943-9949.

29 Goldansaz, H.; Voleppe, Q.; Pioge, S.; Fustin, C.-A.; Gohy, J.-F.; Brassinne, J.; Auhl, D.; van Ruymbeke, E. Controlling the melt rheology of linear entangled metallo-supramolecular polymers. *Soft Matter* **2015**, 11, 762-774.

30 Goldansaz, H.; van Ruymbeke, E.; Gohy, J.-F.; Fustin, C.-A.; Ries, M. E.; Bailly, C. Local molecular dynamics and heterogeneity in PEO-$NiCl_2$ supramolecular networks. *Macromolecules* **2015**, 48, 2290-2298.

31 Auhl, D.; Rasson, A.; Degefa, D. G.; Pioge, S.; Mugemana, C.; Fustin, C. A.; Gohy, J. F.; Bailly, C.; E. Van Ruymbeke. Rheological properties of transient networks from telechelic four-arm star poly(ethylene-oxide) with supramolecular metal-ligand interactions. *In preparation.*

32 Evans, R. M. L.; Tassieri, M.; Auhl, D.; Waigh, T. A. Direct conversion of rheological compliance measurements into storage and loss moduli. *Phys. Rev. E* **2009**, 80, 012501.

33 Vandi, L. J.; Hou, M.; Veidt, M.; Truss, R.; Heitzmann, M.; Paton, R. Interface diusion and morphology of aerospace grade epoxy co-cured with thermoplastic polymers. *ICAS*, **2012**.

34 Gommes, C. J.; Goderis, B. CONEX, a program for angular calibration and averaging of two-dimensional powder scattering patterns. *J. Appl. Crystallogr.* **2010**, 43, 352-355.

35 Brassinne, J.; Gohy, J.-F.; Fustin, C.-A. Controlling the cross-linking density of supramolecular hydrogels formed by heterotelechelic associating copolymers. *Macromolecules* **2014**, 47 (13), 4514-4524.

36 Stadler, F. J.; Pyckhout-Hintzen, W.; Schumers, J.-M.; Fustin, C.-A.; Gohy, J.-F.; Bailly, C. Linear viscoelastic rheology of moderately entangled telechelic polybutadiene temporary networks. *Macromolecules* **2009**, 42 (16), 6181-6192.

37 Radhakrishnan, S.; Schultz, J. M. Polymer-induced crystallization of inorganic salts: PEO-CuCl2. *J. Cryst. Growth* **1992**, 116, 378-386.

38 Radhakrishnan, S. Polymer induced crystallization III. PEO-CdCl2 and in situ formation of PEOCdS composite. *J. Cryst. Growth* **1994**, 141, 437-442.

39 Meurant, G. *Crystal Structure and Morphology*; Academic Press: New York, 1980.

40 Fares, M. M. ; Hacaloglu, J. ; Suzer, S. Characterization of degradation products of polyethylene oxide by pyrolysis mass spectrometry. *European Polymer Journal* **1994**, 30(7) 845-850.

41 Rabek, J. F.; Lindn, L. Å.; Kaczmarek, H.; Qu, B. J.; Shi, W. F. Photodegradation of poly(ethylene oxide) and its coordination complexes with iron(III)chloride. *Polymer Degradation and Stability* **1992**, 37(1) 33-40.

42 Kaczmarek, H.; Sionkowska, A.; Kamiska, A.; Kowalonek, J.; witek, M.; Szalla, A. The influence of transition metal salts on photo-oxidative degradation of poly(ethylene oxide). *Polymer Degradation and Stability* **2001**, 73(3) 437-441.

43 Kaczmarek, H.; Kamiska, A.; Kowalonek, J.; Szalla, A. Changes of poly(ethylene oxide) photostability by doping with nickel(II) chloride. *Journal of Photochemistry and Photobiology A: Chemistry* **1999**, 128(1-3) 121-127.

44 Scheirs, J.; Bigger, S. W.; Delatycki, O. Characterizing the solid-state thermal oxidation of poly(ethylene oxide) powder. *Polymer* **1991**, 32(11) 2014-2019.

45 Han, S.; Kimb, C.; Kwon, D. Thermal degradation of poly(ethylene glycol). *Polymer Degradation and Stability* **1995**, 41, 203-208.

46 Afifi-Effat, A. M.; Hay, J. N. The thermal stabilization of polyethylene oxide. *European Polymer Journal* **1972**, 8(2) 289-297.

47 Yang, L.; Heatley, F.; Blease, T. G.; Thompson, R. I. G. Study of the mechanism of the oxidative thermal degradation of poly(ethylene oxide) and poly(propylene oxide) using H1 and C13 NMR. *European Polymer Journal* **1996**, 32(5) 535-547.

48 Han, S.; Kim, C.; Kwon, D. Thermal/oxidative degradation and stabilization of polyethylene glycol. *Polymer* **1997**, 38 (2) 317-323.

49 Taoda, H.; Hayakawa, K.; Kawase, K.; Kosaka, M. Thermal oxidative aging of poly(ethylene oxide) used as latent-heat-type thermal storage material. *Kobunshi Ronbunshu* **1986**, 43, 353-359.

50 Lai, W.-C. ; Liau, W.-B. Thermo-oxidative degradation of poly(ethylene glycol)/poly(l-lactic acid) blends. *Polymer* **2003**, 44 (23) 8103-8109.

51 Pike, R. D.; Starnes, W. H.; Jeng, J. P.; Bryant, W. S.; Kourtesis, P.; Adams, C. W.; Bunge, S. D.; Kang, Y. M.; Kim, A. S.; Macko, J. A.; O'Brien, C. P. Low-valent metals as reductive cross-linking agents: a new strategy for smoke suppression of poly(vinyl chloride). *Macromolecules* **1997**, 30, 6957-6965.

Chapter 5

Local Molecular Dynamics and Heterogeneity in PEO-$NiCl_2$ Supramolecular Networks

Outline

The melt dynamics of PEO -$NiCl_2$ systems are analyzed by proton NMR relaxometry and rheology. A consistent picture of the corresponding microstructure is proposed based on the combined results. Rheology reveals the presence of a weak gel due to PEO-metallic salt complexation, evidenced by a low second storage modulus plateau ($< 10^4 \ \ Pa$) well below the timescale of PEO terminal relaxation. NMR relaxometry shows that transverse magnetization relaxes faster with increasing salt content. Eventually a bi-exponential behavior is observed, manifesting the coexistence of two distinct environments, with slow and fast dynamics. The chain dynamics in the slow (hindered) domains is temperature, salt content and molecular weight independent within experimental limits, whereas the fast (mobile) domains exhibit similar properties to that of pure PEO. The size of the hindered domains is calculated to be at least 4 times larger than that of the PEO chains, proving that hindered domains encompass many chains. The fraction of hindered domains shows an experimental upper limit of 63%. Based on these observations we propose a microstructure picture for the PEO-$NiCl_2$ gels in which PEO chains are bound together via PEO-metallic salt complexes, and eventually form hindered mobility clusters. These clusters are immersed in the matrix of PEO (mobile domains). In this microstructure picture, in the linear viscoelastic regime the terminal flow of the PEO-$NiCl_2$ system is dominated by the dynamic constraint of PEO-$NiCl_2$ complexes, which arrest a fraction of PEO segments.

5.1 Introduction

In chapter 4 we demonstrated that the interactions between $NiCl_2$ and PEO leads to gel formation. These gels exhibits a second plateau after the plateau modulus of PEO which originates from long complexation time between Ni^{2+} cations and PEO ether oxygens. The system exhibits highly prolonged terminal relaxation time or no terminal relaxation depending on the ion concentration, degree of distribution and molecular weight of the polymer. Another key observation in the previous chapter was the alteration of segmental motion of PEO, manifested by the departure of the plateau modulus of the PEO-salt network from the one of PEO at high salt concentrations. To reach the main objective of this work, *i.e.* understanding the effect of transient supramolecular interactions on chain dynamics over entire timescales, a detailed investigation of the segmental mobility of the PEO-$NiCl_2$ is desired. Nonetheless there are several limitations in studying molecular dynamics of PEO-metal salt systems via rheometry. Primarily crystallinity of PEO and thermo-rheological complexity of PEO-$NiCl_2$ system prevent us from acquiring information about segmental dynamics of PEO chains in the annealed system at low temperature. In addition, the brittle nature of the network disables us from obtaining linear viscoelastic data, which is needed for a quantitative analysis. Therefore we use NMR relaxometry to acquire quantitative information about the molecular motion of these systems.

Ries *et al.*[1,2] investigated Rouse dynamics of PEO-$LiCF_3SO_3$ complexes in the melt using proton NMR relaxometry. They reported that PEO-Lithium complexation hinders Rouse dynamics of the chain but neither alters the entanglement molecular weight, M_e, nor the size of the smallest statistical (Kuhn) segment. Ries *et al.* concluded that the conformation of PEO chains remains intact upon formation of PEO-$LiCF_3SO_3$ complexes, meaning that complexes do not act as physical crosslinks.

Contrary to the PEO-$LiCF_3SO_3$ systems, in PEO-$NiCl_2$ ones we evidenced decrease of M_e, due to PEO-metallic salt complexation, proving that PEO-Ni^{2+} complexes can act as physical crosslinks.[3,4] Unlike PEO-$LiCF_3SO_3$ systems where no network microstructure was observed, our viscoelastic studies suggest two separate network length scales for the PEO chains in the presence of Ni^{2+} cations as observed from the increase of the plateau modulus and the formation of a second plateau.

In this work we aim to investigate the PEO segmental dynamics in the PEO-$NiCl_2$ networks using NMR relaxometry. Specifically we quantitatively study the relaxation of PEO strands adjacent to and far from PEO-metal complexes. The effect of temperature on the dynamics of each of these strands is also reported. In addition, we quantitatively determine the length scale below which the system is heterogeneous due to the PEO-metal interactions. Density, approximate size and vicinity of local homogenous domains are quantified from the transverse NMR relaxation decays. Finally, we present a conclusive microstructure picture for PEO-$NiCl_2$ systems which is consistent with the local and bulk dynamic observations made by NMR transverse relaxometry and rheology, correspondingly.

5.2 Materials and Methods

PEO-$NiCl_2$ samples were prepared using the same method described in section 4.2.

The paramagnetic properties of absorbed oxygen can cause the decay of PEO nuclear magnetization. Hence, oxygen must be thoroughly removed. NMR tubes containing the PEO-metallic salt samples, while attached to a vacuum line, were put through a number of freeze-melt cycles using liquid nitrogen and boiling water. The tubes were then sealed without breaking the vacuum and placed in an oven at 90 $^{\circ}C$ at least for 48 h to give PEO-$NiCl_2$ the time to establish a network and reach equilibrium, as reported in our previous work.[4]

To quantify the ion content, we define the ion equivalence as the number of metallic ions per PEO repeating unit (which is identical to metal/oxygen ratio). In order to identify samples, we use the $''$PEO $X_k - Y$ $''$ formalism, in which X and Y represent the rounded number average molar mass of PEO in kg/mol and ion equivalence, respectively. Table 5.1 summarizes the samples used in this work.

A MARAN bench-top pulse NMR analyzer, manufactured by Resonance Instruments Ltd, U.K., operating at 20 MHz for protons, was used to acquire data. The transverse relaxation was measured by the Carr-Purcell-Meiboom-Gill (CPMG) sequence:

$$90_x - \tau - (180_y - 2\tau)_n$$

This is a sequence that self-compensates for errors in pulse widths at every second echo.[5] The 90_x pulse width was optimized for each sample at every temperature and was typically 3.8 μs. The time between echoes 2τ was ~ 1 ms depending on the rate of decay of the signal. A thousand echoes were used to record the complete decay of the transverse magnetization. Each free induction decay is the result of 100 averaged scans with a recycle delay at least 5 times the longitudinal relaxation time. The recovery of the longitudinal relaxation was measured with the inversion-recovery pulse sequence:[5]

$$180_x - \tau_{var} - 90_x; \quad 0 \leq \tau_{var} \leq 5T_1$$

When single exponential decay did not provide satisfactory fitting, longitudinal and transverse data were adequately fitted by bi-exponential functions with two characteristic time scales and a weight fraction, optimized by least square regression.

$$LM(t) = 1 - 2[A\exp(\frac{-t}{T_{1f}}) + (1-A)\exp(\frac{-t}{T_{1s}})] \tag{5.1}$$

$$TM(t) = B\exp(\frac{-t}{T_{2f}}) + (1-B)\exp(\frac{-t}{T_{2s}}) \tag{5.2}$$

where $LM(t)$ and $TM(t)$ describe the recovering longitudinal and decaying transverse magnetization $vs.$ time, respectively. A and B are the weight fractions of the fast relaxation process, T_{1f}, T_{2f}, T_{1s} and T_{2s} are the time scales of

Table 5.1: Number (M_n), weight (M_w) average molar mass and polydispersity index (PDI) of pure PEO as well as the concentration of $NiCl_2$ in the samples used in this work.

Name	M_n	M_w	PDI	$NiCl_2$ equivalence
	g/mol	g/mol		$ion/monomer$
$0.35k$	-	350	-	1.8, 1.48, 1.71, 1.95
$0.75k$	-	750	-	1.18, 1.48, 1.71, 1.95
$2k$	1954	2047	1.05	1.8, 1.18, 1.48, 1.71, 1.95
$3k$	2532	2736	1.08	1.48, 1.71, 1.95
$4k$	3827	4014	1.05	1.48, 1.71, 1.95
$5k$	4731	4942	1.04	1.48, 1.71, 1.95
$11k$	10336	11159	1.08	1.18, 1.48, 1.71, 1.130, 1.260

the longitudinal and transverse magnetization for fast and slow processes. Viscoelastic properties of the PEO-metallic salt systems were investigated using the same method described in section 4.2.

5.3 Results and Discussion

5.3.1 Rheology

A detailed discussion of the viscoelastic behavior of PEO-metallic systems was reported in the previous chapter. However to make this chapter self-contained and to account for different samples used in this work, we briefly present the rheological characterization of the highest molecular weight PEO ($M_w = 11 \ \ kg/mol$) used in this study.

The complex modulus of the PEO $11k$ samples equilibrated with various amounts of nickel chloride is shown in Figure 5.1. While the pure PEO shows a slope of 1 *vs.* frequency, indicating Newtonian behavior, the nickel containing samples exhibit a gel behavior. The plateau, which is located beyond the reptation time of the PEO chains and has a very low value compared to the plateau modulus of PEO ($\sim 1.8 \ \ MPa$), is a consequence of the complexation between ether oxygen atoms of PEO chains and divalent transition metals. The life time of PEO-metal ion complexes is much longer than the reptation time of the PEO chains, as complex formation hinders chain mobility and eventually jams the system at high concentration. It can be seen that the level of the plateau observed in PEO-Ni^{2+} systems increases upon increasing salt content.

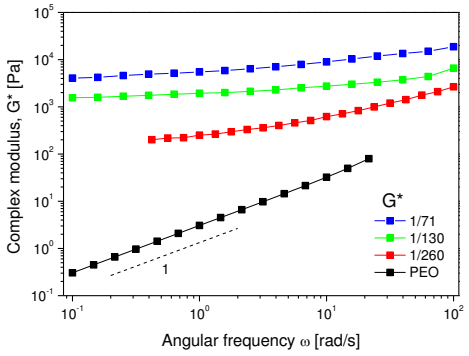

Figure 5.1: Complex modulus vs. angular frequency of PEO $11k$ with different amount of nickel chloride salt. PEO-nickel systems exhibit gel like behavior.

5.3.2 NMR Relaxometry

Figure 5.2 illustrates the effect of nickel salt on the T_2 relaxation signal of PEO $2k$. Upon increasing ion content, the T_2 relaxation time is decreased, though the transverse relaxation signals can still be well represented by a single exponential decay. Eventually, at higher concentrations, the relaxation becomes bi-exponential. This feature is more and more pronounced upon further addition of the salt. Figure 5.3 shows similar trend in transverse magnetization decay of PEO $11k$ with different concentrations of nickel chloride salt at different temperatures.

T_1 relaxation signals exhibit a parallel trend to T_2 , *i.e.* the higher the ion content, the smaller the T_1 relaxation times. T_1 relaxation also decomposes into a bi-exponential function at high salt concentration. In other words, incorporation of ions drastically increases the local microviscosity of the PEO-$NiCl_2$ system, as reported above and in our previous work. However, the ion content threshold for the onset of T_1 bi-exponential behavior is higher than that for the T_2 relaxation. Meaning that at medium concentrations in which T_2 relaxation exhibits bi-exponential features, T_1 signals are still adequately described by a single exponential decay. This is to be expected, as the T_1 measurement averages over the local environment, because it is sensitive to the spectral density of motion occurring around each proton (spin-lattice interactions), whereas T_2 relaxation is more sensitive to the local dynamics of the chain that the proton is attached to (spin-spin interactions) and therefore reveals inhomogeneities in the system.

As the question of the bi-exponential decay of transverse magnetization at low salt concentrations is rather central to our interpretation, we have done additional NMR experiments to clarify the situation. As a matter of fact, fast relaxing components, *i.e.* signals with relaxation times much shorter than that of the echo time, are not effectively refocused by the CPMG spin-echo sequence. The solid echo pulse sequence (SEPS), in contrast, can reveal these

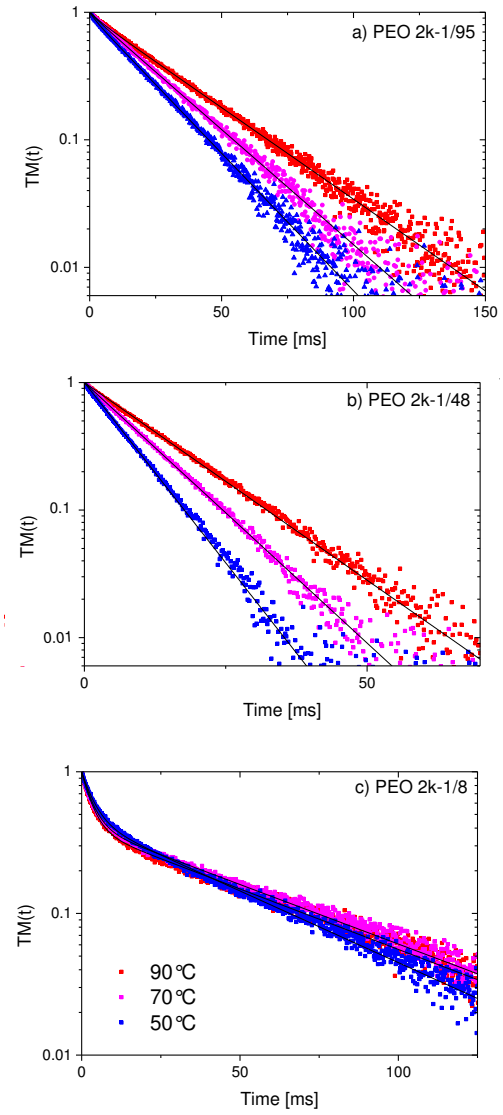

Figure 5.2: Transverse magnetization decay of PEO $2k$ with different concentrations of nickel chloride salt (a) 1/95, (b) 1/48 and (c) 1/8 at different temperatures. Upon increasing ion content, T_2 relaxation time decreases significantly and eventually the relaxation shows strong bi-exponential features. Lines are fits of the decaying signal using equation (5.2).

rapidly relaxing signals. It must be noted though that the ratio between the fractions of fast and slow relaxing components can still be incorrectly estimated by the SEPS because of incomplete refocusing of dipolar interactions. Figure

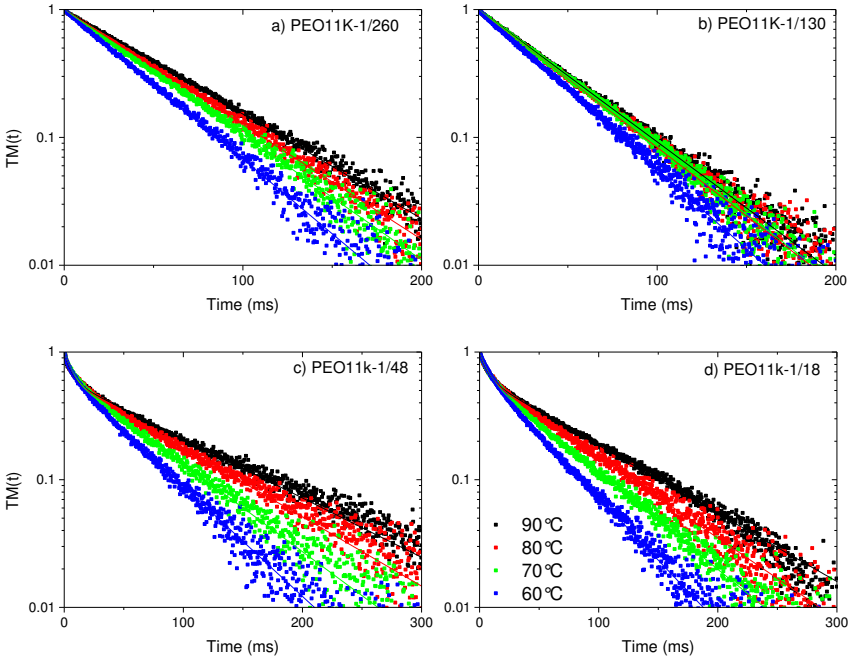

Figure 5.3: Transverse magnetization decay of PEO 11k with different concentrations of nickel chloride salt at different temperatures.

5.4 shows that while in PEO 2k-1/48 CPMG does not capture bi-exponential decay, SEPS proves existence of a small fraction of a fast decaying component.

The T_2 relaxation of oligomers is usually described by a single exponential function that arises from the averaging across all the Rouse modes as described by Brereton[6] and demonstrated experimentally.[1,2,7] On the other hand, a bi-exponential behavior can be assigned to several phenomena, *e.g.* bimodal distribution of molecular weights, difference in mobility of chain segments due to physical or chemical crosslinks, case specific interactions between chains such as end to end hydrogen bonding, coupling between the molecular mobility of the chains and possible contaminations or solvent residues (which can result in a distribution of the correlation times), phase separation or crystallization.[8–15]

In our systems, the significant influence of nickel salt concentration on the shape of both the transverse and longitudinal relaxations (from mono- to bi-exponential behavior as salt concentration increases) as well as the corresponding effect on time scales (see below) strongly suggest that PEO-Ni^{2+} complexation along the PEO chains is the main reason behind the bi-exponential relaxations. As described in the rheology section, supramolecular association between Ni^{2+} and PEO results in higher elasticity and eventually arrests the flow above the melting point. This gelation mechanism induces a second plateau of the dynamic storage modulus *vs.* frequency with correspondingly retarded terminal relaxation.

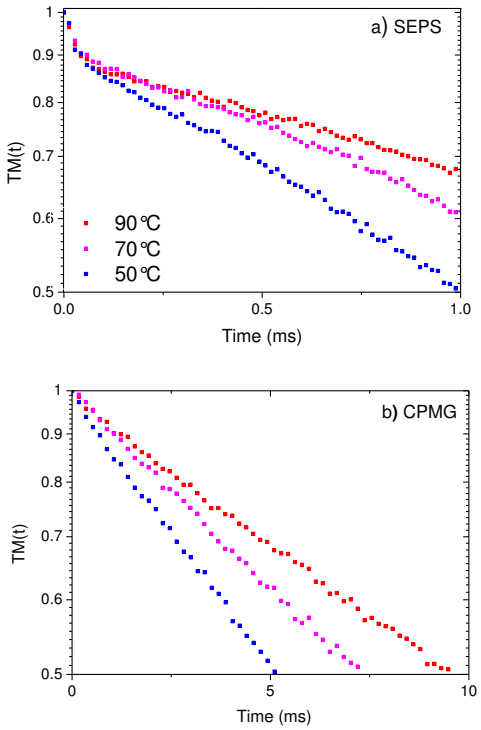

Figure 5.4: FID signal of transverse magnetization of PEO $2k$-1/48 using (a) solid echo pulse sequence (SEPS) and (b) Carr-Purcell-Meiboom-Gill sequence (CPMG).

Using equations (5.1) and (5.2), longitudinal and transverse relaxation times can be extracted. Figure 5.5 shows T_1 and T_2 for PEO $11k$ with different ion contents against reciprocal temperature. According to the theoretical result from the Rouse model, reciprocal T_2 is proportional to the longest Rouse relaxation time of the polymer chain,

$$\frac{1}{T_2} = \frac{6\Delta^2}{\pi}\tau_R \ln(N) \tag{5.3}$$

where Δ delta is the dipolar interaction strength, and N is the number of Rouse segments in the chain.
As the experimental temperature range $(90 - 60\ \ ^\circ C)$ is far from the glass transition of PEO, we can describe the temperature dependent Rouse relaxation time by the Arrhenius formalism over this limited range.

$$\tau_R = \tau_0 \exp(\frac{\Delta E}{RT}) \tag{5.4}$$

where ΔE is the activation energy in J/mol, τ_0 is the relaxation time in the limit that ΔE goes to zero and R is the ideal gas constant.

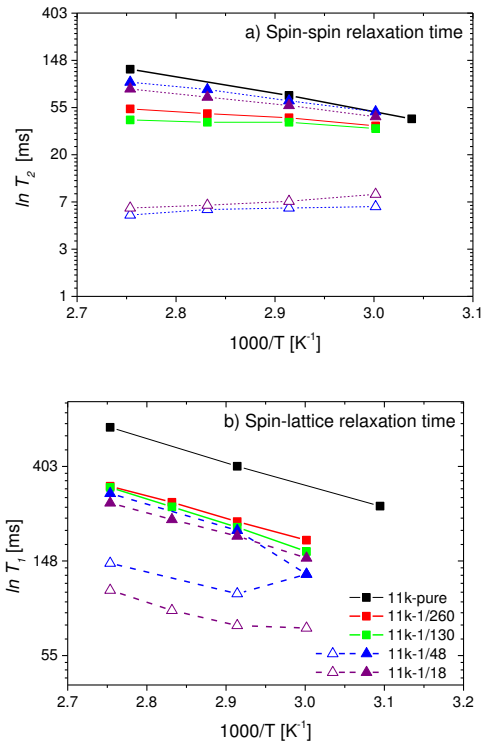

Figure 5.5: (a) Transverse and (b) longitudinal relaxation times of PEO 11k with different ion contents *vs.* reciprocal temperature. While in 1/260 and 1/130 solely single exponential decay of magnetization is observed (closed squares), at higher concentrations, *i.e.* 1/48 and 1/8, bi-exponential decays, with slow (closed triangles) and fast (Open triangles) relaxing components, are found.

Combining equations (5.3) and (5.4), one finds that the plot of $\ln(T_2)$ against reciprocal temperature is proportional to the activation energy of the Rouse relaxation of PEO chains. According to Figure 5.5, PEO-Ni^{2+} complexation, even at ion equivalence as low as 1/260 ,not only reduces T_2 relaxation time, but also significantly decreases the apparent activation energy of segmental motions of PEO chains.

In Figures 5.5.a and 5.6, decomposition of T_2 reveals two distinct dynamics at high salt concentrations. The fast decaying dynamic is entirely temperature independent, whereas the slow one exhibits pure PEO-like temperature dependence. Furthermore, T_2 of the slow decaying component in bi-exponential samples is higher than that of any of the single exponent ones *i.e.* PEO 11k-1/260 and PEO 11k-1/130, which evidently decreases as ion content increases.
Similarly to transverse magnetization, Figure 5.7 shows that the longitudinal retardation signal of PEO also exhibit bi-exponential behavior upon addition of nickel salt. It cannot be assumed a-priori that bi-exponential behavior of

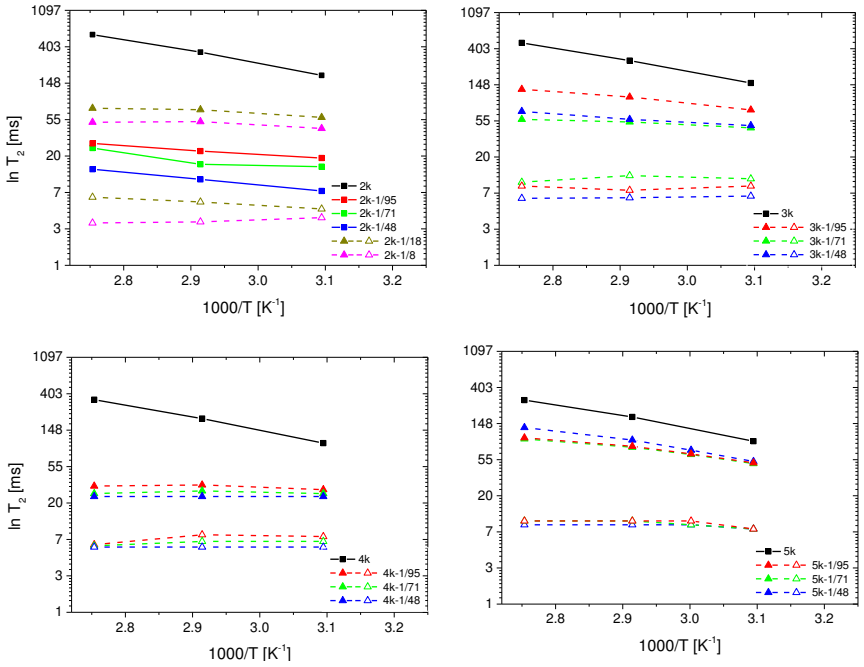

Figure 5.6: Transverse relaxation times of PEO-$NiCl_2$ systems *vs.* reciprocal temperature at different ion contents. Single exponent relaxation times are illustrated with closed squares. Bi-exponential ones are presented with closed and open triangles corresponding to mobile and hindered domains, respectively.

the spin-lattice and the spin-spin relaxations are due to the same processes occurring within a sample. For a simple liquid system that follows the classical Bloembergen-Purcell-Pound theory it is true that the fluctuating magnetic fields that determine the measured T_1 time also determine the measured T_2 time. In a more complex system such as an entangled polymer melt above its glass transition temperature, a mono-exponential spin-lattice relaxation signal is observed, whilst the transverse relaxation becomes bi-exponential and indeed adopts a more complex algebraic form on the increase of the molecular weight of the chains constituting the entangled melt.[6] The claim that the two NMR bi-exponential regimes are concomitant in our work is a-posteriori. On the addition of salt both NMR relaxation signals develop a bi-exponential form. The weight fractions determined from the spin-lattice and the spin-spin bi-exponential relaxation fits coincide, within experimental uncertainty, and do so as a function of salt concentration, molecular weight and temperature. It is this correlation between the fitting parameters that leads us to suggest that both relaxation signals are a result of the same processes within our samples. These observations suggest the coexistence of two dynamic environments in PEO-$NiCl_2$ systems. The first environment is highly affected by the presence

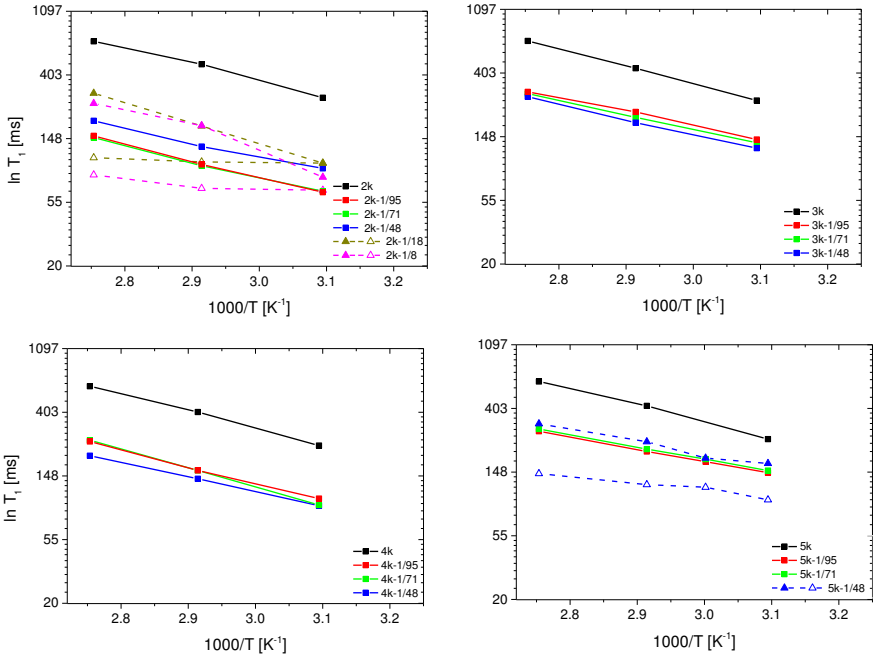

Figure 5.7: Longitudinal retardation times of PEO-$NiCl_2$ systems *vs.* reciprocal temperature at different ion contents. Single exponent relaxation times are illustrated with closed squares. Bi-exponential ones are presented with closed and open triangles corresponding to mobile and hindered domains, respectively.

of ions, and molecular motions are significantly hindered. These domains thus exhibit a fast decay of the induced magnetization and correspondingly small T_2 relaxation times. The second environment corresponds to PEO chain segments which are much less affected by the PEO-Ni^{2+} complexation. However, even in these domains, molecular motions are slowed down, which might be due to either the presence of ions or the presence of fast decaying domains. Here under we refer to the fast and slow decaying domains as hindered and mobile ones, respectively.

The presence of a high temperature plateau in the T_2 *vs.* reciprocal temperature plot (see Figures 5.5.a and 5.6) at medium and high concentrations illustrates network formation. In a solid polymer, hydrogen dipole-dipole interactions are usually the dominating terms of the spin Hamiltonian. Above glass transition, extensive molecular motions occur at a rate larger that T_2^{-1}. As a consequence of high molecular mobility, dipole-dipole interactions are averaged out. Therefore at temperatures above T_g, the T_2 relaxation time for networks is very sensitive to the conformational mean position of network chains. Nonetheless, even at temperatures $100 - 150\ ^\circ C$ above T_g, the presence of physical or chemical crosslinks constrains the possible molecular conformations and makes

the T_2 relaxation independent of temperature and thus forms a high temperature plateau in T_2.[16]

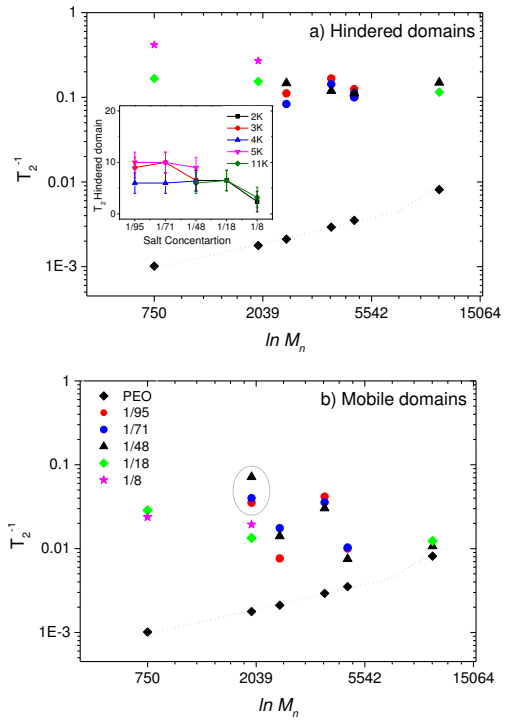

Figure 5.8: Reciprocal transverse relaxation times of (a) hindered and (b) mobile domains vs. PEO molecular weight, at 90 $^{\circ}C$. Insert in (a) shows transverse relaxation time of hindered domains at 90 $^{\circ}C$ against salt concentration. Mobility of hindered domains is independent of ion content, temperature and molecular weight, while molecular motions in mobile domains exhibit no trend of dependency. The line shown is a guide to the eye.

Figure 5.8 illustrates T_2^{-1} against $\ln(M_n)$, for both mobile and hindered domains. The T_2 relaxation time of pure PEO against molecular weight gives straight lines, as predicted by equation (5.3), with slopes being the product of the Rouse relaxation time and the dipolar interaction squared. The intercepts are a function of the length of the shortest statistical segment. Figure 5.8.a shows that the spin-spin relaxation time of the hindered domain is independent of molar mass. The insert in Figure 5.8.a suggests that T_2 of hindered domain remains independent of salt concentration, up to very high concentrations *i.e.* 1/8 equivalence. At this concentration, the maximum volume fraction of hindered domain is typically reached (see Figure5.10), hence added salt has to be accommodated inside already existing hindered domains. The authors believe that the increase of salt density inside hindered domains, would

result in the increase of metal-PEO interactions and hence the chain dynamics in these domains is further slowed down. In addition, from the plateau in the activation plots of PEO-$NiCl_2$ systems presented in Figures5.5 and 5.4 it can be concluded that the transverse relaxation times of hindered domains are temperature independent.

On the contrary, mobile domains show no trend of dependency on molecular weight and ion content. It can be seen in Figure 5.8.b that in the systems with bi-exponential T_2 decay, the smaller the PEO molecular weight, the higher the discrepancy between the dynamics of pure PEO and of the mobile domains in PEO-$NiCl_2$ systems. For instance PEO $0.75k$-1/8 shows about two orders of magnitude higher T_2^{-1} compared to PEO $0.75k$. On the other hand, for molecular weights as high as 11 kg/mol the difference between molecular mobility in pure polymer and salt-modified polymer becomes negligible even at very high ion contents.

The gray ellipse in Figure 5.8.b contains samples with single-exponent T_2 decay. These samples exhibit faster dynamics than hindered domains in the bi-exponential samples but slower than the pure PEO or mobile domains in their bi-exponential counterparts. They also exhibit pronounced temperature dependence.

5.4 Estimate of Hindered Domain Size, Shape and Distribution

Using the recovery of longitudinal magnetization (T_1) and effective spin-diffusion coefficient, D_{eff}, of hindered domains, it is possible to approximate the minimum size of these domains using the equation:

$$X^2 = 2SD_{eff}T_1 \tag{5.5}$$

where X^2 represents the mean square displacement of spin magnetization across the hindered phase on the T_1 time scale. A region must be bigger than X^2 to appear distinct from its surroundings, as X^2 represents the distance over which spin-diffusion can average out the relaxations. S is the number of orthogonal directions determined by the shape of the domain. S is 1 for lamellar systems, 2 for cylindrical and 3 for spherical ones.[5]

As the effective spin-diffusion coefficient cannot be accurately determined for polymers with disordered complex structures or materials with undetermined morphologies, we use a typical value of 0.7 nm^2/ms for D_{eff}.[8] Assuming spherical shape for the hindered domains and also considering there is presumably no long range regularity in the systems, Figure 5.9 shows the minimum diameter of those domains in the systems which exhibit bi-exponential recovery of T_1, for different molecular weights and ion concentrations.

It is obvious from Figure 5.9 that the minimum size of hindered domains is $4-8$ times bigger than the unperturbed size of the chains. This leads to an important conclusion that each hindered domain is composed of a large number of chains. The degree of homogeneity of the PEO-Ni^{2+} interaction at

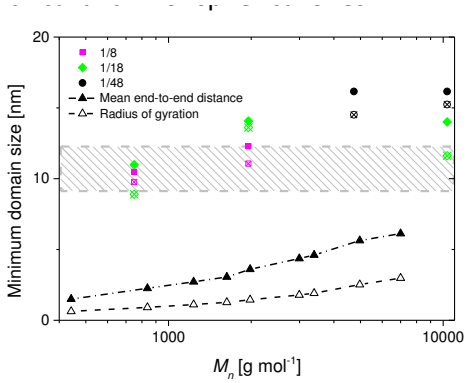

Figure 5.9: Minimum size of hindered domains *vs.* molecular weight at different ion contents, estimated using T_1 at 90 and 70 $^\circ C$ (Solid and open symbols respectively). The black triangles are the simulated unperturbed root mean square end to end distance and radius of gyration of PEO, adopted from reference.[17] The grey-dashed box shows the average length scale between physical junctions in the perfect elastic (entropic) networks, predicted by NMR relaxometry.

the molecular level is an important question and is investigated in the next paragraphs.

In principle, using the main observations presented so far, *i.e.* the formation of fast and slow domains upon network formation which are larger than PEO chains used in this work, one can suggest two molecular scenarios. Either the PEO-$NiCl_2$ gel results from the presence of large clusters due to molecularly heterogeneous interactions between PEO segments and metallic salt, or from a uniform homogenous cross-linked network with possibly dangling PEO strands and a certain number of defects.

If we assume that the gelation is the result of homogenous physical cross-links of PEO via nickel salt that causes a conventional binary cross-linked network of polymer chains, we can approximate the length of cross-linked strands using transverse relaxation times. Hereunder we test this working assumption. The distance between physical or chemical junctions in a rubber can be estimated by a theoretical model relating ^{1}H NMR spin-spin relaxation times with cross-link densities developed by Gotlib *et al.*[18] for lightly cross-linked networks and generalized by Fry and Lind[16] to highly cross-linked elastomers. This theory relates the high temperature plateau of the fast decaying component in a perfect elastomer to the number of statistical segments, Z, between chemical and physical network junctions.

The Fry and Lind[16] theory assigns the fast decaying component of the T_2 relaxation to strands between physical or chemical junctions. It also assumes that these strands are freely jointed, and the distance between the two physical or chemical junctions is constant at the time scale of the experiment ($< 0.5\ \ s$) while freely jointed statistical segments between junctions can reorient by exploring new conformations.

Our viscoelastic study has shown that for the PEO-$NiCl_2$ system the life time of PEO-Ni^{2+} complexation is much larger than the full relaxation time of the chain as well as the time of T_2 experiments. The freely jointed chain is also the main hypothesis of this calculation.

According to Fry and Lind, the number of statistical segments, Z, between chemical and physical network junctions is

$$Z = T_2^{PI}/aT_2^{RL} \tag{5.6}$$

where T_2^{PI} is the plateau in transvers proton relaxation at high temperatures and a is a theoretical coefficient, which depends on the angle between the segment axis and the internuclear vector for the nearest nuclear spins of the main chain. For polymers containing aliphatic protons in the main chain, the coefficient a is close to 6.2.[16,19] T_2^{RL} is the relaxation time that is measured below T_g for the polymer swollen in a deuterated solvent. T_2^{RL} of PEO varies between $7-9\ \ \mu s$ at -166 $^\circ C$.[9]

Using the number of backbone bonds in the statistical segment, C_∞, the molar mass of cross-linked strands, M_x, is calculated as

$$M_x = \frac{ZC_\infty M_u}{n} \tag{5.7}$$

where M_u and n are the molecular weight and the number of backbone bonds in the elementary chain unit, respectively. C_∞ of PEO is $4-5$ rotatable bonds of the backbone as reported by various authors.[2,20]

Combining equations (5.6) and (5.7), and using the plateau of the spin-spin relaxation time of the hindered domains ($8-12\ \ ms$), M_x is estimated to be $11500-17700\ \ g/mol$, which is much larger than the molar mass of the pristine PEOs used in this work. The dashed-box in Figure 5.9 depicts predictions for end to end distance of strands between physical crosslinks, assuming formation of a homogenous elastic network via PEO-metal complexation, based on the NMR relaxometry. The average end-to-end distance of freely jointed strands (r^2) is calculated using

$$r^2 = M_w r_0^2 \tag{5.8}$$

where r_0^2 is 0.805 $Å^2 g^{-1}$ for PEO as reported by Fetters *et al.*[20].

Using the tube theory prediction for the viscoelastic behavior of PEO 11 k-$NiCl_2$ represented in Figure. 5.1, the above mentioned assumptions, *i.e.* formation of homogenous elastic networks via PEO-Ni^{2+} complexes with a number of defects and dangling ends, can be verified.
According to the tube theory, in an entangled polymer network the relaxation modulus ($G(t)$) is inversely proportional to the molar mass between the topological constraints ($M(t)$):

$$G(t) = \frac{\rho RT}{M(t)^{a_d}}\Phi(t) \tag{5.9}$$

where ρ, R and T are density, ideal gas constant and absolute temperature, respectively. $\Phi(t)$ is the fraction of the chains which are not relaxed, if the

chains are assumed to relax in a fixed network and α_d is the dilution exponent ranging from 1 to 1.3.[21−23]

In the PEO $11k$-$NiCl_2$ networks, topological constraints for PEO chains are both entanglements and PEO-metallic salt complexes. The complexation life time is much longer than the reptation time of the chains, as discussed above, hence PEO-$NiCl_2$ complexes can be treated as permanent constraints. On the other hand entanglements continuously disappear and reform based on the mobility of the surrounding PEO chains. According to dynamic tube dilation theory,[21−23] upon relaxation of the surrounding chains, molar mass between the constraining entanglements rescales as

$$M_e(t) = \frac{M_e(0)}{\Phi(t)^{\alpha_d}} \tag{5.10}$$

and therefore

$$G(t) = \frac{\rho RT}{M(0)^{\alpha_d}} \Phi(t)^{\alpha_d+1} = G_N^0 \Phi(t)^{\alpha_d+1} \tag{5.11}$$

In the assumed network, after relaxation of all the entanglements, the molecular mass between PEO-$NiCl_2$ complexes will only dominate elasticity of the system. In other words, while the plateau modulus originates from entangled segments, the second plateau comes from the PEO strands trapped between PEO-$NiCl_2$ complexes. Using equation (5.11), the molecular mass of these trapped strands corresponding to PEO $11k$-$NiCl_2$ systems, presented in Figure 5.1 is estimated to be over 28 kg/mol, which is much larger than the molar mass of PEO used in this work.

The above calculations indicate that the fast decaying component of the T_2 relaxation does not refer to the cross-linked strands between complexes forming an elastic network. In fact, the fast decaying component of T_2 must arise from regions in which several chains are interconnected through PEO-nickel complexation, and hence form cluster structures. The chains inside these cluster domains are forming physical networks, thus their dynamics is significantly hindered. These hindered domains are probably in thermodynamic equilibrium with the matrix of PEO chains, thus the mobile domains exhibit similar properties to pure PEO.

The fraction of hindered domains is determined by the weight factors A and B in equations (5.1) and (5.2) describing bi-exponential T_1 recovery and T_2 decay, respectively. Figure 5.10 shows the fraction of hindered domains as a function of ion concentration for different molecular weights calculated from the fit of T_2. It is clear from Figure 5.10 that success in formation of hindered domains is a direct function of molecular weight, the higher the molecular weight, the larger the fraction of hindered domains. It appears that there is a maximum fraction limit around 63%, which is the theoretical maximum random packing of mono-disperse hard spheres. This observation suggests that our hypothesis for the spherical shape of hindered domains, used in approximating their size, is correct.

The strong effect of molecular weight on the formation of hindered domains can be understood in two ways. Increasing molecular weight results in increasing the contour length and decreasing the molecular mobility of chains. Larger

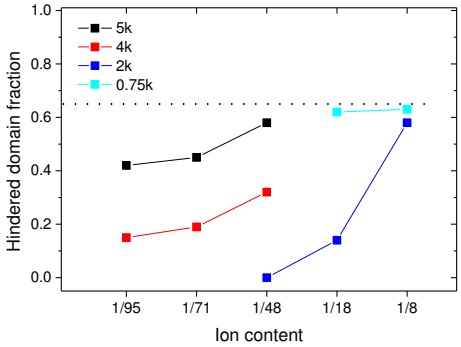

Figure 5.10: Fraction of hindered domains *vs.* ion content for different molecular weights. Fraction of hindered domains is a strong function of molecular weight of PEO chains.

contour lengths increase the likelihood of bridging complexes at constant ion content (constant average distance between ions), while decreasing molecular mobility helps stabilizing these complexes by increasing their association time. As the result of both effects, the probability of formation of hindered domain increases, as observed in Figure 5.10.

It is worth noting that in the PEO-$NiCl_2$ systems where both T_1 and T_2 spectra reveal two distinct environments, the fraction of each domain, determined by the two experiments is identical, within experimental error bars.

5.5 Proposed Microstructure of PEO-$NiCl_2$ Gels in the Melt State

On the basis of the rheology and NMR relaxometry results, we propose a consistent picture for the microstructure for PEO-$NiCl_2$ systems. Ni^{2+} ions and ether oxygen atoms in PEO form complexes which act as physical crosslinks. Some complexes might arise from the folding of a single chain but if such a folding entraps segments of another chain, a crosslinking point will be formed anyway. The inter-connected chains form networks in which the dynamics of PEO segments is significantly hindered. Highly cross-linked domains probably phase separate into spherical cluster domains (hindered domains), in a similar fashion as observed in ionomers. The size of the hindered domains is several times bigger than PEO chains, proving that they are made up of many chains. The remainders of the chains (mobile domains) act as a matrix in which hindered domains are immersed. In this microstructure picture, the mobile domains are composed of at least three components, *i*) free chains capable of relaxing via reptation or Rouse motions *ii*) dangling ends to the chains absorbed in hindered domains relaxing with fluctuations *iii*) tie chains bridging two hindered domain which relax via constraint release Rouse process.

Hence the mobile domain itself is expected to illustrate a complex decay of transverse magnetization, as the relaxation times of these strands are different from each other. Nonetheless it is almost impossible in the frame of this study, to differentiate between different components in the mobile domains and to quantify the weight fraction of each, which presumably depends on molecular weight and salt content. This could be the main reason behind the lack of trend and large scatter observed in Figure 5.8.b.

The existence of clusters with a high density of PEO-Ni^{2+} complexes in a quasi unmodified PEO matrix is a key element to build a consistent picture of the rheology and relaxometry observations since they explain both the second elastic plateau and the features of the biexponential NMR relaxation observed at high salt concentration. The weakness of the clusters is deduced from the shear sensitivity of the gels, as they can be destructured by small deformations.[4]

Upon increasing ion content, the fraction of hindered domains increases until they come into closest proximity (See Figure 5.10). At higher concentrations, the fraction of hindered domains remains constant. Nevertheless the molecular mobility inside the hindered domains is further reduced as the density of PEO-Ni^{2+} complexes increases (See insert in Figure 5.8.a). Figure 5.11 shows a cartoon of the proposed microstructure.

It is important to mention that this picture is in line with the X-ray scattering observations made in chapter 4. The previous work reveals that the hindered domains consist of crystalline complexes of PEO-metal ion, hence they are expected to have internal organization. On the basis of WAXD data, the size of the crystalline structures of PEO-$NiCl_2$ complexes is estimated to be $15-40\ \ nm$ by Scherrer equation (See table 4.2). These results are also consistent with the minimum size of the hindered domains approximated by NMR relaxometry ($>14\ \ nm$). Note that the Scherrer equation is used in section 4.3 to provide a crude minimum estimate of the PEO-$NiCl_2$ crystal size. The word minimum refers at the fact that the true crystal size should be larger than the Scherrer based estimate since instrumental peak broadening and broadening due to paracrystalline distortions or microstrains were not accounted for in the analysis. The crystal size obtained by applying the Scherrer equation to a given reflection is the size measured in a direction perpendicular to the reflecting planes associated with that particular reflection. Since the crystal habit and internal structure of the PEO-$NiCl_2$ crystals are unknown, there is no reason to assume that these crystals are lamellar or that the Scherrer based crystal size would represent *e.g.* a lamellar thickness.

A similar morphology has been reported for Pluronic surfactants, containing PEO chains at extremities, with a saturated solution of $CdCl_2$. Chu *et al.*[24,25] have reported salt induced polymer gelation and spherical disordered nanocrystal growth observed by wide angle X-ray scattering and transmission electron microscopy as a result of complexation between PEO segments and $CdCl_2$ solutions. Radhakrishnan *et al.*[26] has studied complexation of PEO with $CuCl_2$ using WAXS and optical microscopy and have reported crystal domain formation of inorganic phase assisted by PEO in the melt state. The size of the PEO-$CuCl_2$ unit cell was about 6Å.

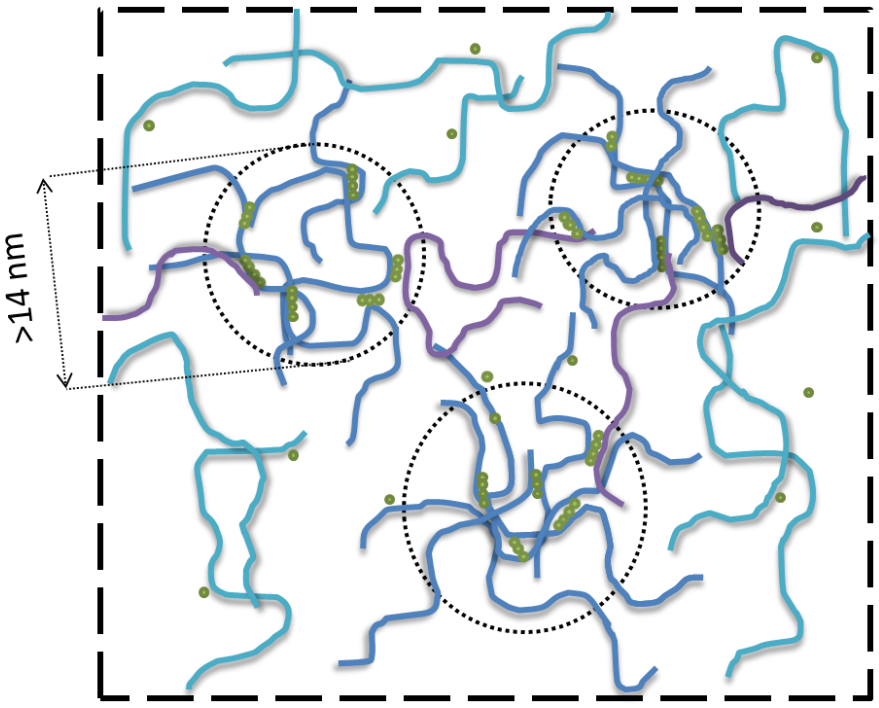

Figure 5.11: Scheme of the proposed microstructure picture of PEO-$NiCl_2$ networks, with weak clusters (hindered domains) shown in dark blue formed through interaction between PEO and Ni^{2+} ions, which are surrounded by relatively mobile PEO chains (mobile domains) depicted in light blue. An elastic network can be formed once the hindered domains are bridged via tie chains (violet).

Formation of individual hindered domains does not explain network formation unless either *i*) there is spatial hindrance between the hindered domains (caging effect) or *ii*) hindered domains form co-continuous morphology or *iii*) hindered domains are interconnected via tie chains. Below, we analyze the three scenarios and draw a conclusion:

In hairy micelles systems with compact hard cores and large flexible coronas, which are analogous to the first scenario, elastic networks are observed when the cores are coming in close proximity and the coronas start to inter-diffuse. Hence networks are only formed at very large volume fraction of hairy micelles.[27] However, in the PEO-$NiCl_2$ systems, network formation is observed at quite small concentrations of $NiCl_2$, in which the fraction of hard domains are so small that they are hardly detected by transverse ^{1}H relaxometry *e.g* PEO 11*k*-1/260 $NiCl_2$. Hence, steric hindrance between hindered domains cannot explain the observed network.

Despite of that fact that co-continuous hindered domains can explain the viscoelastic data and the existence of two distinct domains in NMR relaxometry, this scenario is not consistent with the maximum packing fraction observed in the PEO-$NiCl_2$ systems by T_1 and T_2 signals. In other words, any of the distinct domains in a co-continuous material can occupy an arbitrary volume fraction, yet enabling the other phase to remain continuous.

The authors believe that the third scenario is the most probable: in PEO-$NiCl_2$ systems, elastic networks are formed when some chains start to bridge hindered domains, thus establishing an interconnected network of hindered domains inside a continuous matrix of relatively mobile PEO chains. The effectiveness to bridge the hindered domains and consequently the success of network formation depends on the proximity of hindered domains as well as the size of the bridging chains. Once the network is established, the distance between two adjacent hindered domains is equal or smaller than the size of the tie chains.

As mentioned above, the size of the PEO chain plays a key role in network formation, for instance, despite of high fraction of hindered domains (63%) in PEO $0.75k$-1/8, this sample flows under its own weight above its melting temperature, while a gel is formed in PEO $11k$-1/260, where hindered domains are barely detectable in the FID signal of the transverse magnetization (See Figure. 5.4).

5.6 Conclusion

Network formation in PEO-$NiCl_2$ was studied by proton NMR and rheology. Transverse magnetization signals revealed a bi-exponential decay behavior. A similar trend was observed in the longitudinal recovery, manifesting the coexistence of two distinct environments with slow and fast dynamics. The chain dynamics in the slow (hindered) domains was temperature, salt content and molecular weight independent, whereas the fast (mobile) domains exhibit similar properties to that of pure PEO.

The minimum size of the hindered domains was calculated to be at least 4 times bigger than the PEO chains, proving that they consist of many chains. The tube theory also predicts the effective cross-linked strand to be much larger than that of a PEO chain. The fraction of hindered domains shows an experimental upper limit of 63% in agreement with the maximum packing of mono-dispersed spheres. Based on these observations we propose a microstructure picture for the melt state in which PEO chains are bound together via ion-dipole interactions, and form clusters. These spherical clusters (hindered domains) are immersed in a matrix of PEO chains (mobile domains).

5.7 Appendix

This section is intended to provide some last remarks on the PEO-salt systems presented in Chapters 3-5. Some discussions are inspired by the reviewer comments, others are just for further clarifications.

Ion Equivalence: In studying PEO-salt systems, we used different definitions to quantify salt contents. Ion equivalence has been addressed in three different ways:

In terpyridine functionalized PEO samples of Chapter 3, ion equivalence was defined as moles of ions per one mole of terpyridine end group. Hence, for instance, the weight fraction of salt in 1 eq Bi-PEO systems is two times higher than that of 1 eq Mono-PEO.

In Chapter 4, ion equivalence is defined as moles of ions per moles of chains, while in Chpater 5 it addresses moles of ions per moles of monomers. These two definitions are related by mean degree of polymerization of the PEO chains.

To establish a common basis for comparing systems in the three Chapters, weight fraction of salt in all systems is tabulated in the corresponding Material and Method sections (See Tables 3.1, 4.1 and 5.1).

Choice of Nickel ions: The discussions of this PhD dissertation are only limited to PEO-Ni^{2+} systems, mainly $NiCl_2$, although most transition metals are reported to interact with PEO. The choice of nickel is based on previous viscoelastic investigations in this group, which at the time of writing this document are not yet publically communicated. Briefly, the effect of PEO-salt interactions on viscoelastic properties was tested using chloride salts of Ni^{2+}, Fe^{2+} and Zn^{2+}. It was shown that small fractions of nickel and iron salts alter terminal relaxation and viscoelasticity of PEO while $ZnCl_2$ do not induce any effects. Nickel chloride had a superior effect compared to the iron salt. $FeCl_2$ has not been chosen for the viscoelastic studies as Fe^{2+} reduces in time to Fe^{3+}, which adds another level of uncertainty to the PEO-salt systems. In addition the PEO-Fe^{2+} networks were too weak for rheology measurements. For more information, please contact Prof. Evelyne van Ruymbeke.

It is not clear at this stage why completely different viscoelastic behaviors are observed by changing the metal cation, although literature clearly confirms the presence of strong PEO-salt complexation for $NiCl_2$, $FeCl_2$ and $ZnCl_2$. Similar question exists when changing the counter ion for a given metal cation. For instance it was shown in the Section 4.3.1 that PEO-NiI_2 complexation does not impose any viscoelastic changes to the PEO melt, as opposed to network formation in PEO-$NiCl_2$ (See Figure 4.8).

In general, success of network formation via PEO-ion complexation at least depends on the number of chains contributing in each complex and its association time as well as long range arrangements of the complexes in the PEO melts, *i.e.* crystallization. If a metal cation is only wrapped by a single chain in the PEO-salt complex structure or there is no ordering of complexes which enable the systems to carry stress, network formation is not anticipated. Likewise if the complex is too labile, stress can relax by the fast hopping processes. Additional SAXS and WAXS data can indeed help in better understanding the underlying mechanisms of network formation in PEO-salt systems.

Morphology of PEO-salt networks: As reported in Chapter 3, viscoelastic behavior of telechelic PEO systems functionalized with terpyridine ligands (Mono_ and Bi_PEO) strongly depends on the salt content. Up to stoichiometric ratio *i.e.* 0.5 eq Ni^{2+}/terpyridine, in which all ligands are saturated with metal ion, the Mono_ and Bi_PEO systems exhibit fluid-like behavior.

Upon infinitesimal increase of nickel salt content beyond the stoichiometric ratio, for instance 0.85 eq, an elastic gel is observed, which exhibits a second plateau similar to the case of PEO-Ni^{2+} system. It is impotent to note that the second plateau modulus of Bi-PEO is more than one order of magnitude higher than that of PEO-Ni, and it can eventually reach G_N^0 of PEO (See Figure 3.10). This means that with such functionalized chains nearly the whole sample can be trapped into the transient network. Thus, this result cannot be explained based on only interactions of PEO assemblies with nickel salt since it has been shown in Chapter 4 that the corresponding transient network is very weak, and consequently, the maximum level of the low-frequency plateau is limited due to the breaking of the network under very small shear deformation (see Figures 4.7 and 4.8). This allows us to conclude that for Mono_ and Bi_PEO–$NiCl_2$ with excess of ion the network properties are also due to phase separation of the terpyridine ligands into distinct domains via lateral stacking driven by the $\pi-\pi$ interactions between the aromatic planes of terpyridine. This process leads to larger reduction of mobility of the PEO chains in the terpyridine functionalized PEO–$NiCl_2$ systems. Hence a hierarchy of various modes of self-assembly, *i.e.* coordination interaction, $\pi-\pi$ stacking of terpyridine groups (*i.e.* respectively binary and collective assembly of terpyridine-ion complexes) as well as PEO-salt complexation is expected in telechelic PEO-$NiCl_2$ samples.

The morphology of pure PEO-$NiCl_2$ systems is slightly simpler, though the proposed model suggest that at least 3 levels of self-assembly are evolved, *i.e.* cation-ether oxygen complexation, arrangement of PEO-ion complexes into crystalline structures followed by phase separation of a fraction of PEO chains as hindered domains. These various processes occur at different levels. From literature we know that the complexation process certainly occurs at atomic level ($< 1\ nm$), while the crystallization process happens at the scale of $10-40\ nm$, as revealed by the WAXS data. Yet there is a clear gap between these microscopic levels and the macroscopic level at which rheology works. The hierarchy of self-assembly requires a description of the mesoscopic structures. The experimental data certainly lacks observation at mesoscopic levels ($> 100\ nm$). Porod regime in annealed PEO-231k 200 eq $NiCl_2$ (see Figure 4.11) is perhaps the only piece of data which suggests presence of mesoscopic structures with over 90 nm characteristic sizes. Hence the PEO-salt microstructure proposed in Figure 5.11 might be too restrictive.

As a matter of fact, the two phase model of Figure 5.11 is based on assuming a two component system from the complex shape of T_1 and T_2 relaxation spectra. Therefore bi-exponential functions were used to fit the NMR relaxometry data. However other relaxation modes or different distribution functions such as Gaussian or Lorentzian could have been considered in fitting the experimental data. For instance according to the proposed model, in the relevant time/length scale of the NMR measurements, the mobile phase itself contains at least three types of chain strands with well separated relaxation times *i.e.* trapped segments, dangling ends and mobile chains. Hence, together with the hindered domains, at least a four component mathematical function is required to describe the T_2 spectra of the PEO-$NiCl_2$ networks. Using a 4 component model with at least 7 independent variables (4 time scales and 3 volume frac-

tions) is certainly way too much for a reasonable fit to this short range of T_2 data, considering the inherent scattering of data points. The ill-posed nature of the fitting processes restricts our observation in these systems. Although the multi-phase microstructure is well supported by the NMR and scattering experiments, information on the shape, size and distributions of hindered domains, as well as the link between crystallization of complexes and formation of hindered domains, remains elusive. For instance, the spherical shape of hindered domain was only speculated based on maximum packing, although they are not likely to be monodisperse hard spheres. We will present evidences of non-spherical collective assemblies with a wide distribution of shape and size in PnBA-*g*-UPy supramolecular networks (Chapter 7), which are analogous to the hindered domains in PEO-salt systems.

Despite several limitations and shortcomings, the present model provides a crude picture for the complex microstructure of the PEO-salt systems and help correlating viscoelastic and NMR relaxometry data.

Non-equilibrium viscoelasticity: It was shown in Chapter 4 that the viscoelastic behavior of PEO-$NiCl_2$ systems depends on the time and the temperature of annealing. In addition amplitude sweep tests illustrated that the LVE response is out of reach and any rheology measurements is in NLVE region. Although considerable efforts were made to report the viscoelastic data at a comparable state, for instance all frequency sweep measurement are performed at 0.1% strain (otherwise the corresponding shear strain is mentions), it is not surprise to see differences between various measurements of one sample. For instance in PEO 200 k 231 eq $NiCl_2$ the value of the storage modulus at 0.01 differs by about factor 3 in Figures 4.3 and 4.6. The reason is evidently different shear history of the samples which yielded to different network states. Consequently, the rheology results in Chapters 4 and 5 are not meant to be viewed quantitatively. They rather demonstrate general viscoelastic features in the PEO-salt systems.

Last but not least, viscoelastic data were extensively duplicated over and over using various fresh samples, geometries and gap sizes. The main observations such as network formation, shear sensitivity and ion content dependency have been reconfirmed several times. Hence network breakage-reformation behavior should not be assigned to typical experimental errors like surface slippage or slip-stick phenomena.

PEO Degradation: Evolution of the chemical structure, either degradation or crosslinking, can alter network dynamics. This alteration is seen by rheology through changes in network viscoelasticity and relaxation times. As structural evolutions add to the inhomogeneity in the macromolecular systems and broadens the relaxation spectra, the T_2 decay of the NMR relaxometry is expected to alter. In principle, longer the chains, smaller the T_2 time scales.

Degradation produces low molecular weight PEO chains, hence a greater T_2 is expected for the systems. On the contrary chain extension or cross linking, as observed by MALDI and GPC, can produce longer chains, which will exhibit smaller T_2 and eventually produce biexponential decay of transverse relaxation spectrum. Despite this possibility, we have conclusive arguments and evidences that observed bi-exponential behavior is not due to PEO crosslinking:

i) Although structural changes can produce bi-exponential T_2 behavior, the T_1 retardation spectrum remains mono-exponential in these systems.[6,7] The (semi)biexponential T_1 spectra are only observed when multiple distinct phases are present in the sample.

ii) If we assume that the biexponent decay is a result of high Mw PEO formation, then the fast decaying initial component of T_2 would correspond to entangled strand and the slow decaying final component would be the signature of free ends. Then there is no reason to have a maximum fraction of 63% for entangled strands (See Figure 5.11). In addition the T_2 relaxation time of the fast decaying component ($3-7\ ms$) is too small to be assigned to the entangled PEO strands.[1,2]

iii) Moreover, it is unlikely that the long or cross-linked chains which are forming can entangle in the sea of oligomers, for instance in PEO 0.35 k-$NiCl_2$ system. In the case of PEO, chains as long as $60-100\ kg/mol$ will exhibit T_2 decay similar to those in Figures 5.2 and 5.4[7] (PDI is less important, see reference[14]). Oligomers as short as 350 g/mol cant produce such long polymer chains with any statistical combination reaction.

From these arguments, we confidently conclude that the structural changes caused by simultaneous degradation and crosslinking of PEO chains (see Section 4.3.3) do not have significant contributions in producing the observed bi-exponential decay of T_2 behavior in PEO-$NiCl_2$ systems. The T_2 behavior definitely originates from multiphasic microstructure of the PEO-salt systems.

5.8 Bibliography

1 Ries, M. E.; Brereton, M. G.; Cruickshank, J. M.; Klein, P. G.; Ward, I. M. NMR study of poly(ethy1ene oxide) complexes with $LiCF_3SO_3$. *Macromolecules* **1995**, 28, 3282-3289.

2 Ries, M. E.; Klein, P. G.; Brereton, M. G.; Ward, I. M. Proton NMR study of Rouse dynamics and ideal glass transition temperature of poly(ethylene oxide) $LiCF_3SO_3$ complexes. *Macromolecules* **1998**, 31, 4950-4956.

3 Goldansaz, H.; Voleppe, Q.; Pioge, S.; Fustin, C. A.; Gohy, J. F.; Brassinne, J.; Auhl, D.; van Ruymbeke, E. Controlling the melt rheology of linear entangled metallo-supramolecular polymers. *Softmatter* **2014**, 11 (4), 762-774.

4 . Goldansaz, H.; Auhl, D.; Goderis, B.; Voleppe, Q.; Fustin, C.-A.; Gohy, J.-F.; Bailly, C.; van Ruymbeke, E. Transient metallo-supramolecular networks built from entangled poly (ethylene oxide) melt, *Macromolecules* **2015**, 48(11), 3746-3755.

5 Levitt, M. H. *Spin dynamics: Basics of nuclear magnetic resonance*, 2nd ed.; Wiley: New York, **2008**.

6 Brereton, M. G. NMR transverse relaxation function calculated for constrained polymer chains: application to entanglements and networks. *Macromolecules* **1990**, 23 (4), 1119-1131.

7 Klein, P. G.; Ries, M. E. Dynamics and physical structure of polymers above the glass transition: transverse relaxation studies of linear chains, star polymers and networks. *Prog.Nucl.Magn.Reson.Spectrosc.* **2003**, 42, 31-52.

8 Litvinov, V. M.; Braam, A. W. M.; van der Ploeg, A. F. M. J. Telechelic ionomers: molecular structure and kinetics of physical Gelation of unsaturated polyester as studied by solid State NMR and *X*-ray. *Macromolecules* **2001**, 34 (3), 489-502.

9 Litvinov, V. M.; Dias, A. A. Analysis of network structure of UV-cured acrylates by 1H NMR relaxation,13C NMR spectroscopy, and Dynamic Mechanical Experiments. *Macromolecules* **2001**, 34 (12), 4051-4060.

10 Saito, Y.; Kataoka, H.; Manuel Stephan, A. Investigation of the conduction mechanisms of lithium gel polymer electrolytes based on electrical conductivity and diffusion coefficient using NMR. *Macromolecules* **2001**, 34 (20), 6955-6958.

11 Sekine, S.; Akieda, H.; Ando, I.; Asakura, T. A Study of the relationship between the tensile strength and dynamics of as-spun and drawn poly(glycolic acid) fibers. *Polym. J.* **2008**, 40, 10-16.

12 Montes de Oca, H.; Ward, I. M.; Klein, P. G.; Ries, M. E.; Rose, J.; Farrar, D. Solid state nuclear magnetic resonance study of highly oriented poly(glycolic acid). *Polymer* **2004**, 45, 7261-7272.

13 Litvinov,V.M.; Persyn,O.;Miri, V.; Lefebvre, J.M. Morphology, phase composition, and molecular mobility in polyamide films in relation to oxygen permeability. *Macromolecules* **2010**, 43 (18), 7668-7679.

14 Litvinov, V. M.; Ries, M. E.; Baughman, T. W.; Henke, A.; Matloka, P. P. Chain entanglements in polyethylene melts. Why is it studied again ? *Macromolecules* **2013**, 46, 541-547.

15 Wouters, M. E. L.; Litvinov, V. M.; Binsbergen, F. L.; Goossens, J. G. P.; van Duin, M.; Dikland, H. G. Morphology of ethylene-propylene copolymer based ionomers as studied by solid state NMR and small angle *X*-ray scattering in relation to some mechanical properties. *Macromolecules* **2003**, 36, 1147-1156.

16 Fry, C. G.; Lind, A. C. Determination of crosslink density in thermoset polymers by use of solid-state proton NMR techniques. *Macromolecules* **1988**, 21 (5), 1292-1297.

17 Lee, H.; de Vries, A.H.; Marrink, S.-J.; Pastor, R. W. A coarse-grained model for polyethylene oxide and polyethylene glycol: conformation and hydrodynamics. *J. Phys. Chem. B* **2009**, 113 (40), 13186-13194.

18 Gotlib, Y. Y.; Lifshits, M. I.; Shevelev, V. A.; Lishanskii, I. S.; Balanina, I. V. Influence of the chemical crosslinking network on the spin-spin relaxation of crosslinked and swelling polymer systems. *Polym. Sci. U.S.S.R.* **1976**, 18 (10), 2630-2636.

19 Litvinov, V. M.; De, P. P. *Spectroscopy of rubbers and rubbery materials*; Smithers Rapra Publishing: Shawbury, U.K., **2002**.

20 Fetters, L. J.; Lohse, D. J.; Colby, R. H. Physical properties of polymers handbook; Springer: New York, **2007**, 447-454.

21 van Ruymbeke, E.; Liu, C.Y.; Bailly, C. Quantitative tube model predictions for the linear viscoelasticity. *Rheol. Rev.* **2007**, 53-134.

22 van Ruymbeke, E.; Masubuchi, Y.; Watanabe, H. Effective value of the dynamic dilution exponent in bidisperse linear polymers: from 1 to 4/3. *Macromolecules* **2012**, 45 (4), 2085-2098.

23 van Ruymbeke, E.; Shchetnikava, V.; Matsumiya, Y.; Watanabe, H. Dynamic dilution effect in binary blends of linear polymers with well-separated molecular weights. *Macromolecules* **2014**, 47(21), 7653-7665.

24 Liu, T.; Xie, Y.; Liang, D.; Zhou, S.; Jassal, C.; McNabb, M.; Hall, C.; Chuang, C.-L.; Chu, B. Formation of a salt-polymer complex in L_{64}/Water/$CdCl_2$ systems. *Langmuir* **1998**, 14, 7539-7542.

25 Liu, L.-Z.; Wan, Q.; Liu, T.; Hsiao, B. S.; Chu, B. Salt-induced polymer gelation and formation of nanocrystals in a polymer-salt system. *Langmuir* **2002**, 18 (26), 1040210406.

26 Radhakrishnan, S. Polymer induced crystallization III. PEO:$CdCl_2$ and in situ formation of PEO:CdS composite. *J. Cryst. Growth* **1994**, 141, 437-442.

27 van Ruymbeke, E.; Pamvouxoglou, A.; Vlassopoulos, D.; Petekidis, G.; Mountrichas, G.; Pispas, S. Stable responsive diblock copolymer micelles for rheology control. *Soft Matter* **2010**, 6, 881-891.

Chapter 6

How Supramolecular Assemblies Control Dynamics of Associative Polymers: Towards A General Picture

Outline

The dynamics of supramolecular networks made up of partially hydrolyzed poly(n-butyl acrylate) [PBA] is investigated. These linear entangled random copolymers [PBA-r-AA] self-assemble via hydrogen bonding interactions between carboxylic acid groups. Two types of supramolecular assemblies are revealed,*i.e.* binary assembly of carboxylic acid dimers and collective assembly of dimers into distinct poly (acrylic acid) [PAA] domains. The latter is proved by emergence of new relaxation processes in broad band dielectric spectroscopy while the former is evident by an increase of the glass transition temperature as well as retardation of segmental mobility observed by rheology. Therefore a ″sea-island″ morphology containing geometrically confined PAA nanodomains embedded in a PnBA-rich matrix is suggested for the supramolecular network. Thermodynamic theories are employed to rationalize the existence of an interlayer with restricted mobility between the two phases.

A fraction of PBA-r-AA segments which are trapped between more than one PAA domain is considered to describe the low frequency plateau in storage modulus that is seen beyond the plateau modulus of PnBA as well as strain hardening in both shear and elongation fields.

Finally, based on the observation in this work and wealth of literature on supramolecular systems, a general microstructure is proposed for the associating polymers in which supramolecular moieties are situated along the contour

length. This microstructure appropriately describes different dynamic observations made by rheology, calorimetry and dielectric spectroscopy.

6.1 Introduction

In this work, we address dynamics of supramolecular networks based on partially hydrolyzed entangled PnBA. These random copolymers [PBA-*r*-AA] are self-associating via hydrogen bonds between carboxylic acid groups. We use rheology to characterize segmental and bulk dynamics of the polymer chains, and BDS to independently investigate binary and collective dynamics of the supramolecular moieties. By combining the two techniques we show that the segmental Rouse dynamics of the associating polymers is affected by the friction imposed by the binary supramolecular pairs, whereas the bulk dynamics is controlled by the collective assemblies. The time scale of these collective dynamics is revealed to be a function of the composition of the supramolecular aggregates. We then propose a microstructure for entangled supramolecular networks in which both binary and collective dynamics of supramolecular moieties are taken into account. We believe that this picture in applicable to any system in which associating side groups are distributed along the polymer backbone.

6.2 Materials and Methods

Linear PnBA and PAA were purchased form Polymer Source (Montreal, Canada). PnBA was hydrolyzed in basic environment to transform a fraction of butyl acrylate [BA] units to acrylic acid [AA]. 1 g PnBA was dissolved in 30 mL distilled THF. 200 mg anhydrous potassium hydroxide (KOH) was added to the PnBA solution. Hydrolysis reaction proceeded under reflux condition and argon atmospheres at 70 $^{\circ}C$.

After a desired time, the reaction mixture was cooled down to room temperature, neutralized with excess amount ($15 - 20$ mL) of hydrochloric acid (HCl), and then dried by rotavapor to ensure complete removal of THF and the *n*-butanol generated by the hydrolysis.

To remove potassium chloride (KCl) salt from the PBA-*r*-AA systems, the dried polymers were dissolved in 10 mL of ethyl acetate and then 50 mL ultrapure water were added to this solution. The mixture was stirred for 10 min and the ethyl acetate was removed by rotavapor, which causes polymer to precipitate while KCl salt remains soluble in water. This step was repeated 4-5 times to ensure complete removal of the inorganic salt. Finally, the polymers were extensively dried under vacuum at 50 $^{\circ}C$ for 15 days. EDX confirms high purity of the PBA-*r*-AA samples with respect to metal salts. The AA monomer fraction in PBA-*r*-AA polymers was quantified using ^{1}H NMR spectroscopy. Table 6.1 summarizes properties of different systems used in this work.

To quantify the residual metal contamination after purification of the PBA-*r*-AA polymers, EDX was performed using a JEOL FEG SEM 7600F scanning

Table 6.1: Physical and chemical properties of the PBA-*r*-AA samples used in this study.

Name	M_w	M_w/M_n	Acrylic acid monomer content	Hydrolysis time at 70 $°C$	Glass transition temperature at 10 $°C/min$
	(kg/mol)		$(mol\%)$	(h)	$(°C)$
PnBA	210	1.38	$3 \pm 2\%$	-	-51 ± 0.5
PBA-*r*-AA13%	198*	1.38	$13 \pm 2\%$	4.5	-49.5 ± 0.5
PBA-*r*-AA38%	175*	1.38	$38 \pm 2\%$	7	-47 ± 0.5
PAA	15	1.1	100%	-	108 ± 1.5

** Calculated based on acrylic acid monomer content*[5]

electron microscope equipped with an EDX system (Jeol JSM2300 with a resolution $< 129\ eV$) operating at 15 keV with a working distance of 8 mm. The acquisition time for the chemical spectra lasted 300 s with a probe current of 1 nA. Specimens for EDX were mounted on stubs and analyzed without metallization. The quantitative analysis of the atomic elements was performed with the integrated software which subtracts the bremsstrahlung effect with the classical ″Top Hat Filter″ and then quantifies the area under each atomic peak determined by the $\varphi(\rho z)$ model.

The extent of hydrolysis was determined by ^{1}H NMR in solution by analyzing approximately 10 mg PBA-*r*-AA dissolved in 0.6 mL $CDCl_3$ using > 200 scans separated by recycling times $> 5T_1^{polymer}$. A Bruker AVANCE 500 MHz spectrometer was used for recording ^{1}H NMR spectra. The average fraction of hydrolyzed units was determined using the ratios between the methyl protons of the butyl side chain (< 0.9 ppm), and methylene protons of the butyl side chain next to the ester (~ 4.3 ppm), and the rest of the protons of the backbone and side chain ($1 < chemical\ \ shift < 2.4$ ppm), CH_3/polymer and $COOCH_2$/polymer, respectively.

DSC analysis was performed using a Mettler Toledo DSC821^e calorimeter calibrated against indium. The sample weights were $7-12$ mg. Heating ramps of $5-40$ $°C/min$ between 90 and 0 $°C$ were used to determine glass transition temperatures.

Viscoelastic properties of the PBA-*r*-AA samples were investigated by small and large amplitude oscillatory shear rheology using a MCR 301 (Anton Paar, Germany) rheometer. Temperature was controlled using a convection oven operating under nitrogen. A parallel plate geometry (diameter $8, 15$ or 20 mm) was used depending on the viscosity level of the system at the given temperature. Different geometries were used to ensure accounting for the setup compliance and inertia effects. No slip problem was observed due to good adhesion of the PnBA based polymers to the surface of the steel geometries.

The extensional stress growth coefficient as a function of time was measured using a filament stretching rheometer (DTU-FSR). Cylindrical stainless steel sample plates with a diameter of 5.4 mm were used for all measurements. The mass of each sample varied from 0.04 to 0.06 g. The aspect ratio, L/R, varied from 0.36 to 0.75. Measurements were performed at a constant Hencky strain rate imposed at the midfilament diameter using an online control scheme. All experiments were performed at 22 $^{\circ}C$. The imposed strain rates were varied from 0.0006 to 1 s^{-1}.

BDS was performed using a high resolution Alpha analyzer (Novocontrol, Germany) over the frequency range of 0.1 $Hz - 10$ MHz in combination with a cryostat operating under nitrogen atmosphere. Materials were sandwiched between $20 - 10$ mm gold coated flat circular electrodes using 100 μm thick glass fiber spacers. Frequency sweep measurements were performed in heating and cooling ramps between 110 and -130 $^{\circ}C$ with 2.5 $^{\circ}C$ spacing. PBA-r-AA polymers were then quenched from 110 $^{\circ}C$ using liquid nitrogen bath and the transition to the equilibrium state was monitored by a heating ramp from -130 to $110^{\circ}C$. To correct for geometry discrepancies arising from variation of the spacer thickness or the quenching step, the BDS measurements were repeated for selected temperatures between 60 to -60 $^{\circ}C$ using MCR 301 as the dielectric cell, in which the distance between electrodes can be controlled within ± 1 μm precision.

Imaginary part of permittivity ($\varepsilon^{''}(\omega)$) in dielectric relaxation spectra was decomposed using a set of empirical Havrilik-Negami equation to extract mean relaxation time, τ, and the shape factors describing broadness, a, and asymmetry, b, of the relaxation peaks:

$$\varepsilon^{''}(\omega) = \frac{\Delta\varepsilon}{(1 + (i\omega\tau)^a)^b} + \frac{i\sigma_0}{\omega\varepsilon_0} \tag{6.1}$$

$\Delta\varepsilon$ and ε_0 are the strength of relaxation and the permittivity of free space, respectively. ω and σ_0 denote the angular frequency and frequency independent dc conductivity.

To investigate relaxation processes which are masked by the strong dc conductivity in $\varepsilon^{''}(\omega)$ above the glass transition of PnBA, a one dimensional numerical derivative based on Kramer-Kronig transformation proposed by and van Turnhout and Wübbenhorst[1] was used

$$\varepsilon^{''}_{der}(\omega) = -\frac{\pi}{2}\frac{\partial\varepsilon^{'}(\omega)}{\partial\ln(\omega)} \approx \varepsilon^{''}(\omega) \tag{6.2}$$

$\varepsilon^{''}_{der}(\omega)$ and $\varepsilon^{'}(\omega)$ are the conductivity free part of $\varepsilon^{''}(\omega)$ and real part of complex permittivity, respectively.

6.3 Results and Discussion

6.3.1 Energy Dispersive X-Ray Spectrometry

In the presence of high concentrations of metal salts, the PBA-r-AA systems are expected to behave like ionomers, in which carboxylic acid groups are absorbed

to the ionic aggregates. The association strength of the metal-acid interactions and consequently both linear and non-linear rheology strongly depend on the nature of the metal cation as well as the counter ion. Moreover the viscoelastic behavior depends on the concentration of the metal salt.[2–4] Since after hydrolysis a high fraction of metal salts, especially KCl, exists in the PBA-*r*-AA, it is crucial to purify the supramolecular networks from metallic contaminations, prior to any dynamic experiment. EDX were used to evaluate the success of the purification step. The metallic and organic residues in the PBA-*r*-AA samples are given in Table 6.1. Data are averaged by repeating the measurements at several spots on the specimen.

Table 6.2: Metallic residue in PBA-*r*-AA saples.

Name	Na residue ($wt\%$)	K residue ($wt\%$)	Cl residue ($wt\%$)
PBA-*r*-AA13%	0.36 ± 0.18	0.10 ± 0.14	0.1 ± 0.09
PBA-*r*-AA38%	0.05 ± 0.04	0.08 ± 0.05	0.27 ± 0.74

6.3.2 Broadband Dielectric Spectroscopy

Figure 6.1 shows a 3D plot of $\varepsilon''_{der}(\omega)$ against temperature and frequency for the sample PBA-*r*-AA13%. Four individual processes can be identified. Besides α, β and γ relaxations, which are present in pure PnBA, a set of dielectric relaxations occurs in the supramolecular networks beyond the α relaxation. These new emerging relaxation processes will be referred to as α^*. The sharp rise of $\varepsilon''_{der}(\omega)$ at low frequencies is due to electrode polarization (E_P), which is a consequence of partial accumulation of charge carriers at the interface between electrodes and sample. E_p leads to a drastic increase in the real part of permittivity and reduces the slope of imaginary part with respect to the frequency ($d \log \varepsilon''(\omega)/d \log \omega < 1$). We confidently assign the last rise to E_P since it shows dependency on the geometrical aspect ratio of the dielectric sample.[6]

It is clear from Figure 6.2 that the α^* process is composed of at least 3 different relaxation modes, here under referred to as α_1^*, α_2^* and α_3^*. α_1^* is a small and extremely broad relaxation which can be described by a Cole-Cole formalism. On the contrary, α_2^* is essentially a Debye relaxation. To account for the extended plateau observed in of the PBA-*r*-AA38%, it is obvious that apart from the α_1^* and α_2^* relaxation modes a third contribution, α_3^*, is required. As no information on the shape of this relaxation is available, another Debye process was used just to capture the plateau. E_p was also fitted by a Debye term according to the Macdonald theory.[7] Based on the discussion of this section the α_3^* relaxation shall exist in PBA-*r*-AA13%, though it is obscured under the strong E_p upturn.

The activation plots for the α, β and γ relaxations are presented in Figure 6.3 for all samples. While the γ process is unaffected by modification of

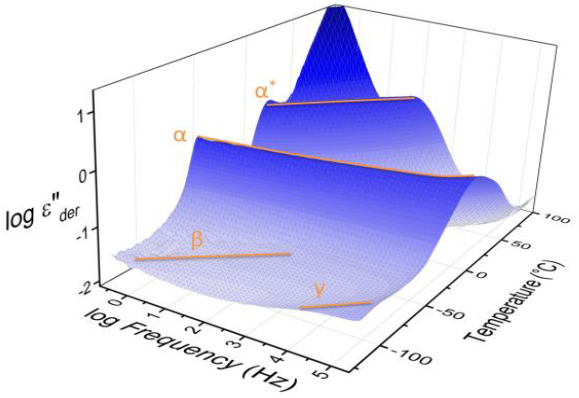

Figure 6.1: 3D representation of ε''_{der} against temperature and frequency for PBA-*r*-AA13%. In PBA-*r*-AA supramolecular networks a new set of processes, α^*, is observed beyond the glass transition of PnBA. The upturn at high temperatures and low frequencies is due to electrode polarization (E_P).

the butyl acrylate side groups to acrylic acid ones, the relaxation time of the β process significantly increases from the reference PnBA sample to PBA-*r*-AA38%. The departure of the time scale of α relaxation upon increasing the AA monomers is in line with a minute increase of the glass transition temperature observed by differential scanning calorimetry (See Table 6.1).

Hayakawa and Adachi[8] studied dielectric relaxation of PnBA and reported three characteristic α, β and γ relaxation phenomena around $230, 190$ and $140\ \ K$, respectively. They assigned the α relaxation to a cooperative process of rotation of the ester bonds (β relaxation) followed by segmental motion of polymer backbones. In a systematic study on Poly(alkyl (meth)acrylates), Gaborieau *et al.*[9] found that both α and β processes occur at lower frequencies with increasing side chain length whilst the γ process is independent of the side chain size. Gaborieau *et al.* reported that the β relaxation exhibits the highest sensitivity to any alteration in the side chain chemistry. Our data are in good agreement with these studies.

The evolution of the relaxation time of the α^*-process against reciprocal temperature is presented in Figure 6.4.a. It is worth noting that similar relaxation times are observed in heating and cooling ramps for all the relaxation processes in the supramolecular systems, *i.e.* γ, β, α and α^* relaxations, within experimental error. This observation suggests that the PBA-*r*-AAs are in equilibrium within the experimental conditions. On the other hand, once the supramolecular networks are quenched, the α^* relaxations clearly accelerate compared to the equilibrium state (See Figure. 6.4.b). Though upon heating, the equilibrium behavior is again reached after a critical temperature (T_C).

In the equilibrium state (open symbols in Figure 6.4), the α_1^* relaxation exhibits a VFT behavior while α_2^* and α_3^* are Arrhenius-like. The relaxation

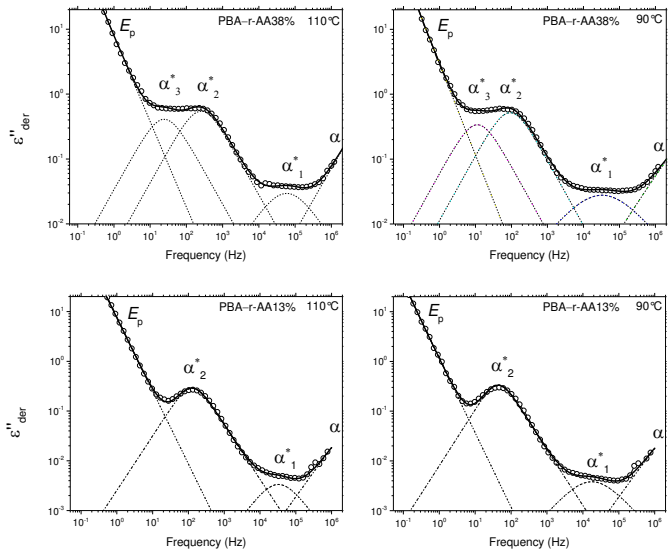

Figure 6.2: $\varepsilon''_{der}(\omega)$ of (top) PBA-*r*-AA38% and (bottom) PBA-*r*-AA13% supramolecular polymers decomposed into different contributions, *i.e.* $\alpha_1^*, \alpha_2^*, \alpha_3^*$ and E_p at various temperatures. In each data set the dashed and solid lines represent individual and sum of all contributions, respectively.

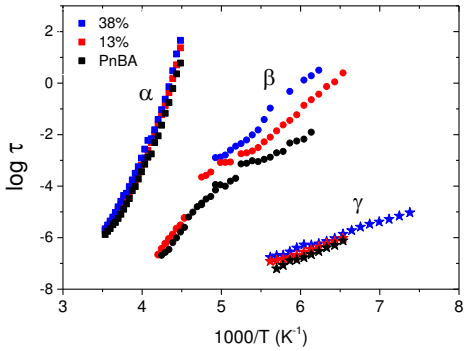

Figure 6.3: Activation plot of the α, β and γ relaxations of thePBA-*r*-AA supramolecular networks.

time of the α_1^* process is identical within the experimental error for both PBA-*r*-AA13% and 38% samples. On the other hand the α_2^* process in PBA-*r*-AA38% is clearly faster than that for the 13% sample. For the case of PBA-*r*-AA38%, α_3^* and α_2^* relaxations exhibit similar temperature dependency, and close relaxation times. It can also be seen that in the heating ramp after quenching, the two relaxations have equal T_C. Figure 6.4.b shows that the

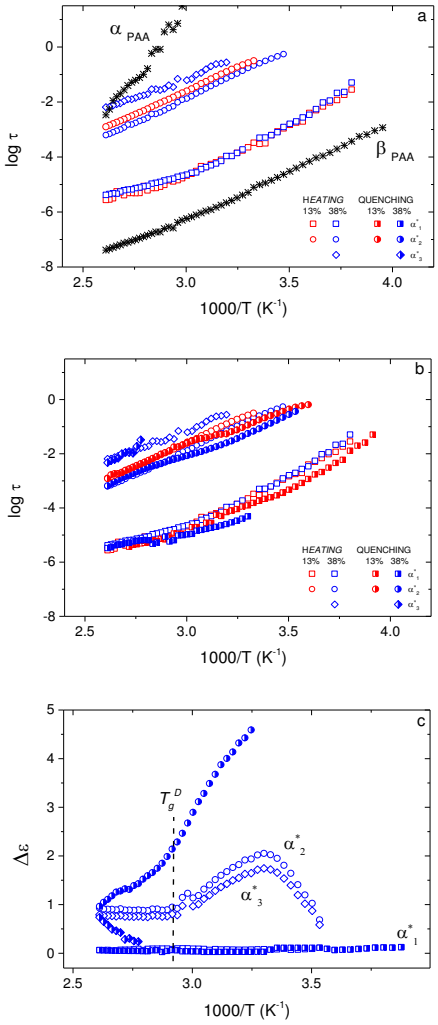

Figure 6.4: Activation plot of the α^* relaxations of the PBA-*r*-AA supramolecular networks (a) in equilibrium and (b) after quenching. (c) Evolution of the intensity of the α^* relaxations of the PBA-*r*-AA38%. Data captured in heating ramps for equilibrated and quenched samples are shown with open and half-filled symbols, respectively.

quenched supramolecular networks recover the α_2^* equilibrium dynamics above the dielectric glass transition ($T_C = T_g^D$) of pure PAA, which is the temperature at which the α-relaxation time of PAA is equal 100 s ($T_g^D = T|\tau_{\alpha\ PAA} = 100\ s$). Unlike α_2^*, the α_3^* relaxation disappears ($\Delta\varepsilon_{\alpha_3^*} = 0$) in the quenched sample and just recovers $> 90\ ^\circ C$. Figure 6.4.c shows that the intensities of the two relaxations in the equilibrium state are highly correlated. The correlation

between the two relaxation processes suggest that the α_2^* can be a sub process of α_3^* relaxation.

The black asterisks in Figure 6.4.a correspond to the α and β relaxation times of a pure PAA ($M_w = 15\ \ kg/mol$). The quantitative agreement between the α^* relaxations in the PBA-*r*-AA samples, particularly in the heating ramp after quenching, with the α and β relaxations of PAA suggest that there are distinct PAA domains embedded in a PnBA-rich matrix. These phases are formed via aggregation of AA monomers belonging to a single chain or several chains into individual domains. It should be mentioned that the very small alteration of the time scale and relaxation intensity of the α relaxation for the supramolecular polymers compared to PnBA strongly suggest that most of the associated supramolecular pairs are excluded from the PnBA rich matrix, by aggregation in the PAA rich domains.

Based on this argument the α_1^* and α_3^* relaxations are assigned to accelerated β and α relaxation in the PAA rich domains respectively. The deviation of these relaxation processes from the equilibrium behavior in pure PAA suggests confinement-induced accelerated dynamics, resulting in a substantial reduction of the glass transition temperature of nanometer sized PAA domains.[10] A comprehensive discussion on the microstructure of PBA*r*-AA samples is given in section 6.4. Using Maxwell-Wagner-Sillars (MWS) and Looyenga models for dielectric mixtures[11–13] the volume fraction of the PAA domains was estimated to be about 6% in the PBA-*r*-AA38% (See Appendix).

Generally there are two main possibilities for the origin of the α_2^* relaxation: i) A mesoscopic relaxation arises from polarization at the interface between the PAA and PnBA rich domains ii) A molecular relaxation of the associated supramolecular moieties. In the following we will discuss these two scenarios. Interfacial polarization (I_P) occurs due to the accumulation of charge carriers in the electric field at the interface of two phases with large differences in conductivity and permittivity. The hopping relaxation time of these charge carriers at the interface can give rise to an additional relaxation process. I_P strongly depends on the shape[11,12] and size[14] of the domains.

Figure 6.5 shows the evolution of *dc* conductivity of the PBA-*r*-AA samples against temperature. In the equilibrium state, *dc* conductivity of the supramolecular samples is almost one order of magnitude lower than that of PnBA. However, upon quenching the conductivity level of PnBA can be retrieved in the supramolecular polymers. Figure 6.5 proves that the presence of supramolecular moieties significantly decreases the diffusion coefficient of charge carriers in the PnBA-rich matrix, since AA groups interact with metallic cations, which are the major fraction of charged impurities in the system.

As a matter of fact, a very low conductivity level is expected inside the PAA domains below 100 $\ ^\circ C$, since the conductivity highly depends on the distance from T_g and also higher density of interaction between metallic cations and the supramolecular moieties are expected.

Since the charge transport in the continuous PnBA-rich matrix is much faster than that in the isolated PAA domains, the system has to be treated as inclusions of insulating particles suspended in a partially conductive matrix. In addition, diffusion of ions away from the boundaries has to be considered due

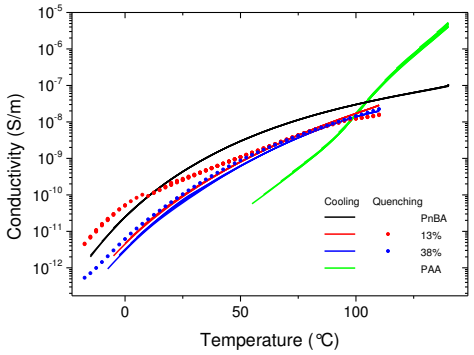

Figure 6.5: Evolution of the dc conductivity in the PBA-*r*-AA supramolecular polymers against temperature in the equilibrium (solid lines) and after quenching (dotted lines) states.

to nonmetric size of PAA domain. It is shown in the Appendix that proper dielectric mixture models do not predict I_P relaxations in the frequency window relevant to that of α_2^*. Therefore the α_2^* relaxation cannot be attributed to I_p. The second possible scenario for rationalizing the α_2^* relaxation is a molecular relaxation involving binary supramolecular associations. Müller *et al.*[15] proposed that both dissociation of the supramolecular pairs or reorientation of the pairs with respect to the electric field can give rise to fluctuation of the polarization vector in time, which is manifested by the relaxations in the dielectric permittivity. These authors proved that the macroscopic dielectric relaxation is dominated by the relaxation process which occurs faster. When the dissociation occurs faster than the reorientation of the binary assembly, a Debye process, which is the main characteristic of chemical relaxations, is expected on the macroscopic scale. On the other hand, if reorientation of the binary assemblies happens prior to dissociation, a broad asymmetric permittivity peak is expected since reorientation of the associated supramolecular moieties couples with the cooperative motion of the surrounding environment.[15]

As mentioned in the discussion of Figure 6.2, the α_2^* is strictly a Debye relaxation. Therefore, based on the arguing of Müller *et al.*, the α_2^* relaxation is assigned to the dissociation of AA dimers in the PAA domain. The Arrhenius activation energy of this process is $\sim 29 \;\; kJ/mol$.

The close correlation between the α_2^* and α_3^* relaxations can be explained based on the assigned molecular origins. Upon heating, the thermal energy of the system increases and eventually a large fraction of the supramolecular pairs will have the energy to dissociate due to shift in the equilibrium. As a result of this lower connectivity level and smaller friction between the adjacent segments, the energy barrier for the glass transition reduces, and eventually leads to structural relaxation in the glassy PAA domain. The structural relaxation process in the PAA domain is indeed a collective motion of the supramolecular

moieties, which occurs after progressive dissociation of the binary supramolecular associations. (See section 6.4 for detailed discussion)

In summary, in this part we have compelling evidence that the PAA-*r*-BA supramolecular networks are heterogeneous materials in which PAA domains are formed by aggregation of the supramolecular moieties (collective assembly). The internal dynamics of these domains are controlled by the dissociation of the binary supramolecular assemblies (manifested by the α_2^* relaxation) which give rise to the collective dynamics of the supramolecular groups (the α_3^* relaxation).

6.3.3 Rheology

In this section we investigate linear (LVE) and non-linear viscoelastic (NLVE) response of PBA-*r*-AA supramolecular networks. Our aim is to establish a direct relationship between segmental and bulk dynamics of supramolecular networks and the transient frictions imposed on the polymer chains by both binary supramolecular assemblies in PnBA-rich matrix and collective assemblies in the PAA domains. LVEs of PBA-*r*-AA networks and pristine PnBA at 25 $^\circ C$ are compared in Figure 6.6. While PnBA is almost flowing at this temperature, the supramolecular samples show delayed terminal relaxation time. At low frequencies, a second plateau is emerging which becomes more pronounced by increasing the AA monomer content. It is obvious from Figure 6.6 that the friction imposed by the supramolecular moieties also causes departure from the plateau modulus of PnBA. Just like the second plateau, the classical plateau modulus also increases with increasing supramolecular groups (Also see Figure 6.8 and discussion there).

The LVE response of the supramolecular networks is highly temperature dependent. Figure 6.7.a shows that by increasing temperature the second plateau decreases and shifts to lower frequencies. It is important to mention that the transition region between the first and the second plateau extends over several orders of magnitude by a slope of $\sim \frac{1}{2}$ against frequency axis (See Figure 6.7.a). This slope manifests that a Rouse process is the dominating stress relaxation mechanism on this time scale. By increasing the temperature or decreasing the AA content, the second plateau eventually disappears and is replaced by nearly parallel dynamic moduli. This parallel region dominates the LVE behavior over > 4 decades of frequency (See Figure 6.7.b), a behavior that is indicative for hydrogen bonding systems,[16] since the transient bonds are becoming weaker but do not vanish up to very high temperatures.[17,18]

Thixotropy is another well-known feature of many supramolecular polymers which arises from the competition between the equilibrium thermodynamics and hindered molecular motion in these systems. Despite a highly retarded terminal relaxation, the PBA-*r*-AA supramolecular networks, up to 38% AA content used in this work, exhibit equilibrium linear viscoelastic dynamics. In other words the LVE data presented in Figures 6.6 and 6.7 is independent of the thermal history of the supramolecular systems. To account for the possible role of slow relaxation mechanism during storage, the LVE of PBA-*r*-AA38% were re-measured at intervals of 3 and 9 months after the first measurement and the original data were reproduced within experimental errors. The equilibrium

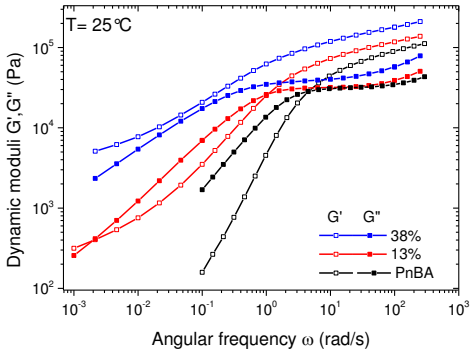

Figure 6.6: linear viscoelastic response of PBA-*r*-AA supramolecular networks at 25 $^{\circ}C$. LVE of pristine PnBA is also shown for comparison.

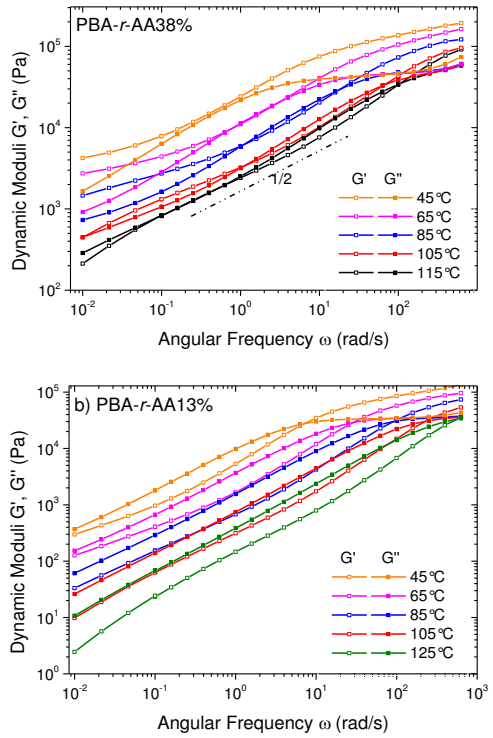

Figure 6.7: Temperature dependent storage and loss moduli (open and solid symbols, respectively) for (a) PBA-*r*-AA38% and (b) PBA-*r*-AA13% in the linear viscoelastic region.

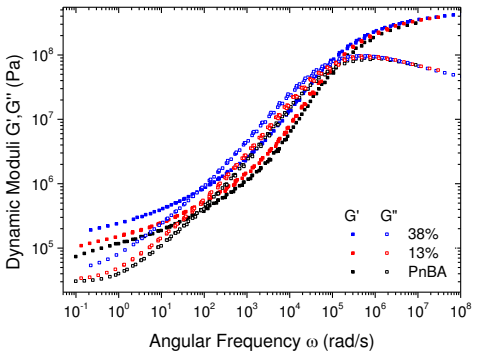

Figure 6.8: Master curve of dynamic moduli for PBA-*r*-AA supramolecular networks at iso-friction state ($T_g + 36\ ^\circ C$). Segmental Rouse dynamics of the supramolecular polymer are systematically delayed due to friction imposed by the binary supramolecular assemblies. Different measurements are only horizontally shifted using shift factors of the reference PnBA.

viscoelastic indeed originates from the equilibrium dynamics of PAA aggregates in the conventional heating and cooling ramps (See discussion of Figure 6.4).

In addition to bulk dynamics, segmental motion of the supramolecular polymers is also altered with respect to that of pristine PnBA. Figure 6.8 shows the dynamic moduli master curves of PBA-*r*-AA samples at the iso-friction state ($T_g + 36\ ^\circ C$) constructed using frequency sweeps at 6 different temperatures between $-45\ ^\circ C$ and $-15\ ^\circ C$. No vertical shift was used in constructing the master curves in Figure 6.8. For the supramolecular samples, different measurements are reduced to indivitual master curves using the shift factors of the reference PnBA, *i.e.* $C_1 = 8.17$ and $C_0 = 110$. Apart from well-known systematic scattering in the transition region between glassy and Rouse dynamics,[19] time temperature superposition (tTs) can be successfully applied to construct master curves in this time/length scales, *i.e.* the system shows thermorheological simplicity that is known for supramolecular polymers close to glass transition.[2,20,21] It is clear from Figure 6.8 that increasing AA monomer content results in delayed Rouse relaxation times, as well as higher plateau modulus compared to PnBA. Nonetheless, it is expected that upon increasing temperature, which leads to lower density of assemblies in the supramolecular networks, the plateau modulus and the Rouse relaxation time of pristine PnBA is recovered in the PBA-*r*-AA systems

Figure 6.9.a shows the extensional rheology of PnBA-*r*-AA38% and the reference PnBA for various strain rates. The strain rates are always increasing from right to left; *i.e.*, for PnBA the farthest curve to the right in Figure 6.9.a corresponds to the smallest strain rate 0.3 s^{-1} , and the farthest to the left corresponds to the highest strain rate 3 s^{-1}. In the case of PnBA-*r*-AA38%, strain rate ranges from 0.001 to 1 s^{-1}. The solid lines represent the corresponding LVE envelope determined from a multimode Maxwell fit

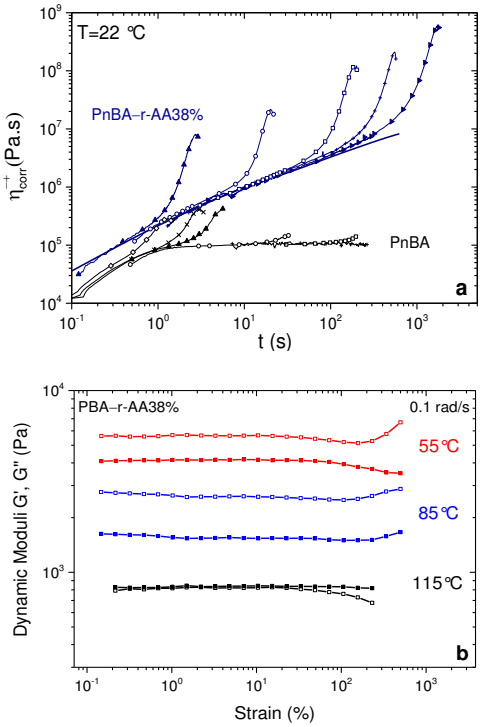

Figure 6.9: (a) Stress growth coefficient of PnBA-*r*-A38% and the reference PnBA measured using the filament stretching rheometer. The solid lines represent the best fit of the multimode Maxwell model to the LVE data. (b) Evolution of storage (open symbols) and loss (solid symbols) moduli of PBA-*r*-AA38% upon progressive increasing of strain in oscillatory shear at different temperatures. The oscillation frequency is fixed to 0.1 rad/s for all curves.

to the LVE data shown in Figure 6.6. It is evident from the LVE envelope that the shear viscosity is increasing with increasing AA content. Note that a terminal regime was not observed in the LVE data, and therefore a zero shear rate viscosity cannot be reported. Thus, any flattening observed in the LVE envelope (solid lines) is due to a finite number of modes used to fit the linear viscoelastic data and not the asymptotic approach to a zero shear rate viscosity. Typically in extensional rheology of monodisperse entangled linear polymer melts, the measured stress growth coefficient follows the LVE envelope for strain rates much less than the inverse Rouse time, $1/\tau_R$. For strain rates greater than $1/(0.5\tau_R)$, the stress growth coefficient deviates upward from the LVE envelope. This upward deviation is referred to as strain hardening. It is convenient to discuss the relative magnitude of strain rate ($\dot{\varepsilon}$) to τ_R in terms of the Weissenberg number, $Wi = \dot{\varepsilon}\tau_R$; *i.e.*, for monodisperse entangled linear polymers when $Wi < 0.5$ no strain hardening is expected and when $Wi \geq 0.5$

strain hardening is expected. Figure 6.9.a illustrates that the transient frictions of binary and collective assemblies in PnBA-r-AA38% significantly decrease the onset of strain hardening to $Wi \leq 4 \times 10^{-5}$. At small times, all curves follow the LVE envelop. At larger times there is a sharp strain hardening behavior observed for all measured strain rates. The strain hardening achieves a magnitude 2 order higher than the LVE envelope and 4 orders of magnitude higher than the zero shear rate viscosity of PnBA.

Figure 6.9.b indeed shows that strain hardening can also be observed in the large amplitude oscillatory shear flow. Like LVE, NLVE behavior of the PBA-r-AA supramolecular polymers has complex temperature dependency. PBA-r-AA38% shows strain hardening at 55 and 85 $^{\circ}C$, while at 115 $^{\circ}C$ strain softening is observed.

Summarizing the above made observations, we illustrated that both linear and nonlinear viscoelastic properties of the entangled PBA-r-AAs are dominated by the supramolecular groups. The important dynamic features are emergence of a second plateau, strain hardening and retardation of segmental motion. Strong temperature dependency is observed for all these dynamic features.

6.4 Correlation Between Microstructure and Dynamics of the Supramolecular Networks: Towards A General Picture

In this section we propose a molecular microstructure for the PBA-r-AAs based on the viscoelastic and dielectric results. We will couple our findings to the existing literature on associating polymers, with the objective to generalize our understanding on the microstructure of entangled supramolecular networks. In doing so, we take advantage of analogies between self-assembling block copolymers and supramolecular networks, yet carefully consider critical distinctions of the two class of systems. We first introduce the main ingredients of our model.

Collective assemblies lead to PAA domains: It was argued in the section 6.3.2 that the PBA-r-AA supramolecular polymers are inherently heterogeneous materials with supramolecular collective assemblies embedded in a polymer-rich matrix. The deviation of the glass transition dynamics of PAA domains from the one of bulk PAA, suggest that the structural relaxations in the supramolecular aggregates are affected by chain connectivity. With respect to PAA phase there are three main observations: i) acceleration of the structural relaxation dynamics (α_3^*) with respect to the that in the bulk (α_{PAA}) ii) complete breakdown of VFT temperature dependency of structural relaxation dynamics to an Arrhenius one and iii) emergence of a highly correlated subprocess (α_2^*) with relaxation time close to the structural relaxation dynamics (α_3^*).

These three observations are typical consequences of geometrical confinement in soft matter (See chapter 7 in reference[10]) and prove that PAA domains of the size of a few nanometer exist, being dispersed in the PnBA-rich

matrix. According to Adams and Gibbs, who introduced the idea of cooperative glass transition dynamics by postulating cooperative rearranging regions (CRR), cooling a super cooled liquid increases the size of CRR (ξ), which is manifested by progressive increase of the structural relaxation time. The typical size of CCR have been found to be in the order of $2-3$ nm for most glass formers at T_g, which reduces accordingly for higher temperatures with increasing distance to T_g.[22] Upon cooling a glass forming liquid, confinement effects are observed when ξ approaches the size of geometrical confinement. Although the present picture ignores the diversity in shape and heterogeneous nature of the dynamically correlated regions, it helps in acquiring information about the size of collective assemblies in PBA-r-AAs.

A second consideration concerns the impact of supramolecular association on the free energy of the system, which can be decomposed into 4 main contributions:

i) The supramolecular forces between moieties which are situated adjacent to each other.

ii) Interfacial tensions between matrix and collective assemblies.

iii) The entropic-elastic forces required to deform and stretch the polymer coil (see below)

iv) The hard core (steric) repulsions preventing the system from collapsing under influence of van der Waals and supramolecular interaction. Neglecting thermal expansion steric repulsions lead to constant density (uniform packing) of the material.[23]

The decrease of thermal energy (kT) results in lower entropic-elastic forces and a larger equilibrium constant for binary supramolecular assemblies. The latter is the driving force towards collective assembly and the former is the resistance against it.[24] Hence upon cooling larger number of AA groups can be accommodated inside the existing PAA domains and new domains are expected to form.[25] Minimization of the interfacial tensions implies enlargement of existing PAA domains rather than formation of a large fraction of new ones. Hence just like ξ, upon cooling, the PAA domains grow in size.
According to the Adam Gibbs model, if ξ grows faster and eventually exceeds the size of the PAA domains (r_{PAA}), a breakdown of the VFT-type dynamics due to geometrical confinement will be observed. Figure 6.4.b illustrates that the confinement effect is observed below 100 $^{\circ}C$, where a sizable deviation from the structural relaxation time of bulk PAA is observed. Hence it can be suggested that $r_{PAA} \sim \xi_{PAA}$ at 100 $^{\circ}C$. In other words PAA domains are only a few nanometers in size (< 5 nm).

Using a statistical approach we can draw crude guidelines for sequences of AA monomers to participate in PAA domains. The randomness of hydrolysis implies that in addition to a large fraction of isolated AA monomers, there are sequences of consecutive AA monomers along the PBA-r-AA copolymer chains. The probability of having a sequence of X AA monomers, $P_{seq}(X)$, depends on the total AA monomer content as well as their distribution along

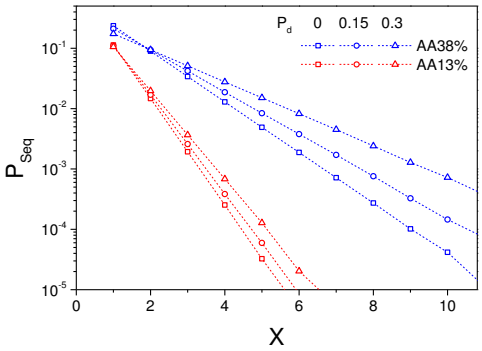

Figure 6.10: Probability of having sequences with X consecutive AA monomers in chains containing 1640 monomer and in average 13 or 38 $mol\%$ acid groups at 3 degrees of distribution . For clarity, $P_{seq}(x)$ is printed for selected points.

the chain (P_d). Depending on the P_d a full spectrum of samples ranging from complete randoms ($P_d = 1$) to two block copolymers ($P_d = 0$) can be formed. P_d is dependent upon the hydrolysis reaction conditions such as choice of salt, temperature and concentration. $P_{seq}(X)$ for chains having 1640 monomers and in average 38 and 13 $mol\%$ AA monomers at 3 degrees of sticker distribution is illustrated in Figure 6.10. Note that $P_{seq}(X)$ decreases exponentially with increasing X.

Figure 6.10 shows that $P_{seq}(2)$ is just $\sim$ 0.015 and $\sim$ 0.09 in PBA-r-AA 13% and 38% respectively and that the major fraction of AA monomers are isolated by BA monomers in both systems. Larger sequences are extremely scarce in both random copolymers. We remind that ″conventional″ dielectric mixing models estimate the volume fraction of PAA domains inside PBA-r-AA 38% to be roughly 6%. Considering the low probabilities of having AA sequences and assuming that the monomeric volume of AA and BA are similar in both PAA domains and PnBA-rich matrix, we can argue that any sequence with at least 2 AA monomers largely participates in the PAA domains. Of course, thermodynamic equilibrium urges that a fraction of the AA sequences remains in the PnBA-rich matrix. Note that we do not exclude the possibility that the isolated AA monomers participate in the PAA domains, however with respect to the small activation energy of hydrogen bonds between carboxylic acid dimers which is in the range of entropic-elastic forces of the chains, it is not likely that a sizable fraction of the isolated AA monomers are involved in the PAA domains. This conclusion is in line with the large systematic increase of the β relaxation by increasing AA content from the values of PnBA matrix which confirms the presence of a considerable amount of AA monomers in this phase.[9]

Interlayer between the PAA domains and the PnBA-rich matrix: Experimental and theoretical frameworks for the self-assembly of immiscible block copolymers are well established. For a given AB bock copolymers, in

which volume fraction of A block (Φ_A) is much smaller than that of B block (Φ_B), it is known that the A block phase separate into spherical micelles and the B block form the matrix. The theoretical thermodynamic driving force at the initial step of phase separation is the exponential decrease of the free energy by local fluctuations of the A block with respect to the Φ_A. In the later stages, known as strong segregation region (SSR), formation of sharp interfaces between pure A and B self-assembled regions results in further stability of the immiscible block copolymer.[26]

Semenov[27] theoretically illustrated that this phase separation of incompressible copolymers in SSR results in extended conformation of A segments inside the domains. In other words one end of the segments has to reach the center and the other end will place itself at the boundary of the A domains. Hence the radius of the micelle (r_A) is expected to be bigger that the unperturbed end-to-end distance of the A block. Since A and B bock are connected in the block copolymer, he proved that an interlayer exists between the two phases, in which the junctions of A and B blocks are concentrated. The segments in the interlayer must be highly extended and no foreign B chain can enter this region otherwise conservation of mass is violated in the region ($\Phi_B >> 1$). The segments in the interlayer have restricted mobility compared to those in the bulk. Nyrkova *et al*[25] have extended Semenov theory[27] to multi-block copolymers as well as the limiting case of random copolymers, and proposed that size and number of chains in the A domain as well as the inter-distance between individual domains (D) all scale with the surface tension between the blocks (δ). Note that in the derivation of this theory in the reference.[25] only interfacial and entropic-elastic forces were considered. To avoid singularity of the model and infinite r_A when $\delta \to 0$ by reducing temperature, the authors developed theoretical framework for a regime where either r_A is equal to the size of A block or the surface of the A block is completely covered by the A-B junctions, hence the domains cannot grow further. This regime, which is called superstrong segregation regime (sSSR), is relevant to copolymers with extremely short A blocks and bearing strongly interacting groups, for instance random ionomers. Nyrkova *et al.*[25] proved the existence of the interlayer for random ionomers and in general random supramolecular polymers in the sSSR, as well.

It was stated that the size of PAA domains change with temperature, hence phase separation in the PBA-*r*-AA polymers occurs in the SSR. Either case, whether collective assembly takes place in the SSR or sSSR, the aggregates are separated from the matrix by interlayer of extended segments, which has lower mobility compared to the bulk segments.

The thickness of an interlayer is believed to be in the order of persistence length of the polymer[28–30] which is shown to be temperature independent.[31] In other words the region of restricted mobility increases in size by increasing chain rigidity. Interesting observations were made in systems with sizable fraction of interlayer. For instance in sulfonated polystyrene ionomers where a large volume fraction of interlayer is surrounding domains of collective assemblies (multiples) a second glass transition higher than the one of neat polystyrene is observed. This second glass transition was attributed to coalescing interlayers

which eventually form a continuous phase.[28,32] It was shown that dynamics of chains in the interlayer can be modified independently from the bulk (See chapter 8 in the reference[33]).
Combining the dielectric observations with the theoretical works in the references [27,25], we conclude that the PAA domains are essentially small aggregates of binary associated AA units, which are isolated from the matrix by an interlayer of PnBA segments being covalently connected to the AA monomers. These segments adopt extended conformations in both PAA domains and the interlayer. The interlayer is most probably free from AA monomers, as these monomers in the interlayer would experience strong supramolecular interactions, and would tend to be incorporated in the PAA domains.

Trapped segments: The second plateau observed in LVE response of PnBA is attributed to the fraction of segments which are bound between two PAA-rich domains,[34] here we refer to them as trapped segments. There are mainly two types of constraints acting on the trapped segments, the PAA domains pinning ends and hence disabling stress relaxation via fluctuation and reptation mechanism, as well as the entanglements with the other chains or trapped segments. Therefore the trapped-segments can only relax by Rouse process up to the longest Rouse segments and later by activated constraint release Rouse process when the entanglements are relaxed. This scenario justifies the slope of the transition region between the two plateaus. The lack of mobility of trapped segments will result in stress concentrations and eventually stretched conformation of these segments in the NLVE field. Hence the strain hardening in the initial stage mainly originates from the long relaxation time of trapped segments. In the highly stretched regime one can also consider a contribution to stain hardening coming from higher fraction of binary supramolecular assemblies in the matrix, since chains are aligned in close proximities, which cause higher density of elastically active chains.[35]

The temperature dependence of the second plateau and the strain hardening in PBA-*r*-AA supramolecular networks can be rationalized by taking into account thermodynamic equilibrium between binary and collective assemblies. Upon increasing temperature the rate of exchange between binary and collective assemblies increases and the equilibrium shifts toward larger fraction of binary assemblies. Once a binary supramolecular assembly is detached from the PAA domains the trapped segment will be able to relax the stress by fluctuations. As a results of smaller number of trapped chains at high temperature, the second plateau modulus and strain hardening become less pronounced, until eventually disappear.

Semenov[27] calculated that the interdistance between the A domains (λ), scales with the number of monomers as $\lambda \propto N_B^{1/3}$. Similar scaling law was suggested for ionomers.[36] As the interdistance grows slower than the end-to-end distance of trapped chains ($\propto N_B^{1/2}$) one can conclude that the trapped chains have to connect remote A domains and not adjacent ones. In other words a small fraction of trapped chains are expected in entangled supramolecular polymers. In the case of PBA-*r*-AA13 and 38% respectively, solely the stress carried by $2-4$ and $7-10$ $mol\%$ of the chains give rise to the low frequency second plateau.

Segmental mobility alters by binary assemblies: Large deviation of the β relaxation of the PnBA-rich matrix suggests the presence of a considerable amount of AA monomers in this phase.[8] On the other hand, minute changes of the α relaxation and glass transition, imply that only a small fraction of these AA monomer are in the associated state. The binary associations of supramolecular groups justifies the alteration of the segmental dynamics at low temperature, since they constraint the longest statistical segment which can relax by the Rouse process.[37] In contrast, the life time and density of the binary supramolecular associations decrease at high temperatures, making significant deviations from the segmental dynamics of pure PnBA unlikely for the PBA-rich matrix in the supramolecular polymers.

Based on our dynamic study and the wealth of publications on supramolecular polymers we propose the following molecular picture for entangled associative polymers in which the supramolecular moieties are distributed along the backbone. Strong binary supramolecular interactions and surface tension between the polymer backbone and the moieties drives the latter to collectively self-assemble into distinct domains. The size of the domains depends on the chemical structure of both supramolecular groups and the polymer backbone as well as the surface tension. Hence it varies from a few nanometers to several microns in different supramolecular systems. An interlayer exists between the supramolecular aggregates and the polymer matrix, in which only the chains which are contributing to the supramolecular domains are present. The segments are expected to have extended conformation and restricted mobility compared to the bulk segments. If the chains are long enough (*e.g.* entangled), a fraction of the chains may enter more than one collective assembly therefore trapped segments are formed. If at the time scale of the experiment the trapped segments cannot escape from the constraints of the supramolecular domains, then a second plateau is formed. Since the thermodynamic equilibrium between binary and collective assemblies drive the possibility that a trapped chain detaches from the constraining aggregate, the second plateau is expected to exhibit Arrhenius temperature dependency. Finally if some scarce supramolecular moieties which are not excluded from the polymer matrix by collective assembly, form binary associations with life time larger than the longest Rouse time (τ_R^{Max}) a slowing down of the segmental motion is also observed. Since three types of constraints are imposed on the chains, *i.e.* entanglements, binary and collective assemblies of supramolecular groups, the classical plateau modulus (G_N^0) is expected to increase, if the time scale of any of the transient frictions is comparable to the Rouse time of the entangled strands (τ_e). Figure 6.11 schematically depicts the proposed microstructure.

6.5 Conclusion

Partially hydrolyzed, entangled, associating polymers based on PnBA were used to examine the influence of binary and collective assemblies of supramolecular moieties on the dynamics of these systems. It was shown that PBA-*r*-AAs organize in nanometer-sized (confined) PAA domains dispersed in a PnBA-rich matrix. BDS were successfully used to study dynamics of binary assem-

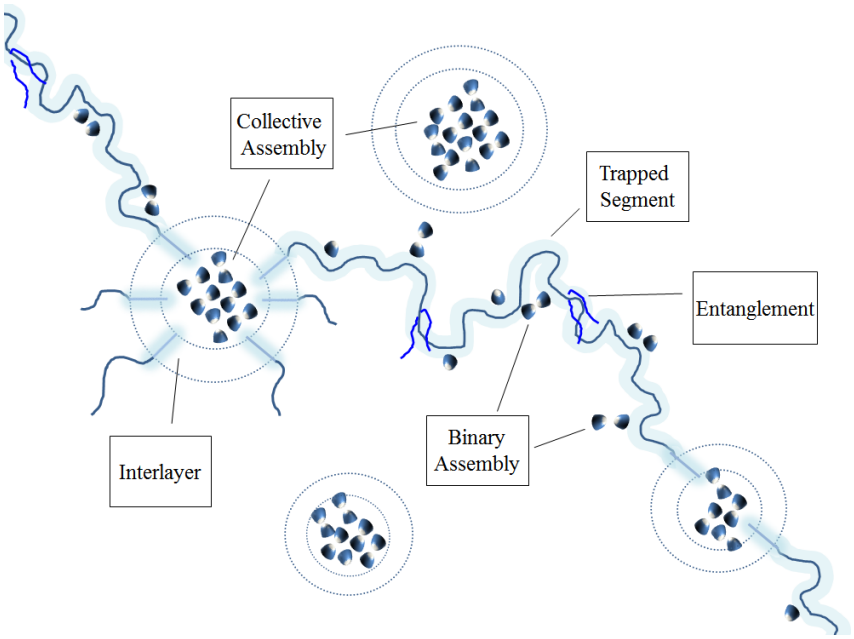

Figure 6.11: Schematic representation of the proposed microstructure of PBA-*r*-AAs. The AA monomers are depicted by cones. Binary assembles are shown by two cones pointing toward each other in close proximity. The picture is valid for any entangled supramolecular network in which moieties are distributed along the polymer backbone.

blies in the PAA domains, as well as internal structural relaxation of these collective assemblies. A distinct relaxation process, closely linked to the structural relaxation dynamics of these glassy domains, is ascribed to the association/dissociation dynamics of binary assemblies in the PAA domains.

Using rheology we showed that segmental and bulk dynamics of PBA-*r*-AA supramolecular systems depend on the concentration of supramolecular moieties (*i.e.* degree of hydrolysis). Moreover, a strong temperature dependence was observed in both linear and nonlinear viscoelastic behavior of PBA-*r*-AAs, namely low frequency second plateau level and relaxation times. Based on these observations and the theoretical framework of self-assembly in copolymers, we proposed a general microstructure for entangled, supramolecular networks in which ″sticky″ moieties are located along the chains. In this picture binary assemblies phase separate into collective ones, which are separated by an interlayer from the matrix. The chains are stretched inside the collective assemblies and the interlayer. A small fraction of chains bridge the collective assemblies. The stress carried out by the trapped segments between collective domains give rise to a low frequency second plateau in LVE and strain hardening in NLVE regimes. In the temperature window were the life time of binary assembles inside matrix is longer than the longest Rouse relaxation time of the chain,

alteration of segmental dynamics is also expected. The plateau modulus can also increase due to long life constraints imposed by either binary or collective assemblies, which are temperature dependent.

6.6 Appendix

In the ″conventional″ dielectric mixture theories the size of the inclusions is not considered and emphasis has put on the shape factor.[11] There is a critical assumption in the conventional models, such as MWS, Looyenga and Hanai-Bruggman, that the free charges are accumulated at the boundaries. In reality, when an electric field is applied to a (partially) conductive heterogeneous dielectric, the charges can move and accumulate near the boundaries. The diffusion of the charges away from the boundaries leads to a charged layer. The thickness of this layer is known as Debyes screening length $(1/\kappa)$. When the inclusion size (r_p) is comparable to the Debyes length, strong mismatch with the prediction of the ″conventional″ mixture models are observed because these models treat space charges as surface ones[14,38,39].

In suspensions of conducting particles in insulating matrix, Boersma and van Turnhout[14] showed that when Debyes length is much larger than the thickness of the conductive layer $(r_p\kappa \ll 0)$ there is no charge accumulation at the boundaries. These authors calculated Debyes length in a few polymeric interfaces to be around 1 μm. Garcia *et al.*[38] treated diffusive effects in the boundaries of conductive spheres and a conductive matrix, where spheres are surrounded by an insulating shell. This model has the final form of:

$$\varepsilon_c^* = \varepsilon_m^*(1 + 2\Phi_p A_m)(1 - \Phi_p A_m) \tag{6.3}$$

In the suspensions of insulating particles in conductive matrix A_m is defined as

$$\begin{aligned} A_m &= \left[\varepsilon_p^* - (\varepsilon_m^* + \varepsilon_p^*\Xi)\right] / \left[\varepsilon_p^* + 2(\varepsilon_m^* + \varepsilon_p^*\Xi)\right] \\ \Xi &= \frac{\sigma}{i\omega\varepsilon_0\varepsilon_m^*} \frac{\Lambda_m r_p + 1}{(\Lambda_m r_p)^2 + 2(\Lambda_m r_p + 1)} \\ \Lambda_m^2 &= \kappa^2(1 + i\omega\frac{\varepsilon_0\varepsilon_m^*}{\sigma_m}) \end{aligned} \tag{6.4}$$

where subscripts c, m and p address composite, matrix and particle respectively and ε_0 is the permittivity of vacuum $(8.854^*10^{-12}\ \ F/m)$.

It was argued in the section 6.4 that the size of the PAA domains does not exceed 5 nm. Considering $1/\kappa$ to be only 0.1 μm, we applied the Garcia model to the PBA-r-AA systems. Results are shown in Figure 6.12, where the real part of permittivity and its derivative are separated in the left and right panels, respectively. It should be mentioned that the experimental data of PnBA and PAA (black and green solid circles, respectively) are significantly affected by the E_P which depends on the aspect ratio of the geometry. E_P contribution was subtracted by fitting the data with Havriliak-Negami formalism, shown by black and green open circles. Note that contrary to MWS and Looyenga

models which predict an increase of dielectric permittivity compared to PnBA, Garcia model estimates lowed permittivity plateau for the PBA-r-AA in this range of $r_p\kappa$ (For a discussion on different regimes of $r_p\kappa$ see[39]). MWS and Looyenga models suggest that there is almost 6 $vol\%$ PAA domains in the PBA-r-AA38% network.

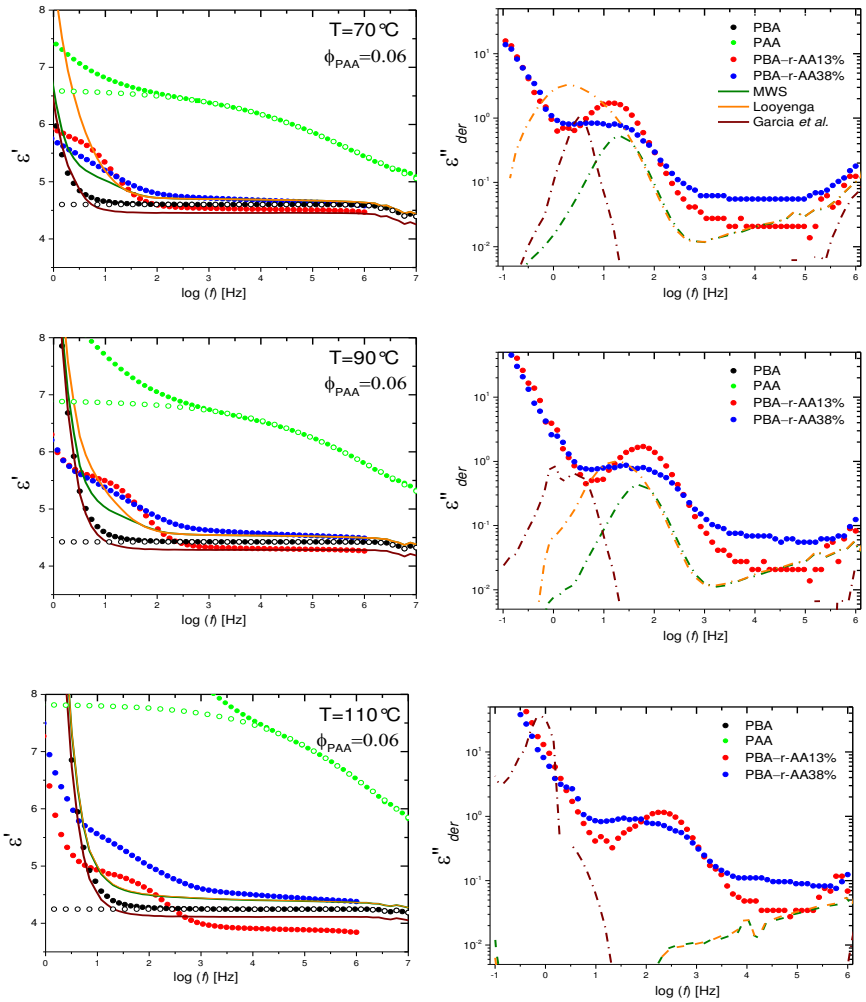

Figure 6.12: Crude estimate of the volume fraction of the PAA aggregates (Φ_{PAA}) in the PBA-AAs and interfacial relaxation process at different temperatures, using Maxwell-Wagner- Sillars (MWS), Looyenga and Garcia *et al.* models (Olive, orange and wine respectively). Solid circles and lines show experimental data and the predictions of the models based on that, whilst open circles and dashed lines represent the case where E_p is truncated from the experimental data and subsequently used in the models to predict mixture properties.

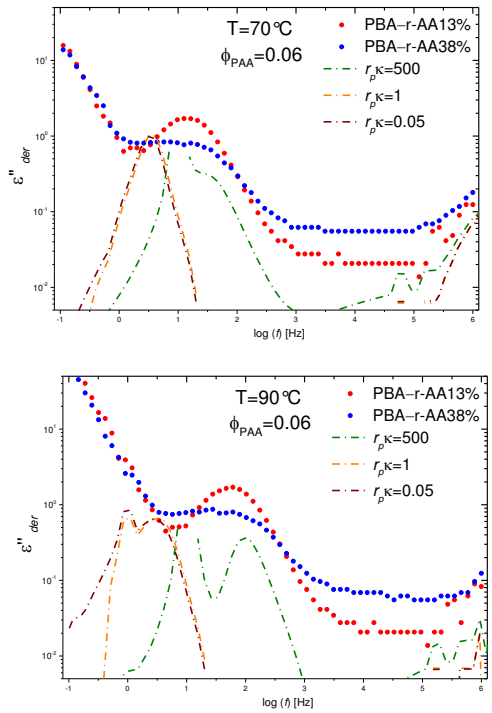

Figure 6.13: Prediction of the Garcia model for three sets of r_pK

Interpretation of the interfacial relaxation time in the system is very delicate. All models predict I_P relaxations at 70 and 90 $^\circ C$. On the other hand, while no relaxation is predicted by MWS and Looyenga at 110 $^\circ C$, Garcia model predict a strong I_P process, albeit in very low frequencies. Hence the α_2^* relaxation which is observed at all temperature range > 25 $^\circ C$ cannot be assigned to the accumulation of charges at the boundaries. Not that although MWS captures the relaxation process at lower temperatures but as mentioned above its validity in the current system is questionable since diffusion effects are not considered in this model. On the other hand, the predictions do not exclude the possibility of having I_P. From the relaxation process estimated by the Garcia model one can deduce that the interfacial polarization might be masked underneath the strong electrode polarization. However the intensity and position of the I_P relaxation predicted by the Garcia model strongly depends on the $r_p\kappa$ value. In lack of information about the Debyes length in the PBA-r-AA system we performed a parametric study to evaluate the trends in the model predictions, shown in Figure 6.13.

It can be concluded from Figure 6.13, that in situations where $r_p\kappa \leq 1$, the prediction of the Garcia model is not heavily influenced by the error induced in determination of the Debyes screening length. Therefore the main conclusion of this section *i.e.* neither α_2^* nor α_3^* relaxations arise from interfacial polarization

phenomena, which was established with respect to the prediction of the mixture models, is valid.

6.7 Bibliography

1 Wübbenhorst, M.; Van Turnhout, J. Analysis of Complex Dielectric Spectra. I: One-Dimensional Derivative Techniques and Three-Dimensional Modelling. *J. Non. Cryst. Solids* **2002**, 305 (1-3), 40-49.

2 Stadler, F. J.; Pyckhout-Hintzen, W.; Schumers, J.-M.; Fustin, C.-A.; Gohy, J.-F.; Bailly, C. Linear Viscoelastic Rheology of Moderately Entangled Telechelic Polybutadiene Temporary Networks. *Macromolecules* **2009**, 42 (16), 6181-6192.

3 Ahn, D.; Shull, K. R. Effects of Methylation and Neutralization of Carboxylated Poly(n-Butyl Acrylate) on the Interfacial and Bulk Contributions to Adhesion. *Langmuir* **1998**, 14 (13), 3637-3645.

4 Bose, R. K.; Hohlbein, N.; Garcia, S. J.; Schmidt, A. M.; van der Zwaag, S. Relationship between the Network Dynamics, Supramolecular Relaxation Time and Healing Kinetics of Cobalt Poly(butyl Acrylate) Ionomers. *Polymer (Guildf).* **2015**, 69, 228-232.

5 Shabbir, A.; Goldansaz, H.; Hassager, O.; Ruymbeke, E. Van; Alvarez, N. J. The Effect of Hydrogen Bonding on Linear and Nonlinear Rheology of Entangled Polymer Melts; **2015**.

6 Kremer, F.; Schnhals, A. *Broadband Dielectric Spectroscopy*; 2003.

7 Macdonald, J. R. Theory of Ac Space-Charge Polarization Effects in Photoconductors, Semiconductors, and Electrolytes. *Phys. Rev.* **1953**, 92 (1), 4-17.

8 Hayakawa, T.; Adachi, K. Dielectric Relaxation of Poly(n-Butyl Acrylate). *Polym. J.* **2000**, 32 (10), 845-848.

9 Gaborieau, M.; Graf, R.; Kahle, S.; Pakula, T.; Spiess, H. W. Chain Dynamics in Poly(n-Alkyl Acrylates) by Solid-State NMR, Dielectric, and Mechanical Spectroscopies. *Macromolecules* **2007**, 40 (17), 6249-6256.

10 Kremer, F. *Dynamics in Geometrical Confinement*; 2014.

11 Bánhegyi, G. Comparison of Electrical Mixture Rules for Composites. *Colloid Polym. Sci.* **1986**, 264 (12), 1030-1050.

12 Bánhegyi, G. Numerical Analysis of Complex Dielectric Mixture Formulae. *Colloid Polym. Sci.* **1988**, 266 (1), 11-28.

13 Steeman, P. A. M.; Maurer, F. H. J.; Van Turnhout, J. Dielectric Properties of Blends of Polycarbonate and Acrylonitrile-Butadiene-Styrene Copolymer. *Polym. Eng. Sci.* **1994**, 34 (9), 697-706.

14 Boersma, a.; van Turnhout, J. Dielectric Study on Size Effects in Polymer Laminates and Blends. *J. Polym. Sci. Part B Polym. Phys.* **1998**, 36 (15), 2835-2848.

15 Müller, M.; Stadler, R.; Kremer, F.; Williams, G. On the Motional Coupling between Chain and Junction Dynamics in Thermoreversible Networks. *Macromolecules* **1995**, 28, 6942-6949.

16 Lewis, C. L.; Stewart, K.; Anthamatten, M. The Influence of Hydrogen Bonding Side-Groups on Viscoelastic Behavior of Linear and Network Polymers. *Macromolecules* **2014**, 47 (2), 729-740.

17 Zhang, S.; Painter, P. C.; Runt, J. Coupling of Component Segmental Relaxations in a Polymer Blend Containing Intermolecular Hydrogen Bonds. *Macromolecules* **2002**, 35 (25), 9403-9413.

18 Isasi, J. R.; Cesteros, L. C.; Katime, I. Hydrogen Bonding and Sequence Distribution in Poly(vinyl Acetate-Co-Vinyl Alcohol) Copolymers. *Macromolecules* **1994**, 27 (8), 2200-2205.

19 Matsumiya, Y.; Uno, A.; Watanabe, H.; Inoue, T.; Urakawa, O. Dielectric and Viscoelastic Investigation of Segmental Dynamics of Polystyrene above Glass Transition Temperature: Cooperative Sequence Length and Relaxation Mode Distribution. *Macromolecules* **2011**, 44 (11), 4355-4365.

20 Chen, Q.; Masser, H.; Shiau, H. S.; Liang, S.; Runt, J.; Painter, P. C.; Colby, R. H. Linear Viscoelasticity and Fourier Transform Infrared Spectroscopy of Polyether-Ester-Sulfonate Copolymer Ionomers. *Macromolecules* **2014**, 47 (11), 3635-3644.

21 Van Ruymbeke, E.; Vlassopoulos, D.; Mierzwa, M.; Pakula, T.; Charalabidis, D.; Pitsikalis, M.; Hadjichristidis, N. Rheology and Structure of Entangled Telechelic Linear and Star Polyisoprene Melts. *Macromolecules* **2010**, 43 (9), 4401-4411.

22 Erwin, B. M.; Colby, R. H. Temperature Dependence of Relaxation Times and the Length Scale of Cooperative Motion for Glass-Forming Liquids. *J. Non-Crystalline Solids*, **2002**, 307-310, 225-231.

23 Dreyfus, B. Model for the Clustering of Multiplets in Ionomers. *Macromolecules* **1985**, 18 (2), 284-292.

24 Goldansaz, H.; Auhl, D.; Goderis, B.; Voleppe, Q.; Fustin, C.-A.; Gohy, J.-F.; Bailly, C.; van Ruymbeke, E. Transient Metallosupramolecular Networks Built from Entangled Melts of Poly(ethylene Oxide). *Macromolecules* **2015**, 48 (11), 3746-3755.

25 Nyrkova, I. A.; Khokhlov, A. R.; Doi, M. Microdomains in Block Copolymers and Multiplets in Ionomers: Parallels in Behavior. *Macromolecules* **1993**, 26 (14), 3601-3610.

26 Rubinstein, M.; Colby, R. H. *Polymer Physics*; OUP Oxford, 2003.

27 Semenov, A. N. Contribution to the Theory of Microphase Layering in Block-Copolymer Melts. *J. Theor. Exp. Phys.* **1985**, 61 (4), 733-742.

28 Eisenberg, A.; Hird, B.; Moore, R. B. A New Multiplet-Cluster Model for the Morphology of Random Ionomers. *Macromolecules* **1990**, 23 (18), 4098-4107.

29 Tant, M. R., Mauritz, K. A., Wilkes, G. L., Eds. *Ionomers: Synthesis, Structure, Properties and Applications*; Springer Netherlands: Dordrecht, 1997.

30 Semenov, A. N.; Nyrkova, I. A.; Khokhlov, A. R. Polymers with Strongly Interacting Groups: Theory for Nonspherical Multiplets. *Macromolecules* **1995**, 28 (22), 7491-7500.

31 Wignall, G. D.; Ballard, D. G. H.; Schelten, J. Measurements of Persistence Length and Temperature Dependence of the Radius of Gyration in Bulk Atactic Polystyrene. *Eur. Polym. J.* **1974**, 10 (9), 861-865.

32 Gauthier, M.; Eisenberg, A. Matrix Polarity Effects on Ionic Aggregation in a Nitrated Styrene Ionomer. *Macromolecules* **1989**, 22 (9), 3756-3762.

33 Eisenberg, A.; Kim, J.-S. *Introduction to Ionomers*; Wiley, 1998.

34 Hawke, L. G. D.; Ahmadi, M.; Gondansaz, H.; van Ruymbeke, E. Viscoelastic Properties of Linear Associating Poly(n-Butyl Acrylate) Chains; **2015**.

35 Xu, D.; Hawk, J. L.; Loveless, D. M.; Jeon, S. L.; Craig, S. L. Mechanism of Shear Thickening in Reversibly Cross-Linked Supramolecular Polymer Networks. *Macromolecules* **2010**, 43 (7), 3556-3565.

36 Eisenberg, A. Clustering of Ions in Organic Polymers. A Theoretical Approach. *Macromolecules* **1970**, 3 (2), 147-154.

37 Seidel, U.; Stadler, R.; Fuller, G. G. Relaxation Dynamics of Bidisperse Temporary Networks. *Macromolecules* **1994**, 27 (8), 2066-2072.

38 Garcia, A.; Barchinit, R.; Gross, C. The Influence of Diffusion on the Permittivity of a Suspension of Spherical Particles with Insulating Shells in an Electrolyte. *J. Phys. D. Appl. Phys.* **1985**, 18, 1891-1896.

39 Garcia, A.; Grosse, C.; Brito, P. On the Effect of Volume Charge Distribution on the Maxwell-Wagner Relaxation. *J. Phys. D Appl. Phys.* **1985**, 18, 739-745.

Chapter 7

Entangled Supramolecular Networks Based on Poly (n-butyl acrylate-g-Ureidopyrimidinone)

Outline

Most of the studies on supramolecular transient networks have avoided dealing with complex polymer dynamics, by utilizing chains shorter than entanglement molecular weight, while in most applications polymer chains are well-entangled. This work aims to address properties of this important class of associating polymers. We have therefore used atom transfer radical polymerization (ATRP) to synthesize high molecular weight poly (n-butyl acrylate)s with low polydispersities and functionalized them with strong hydrogen bonding Ureidopyrimidinone (UPy) groups.

Even though PnBA precursor is amorphous, the supramolecular networks show several melting peaks which are attributed to the diversity of shape and size of the collective assemblies (UPy stacks), as confirmed by optical microscopy. Non-spherical collective assemblies are formed at high UPy contents. Viscoelastic properties are significantly affected by UPy associations. There is a clear relationship between rearrangement of collective assemblies and stress relaxation in these supramolecular networks. The results confirm the universal microstructure picture proposed in Chapter 6.

A low frequency second plateau is once again observed in storage modulus. The magnitude of the plateau modulus and the second plateau increases, by increasing the UPy content. A transition region between the two plateaus is observed with a clear slope of $\frac{1}{2}$ against frequency. Segmental relaxations are also altered comparing to that of PnBA. Based on the proposed microstructure picture, a hierarchical relaxation mechanism for PnBA-g-UPy networks

is described which accounts for both collective and binary assemblies in the supramolecular systems.

7.1 Introduction

Hydrogen bonding moieties demonstrate very broad range of strength, controlled by the number and the configuration of the hydrogen bonded sites.[1,2] The arrangement of donor (D) and acceptor (A) bonds inside the hydrogen bonding motifs determines the strength of association. For instance DDAA arrangement is stronger than DADA array, because of the secondary electrostatic interaction.[3] One of the promising multiple hydrogen bonding groups is Ureidopyrimidinone (UPy) introduced by Sijbesma *et al.*[4] UPy has high bond strength and its dimerization constant is 5.7×10^7 in chloroform and 5.9×10^8 in toluene. This group has three spatial configurations, referred to as tautomeries, being affected by solvent polarity and substituent groups.[5] Different low molecular weight polymers such as poly(ethylene-co-butylene), polycarbonate, polycaprolactone and polydimethylsiloxane with hydroxyl end groups have been functionalized by UPy.[6–9] Mechanical properties of these unentangled supramolecular systems were similar to that of conventional elastomers at ambient temperature. For instance, poly(ethylene-co-butylene) that was a viscous liquid at ambient temperature was converted to a viscoelastic solid with over 5 MPa plateau modulus upon functionalization with UPy.[8]

Apart from binary associations, lateral interactions can also influence mechanical behavior of the supramolecular systems. When UPy is connected to the chain with urethane or urea linkage, the lateral interactions derived by $\pi-\pi$ stacking create UPy stacks.[8] The melting temperature of these stacks depends on several parameters. For instance, in polycaprolactone based supramolecular polymers the melting temperature of the stacks, which depends on the molecular weight and the structure of polycaprolactone as well as the UPy density, was reported between $40 - 90\ ^\circ C$,[10] while in network made up of high molecular weight, semi-crystalline and entangled poly(ethylene-co-vinyl alcohol) it was measured between $90 - 120\ ^\circ C$.[11] Thermoplastic elastomers were made via UPy stacking in functionalized amorphous polymer with low glass transition temperature.

In this research supramolecular copolymers based on entangled poly (n-butyl acrylate-co-hydroxyl ethyl acrylate) are synthesized using atom transfer radical polymerization (ATRP) and functionalized with UPy groups. Special care has been paid to the synthesis of high molecular weight precursor with low polydispersity using special reaction conditions. While entanglement seems to be crucial for designing structural supramolecular polymers with good mechanical properties, the dynamics of supramolecular polymer systems with well entangled precursor is not studied as extensively as non-entangled ones. Understanding dynamics of supramolecular polymer is necessary in designing systems for special applications. The primary objective of this chapter is to investigate polymer dynamics in an entangled supramolecular network with strong binary and collective associations. In addition we seek for direct evidences to confirm the universal microstructure model proposed in Chapter 6. We also aim

to highlight similarities in the viscoelastic behavior of these strongly associating supramolecular networks with weak hydrogen bonding PnBA– r-AAs, addressed in the previous chapters.

It should be noted here that the supramolecular systems of this study are not in their thermodynamic equilibrium, as large frictions imposed by binary and collective assemblies of the UPy groups considerably slow down the motion of the polymer chains. Attempts are made to equalize thermal history of all samples, by annealing at similar conditions before measurements, in order to insure a common starting point. Yet the data, especially the viscoelastic ones, may suffer from the strong non-equilibrium behavior. Although difficulties in achieving equilibrium limit our understanding of the dynamics and microstructure of these supramolecular networks, the current data helps in testing the universal model of Chapter 6.

7.2 Materials and Methods

n-butyl acrylate (BA, 99%) was purchased from Aldrich and purified by passing through a column of basic alumina. Unstabilized trimethylsiloxy protected ethyl acrylate (HEA-TMS, 97%) was purchased from abcr and was used without any purification. Ethyl 2-bromopropionate (EBP, 98%), N, N, N', N'', N''-pentamethyl diethylene triamine (PMDETA, 99%) and copper(I) bromide (CuBr, 99,999%) were purchased from Aldrich and used without extra purification. Methyl isocytosine was purchased from Aldrich. 1,6-diisocyanatohexane, and dibutyl tin dilaurate (DBTDL) were purchased from Merck. The rest of used materials were commercially available, synthesis grade and were used without further purification.

UPy synthon was synthesized according to the literature.[6]

7.2.1 Synthesize of PnBA Homopolymer and P(nBA-co-HEA-TMS) Copolymers

In a 25 mL schlenk flask, anisole (4.12 mL, 25% v/v, for the case of PnBA-b4; see Table7.1) as the solvent and the internal standard of ^{1}H NMR measurements, EBP (7.2 $\mu L, 55.2$ μmol) as the initiator, BA (12.35 $mL, 86.2$ $mmol$) and HEA-TMS (3.4 $mmol$), for copolymer, as the monomers and PMDETA (11.5 $\mu L, 55.2 \mu mol$) as the ligand were added and the resulting solution was bubbled with argon (Ar) for 30 minutes. CuBr (7.9 $mg, 55.2$ μmol), as the catalyst, was added to a 25 mL round-bottom flask, the flask was degassed by vacuum and the internal atmosphere was replaced by Ar. The solution was transferred to the catalyst containing vessel and was placed in an oil bath. The reaction mixture was stirred for at most 120 h using a magnet bar. During polymerization samples were removed by a degassed syringe in order to determine the conversion using ^{1}H NMR. After reaching the desired conversion, the reaction was stopped and mixture was dissolved in CH_2Cl_2 and passed through a column of natural alumina in order to remove the copper complex. The solution was precipitated in excess amount of methanol and the precipitate was dried under vacuum. For the case of PnBA-b4 (see Table7.1), SEC :

$M_n = 143\ kg/mol, PDI = 1.19$; ^{1}H NMR (300 MHz, $CDCl_3$): δ HEA-TMS peaks: 0.13 (s, $Si(CH_3)_3$), 1.7 and 1.9 (m, CH_2 in polymer main chain), 2.34 (m, CH in polymer main chain), 3.75 (m, CH_2-OSi), 4.10 (m, $C(O)O-CH_2$); BA peaks : 0.95 (t, CH_3), 1.36 and 1.6 (m, $2CH_2$), 1.7, 1.9 and 2.3 (m, CH_2 and CH in polymer main chain), $4.0-4.1$ (m, $C(O)O-CH_2$). Composition (^{1}H NMR): BA/HEA-TMS = 96.4/3.6 (approximately 96/4).

7.2.2 Grafting of UPy on Poly(nBA-co-HEA)

To cleave TMS protections, poly(nBA-co-HEA-TMS) were hydrolyzed completely using concentrated HCL, in THF at 25 $°C$ for $12h$. Poly(nBA-co-HEA) was then grafted with UPy in different ratios to obtain a series of supramolecular networks according to the following procedure; deprotected poly(nBA-co-HEA) was mixed with UPy synthon and two drops of DBTDL in toluene at 80 $°C$. The mixture was stirred for 10 min, and then centrifuged. The solvent was removed under vacuum. Functionalized copolymer was dried under reduced pressure at 50 $°C$ for 24 h. PnBA-g-UPy samples were then annealed at 90 $°C$ for 24 h to insure that they all have been subjected to similar thermal history (See Section 7.3.3 for more details).

7.2.3 Characterization Methods

Synthesis of UPy synthon was studied by FTIR spectra recorded on a Bomem spectrometer (ABB Bomem Inc., Canada). Monomer conversions, copolymer compositions and grafting of UPy on copolymer were determined by proton nuclear magnetic resonance (^{1}H NMR) spectroscopy. ^{1}H NMR spectra were recorded on a Bruker Avance 500 MHz spectrometer. Chemical shifts were reported downfield from tetramethylsilane in $CDCl_3$ as the internal standard at room temperature. In the supramolecular networks, UPy percent was calculated through the ratio of integration of UPy characteristic peaks to the integration of acrylate characteristic peak.

Polymer molecular weights and polydispersity indices were determined using a Waters gel permeation chromatography (GPC), Waters 410 refractometer as the detector and Waters WISP 712 auto injector with injection volume of 150 μL using three PLgel 5 μ columns: 10^2 Å, 10^3 Å and 10^4 Å.

Dynamic mechanical properties were studied by temperature sweep tests on a Triton-TTDMA instrument. A rectangular bar of supramolecular polymer of size about $20 \times 2 \times 2\ mm$ was subjected to a sinusoidal deformation in torsion mode. Annealed samples were loaded to the setup at room temperature and then cooled down to $-100\ °C$. Using a heating rate of 3 $°C$/min viscoelastic properties were measured at constant frequency, 1 Hz, under nitrogen atmosphere.

Viscoelastic response of the PnBA-g-Upy supramolecular networks was measured in frequency domain using 8 mm parallel plate geometries of MCR301 rheometer (Antone Paar, Germany). Annealed supramolecular samples were loaded to the rheometer at room temperature. The systems are then heated up to 75 $°C$ where 2 consecutive frequency sweep measurements between $628-0.01$

rad/s are performed. Next the samples were cooled down to 35 $°C$ and similar frequency sweep experiments were repeated. At each temperature, discrepancy between the two consecutive measurements was less than 5% for all samples, which shows that the annealing protocol is good enough for this range of temperature and frequency. The second frequency sweep measurement at each temperature is reported.

For optical microscopy, fresh and annealed supramolecular samples were cooled down to $-60\ °C$ and microtomed without using any chemicals, including water. Ultrathin sections were immediately placed on copper grids, sandwiched with glass lames, and placed under optical microscope. Silicon oil was used to fill the cavity between the microscope lens and the lame. Special attention was made to minimize exposure to air, as absorbed water may change the microstructure by plasticizing UPy stacks. Microstructure was photographed at room temperature.

7.3 Results and Discussion

7.3.1 Synthesis

For UPy synthon, the molecular structure is confirmed by FTIR. The peaks at 1553, 1582, 1667 and 1706 cm^{-1} represent the UPy group. Isocyanate group is confirmed by peak at 2270 cm^{-1}. Furthermore, ^{1}H NMR contains 3 peaks above 10 ppm. These peaks are related to the hydrogen bonded amine groups and are considered as characteristic peaks of UPy.[6]

PnBA and random (PnBA-co-HEA-TMS) copolymers were synthesized by ATRP at different HEA contents. In controlled radical polymerizations all chains grow simultaneously which leads to low polydispersity.[12,13] This specificity helps to separate polydispersity effects from other parameters that influence dynamic behavior.

ATRP has opened new opportunities for synthesis of complex architectures from broader range of monomers and under milder reaction conditions.[14] However there are limited reports on successful incorporation of polar comonomers like HEA in narrow dispersed high molecular weight copolymers. HEA comonomer was protected with trimethylsilyl (TMS), to minimize the negative effect of polarity on polymerization kinetics.[15,16] Protection was removed and hydroxyl group was provided for anchoring UPy group as explained in the experimental section. Details of the reaction conditions and the molecular characteristics of the final copolymers are depicted in Table 1. Table 7.1.

Figure 7.1 shows the ^{1}H NMR spectrum of purified PnBA-b4. The absence of any peaks around 5.8, 6.1 and 6.3 ppm, which are the characteristic peaks of monomers, confirms complete removal of unreacted monomers. Instead, the presence of broad peaks between 3.9 and 4.2 ppm arising from the OCH_2 in BA and HEA units (labeled as a and e, respectively) and the methyl of the pendant in BA units in 0.96 ppm (labeled d) as well as 0.13 ppm belonging to methyl of TMS groups in HEA units (labeled g), illustrates the presence of poly(nBA-*co*-HEA-TMS). The final copolymer compositions were determined by ^{1}H NMR spectroscopy. The integration area of OCH_2 from BA and HEA-

Table 7.1: Molecular characteristics of PnBA homo and copolymers

Sample	Time	Conv[a]	HEA[a]	$M_{n_{GPC(backbone)}}$ [b]	$M_{nNMR(backbone)}$ [c]	PDI[b]
	h	%	*mol%*	*kg mol*$^{-1}$	*kg mol*$^{-1}$	
PnBA145	120	73	0	144	140	1.13
PnBA-b4	46	63	3.6	143	123	1.19
PnBA-b7	72	65	7	143	129	1.13

[M]:[EBP]:[Cu]:[PMDETA]:1500:1:1:1, [a] determined by ^{1}H NMR spectroscopy. [b] calibrated against PS standards. [c] calculated from conversion.

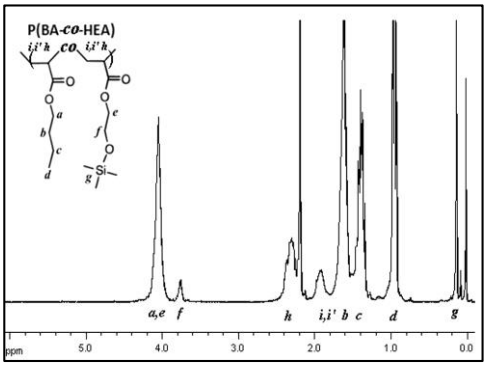

Figure 7.1: ^{1}H NMR spectrum of poly (nBA-co-HEA-TMS), sample PnBA-b4.

TMS units (labeled as a and e) and 9 protons of TMS group and peaks around 0.13 *ppm* (labeled g) from HEA units were compared to get final copolymer composition. The calculated commoner mole fractions were 3.6 and 7% (See Table 7.1).

The ^{1}H NMR results confirm that the cleavage reaction is quantitative, and the level of grafting can be regulated by controlling the feeding of the UPy groups in the reaction with de-protected copolymer. In the ^{1}H NMR spectra of grafted copolymers the methyl peak of TMS groups in HEA units (~ 0.13 *ppm*) is disappeared. The multiplet between 3.9 and 4.2 *ppm* is related to OCH_2 in BA and HEA units. The peaks above 10 *ppm* illustrate hydrogen bonded amines in UPy groups. UPy fraction in final copolymers was determined by comparison of integration area of these peaks. Results are presented in Table 7.2. According to the UPy content, the samples were named U2, U3 and U4. Note that all samples are made from a single backbone.

Table 7.2: Chemical and physical properties of the PnBA-*g*-UPy supramolecular networks

Sample label	Backbone	UPy feed[a] g	UPy content[b] %	T_g^{DMTA} $^\circ C$	T_g^{DSC} $^\circ C$
U2	PnBA-b4	0.9	2.5	−29	−45
U3	PnBA-b4	1.31	3	−28	−42
U4	PnBA-b4	1.83	3.5	−26	−39

[a]Based on 10 g polymer; [b]Calculated from ^{1}H NMR;

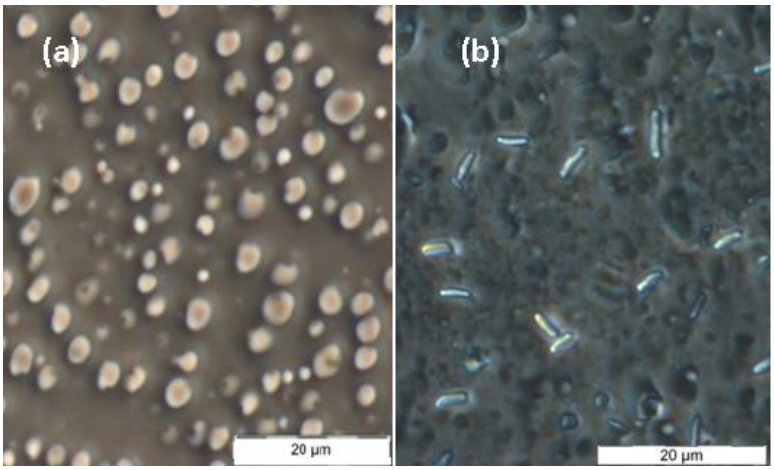

Figure 7.2: Microstructure of (a) U3 and (b) U4, as revealed by optical microscopy. Collective assemblies with various size and shape are observed.

7.3.2 Morphology of the PnBA-*g*-UPy Supramolecular Networks

Sticky groups, such as UPy, contaning aromatic cores are prone to phase separation into microdomains. These microdomains can have different structures depending on stickers density.[17] Figure 7.2 shows the morphology of the U3 and U4 systems as revealed by optical microscopy. A large number of coarse domains with dispersity of size and shape can be seen in the both samples. Unlike the surrounding matrix, these domains are very stiff and show high modulus ($< 10^8$ Pa) as measured by peak-force mode of atomic force microscopy. Supramolecular systems with higher concentration of grafted UPy groups show more diversity in the shape of the phase separated UPy stacks (See also Figure 7.3). As shown in Figure 7.2, UPy stacks demonstrate different shapes. Particularly, one can see spherical and cylindrical domains, with higher fraction of cylindrical stacks at high UPy concentrations.

Furthermore, annealing the PnBA-*g*-UPy samples at 90 $^\circ C$ leads to a higher fraction of cylindrical structures. Semenov *et al.* proposed that in associating

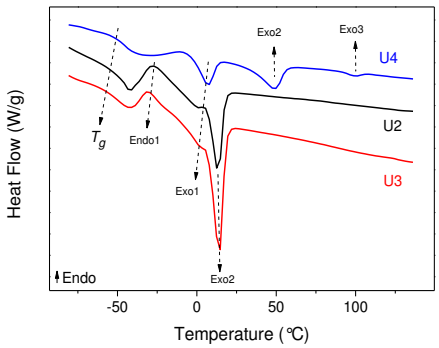

Figure 7.3: Thermal behavior of the PnBA-*g*-UPy supramolecular networks at 10 $°C$/min heating rate. Above glass transition, several exo and endothermic peaks are observed which correspond to the melting and crystallization of UPy stacks.

polymers with strongly interacting groups, such as ionomers, supramolecular aggregates can demonstrate cylindrical or disk like structures rather than spherical shape. The main parameter that controls the shape of the aggregate is surface tension between the supramolecular stacks and the non-associating polymeric backbones. As the surface tension is a function of thermal energy, shape changes can be expected by varying temperature.[18] The presence of non-spherical UPy collective assemblies and morphological changes induced by annealing can be rationalized based on this theory.

Figure 7.3 shows the thermal behavior of the PnBA-*g*-UPy networks measured at 10 $°C$/min heating ramps. It is clear that the glass transition temperature (T_g) of the PnBA-rich matrix increases by increasing the grafted UPy content. Above T_g, all samples show several exothermic peaks. It is trivial that these exothermic peaks are attributed to either the melting or restructuring of the UPy stacks. Exo1, occurring below 0 $°C$, can be unambiguously identified in the three supramolecular networks. In U2 and U3, Exo1 is seen as a shoulder to Exo2, while in the U4, these two peaks are separated. Exo2 in U4 is very different from the one of U2 and U3. Hence they are related to different structures or thicknesses of UPy stacks. In the case of U4, also a small peak is observed around 100 $°C$, which addresses presence of more stable UPy aggregates.

In addition, an endothermic peak is observed above the glass transition of the matrix in the PnBA-*g*-UPy networks. The strength of the Endo1 strongly decreases with increasing the UPy content. Eventually in the U4 network, only small traces of Endo1 can be observed at the vicinity of Exo2. Most probably, Endo1 originates from the cold crystallization of the UPy groups which could not effectively crystalize during the cooling ramp. It can be inferred that at high UPy content, where chain dynamic is significantly hindered due to large number of UPy stacks (see Section 7.3.3), the likelihood of formation of new

UPy domains reduces, as it requires chain motion. Hence the intensity of Endo1 decreases and its peak shifts to higher temperatures. This observation is in line with the results of Weitor *et al.* who reported that the melting temperature of the UPy stacks varies by the molecular weight of polycaprolactone precursor and the density of UPy groups.[10]

In summary, collective assemblies of UPy groups is observed in the PnBA-*g*-UPy supramolecular networks. The shape of the stacks ranges from spherical to cylindrical. Diversity in size and shape of the collective assemblies leads to multiple exothermic peaks above the T_g of the PnBA precursor.

7.3.3 Viscoelastic Properties of the PnBA-*g*-UPy Supramolecular Networks

Just like PEO-$NiCl_2$ systems, viscoelastic properties of the PnBA-*g*-UPy supramolecular networks strongly depend on the annealing conditions. Upon annealing a fresh sample, both elasticity and terminal relaxation time of the transient network increase. Furthermore, the microstructure of the system evolves and higher density of cylindrical stacks is achieved. This time and temperature dependent evolution is either due to restructuring of the present UPy stacks or formation of new ones, which result in higher density of intermolecular supramolecular associations. High density and long life time of the collective assemblies practically freeze the supramolecular networks. Hence **PnBA-*g*-UPy networks of this work are not in their thermodynamic equilibrium**, which suggests that any minor change in the experimental protocol can change the results. To overcome this difficulty all samples were annealed at 90 $°C$ for 24 h, before microstructure and viscoelastic investigations, presented in sections 7.3.2 and 7.3.3. This thermal treatment insures that all samples have been subjected to identical thermal history and enables us to compare the behavior of the PnBA-*g*-UPy networks. Additionally, identical experimental protocols were used for all samples. Hereunder we report viscoelastic data of identically annealed and measured supramolecular networks.

Evolution of the storage and loss moduli of the U3 and U4 networks upon heating is shown in Figure 7.4. Above glass transition, two major relaxations can be observed. The temperatures at which these relaxations occur are correlated to the exothermal processes observed in DSC. In other words after each thermal transition a part of the stress is relaxed in the system. Hence, it can be concluded that the UPy stacking is, at least, partially intermolecular and holds stress. At temperatures below -20 $°C$, the storage modulus of all samples are close to each other. Although minor differences are observed here, the chain dynamics is limited to small segments and is only slightly affected by the presence of binary and collective assemblies of the UPy groups. As U3 sample shows higher moduli compared to U4 right after the glass transition, it can be stated that the cold crystallization process (Endo1 in Figure 7.3) establishes new intermolecular associations. The cold crystallization should occur at a faster rate than chain relaxation in this range of temperature, otherwise the U3 system would behave similarly to U4. As opposed to low temperatures, above Exo1 U4 system is more elastic, which is due to higher number of binary

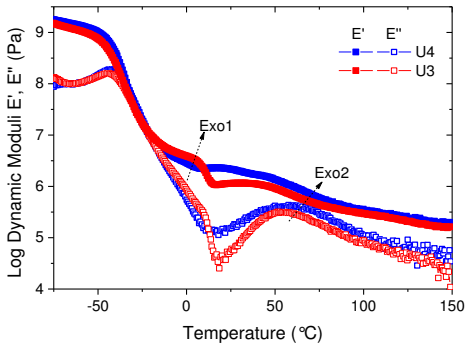

Figure 7.4: Evolution of the storage and Loss moduli, E' and E'', of PnBA-g-UPy networks against temperature at 1 Hz (torsion mode) and 3 $^{\circ}C$/min heating ramp.

and collective assemblies. Above 100 $^{\circ}C$, where collective assemblies of UPy motifs almost disappear, there is a minute difference between the two samples, which is presumably due to higher number of active binary associations. Even at 150 $^{\circ}C$ no signature of terminal regime is observed. Viscoelastic properties are not tracked above 150 $^{\circ}C$ as UPy groups were reported to be unstable beyond this temperature limit. Note that several plateaus in the storage modulus are observed in the U3 and U4 supramolecular systems.

Figure 7.5 illustrates LVE dynamic moduli $G'(\omega)$ and $G''(\omega)$, of PnBA-g-UPy networks measured at 75 and 35 $^{\circ}C$. It is clear from Figures 7.4 and 7.5 that at every measurable temperature binary and collective UPy associations dominate viscoelasticity of the system. Nonetheless the magnitude of dynamic alteration differs at various temperatures and time scales.

Like in most of the supramolecular networks, Figure 7.5 shows that the terminal relaxation of the chains is considerably hindered by inclusion of the supramolecular moieties. At 35 $^{\circ}C$ (Figure 7.5.a) while PnBA precursor is flowing with $G' \sim \omega^2$ and $G'' \sim \omega$, only a small fraction of stress is relaxed after 100 s in all PnBA-g-UPy networks. It is clear from the viscoelastic data that the supramolecular networks have higher plateau modulus compared to the PnBA precursor. Figure 7.5.b illustrates that once again a low frequency second plateau is observed in $G'(\omega)$, which levels up as the sticker density increases in the system. Just like PnBA– r-AA supramolecular networks the transition region between the two plateaus shows a slope of $\frac{1}{2}$. The slope is better seen in PnBA-g-UPy networks. By comparing the shape of viscoelastic curves at 35 and 75 $^{\circ}C$, it can be stated that the networks demonstrate strong thermo-rheological complexity, as anticipated.

In summary, we made the following observations in the PnBA-g-UPy networks.

i) Viscoelasticity is dominated by the collective assembly of UPy motifs at low temperatures. Each exothermal transition which corresponds to the

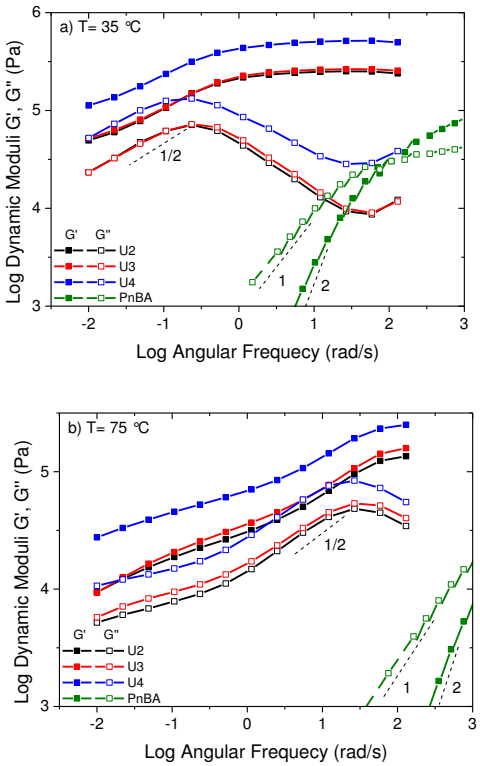

Figure 7.5: Storage and loss moduli G', G'' of PnBA-g-UPy networks against angular frequency at (a) 35 and (b) 75 $°C$. PnBA precursor data are shown for comparison. Dashed lines indicate various slopes.

melting of a fraction of UPy stacks (see Section 7.3.2) is followed by a stress relaxation in the supramolecular network.

ii) Above 100 $°C$, where collective assemblies are either not present or they are so scarce that cannot be detected by DSC, the relaxation time of the network is still significantly hindered. This is perhaps due to strong binary associations of UPy groups.

iii) Chain relaxations are affected by the transient friction of UPy groups. The plateau modulus lifts up, a second plateau is formed and a Rouse dominating relaxation mechanism with $G' \sim \omega^{1/2}$ and $G'' \sim \omega^{1/2}$, between the two plateaus is observed.

7.3.4 Hierarchy of Relaxation Mechanisms in PnBA-*g*-UPy Supramolecular Networks

Based on the observations of Sections 7.3.2 and 7.3.3, we propose a hierarchy of molecular relaxation processes for the present supramolecular systems. At a given temperature polymer strands can be divided into 3 categories: Mobile chains which are not trapped by any collective assembly, dangling ends with one free end and the other fixed to a collective assembly and trapped segments which are fixed at both sides by UPy stacks. Each of these segments can have additional binary associations.

After concomitant Rouse relaxations, trapped segment cannot undergo further relaxation while mobile chains and dangling end strands can relax by contour length fluctuations. If there is no binary contact on mobile chains or the associations are very labile, one can consider reptation as the most probable mechanism for stress relaxation. This assumption is supported by the results of Hackelbusch *et al.* who showed that diffusivity of sticky chains in weakly associating networks is not different from the non-associating precursors.[19] On the contrary, diffusivity of chains bearing strongly interacting supramolecular motifs was shown to be significantly slower than the non-functional counter parts.[19,20] Considering strong association interactions of quadrupole hydrogen bonding UPy groups, reptation of mobile chains is not probable in the supramolecular networks of this work.

Contour length fluctuations of the dangling ends and mobile chains occur at the association-dissociation rhythm of the supramolecular motifs, so called sticker blinking. Presumably, every segment has the chance for fluctuations only if all stickers between the considered segment and the chain ends are dissociated in a specific time period. When association lifetime of the stickers is met, the active stickers, which effectively contribute to the polymeric network, disassociate and new active ones emerge in random places to keep the equilibrium fraction of active stickers constant. After another lifetime step, the current active ones are replaced by randomly positioned new active stickers and so forth. In other words, active stickers start random blinking among all potential stickers. The segments between the first active sticker and the closest chain end are free to fluctuate at time zero. On the other hand, segments located between the first active sticker and the middle of the chain are frozen and would wait for another blinking of the stickers, which may give them the chance for fluctuations (all of the active sticker may randomly locate behind some of the frozen segments by the next blinking). Through time, each segment can accumulate time during which it is not frozen and fluctuations happen gradually based on this accumulated free time.[21]

Considering that the collective assemblies stand still during the accumulated fluctuation process of the mobile chains and dangling strands, there is no possibility for trapped segments to relax stress in this time scale. Nonetheless after accumulated fluctuations, conductive constraint release processes will be activated. Dilated trapped segments, this time can partially relax by further transverse Rouse motions.

7.4 Conclusion

Poly (n-butyl acrylate-co-hydroxyl ethyl acrylate) with relatively high molecular weights and narrow polydispersities were synthesized via ATRP at two different comonomer levels. The copolymers were grafted with UPy group at different fractions to create physical cross-links via strong quadruple hydrogen bonds. Samples at lower density of physical junctions have similar thermal behavior which was different from the ones with higher number of sticky groups. The latter had several melting peaks which were attributed to the diversity of association structures and thicknesses of the stacks as confirmed by the optical microscopy. Specifically, higher UPy grafting density leads to emergence of highly ordered cylindrical stacks.

UPy stacks results in longer relaxation times and higher levels of the second plateau as expected. A clear correlation between thermal and viscoelastic properties were observed. After each exothermal melting of UPy stack a clear relaxation is observed, which suggest that the viscoelastic behavior is highly dominated by the collective assemblies. Viscoelastic observations similar to those in PnBA_ r-AAs, together with a clear visualization of the collective assemblies confirm the validity of the universal microstructure proposed in the last chapter. Based on this microstructure picture a hierarchical relaxation mechanism for PnBA-*g*-Upy network is proposed which accounts for both collective and binary assemblies in the supramolecular system.

7.5 Bibliography

1 Armstrong, G.; Buggy, M. Hydrogen-Bonded Supramolecular Polymers: A Literature Review. *J. Mater. Sci.* **2005**, 40 (3), 547-559.

2 Brunsveld, L.; Folmer, B. J.; Meijer, E. W.; Sijbesma, R. P. Supramolecular Polymers. *Chem. Rev.* **2001**, 101 (12), 4071-4098.

3 Beijer, F. H.; Sijbesma, R. P.; Kooijman, H.; Spek, A. L.; Meijer, E. W. Strong Dimerization of Ureidopyrimidones via Quadruple Hydrogen Bonding. *J. Am. Chem. Soc.* **1998**, 120 (27), 6761-6769.

4 Sijbesma, R. P. Reversible Polymers Formed from Self-Complementary Monomers Using Quadruple Hydrogen Bonding. *Science* **1997**, 278 (5343), 1601-1604.

5 Söntjens, S. H. M.; Sijbesma, R. P.; van Genderen, M. H. P.; Meijer, E. W. Stability and Lifetime of Quadruply Hydrogen Bonded 2-Ureido-4[1 H]-Pyrimidinone Dimers. *J. Am. Chem. Soc.* **2000**, 122 (31), 7487-7493.

6 Folmer, B. J. B.; Sijbesma, R. P.; Versteegen, R. M.; Van Der Rijt, J. A. J.; Meijer, E. W. Supramolecular Polymer Materials: Chain Extension of Telechelic Polymers Using a Reactive Hydrogen-Bonding Synthon. *Adv. Mater.* **2000**, 12 (12), 874-878.

7 Botterhuis, N. E.; van Beek, D. J. M.; van Gemert, G. M. L.; Bosman, A. W.; Sijbesma, R. P. Self-Assembly and Morphology of Polydimethylsiloxane Supramolecular Thermoplastic Elastomers. *J. Polym. Sci. Part A Polym. Chem.* **2008**, 46 (12), 3877-3885.

8 Kautz, H.; Van Beek, D. J. M.; Sijbesma, R. P.; Meijer, E. W. Cooperative End-to-End and Lateral Hydrogen-Bonding Motifs in Supramolecular Thermoplastic Elastomers. *Macromolecules* **2006**, 39 (13), 4265-4267.

9 Dimopoulos, A.; Wietor, J. L.; Wbbenhorst, M.; Napolitano, S.; Van Benthem, R. a T. M.; De With, G.; Sijbesma, R. P. Enhanced Mechanical Relaxation below the Glass Transition Temperature in Partially Supramolecular Networks. *Macromolecules* **2010**, 43 (20), 8664-8669.

10 Wietor, J.-L.; van Beek, D. J. M.; Peters, G. W.; Mendes, E.; Sijbesma, R. P. Effects of Branching and Crystallization on Rheology of Polycaprolactone Supramolecular Polymers with Ureidopyrimidinone End Groups. *Macromolecules* **2011**, 44 (5), 1211-1219.

11 Jangizehi, A.; Ghaffarian, S. R.; Kowsari, E.; Nasseri, R. Supramolecular Polymer Based on Poly (Ethylene-Co-Vinyl Alcohol)-G-Ureidopyrimidinone: Self-Assembly and Thermo-Reversibility. *J. Macromol. Sci. Part B* **2014**, 53 (5), 848-860.

12 Van Herk, A. M. Historic Account of the Development in the Understanding of the Propagation Kinetics of Acrylate Radical Polymerizations. *Macromol. Rapid Commun.* **2009**, 30 (23), 1964-1968.

13 Ahmad, N. M.; Charleux, B.; Farcet, C.; Ferguson, C. J.; Gaynor, S. G.; Hawkett, B. S.; Heatley, F.; Klumperman, B.; Konkolewicz, D.; Lovell, P. A.; et al. Chain Transfer to Polymer and Branching in Controlled Radical Polymerizations of N-Butyl Acrylate. *Macromol. Rapid Commun.* **2009**, 30 (23), 2002-2021.

14 Shipp, D. A.; Wang, J.-L.; Matyjaszewski, K. Synthesis of Acrylate and Methacrylate Block Copolymers Using Atom Transfer Radical Polymerization. *Macromolecules* **1998**, 31 (23), 8005-8008.

15 Beers, K. L.; Boo, S.; Gaynor, S. G.; Matyjaszewski, K. Atom Transfer Radical Polymerization of 2-Hydroxyethyl Methacrylate. *Macromolecules* **1999**, 32 (18), 5772-5776.

16 Robinson, K. L.; Khan, M. A.; de Paz Bez, M. V.; Wang, X. S.; Armes, S. P. Controlled Polymerization of 2-Hydroxyethyl Methacrylate by ATRP at Ambient Temperature. *Macromolecules* **2001**, 34 (10), 3155-3158.

17 Herbst, F.; Schroter, K.; Gunkel, I.; Groger, S.; Thurn-Albrecht, T.; Balbach, J.; Binder, W. H. Aggregation and Chain Dynamics in Supramolecular Polymers by Dynamic Rheology: Cluster Formation and Self-Aggregation. *Macromolecules* **2010**, 43 (23), 10006-10016.

18 Semenov, A. N.; Nyrkova, I. A.; Khokhlov, A. R. Polymers with Strongly Interacting Groups: Theory for Nonspherical Multiplets. *Macromolecules* **1995**, 28 (22), 7491-7500.

19 Hackelbusch, S.; Rossow, T.; van Assenbergh, P.; Seiffert, S. Chain Dynamics in Supramolecular Polymer Networks. *Macromolecules* **2013**, 46 (15), 6273-6286.

20 Colby, R.; Zheng, X.; Rafailovich, M.; Sokolov, J.; Peiffer, D.; Schwarz, S.; Strzhemechny, Y.; Nguyen, D. Dynamics of Lightly Sulfonated Polystyrene Ionomers. *Phys. Rev. Lett.* **1998**, 81 (18), 3876-3879.

21 Ahmadi, M.; Hawke, L. G. D.; Goldansaz, H.; van Ruymbeke, E. Dynamics of Entangled Linear Supramolecular Chains with Sticky Side Groups: Influence of Hindered Fluctuations. *Macromolecules* **2015**, DOI: 10.1021/acs.macromol.5b00733.

Chapter 8

Conclusions

8.1 Final Remarks

Dynamics and morphology of two libraries of supramolecular networks based on linear monodisprese entangled associative polymers were investigated in chapters 3-7. 3D networks are formed via reversible interacting sites, placed along the contour length of the chains. Nature of the transient supramolecular interactions are entirely different in PEO-salt and PnBA based systems. While binary assemblies in the former are due to ion-dipole interactions between metal cations and ether oxygens, in the latter system hydrogen bonds lead to dimerization of the carboxylic acid and UPy side groups. Nevertheless, collective assemblies exist in both libraries. In PEO-$NiCl_2$, crystallization of $''$crown-ether-like$''$ complexes freeze the motion of contributing segments, with respect to those in the bulk, whilst reduction of surface tensions is the dominant driving force of phase separation of AA monomers into PAA domains in partially hydrolyzed PnBAs. Although the collective assemblies could not be visualized in either of these supramolecular networks, NMR relaxometry and WAXS data consistently revealed that the PEO-$NiCl_2$ crystals are rather huge and exceed 14 nm in size. On the contrary, PAA domains are believed to be smaller than 5 nm since geometrical confinement features were observed in the dielectric structural relaxation. Collective assemblies in PnBA-g-UPy networks which are formed by the $\pi - \pi$ stacking of UPy motifs, are coarse enough that can be detected by optical microscopy. It was illustrated that thermal transitions of UPy stacks is followed by stress relaxation processes in the corresponding supramolecular polymer network. This observation well represents the correlation between microstructure and morphology in entangled supramolecular networks.

It was argued that the binary assemblies in both libraries of supramolecular networks mainly affect the segmental relaxation, seen by the depression of the longest Rouse time of polymer strands (τ_R^{Max}). Based on the viscoelastic investigations presented in Chapters 4, 6 and 7 it can be stated that collective assemblies play a key role in controlling dynamics of supramolecular networks, compared to binary ones.

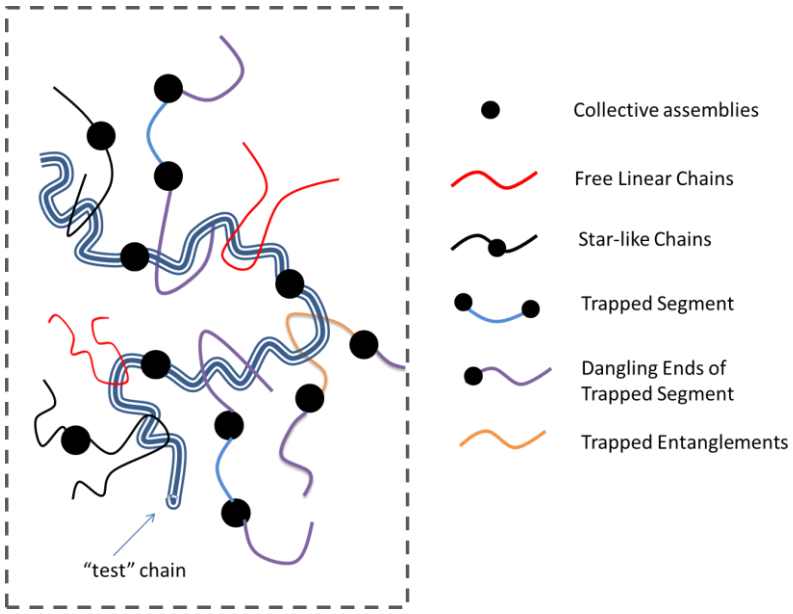

Figure 8.1: Schematic illustration of different categories of segments in enatgled supramolecular networks fromed via collective assemblies of moities. A probe chain is shown. It is surrounded by free linear chains not attached to collective assemblies, star-like chains that are only attached to one collective assembly, and trapped chains that are connected to at least two long life time collective assemblies.

With respect to participation in collective assemblies, polymer segments can be divided into five categories, illustrated schematically in Figure. 8.1. (*i*) free linear chains that are not attached to any collective assembly, and have freely moving extremities (*ii*) star-like chains that are attached to only one long lifetime collective assembly, (*iii*) trapped segments that are connected to more than two collective assemblies, and (*iv*) dangling ends of the trapped segments. Free linear chains, star-like molecules and dangling end of the trapped segments constitute the mobile polymer fraction of the system as they are able to relax by tube escape mechanisms. In contrast, sections of trapped chains between two collective assemblies are essentially immobile since renewal of their orientation is restrained until dissociation of this long lifetime stickers. This classification of segments in a supramolecular network enables us to describe complex shape of the relaxation modulus by considering hierarchy of relaxation times, shown in Figure 8.2. Note that dynamic moduli and angular frequencies are normalized by the plateau modulus (G_N^0) and the reptation time (τ_d) of linear chains, respectively.

Zone 1: At early timescales Rouse motions occur, which involve relaxation of subchains of increasing lengths. At times shorter than τ_R^{Max} the relaxing

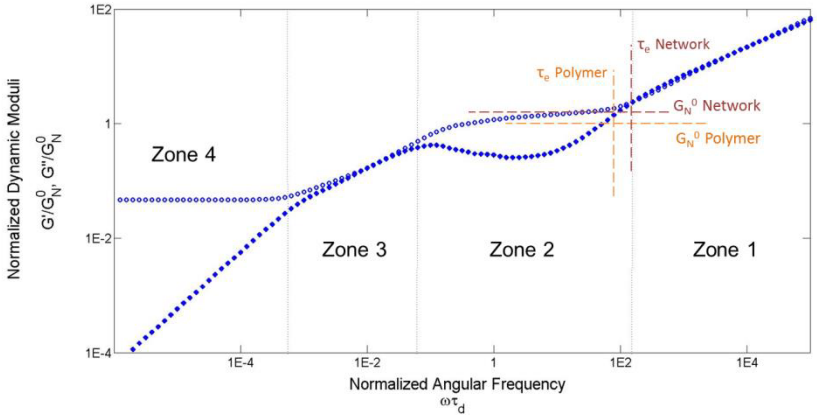

Figure 8.2: Different zones of relaxations in dynamic moduli of entangled supramolecular networks. Zone 1: high frequency Rouse regime. Zone 2: upper plateau zone in which entanglements and supramolecular assemblies contribute to elasticity; Mobile segments gradually start to relax orientation. Zone 3: Constraint Release Rouse (CR) equilibration of the trapped strands. Zone 4: Second plateau modulus; only trapped strands between collective assemblies contribute to elasticity.

segments do not feel the tube. Note that the sgements which can relax by Rouse are shorter than the distance between physical constarints, *i.e.* entanglements , binary and collective assemblies. At longer times, Rouse modes are restricted, as longer segments feel the constraint imposed by the surroundings environment. The transition to the first plateau modulus (Zone 2) marks the saturation of the Rouse modes, and the tube picture starts to be relevant. In other words, the length of the subchains reaches the average spacing between physical constraints. It is worth noting that binary assemblies only alter Rouse modes, when their corresponding association time exceed τ_e .

Zone 2: At the second relaxation step, the dangling branches of the trapped chains as well as the star-like chains will renew orientation by CLF. Moreover, the free linear chains will relax by reptation and CLF. As the level of the first plateua modulus is determined by the average distance between physical constraints, higher plateau modulus can be expected for the supramolecular network, compared to linear chains.

Zone 3: Once the mobile components have relaxed, the CR process becomes active. Trapped strands between successive sticky junctions partially renew configuration through local CR events. In other words, the segments of the trapped strands will undertake Rouse-like hops. These events occur at time scale by which entanglements between the trapped strands and the surrounding mobile material disappear/re-appear. They provide

extra freedom to the trapped strands, which can now explore the surrounding space on a larger length scale than the one corresponding to the original tube diameter.

Zone 4: The terminal relaxation of the trapped chains is delayed until dissociation of the collective assemblies takes place. As mentioned earlier in most cases it is outside the experimental window. Nevertheless, the beginning of this regime can be observed with specific samples at high temperatures.

In summary, using PEO-$NiCl_2$, PnBA-*g*-UPy and PBA-*r*-AA supramolecular networks, we showed that the dynamics of entangled macromolecules can be controlled over the entire length scale by supramolecular assemblies. We investigated the relationship between different modes of self-assembly of supramolecular moieties and chain dynamics over a wide length/time scale. In achieving this goal, we successfully combined different experimental techniques to probe chain motion. Furthermore, we studied transient dynamics of supramolecular moieties in the environment of polymer and showed that the association - dissociation times of supramolecular assemblies strongly depends on their surrounding environment.

Using various methods, we inferred size, shape, internal organization and dynamics of collective assemblies in the both libraries of supramolecular networks. Several anomalous viscoelastic phenomena, *e.g.* emergence of the second plateau and strain hardening, were attributed to these aggregates. It was also shown that formation of collective assemblies can prevent the system from reaching equilibrium and eventually lead to thixotropy or other history dependent behaviors.

Finally taking into account dynamics and morphology studies in the PEO-$NiCl_2$ and PBA-*r*-AA supramolecular system, as well as other investigations, on various entangled supramolecular systems; *i.e.* telechelic terpyridine functionalized PEO, telechelic Coumarin terminated poly(dimethylsiloxane), thermoplastic elastomers based on poly(tetrahydrofuran), and associative polymers based on PnBA functionalized by quadrupole hydrogen bonding ureidopyrimidinone (UPy) groups; a detailed universal microstructure picture is drawn. The microstructure enables us to classify different segments in the systems, with respect to their relaxation times and interpret complex viscoelastic observations. In addition, we can correlate various dynamics and morphology observations in entangled supramolecular networks.

8.2 Future Perspectives

It was illustrated that collective assemblies play the major role in controlling polymer dynamics. Unlike binary assemblies which have been addressed extensively in the literature, the properties of collective assemblies are less known. To the best of our knowledge, research done on understanding and controlling hierarchical assembly, organization and internal dynamics of these aggregates are limited. Today, collective assembly of supramolecular moieties is just a spontaneous phase separation mechanism, which limits application of several

supramolecular systems and gives strength to some others. Nonetheless a detailed study of the formation and properties of collective assemblies is required. In particular, to control viscoelastic properties of the entangled suparmeolcular moieties, we required methodologies to interfere with the spontaneous phenomena of assembling. Having access to competing chemical compounds is a key. Insights to controlling this process can be achieved by selective plasticization of the supramolecular networks.

Failure of tTS is known for the entangled supramolecular systems. In practice, often a complex behavior is observed for viscous and elastic properties. For instance several authors reported successful construction of master curve using storage modulus, while pronounce thermo-rheological complexity was observed in the loss modulus. In other system none of the components were therom-rheologically simple. In lack of experimental data over an extended frequency range, some authors reported success of tTS principle by using strong vertical shifts. From the trend of literature it is clear that there is no common practice in applying tTS principle and interpreting temperature dependency of the dynamics of supramolecular systems. Hence LVE results are partially manipulated, which may give rise to inconsistent, if not wrong, conclusions. Therefore it is highly desired to revisit tTS principle in supramolecular systems, and establish a general validity framework. In doing that one has to take advantage of theoretical model, which can predict LVE dynamics over entire frequency range by considering temperature dependency of supramolecular interactions. Of course, to validate the model, access to detailed experimental data sets on model entangled supramolecular systems is required.

To accelerate our understanding process on dynamics and microstructure of entangled supramolecular systems, several libraries of model well defined samples should be prepared at large quantities, to facilities access of different research groups to these materials. At the current time, hundreds of supramolecular systems are being investigated across the globe. This is indeed an advantage, but on the other hand it makes generalizing the findings very difficult. Today, lots of effort is put on basic characterization of these samples, but often shortage of material or expertise, is the limiting factor in the way of deeper scientific works. Hence widely available libraries of well-defined supramolecular systems can dramatically impact the progress of this field of science.

List of Publications

Journal Papers

Published

Goldansaz, H.; Voleppe, Q.; Piog, S.; Fustin, C. a.; Gohy, J. F.; Brassinne, J.; Auhl, D.; van Ruymbeke, E. Controlling the Melt Rheology of Linear Entangled Metallo-Supramolecular Polymers. *Soft Matter* **2015**, 11 (4), 762-774.

Goldansaz, H.; van Ruymbeke, E.; Gohy, J.-F.; Fustin, C.-A.; Ries, M. E.; Bailly, C. Local Molecular Dynamics and Heterogeneity in $PEONiCl_2$ Supramolecular Networks. *Macromolecules* **2015**, 48 (7), 2290-2298.

Goldansaz, H.; Auhl, D.; Goderis, B.; Voleppe, Q.; Fustin, C.-A.; Gohy, J.-F.; Bailly, C.; van Ruymbeke, E. Transient Metallosupramolecular Networks Built from Entangled Melts of Poly(ethylene Oxide). *Macromolecules* **2015**, 48 (11), 3746-3755.

Goldansaz, H.; Goharpey, F.; Afshar-Taromi, F.; Kim, I.; Stadler, F. J.; van Ruymbeke, E.; Karimkhani, V. Anomalous Rheological Behavior of Dendritic Nanoparticle/Linear Polymer Nanocomposites. *Macromolecules* **2015**, 48 (10), 3368-3375.

Shabbir, A.; Goldansaz, H.; Hassager, O.; Ruymbeke, E. Van; Alvarez, N. J. The Effect of Hydrogen Bonding on Linear and Nonlinear Rheology of Entangled Polymer Melts. *Macromolecules* **2015**, 48 (16), 5988-5996.

Ahmadi, M.; Hawke, L. G. D.; Goldansaz, H.; van Ruymbeke, E. Dynamics of Entangled Linear Supramolecular Chains with Sticky Side Groups: Influence of Hindered Fluctuations. *Macromolecules* **2015**, 48 (19), 7300-7310.

Lambricht, L.; De Berdt, P.; Vanacker, J.; Leprince, J.; Diogenes, A.; Goldansaz, H.; Bouzin, C.; Prat, V.; Dupont-Gillain, C.; Rieux, A. Des. The Type and Composition of Alginate and Hyaluronic-Based Hydrogels Influence the Viability of Stem Cells of the Apical Papilla. *Dent. Mater.* **2014**, 30 (12), e349-e361.

Koussoroplis, S. J.; Paulissen, G.; Tyteca, D.; Goldansaz, H.; Todoroff, J.; Barilly, C.; Uyttenhove, C.; Van Snick, J.; Cataldo, D.; Vanbever, R. PEGylation of Antibody Fragments Greatly Increases Their Local Residence Time Following Delivery to the Respiratory Tract. *J. Control.* Release **2014**, 187, 91-100.

Khorasani, M. M.; Ghaffarian, S. R.; Goldansaz, H.; Mohammadi, N.; Babaie, A. Solid-State Microcellular Foaming of PE/PE Composite Systems, Investigation on Cellular Structure and Crystalline Morphology. *Compos. Sci. Technol.* **2010**, 70 (13), 1942-1949.

Pending

Goldansaz, H.; Fustin, C.-A.; Wübbenhorst, M.; van Ruymbeke, E. How Supramolecular Assemblies Control Dynamics of Associative Polymers: Towards a General Picture; **2015**.

Hawke, L. G. D.; Ahmadi, M.; Gondansaz, H.; van Ruymbeke, E. Viscoelastic Properties of Linear Associating Poly(n-Butyl Acrylate) Chains; **2015**.

Jangizehi, A.; Goldansaz, H.; Shirani, M.; Ahmadi, M.; Ghaffarian, S. R. Dynamics of Entangled Supramolecular Networks Based on Poly (butyl Acrylate)-g-Ureidopyrimidinone.

Peer-reviewed Conference Papers

Goldansaz, H.; van Ruymbeke, E. Super-Lubricity Induced by Soft Dendritic Nanoparticles to Entangled Polymers. *Annual Meeting of the Belgian Polymer Group* **2015**, Houffalize, Belgium.

Goldansaz, H.; Fustin, C.-A.; Wbbenhorst, M; Shabir, A.; Alvarez, N. J.; Hassager, O.; van Ruymbeke, E. Equilibrium Dynamics of Entangled Supramolecular Polymers Based of Poly(n-butyl acrylate), 10^{th} *Annual European Rheology Conference* **2015**, Nantes, France.

Hawke, L. G. D.; Ahmadi, M.; Gondansaz, H.; van Ruymbeke, E. On the Dynamics of Entangled, Linear Associative Polymers in the Melt State, 10^{th} *Annual European Rheology Conference* **2015**, Nantes, France.

Shabir, A.; Goldansaz, H.; Alvarez, N. J.; van Ruymbeke, E.; Hassager, O. The Influence of Hydrogen Bonding on Nonlinear Extensional Rheology of Supramolecular Poly(n-butyl acrylate). 86^{th} *Annual Meeting of The Society of Rheology* **2014**, Philadelphia, U.S.

Goldansaz, H.; Auhl, D.; Ries, M. E.; Fustin, C.-A.; Gohy, J.-F.; Bailly, C.; van Ruymbeke, E. Dynamics of Poly(ethylene oxide) Metallo-Supramolecular Networks, *SoftComp & ESMI Annual Meeting* **2014**, Heraklion, Greece.

Goldansaz, H.; Karimkhani, V.; Goharpey, F.; Afshar-Taromi, F.; Kim, I.; Stadler, F. J.; van Ruymbeke, E. Super-Lubricity Induced by Soft Dendritic Nanoparticles to Entangled Polymers. 9^{th} *Annual European Rheology Conference* **2014**, Karlsruhe, Germany.

Goldansaz, H.; Auhl, D.; Bailly, C.; van Ruymbeke, E. Dynamics and Microstructure of Metallo-Supramolecular Networks, 85^{th} *Annual Meeting of The Society of Rheology* **2013**, Montréal, Canada.

Goldansaz, H.; Auhl, D.; Bailly, C.; van Ruymbeke, E. Dynamics and Microstructure of Metallo-Supramolecular Networks Obtained from Poly(ethylene oxide). 9^{th} *Annual European Rheology Conference* **2013**, Leuven, Belgium.

Auhl, D.; Fustin, C.-A.; Gohy, J.-F.; Bailly, C.; van Ruymbeke, E.; Goldansaz, H. Dynamics of Transient Metallo-Supramolecular Networks Obtained from Poly(ethylene oxide). XVI^{th} *International Congress on Rheology* **2012**, Lisbon, Portugal.